UNIVERSITY OF UDINE

PhD course in Biomedical Science and Biotechnology

Cycle XXVII

Molecular pathways in the response of tumors to photodynamic therapy:

Role of NF-κB /YY1/RKIP loop

PhD Student: Emilia Della Pietra

Tutor: Valentina Rapozzi

Academic year 2014/2015

Summary

1 INTRODUCTION

Photodynamic therapy (PDT) is a clinically approved, not invasive therapeutic treatment that can induce a selective cytotoxic activity in the target cells (Agostinis P et al. 2011). This technique can be used for the treatment of a lot of diseases including psoriasis, age-related macular degeneration and cancer; recently it is interesting the use of PDT in microbiology for the treatment of resistant bacteria (Hamblin MR et al 2004; Jori G et al. 2006). The procedure involves i) the administration of a light-sensitive but, per se, harmless drug (photosensitizer, PS) followed by uptake of this compound and accumulation in the target cells; ii) the subsequent irradiation of the PS at a wavelength corresponding to an absorbance band of the molecule; iii) the oxygen that, reacting with the active PS, induces the production of reactive oxygen species and singlet oxygen (Plaetzer K et al 2009; Agostinis P et al.2011). A lot of studies show that, after PDT treatment, there is also an increase of nitric oxide (NO) due to the activation of the inducible nitric oxide synthase (iNOS) (Gupta S et al. 1998; Rapozzi V et al 2013).

The active PSs are able to produce rapidly a cytotoxic effect through apoptosis and/or necrosis activation; PDT selectivity is derived by the ability of the photosensitizers to localize in the cellular target and by the capability of light to reach in the selected sites. The targets of PDT include (i) tumor cells, (ii) the microvasculature that blood supply the tumor, (iii) and the inflammatory and immune host system that are activated against tumor cells (Dougherty TJ et al. 1998). Thanks to the low invasiveness of this therapy it can be used in different types of solid cancer (bladder cancer, early stages of lung and esophagus cancer, head and neck cancer) in which it is possible to obtain the reduction of tumor growth (Dougherty TJ et al. 1998; Agostinis P et al. 2011).

PDT offers a lot of advantages such as a minimal systemic toxicity, few secondary effects and the combination with other therapies like chemotherapy and radiotherapy.

1.1 The photosensitizer

The ideal photosensitizer would be a chemically pure drug with preferential uptake in tumor cells and a low light degradation molecule (that is optimal for long irradiation

times) with a rapid clearance (to reduce the photosensitivity of the patients). In terms of the administration it is important the solubility of the molecule: an amphiphilic structure is better for the transport in the blood and for the ability to penetrate the cytoplasmic membrane. To perform an optimal treatment it is important that this drug is not toxic in the dark, it should have a strong absorption peak between 600 and 800 nM; in fact, in this range of wavelength there is a deep light penetration in the tissue and the energy is sufficient to produce singlet oxygen (Triesscheijn M et al 2006; Plaetzer K et al 2009; Agostinis P 2011).

The first clinically approved PS was a mixture of purified phorphirins, called hematophorphirin derivates (HpD) and its purified compound, Photofrin, (porfimer sodium), is commercially available and officially approved for clinical application (Moan J 1986;Dougherty TJ et al. 1998; Triesscheijn M et al. 2006).

Today this PS is still the most employed, despite it has some problems like long lasting skin photosensitivity and low absorbance at 630 nM (Agostinis P et al 2011).

Another important PS widely used is 5-Aminolaevulinic acid (ALA) that is a metabolic precursor of protoporfirin IX, the real active molecule (Kennedy et al.1990; Dougherty TJ et al 1998).

To improve the characteristics of the PS and to reduce its toxicity, a lot of new compounds were synthesized; farther there are a lot of new techniques to meliorate the distribution of the PS and its selectivity.

The most well-known and used PSs are cyclic tetrapyrroles (porphyrins, chlorins and bacteriochlorins) and phenothiazenium-based structures that are known as second generation of PSs. The develop of the new generation concerns in the combination of these PSs with carrier molecules, such as monosaccharides, peptides, antibodies, polymers, nanoparticles and liposomes, in agreement with the cellular targets (Yoon I et al. 2013;Benov L 2014).

Host response to PDT treatment depends on the PS used, the type of light, the degree of tissue oxygenation and the type of cells treated. Besides it is important to consider the intracellular localization of the PS from which depends the kind of cell death and the influence of the tumor microenvironment (Moor AC 2000; Gomer CJ et al. 2006)

1.2 Photophysics and Photochemistry

Normally the PS is present in a energetically stable state, called ground state. This condition is characterized by two electrons with opposite spin in the lower energy molecular orbital; this configuration is called singlet state (Plaetzer K et al 2009; Robertson CA et al 2009). After the absorption of a light quantum with appropriate energy, one of them moves from the ground state to a exited state, keeping the same spin. This new condition is called excited singlet state. As the excited state is energetically less stable than the ground state, it has a short live and it can lose its energy in three ways: i) fluorescence light, ii) heat iii) and by intersystem crossing. In this process the spin of the excited electron inverts to form a long lived excited triplet-state. Each process is possible but it is important to know that PS has high probability to moves to triplet state (Ochsner M 1997;Plaetzer K et al 2009). Using the energy of the triplet state, the PS is able to induce chemical changes in the neighbors molecules through two reactions: type I and type II. In type I reaction, the excited PS can react directly with a substrate and transfer an electron to form a radical; the radical is unstable and may react with oxygen producing reactive oxygen species (ROS) (Plaetzer K et al 2009; Robertson CA et al. 2009; Agostinis P et al 2011). The ROS produced are seperoxide anions, hydrogen perosside and hydroxyl radical; the last two radicals are able to pass easily through plasma membrane; in this way the oxidative damage is not limited to the membrane compartment.

Type II reaction occurs when the PS transfers its energy directly to the molecular oxygen present in the tissue. The oxygen moves from its ground state to an excited state named singlet oxygen (with paired electrons). Since this molecule has a very short lifetime in cells, its site of damage is close to the site where the PS is located (Ochsner M 1997;Plaetzer K et al 2009; Robertson CA et al. 2009).

Both reaction happen simultaneously after PDT treatment and their contribution depends on the type of PS and on the quantity of substrate (Plaetzer K et al 2009; Robertson CA et al. 2009) (Figure 1)

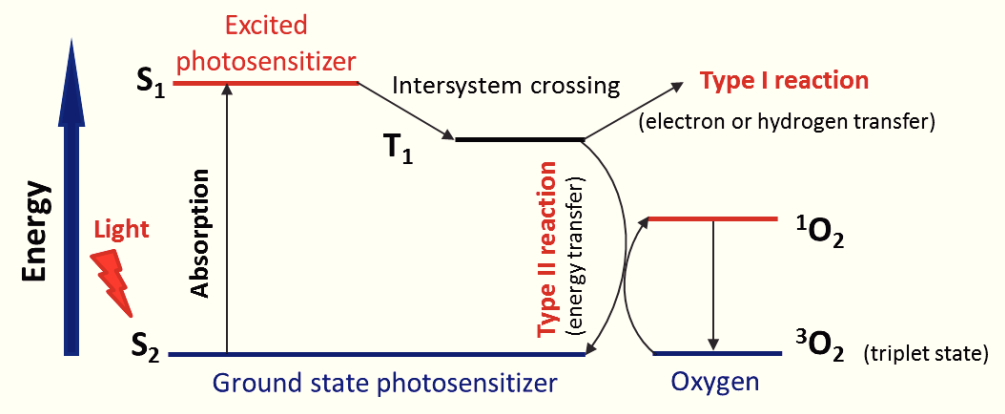

Figure 1.Modified Jablonski diagram *The diagram shows the excitation of the PS to its singlet excited state (S1),followed by intersystem crossing (T1) that relaxes to the ground state by type I (radical production) or type II (energy transfer to molecular oxygen) reaction. (Agostinis P et al.2011)*

1.3 Light delivery

To have an optimal PDT treatment *in vivo*, it is necessary that sufficient light reaches the diseased tissue to destroy tumor cells. The light propagation in the tissue implicates some processes such as reflection, refraction and scattering that can reduce the beam power and the deep penetration in the tissue (Nowis D et al. 2005; Wilson DC et al., 2008; Allison RR et al.2013). Another important phenomenon in light delivery during PDT is light absorption by tissue chromophores such as water, oxyhemoglobin (HbO_2) and deoxyhemoglobin, melanin and cytochrome (Robertson CA et al.2009; Agostinis P et al. 2011), that reduces activation of the PS.

The absorption spectrum of PS defines the optical window of PDT, below 620 nm and above 1200 nm; moreover, the fact that longer wavelengths are energetically insufficient to produces singlet oxygen, reduces again the optical window (600-800 nm); (Nowis D et al. 2005; Plaetzer k et al. 2009). Summary, to make an optimal PDT treatment it is important to know the characteristics of the tissue (amount of chromophores, pH, oxygenation of the tissue) and of the PS: for deeper treatment it is better to use a PS that absorbs red light, while to perform a topical treatment it is possible to use a PS which absorbs blue light (400nm) (Allison RR et al.2013).

It is possible to decide the light source according to PS absorption (fluorescence excitation and action spectra), disease (location, size of lesions, accessibility, and tissue characteristics), cost and size; the light can be provided by halogen, fluorescent, tungsten or xenon lamps (inexpensive); lasers (expensive) and LEDs that are very small and portable (Nowis D et al. 2005; Agostinis P et al. 2013 Allison RR et al. 2013).
It is also important to underline that a lot of PSs are fluorescent dyes that allow to obtain optical imaging to monitor PDT treatment (Robertson CA et al. 2009).

1.4 PDT and microenvironment

PDT not only modulates the direct tumor cell destruction, but it acts also on tumor microenvironment that is made up of malignant cancer cells and connective tissue as well as other cells including endothelial cells, fibroblasts and cell of the immune system (Gomer CJ et al. 2006; Milla Sanabria L et al. 2013). There are a lot of studies that show that PDT treatment is able to activate inflammatory and immune response, angiogenesis, and, in general, pro-survival pathways. These pathways can induce tumor recurrence and occur when one of PDT components (light, photosensitizer or oxygen) is limiting (low-dose PDT) (Piette J et al. 2003;Verna S et al.2007). During PDT treatment, vascular damage and the oxygen consumption may limit the efficacy of the treatment, in fact the hypoxic condition can cause the stabilization of hypoxia-inducible factor 1-alpha (HIF1 alpha) and the increase of vascular endothelial growth factor (VEGF). Some studies reported that antiangiogenic treatments enhance the tumoricidal action of PDT (Ferrario A et al. 2000; Solban N et al. 2006).
Ferrario et al. have shown that the oxidative stress due to PDT treatment can also induce the activation of metalloproteinases (MMPs); these molecules are involved in the degradation of the extracellular matrix and they have an important role in tumor angiogenesis, growth, invasion, and metastasis (Zhang H et al.2014); in *in vivo* studies it has been demonstrated that combining PDT with prinomastat (an MMP inhibitor) the therapeutic efficiency is enhanced (Ferrario A et al. 2004).
However low-dose PDT treatment can also promote the expression of the inducible cyclooxygenase (COX-2), involved in inflammatory response. It has been shown that this

protein is also linked to the development and progression of a variety of cancers, increasing the adhesion to extracellular matrix proteins, the cell motility, the resistance to apoptosis and the induction of cell proliferation (Volanti C et al. 2005). The use of selective NSAIDs, (non-steroidal anti-inflammatory drugs) that reduce prostaglandin production and inhibit COX-2, can ameliorate the single PDT treatment without affecting normal tissue repair (Ferrario A et al. 2002; Ferrario A et al. 2005).

1.5 Nitric oxide in the tumor

Nitric oxide (NO) is recognized as a major effector molecule in a diverse array of physiologic and pathologic processes. The biosynthesis of NO is catalyzed by a family of enzymes called NO synthases (NOS); the catalytic mechanism of NOS involves the electron transport from NADPH to the NOS NH_2-terminal domain, where the oxygen is reduced and incorporated into the guanidine nitrogen of L-arginine, producing NO and L-citrulline (Figure 2) (Singh S et al. 2011). It is evident that this radical not only controls important functions in tumor progression, but may have a major influence on the outcome of cancer therapies, in particular those dependent on oxygen and on ROS generation, such as photodynamic therapy (Korbelik M et al. 2000). This short-lived agent is involved in carcinogenesis, invasion, angiogenesis and modulation of therapeutic response. A lot of studies underline that NO can induce tumor progression or regression in dependence on the local concentration, the spatial and temporal distribution; in fact, when present at low rates (<50nM), NO is able to induce tumor cell proliferation, resistance to apoptosis, angiogenesis, cell migration and invasion; vice versa high rates of NO (>400nM) induce DNA damage, oxidative and nitrosative stress, mitochondrial damage that implicate cell death and tumor regression (Singh S et al.2011; Burke AJ et al.2013).

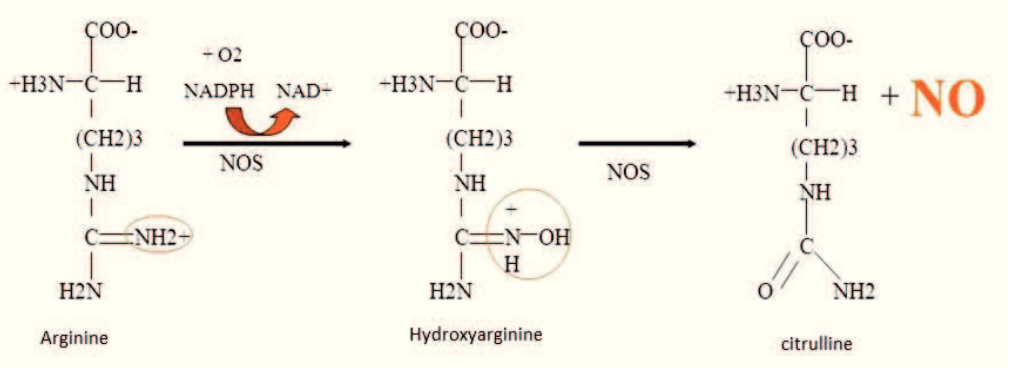

Figure 2 Nitric oxide production: *nitric oxide synthases produce NO by catalyzing a five-electron oxidation of a guanidino nitrogen of L-arginine. Oxidation of Arginine to citrulline occurs via monooxygenation reactions producing the intermediate hydroxyarginine. 2 mol of molecular oxygen and 1.5 mol of NADPH are consumed per mole of NO forme.*

1.6 Nitric oxide in PDT

1.6.1 Nitric oxide during PDT

Nitric oxide is known to directly influence the biological processes activated by PDT: in tumors that produce high levels of NO, the reduction of the blood flow, the vasoconstriction, the ischemia/hypoxia and the inflammatory reaction, induced by photodynamic treatment can be reduced; in fact, tumor models characterized by high NO production are less sensitive than the others (Korbelik M et al. 2000). Probably this is due to the following effects of NO: i) it acts as a potent vasodilator, ii) it prevents platelet aggregation, iii) it reduces the aggregation of neutrophils and iv) it prevents mast cell degranulation (Schmidt HHH et al. 1994; Korbelik M et al. 2000). On the other hand, it is important to consider that, elevated NO levels may maintain vessel dilation during PDT treatment, resulting in increased tumor oxygenation, that enhance the oxygen-dependent generation of oxidative stress (Reeves KJ et al. 2009). The NO-sensitive process that occurs after PDT includes reperfusion post injury, in which NO has a protective role increasing tumor oxygenation, the apoptosis of tumor cells and the modulation of immune reaction against the tumor (Dougherty TJ et al 1998).

1.6.2 Following PDT treatments

Gupta et al.(Gupta S et al. 1998) reported, for the first time, an increase of NO following treatment of A431, human carcinoma cells, with phthalocyanine/PDT. The increase of NO is correlated with an enhanced constitutive expression of nitric oxide synthase (NOS). Other authors confirmed this result in other cell line: prostate cancer PC3 (Rapozzi V et al. 2013; Bhowmick R et al. 2014), murine amelanotic melanoma B78H1 (Rapozzi V et al. 2011) and breast cancer COH-BR1 (Bhowmick R et al. 2011). Another evidence of NO production after PDT was obtained by Dalbasti et al. (Dalbasti T et al. 2002) that, using an electrochemical sensor for on-line measurement of NO changes, has detected a transient rise in NO production in the cerebellum after ALA/PDT.

Oxidative stress is the major cause of damage associated with an elevated NO level. This is due to the rapid reaction between superoxide (O^{2-}) and NO that forms the short-lived perossinitrite (ONOO−); this is a powerful oxidant, more toxic than its precursors (Beckman JS 1994). ONOO− oxidatively damages a wide range of biological molecules, including proteins, lipids and nucleic acids; moreover it is also able to oxidize thiols, to nitrate protein tyrosine residues and to damage mitochondria. Furthermore, ONOO−, as its conjugate acid ONOOH, can diffuse through membranes and cause damage far from its site of synthesis (Beckman JS 1994; Murphy MP 1999). Elevated NO levels increase oxidative stress and DNA damage; in addition it activates PARP, disrupting cellular energy metabolism, mitochondrial function and calcium homeostasis inducing activation of pro-death pathways (both necrosis and apoptosis) (Murphy MP 1999).

NO and reactive nitrogen species (RNS), are also able to modulate important transcription factors such as p53, able to block the cell cycle and to activate apoptotic pathways, and HIF-1 alpha, involved in angiogenesis, inflammation and cell proliferation.

All these functions are depending on the NO concentration involved (Zhou J et al. 2005;Burke AJ et al. 2013). It is also important to underline that NO is able to elicit long-term cytoprotective antioxidant responses resulting in apoptosis inhibition (Gomes ES et al. 2002; Casas A et al.2011). Literature reports that low NO levels induced after PDT treatment are correlated to the resistance, to apoptosis and to the stimulation of cell growth, through cyclic guanosine monophosphate(cGMP)-dependent mechanism (Gomes

ER et al. 2002; Bhowmich R et al. 2013) and through the suppression of pro-apoptotic JNK and p38 MAPK activation (Bhowmich R et al. 2014).

Evidences gathered in recent years indicate that NO participates in the regulation of cell differentiation. It has been demonstrate that a low amount of NO generated either from chemical donors or following eNOS overexpression regulates apoptosis, self-renewal and differentiation of embryonic stem cells (Tejedo JR et al. 2010).

1.7 NF-κB/Snail/YY1/RKIP loop

Nitric oxide is able not only to modulate the oxidative stress induced by PDT, but also to contribute to the molecular pathways activated by ROS.

One of this pathways is the NF-κB/Snail/YY1/RKIP loop, that is normally dysregulated in tumor. This loop is important in the regulation of tumor cell growth, in the tumor cell sensitivity to cytotoxic stimuli (chemotherapeutics drugs) and it has a pivotal role in the regulation of cell invasiveness through epithelial to mesenchymal transition (EMT) (Bonavida B et al. 2011) (Figure 3).

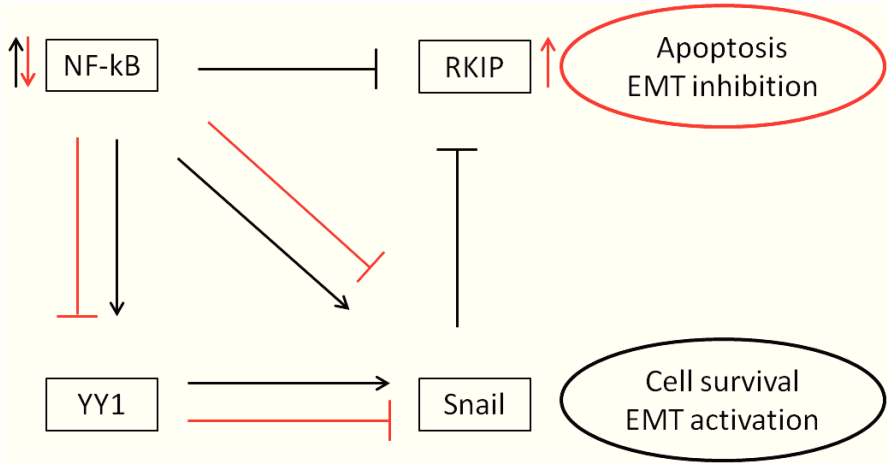

Figure 3 *Schematic diagram of the crosstalk among the members of the NF-κB /Snail/YY1/RKIP loop in the regulation of resistance to apoptotic stimuli and EMT. NO is able to modulate NF-κB in a dose dependent way: low NO levels, activate NF-κB and downstream genes Snail and YY1; these genes act as transcriptional repressor of RKIP, a metastasis suppressor gene. Snail also acts as an essential initiator of EMT ,inhibiting RKIP and E-cadherin, an adhesion protein. It has been demonstrated that high NO levels inhibit the activation of NF-κB, YY1 and Snail and induce RKIP, triggering cell death and EMT inhibition. The NO-mediated regulation of the NF-κB /Snail/YY1/RKIP loop via the above mechanisms result in the modulation of cell survival EMT. Red lines correspond to the effect of high NO level, while black lines correspond to the low NO levels (Bonavida B et al. 2011).*

1.7.1 NF-κB

The NF-κB (nuclear factor kappa-light-chain-enhancer of activated B cells) is a ubiquitously expressed protein complex that controls transcription of DNA. NF-κB is found in almost all animal cell types and is involved in cellular responses to stimuli such as stress, cytokines, ultraviolet radiation, free radicals (ROS or NO) (Matroule JY et al. 2006; Bonavida B et al. 2011; Rapozzi V et al. 2011). The incorrect regulation of NF-κB is linked to inflammatory and autoimmune diseases; moreover several different types of human tumors present the NF-κB expression constitutively active. The activation of this transcription factor implicates expression of genes that keep proliferation and cell protection; on the other hand, defects in NF-κB result in increased susceptibility to apoptosis leading to increased cell death.

The NF-κB consists in homo- or hetero-dimers of five proteins belonging to the Rel/ NF-κB family (p50, p52, p65, RelB, c-Rel). Under basal conditions, NF-κB is sequestered in the cytoplasm by inhibitor proteins of the IκB family but it can be rapidly activated in response to different stimuli. The phosphorylation of IκB proteins by the IKK complex induces the proteasome degradation of these inhibitor proteins, allowing the nuclear translocation of the NF-κB. Once in the nucleus, it can activate the transcription of its target genes (Bonavida B et al. 2011). It has been demonstrated that the iper-activation of NF-κB is related to the downstream activation of anti-apoptotic genes such as Bcl-xl and Yin Yang 1 (YY1); moreover, this transcription factor is able to modulate EMT and metastasis directly through the activation of Snail and indirectly through the down regulation of RKIP, a metastasis suppressor gene and E-cadherin, an adhesion protein (Wang H et al. 2007; Bonavida B et al. 2011).

Following PDT there is a modulation of NF-κB, in particular It has been demonstrated that after a non-optimal PDT treatment there is an increase of NF-κB levels that is linked to the activation of pro-survival pathways (Volanti C et al. 2002). Vice versa the optimal PDT treatment reduces the levels of NF-κB inducing cell death (Rapozzi V et al .2013).

1.7.2 Snail

Snail is a member of Snail superfamily of zinc-finger transcription factors and it is involved, not only in cell division and survival, but also in embryonic development and neural differentiation (Bonavida B et al. 2011). Snail is also involved in the acquisition of invasive and migratory properties during tumor progression, in particular in the activation of epithelial-mesenchymal transition that is the first step for metastasis formation (Nieto MA 2002). It directly down-regulates the expression of both RKIP, a metastasis-suppressor gene, and E-cadherin, a protein involved in cell-cell adhesion (Nieto MA 2002; Bonavida B et al 2011); furthermore Snail stimulates the expression of mesenchymal markers such as vimentin and fibronectin (Nieto MA 2002; Kim YS et al. 2014)

It has been also demonstrated that NF-κB can directly activate Snail promoting EMT and cell survival (Wu Y et al 2009; Bonavida B et al 2011)

1.7.3 YY1

Yin Yang 1 (YY1) is a zinc-finger transcription factor that can activate or repress the transcription depending on the context in which it binds (Castellano G et al. 2009); in this way it controls many cellular process such as proliferation and apoptosis. Its expression is crucial during embryonic development but it has been associated also with tumor progression, in particular it is linked to the metastatic process and to cancer cells survival. YY1 is overexpressed in several cancer (Castellano G et al. 2009) and it has been demonstrated that its silencing can sensitize the resistant tumor cell to apoptosis (Bonavida B et al. 2011). YY1 is identified as a repressor of death receptors like Fas and DR5 (Castellano G et al. 2009) and it has been demonstrated that it can activate DNA repair, promote a reduction of cellular adhesion (EMT activation) and inhibit apoptosis, leading to cellular proliferation, migration, and prolonged cell survival (Gordon S et al. 2006). Bonavida and collaborators demonstrated that NF-κB is directly able to regulate YY1 transcription, YY1 regulates the transcription of Snail and Snail reduces RKIP expression. These genes are therefore involved in the dysregulated NF-κB /YY1/Snail/RKIP loop that is linked in EMT activation and tumor progression (Bonavida B et al. 2011; Kashyap V et al. 2014).

1.7.4 RKIP

Raf kinase inhibitory protein (RKIP) is a highly conserved cytosolic protein, member of the phosphatidylethanolamine-binding family (PEBP); the most important targets of this protein are the pro-survival pathways Raf-MEK-ERK and NF-κB. In this context, RKIP is also able to inhibit STAT (Signal Transducer and Activator of Transcription) that regulates some genes involved in cell growth, apoptosis, survival and differentiation (Bonavida B et al. 2011; Deiss K et al. 2012).

RKIP is also important in chemotherapeutic resistance; in fact, it has been demonstrated that the depletion of RKIP determinates an increase of Nrf2 (Nuclear factor (erythroid-derived 2)-like 2), a transcription factor involved in antioxidant defenses, that is correlated to cell resistance (Bonavida B et al. 2011; Deiss K et al. 2012).

RKIP expression is down-regulated in several tumors and especially in metastatic tumors (Bonavida B et al. 2011). It is known that this gene plays a role as a metastasis suppressor in different types of cancer; moreover, it has been demonstrated that the overexpression of RKIP is correlated with EMT inhibition and activation of pro-apoptotic stimuli through the down-regulation of NF-κB, Snail and YY1 (Bonavida B et al.2011).

1.8 Epithelial-Mesenchymal Transition

Epithelial to mesenchymal transition (EMT) is a phenotypic conversion linked to metastasis. The concept of EMT was originally defined as a feature of embryogenesis, essential for the development of tissues and organs (Polyak K et al. 2009). EMT process is important also in cancer, in fact similar behaviors have been found during tumor invasiveness and metastasis (Mani SA et al. 2008). In addition it contributes to drug resistance (Singh A et al. 2010). Epithelial and mesenchymal cells have different phenotypes and functions: the first ones are characterized by closely cell-cell adhesion, planar and apical polarity, a polarized actin cytoskeleton and they are able to adhere to the basal surface. In contrast, the other ones are characterized by loosely associated cells that lack polarity and are surrounded by a large extracellular matrix, farther these cells are able to migrate easily and differentiate into connective, lymphatic and circulatory tissues. The term EMT refers to a multistep program by which epithelial cell lose their

differentiated characteristics and acquire mesenchymal features (Figure 4) (Wang Y 2014).

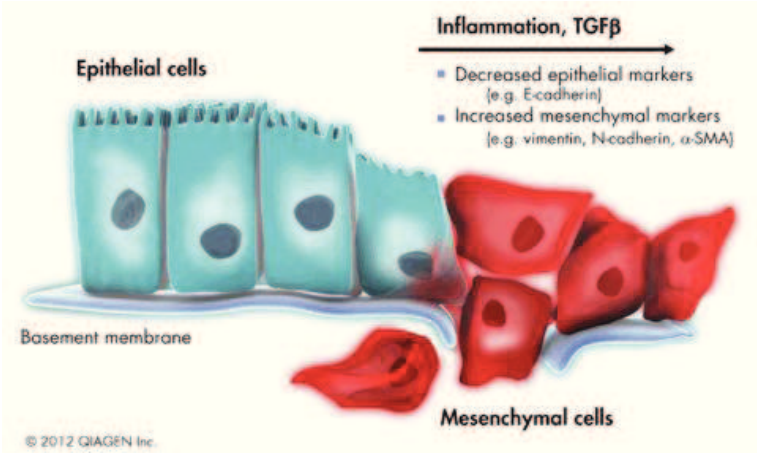

Figure 4. Epithelial to mesenchymal transition*. EMT takes place during embryonal development and plays a role in cancer invasion. It involves the decrease of the epithelial features (e.g. E-cadherin) and the increase of the mesenchymal ones (e.g. vimentin, N-cadherin)*

During EMT the adherent cells lose some typical markers of this phenotype such as MUC-1, ZO-1, Laminin-1 and E-cadherin, increasing the expression of mesenchymal proteins like, fibronectin, N-cadherin and vimentin (Gupta PB et al. 2009; Van der Pluijm G 2011).
E-cadherin is a transmembrane protein that mediates cell-cell adhesion and that has an important role in cell polarity and tissue morphogenesis. In cancer, loss of E-cadherin in epithelial cells is correlated to migration and invasion. Moreover, it has been found that a soluble extracellular fragment of E-cadherin, detectable in serum, is considered a diagnostic factor in cancer research because it is present in more quantity in cancer patients respect to the healthy ones (Repetto O et al. 2014).
On the other hand vimentin is the major cytoskeletal component of mesenchymal cells and it is often used as a marker of cells undergoing on EMT during both normal development and metastatic progression.
EMT is a reversible process; in fact, once migrating to the new site, tumor cells are able to re-express epithelial markers that permit adhesion, in a process named mesenchymal-to epithelial transition (MET). In this way, this process seems to be pivotal in the formation of distant metastasis (Polyak K et al.2009; Jing Y et al. 2011).

EMT activation is linked to different types of stimuli that include ROS (Wang Y et al. 2014) and NO; this one can both promote (directly by induction of tumor cell migration and invasion and indirectly through expression of angiogenic factors in tumor cells) and inhibit (through DNA damage, gene mutation and apoptosis) this process in a dose dependent way (Wink DA et al. 1998; Fukumura D et al. 2006; Burke AJ et al. 2013).

EMT is correlated to several pathways, the most common are TGF-beta, Wnt, Notch, Hedgehog and NF-κB pathways. There is a lot of crosstalk between these pathways, for example Notch can induce EMT through NF-κB activation but also modulating the activity of TGF-beta (Polyak K et al 2009). Hedgehog pathway is also implicated in EMT activation because it is correlated to an increase of Snail protein expression and to a decrease in E-cadherin and tight Junctions formation. It appears to be a crucial regulator of angiogenesis, metastasis and in the conservation of a more aggressive tumor phenotype (Polyak K et al. 2009;Lu Y et al. 2015). Several studies reported that NF-κB is strictly involved in EMT because it is able to suppress the expression of epithelial specific protein E-cadherin (Chua HL 2007;) and to induce the expression of mesenchymal specific protein, vimentin (Julien S et al. 2007).

The crucial role of NF-κB in EMT triggering is due to its ability to modulate some downstream genes such as YY1 and Snail; YY1 is able to activate the Snail transcription (Bonavida B et al. 2011) and Snail is able to repress the E-cadherin adhesion protein. Epithelial cells that overexpress Snail acquire metastatic and invasive potential and EMT phenotype; moreover, Snail is able to activate EMT through the modulation of claudins and occludins, important proteins for the cell polarity (Lin K et al. 2010). The modulation of these genes (YY1 and Snail) reflect on the modulation of RKIP (Bonavida B et al. 2011), that is also important in EMT and metastasis. In several reports RKIP results a metastasis suppressor, in fact it has been shown that the RKIP knockdown in LNCap cells results in increase of their invasive ability (Escara-Wilke J 2012) Moreover, Beshir et al. demonstrated that the inhibitory function of RKIP in metastasis and migration may be due to its ability to down-regulate the expression of some matrix metalloproteinases (Beshir et al. 2010)

1.9 Resistance

Resistance in cancer photodynamic treatment is an important limit that is still poorly understood. As for other forms of cancer therapy, PDT has to deal to a set of strategies that are employed by tumors to mitigate the cytotoxic effects of treatment. The mechanism of resistance developed by treated cells is the general mechanism of drug resistance and it can be summed up in these points: i) different uptake, rate of efflux of the drug (the photosensitizer in this case), ii) activation of cytoprotective mechanisms into the cells iii) decreased drug activation, or iv) increase of its inactivation (Casas A et al. 2011). It has been demonstrated that the cause of resistance is dependent on the cell type and the PS used.

1.9.1 PS uptake, intracellular localization and efflux.

PS uptake by cells is crucial for effective PDT because ROS and $^1O_2$ have a short half-life and act close to their site of generation so the most important oxidative damage happens in the localization site of the PS. Several factors can modulate the localization of the PS, such as its chemical structure, the drug delivery, the time interval between drug administration and light exposure and tumor type. The structural characteristics that determine the subcellular localization pattern are: (a) the net ionic charge which can range from -4 (anionic) to +4 (cationic); (b) the degree of hydrophobicity expressed as the logarithm of the n-octanol/water partition coefficient; (c) the degree of asymmetry present in the molecule. Hydrophobic PSs, can diffuse across the plasma membrane, and then relocate to other intracellular membranes. These PSs present a good uptake by tumor cells. Less hydrophobic PSs are taken up by endocytosis because they are too hydrophilic to diffuse across the plasma membrane (Castano AP et al. 2004; Benov L. 2014).

Plasma membrane targeting by PSs may lead to apoptosis inhibition and rescue response (A Casas et al. 2011). PSs which present positive charged and are also hydrophobic can localize in mitochondria; probably this is due to the influence of the mitochondrial membrane potential as well as the lipid bilayer of the membrane (Castano AP et al. 2004). This type of PSs is able to induce apoptosis very rapidly, causing the inactivation of

numerous mitochondrial enzymes and inducing the release of cytochrome c with the consequent caspases activation (Casas A et al. 2011). Lysosomal membrane rupture, actuated by PS targeting this organelle, and leakage of cathepsins from photo-oxidized lysosomes induce Bid (member of Bcl-2 family) cleavage and mitochondria outer membrane permeabilization, inducing rapid apoptosis activation (Agostinis P et al. 2011). When endoplasmic reticulum is targeted, Bcl-2 family is sensitive to oxidative damage, activating controlled cell death pathways. PDT, in addition to apoptosis activation, is able to induce autophagy that is used by cells i) to recycle the injured organelles and proteins, ii) to trigger pro-survival response and iii) to increase the resistance to death induced by ROS (Dewaele M et al. 2010). On another hand, it has been demonstrated that autophagy leads to cell death according to subcellular localization and tumor type. PSs that localize in mitochondria, ER and lysosomes can activate autophagy, whose role depends on PDT dose: with low PDT doses autophagy maintain cell viability, whereas at high PDT doses it is correlated to cell death (Inguscio V et al. 2012).

To guarantee PDT efficacy after the uptake, the PS has to remain into the cell until light activation. In this field an important role is attributed to the complex mechanism of multidrug resistance (MDR); this mechanism includes the activity of efflux pump, the activation of pro-survival pathways and other repair mechanisms. The most important family of efflux pump involved in MDR is the ATP binding cassette (ABC), composed by p-glycoprotein (p-gly or MDR1), ABCG2 (BCRP) and ABCC1 (or MRP1). They use the energy of ATP hydrolysis to efflux the endogenous material such as metabolic products, exogenous drugs and toxins from the cytoplasm into the extracellular space (Robey RW et al. 2004; Mo W et al. 2012; Mao Q et al. 2015). It has been demonstrated that the cells that overexpress or have an overactivation of these pumps can increase the degree of resistance; this type of resistance is not common to all the cell lines, in fact it is dependent on the structure of PS, on the cell type and intracellular distribution (Casas a et al. 2011). The most important ABC transporter in PDT is ABCG2 because the function of this protein in cancer stem cells (the most resistant cells in tumor) is to protect cells from heme and porphyrins during hypoxia (Krishnamurthy P et al. 2006). A lot of photosensitizers have been reported to be a substrate of this efflux pump. Indeed,

literature data show that overexpression of ABCG2 reduces the effects of photodynamic treatment and that the inhibition of ABCG2 transport is able to enhance the efficacy and selectivity of PDT (Robey RW et al.2004; Robey RW et al.2005;Selbo KP et al. 2012).
During PDT, different factors can modulate ABCG2 expression: i) the oxidative stress, via Nrf2 activation (Ishikawa T et al. 2010); ii) the hypoxia, often present in the tumor and iii) the same PS sometimes is involved in the overexpression of this pump (Casas A et al. 2011).

1.9.2 Cytoprotective mechanisms

After the activation of the PS reactive oxygen species are produced. This is the base for the pro-death role of these radicals but in the same way, there is an activation of antioxidant defense mechanism to contain the cell damage. Also these mechanisms are dependent on the treatment modality and on the cell type; in fact the cells can have different levels of antioxidant molecules such as glutathione, vitamin A and E; and also different rates of enzymes involved in ROS detoxification like superoxide dismutase, catalase or lipoamide dehydrogenase. All these molecules are involved in antioxidant defense that antagonize PDT (Agostinis P et al. 2011; Casas A et al. 2011). PDT was shown to up-regulate heme oxygenase-1 (HO-1) expression and the mechanism is regulated through the PI3K/Akt pathway and Nrf2 nuclear accumulation (Ishikawa T et al. 2010). Because of the antioxidant activity of HO-1, it can be expected that Nfr2-dependent signal transduction can control cellular protection against PDT-mediated cytotoxic effect. Oxidative stress can form oxidized proteins that can be refolded by molecular chaperones, for this reason an important role in PDT rescue response is assigned to heat shock proteins, involved in the modulation of cell damage. After PDT treatment there is an increase of HSP 27, HSP 70, HSP 90 and HSP 60 that is the chaperon protein mainly found in mitochondria of PDT resistant cells (Halon J et al. 2001). The intracellular function of HSPs is correlated both to protein refolding and to regulation of pro-survival pathways (Agostinis P et al. 2011).
The oxidative damage is also linked to the activation of DNA repair mechanism and to the activation of stress response genes involved in the modulation of proliferation and inducing cell detachment, resistance and activation of pro-survival pathways. The

modification on the expression of NF-κB was found after PDT treatment; the nuclear accumulation of this transcription factor is correlated to prosurvival pathways activation. It has been demonstrated that PDT can both increase and decrease the NF-κB level in a dose dependent way (Rapozzi V et al. 2011). Other common early response gene induced by PDT concerns the expression of JUN and FOS that form the activator protein-1 (AP-1), involved in apoptosis modulation, cell proliferation and survival (Casas A et al. 2011).

The activation of several cell survival signal transduction pathways have also been reported after PDT; the mitogen-activated protein kinases (MAPK) are involved in the regulation of growth, invasion and in the mechanisms against oxidative stress due to PDT. Cytotoxic oxidants, such as hydrogen peroxide and peroxynitrite, produced after treatment, have been shown to stimulate Akt/protein kinase B survival pathway (Zhuang S et al. 2003).

Ras proteins include a group of small GTP-binding proteins that are important molecular switchers for a variety of signal pathways that control proliferation, apoptosis, cytoskeleton modification, cell migration and adhesion. It has been found that Ras oncogene confers resistance to photodynamic treatment and this type of resistance is toward PDT and not to a particular PS (Casas A et al. 2011;Di Venosa G et al. 2012).

1.9.3 Morphology, cytoskeleton modification

The PDT resistance mechanism can be also mediated by proteins that interact with extracellular matrix (ECM). ECM is a collection of extracellular molecules such as collagens, elastin, proteoglycans, polysaccharides like hyaluronic acid and glycoproteins like fibronectin and laminin. These macromolecules are able to modulate a lot of phenomena involved in resistance and aggressiveness: cell adhesion, migration, proliferation (Casas A et al. 2011). Cell adhesion proteins mediate cell-cell adhesion (E-cadherin, catenin) and cell-ECM adhesion (integrins, vinculins,FAK).

The proliferative rate is anchorage dependent (Milla LN et al. 2011). Experimental evidences show that the cell that adhere to ECM are protected from apoptosis induced by anticancer therapies and in contrast, the loss of adhesion can be associated to apoptosis (Casas A et al. 2008; Milla LN et al. 2011). Also in PDT, It has been shown that in more resistant cells there is an increase of integrin that induces the activation of prosurvival

pathways (PI3K/Akt) and reduces apoptosis (inhibition of caspase 8); moreover, the PDT resistant cells show an increase of vinculin and p-FAK (Focal adhesion kinase, involved in cell adhesion and spreading process), that can facilitate three-dimensional invasion (Milla LN et al. 2011).

vimentin that is one of the cytoskeletal component responsible for maintaining cell integrity, is degraded by a lot of apoptosis inducers; moreover is overexpressed during EMT and in PDT resistant cells (Singh A et al. 2010; Casas A et al. 2011).

In addition, these cells show a general reorganization of the cytoskeleton and of the adhesion proteins, that confer a fibroblastic morphology, an alteration of actin, vinculin, catenin and cadherin distribution and an increase of stress fibers respect to normal cells. This reorganization can be correlated with a lower metastatic phenotype (Casas A et al. 2008; Milla LN et al. 2011).

1.9.4 Survivin

Survivin is an inhibitor of apoptosis protein, its function is to inhibit caspase activation and then apoptosis; it has an important role during the development and it is completely absent in the differentiated tissue. Over-expression of this protein was found in most human tumors and for these reasons this molecule is considered a prognostic marker and a possible target for anticancer therapies. Survivin is able to promote tumor progression, angiogenesis and chemo/radio-resistance.

It has been shown that cell lines resistant to PDT has an increased level of phospho-survivin (Milla LN et al. 2011; Casas A et al. 2011). This protein, as well as Bcl-2 and p-Akt is involved in cell proliferation and in apoptosis inhibition. All these proteins are client of HSP90, this consideration suggests that the target of survivin and HSP90 client proteins can be a strategy to increase PDT efficacy (Ferrario A et al. 2007).

1.9.5 Nitric Oxide:

As mentioned before, is known that PDT can induce the NO release in a dose dependent manner and so through it, PDT can modulate resistance and survival. The cytoprotective role of nitric oxide in resistance, appear when it is present in low rate. It is still important to underline that, in general, when the tumor shows high levels of endogenous NO, it is

less sensitive to therapies. Moreover NO can be a modulator of angiogenesis, invasiveness and evasion of apoptosis (Bhowmick R et al. 2009; Burke AJ et al.2013).
NO can reduce the activation of p38-MAPK and JNK that are proteins involved in cell death and it can activate ERK and NF-κB pro-survival proteins. NO might have a cytoprotective role through the increase of cGMP, an activator of the pro-survival and anti-apoptotic protein PKG that is able to inhibit caspases activation (Bhowmick R et al. 2013). Its role in PDT resistance is linked also to its capability to modulate the expression of the ABC transporter influencing chemo-resistant phenotype (Porro A et al. 2010) and further, modulating anti-apoptotic proteins such as survivin (Casas A et al. 2011).

1.10 Cancer stem cells

Most of tumors are histologically heterogeneous and present a subset of cells characterized by some biological, molecular and biochemical features associated with normal stem cells; these cells are identified in both solid and hematopoietic tumors and are called cancer stem cells. This is a minor population in the tumor and it is characterized by particular features: i) the capability to form tumorspheres in vitro cell cultures , ii) unlimited cell renew, iii) the capability to resist to several therapies (chemotherapy, radiotherapy), iv) the capability to be tumorigenic at low cell number, v) and the capability to hoechst dye-exclusion (Gupta PB et al. 2009; Singh A et al. 2010; Li Y et al. 2012). The existence of this more aggressive population, can in part explain the ability of tumor to escape from the action of chemotherapeutic agents and to induce tumor recurrence. Several papers speculate about the origin of these cells; some of them propose a hierarchically organization of cancer in which CSC or cancer initiating cells are in the top and they are the only one capable to reconstituting the whole upon transplantation (Pfeiffer MJ et al. 2010; Cruz MH et al. 2012). Cruz MH and coworkers (Cruz HM et al. 2012) propose a glioma model in which all the cells have the potential to develop cancer stem features and the stemness degree depend on the microenvironment. Anyhow the identification, the study and the elimination of this population is important to understand resistance mechanisms and to propose an effective cancer therapy. CSC population is identified using several surface markers that

can be different according to the type of cancer. The more common markers are CD44 CD133, CD24, ALDH-1 and ABCG2 (BCRP), found in different types of cancer such as breast, prostate (Salvatori L et al. 2012; Fan X et al. 2011), pancreatic cancer (Xue ZX et al. 2014) and glioma (Cruz HM et al. 2012). CD44 is a trans-membrane glycoproteins that is the major cell adhesion molecule for hyaluronic acid, an important component of ECM. It permits the interaction with the extracellular matrix and the actin cytoskeleton; it has both physiological and pathological function such as lymphocyte homing, wound healing, cell migration, tumor cell growth and metastasis activation (Marhaba R et al. 2004; Nagano O et al.2004). CD24 and CD133 (also known as Prominin1) are two membrane glycoproteins involved in cell adhesion, the first is characteristic of B cells, mature granulocytes and in differentiate neuroblast; the second is present in progenitors cells. When express in cancer, these markers are correlated to metastasis and tumor recurrence (Vaz PA et al. 2014). Aldehyde dehydrogenase 1 (ALDH-1, enzyme involved in the production of retinoid acid and in alcool detoxification) activity detection is also used for the identification of CSC; in fact, retinoic acid pathway is important for cell differentiation during development and in organism defense from toxic; moreover the high expression of this enzyme in breast cancer is correlated to poor prognosis (Croker AK et al. 2009; Kunju LP et al. 2011).

The development of the cancer stem cells is tightly correlate to EMT phenotype, in fact the metastatic cancer cells, which have presumably undergone EMT, may exhibit CSC phenotype (Singh A et al. 2010). In several studies it has been demonstrated that the expression of EMT-inducing transcription factors such as SNAIL1 and TWIST, increase the number of CSC that have been identified using the specific CSC marker for the particular type of cancer analyzed (Polyak K et al. 2009; Morel AP et al. 2008).

2 AIM

Tumor recurrence in cancer photodynamic therapy (PDT) is an important limit that is still poorly understood. The study of the relationship between the PDT cancer resistance and the development of a more aggressive population (CSC) is potentially useful to predict the PDT efficacy and to develop more effective and specific photosensitizers.

The knowledge of the molecular pathways involved in tumor recurrence is an important step in the development of new strategies to improve PDT treatment. In this study we focused our attention on the NF-κB YY1/RKIP loop, normally dysregulated in cancer. Considering that i) this loop is involved in tumor progression and resistance, ii) this loop can be modulated by NO in a dose dependent way, and that iii) after PDT treatment there is an induction of NO release, we analyzed the involvement of the loop in tumor recurrence after PDT in order to find new strategies to prevent the development of PDT resistance.

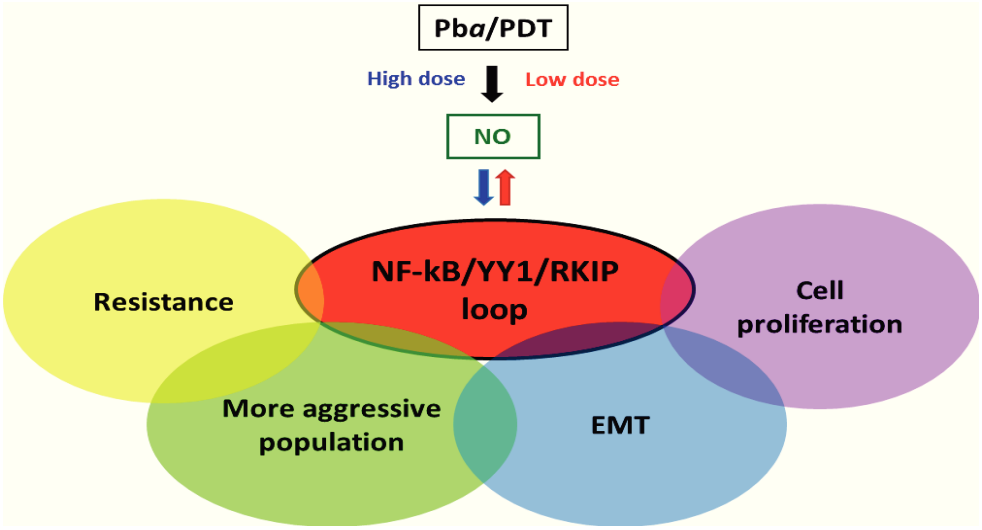

Figure 5. Schematic representation of the involvement of the NF-κB /YY1/RKIP loop in tumor recurrence

3 MATERIALS AND METHODS

Cell culture

The human prostate cancer PC3 and LNCaP cell lines were cultured in RPMI medium which contained 10% fetal bovine serum, antibiotics (penicillin 100 U/ml, streptomycin 100 µg/ml) and glutamine 2 mM. Cells were maintained in a humidified atmosphere with 5% CO_2 air at 37 °C. PC3 cells are characterized by two population, one in adhesion and one in suspension. PC3 cell line is considered a cell line with high metastatic potential. In contrast, LNCaP cell line is an adherent cell line with low metastatic potential.

Photodynamic treatment and reagents

Pheophorbide *a* (Pb*a*)(C35H36N4O5; MW 592.69) was purchased from Frontier Scientific Inc, Logan, UT. Pb*a* was dissolved in dimethylsulfoxide (DMSO) and conserved in aliquots of 0.5 mM at -80°C. The stability in solution of Pb*a* was checked by measuring its UV–vis spectrum at weekly intervals. Cells were treated with Pb*a* in the dark for 3h, then irradiated with a metal halogen lamp with red filter for 7 min (0.84 J/cm^2).

m-THPP (meso-tetra (m-hydroxyphenyl)porfirine)(C44H30N4O4; MW 678.74) was purchased from Frontier Scientific Inc, Logan, UT. m-THPP was dissolved in dimethylsulfoxide (DMSO) and conserved in aliquots of 0.5 mM at -80°C. The cells were treated with m-THPP in the dark for 3 h, then irradiated with a white, metal halogen lamp for 30 min (14 J/cm^2).

DRPDT2 (DR2) was synthesized by Dr.Greta Varchi (National Research Council Institute for Organic Syntheses and Photoreactivity ISOF, Bologna, Italy); it was dissolved in DMSO and conserved in aliquots at -80°C. The stability in solution was checked by measuring its UV–vis spectrum at weekly intervals. To perform a comparison between Pb*a* and DRPDT we calculated the same concentration of Pb*a* in both solutions; we confirmed the data with the overlay of the two spectra obtained by the spectrophotometer UV-vis Jasco (Jasco

s.r.l, Lecco, Italy). Cells were treated with DRPDT2 for 6h in the dark and after irradiated with a white, metal halogen lamp for 30 min (14 J/cm^2).

L-NG-nitroarginine methyl ester (L-NAME), NOS inhibitor, was obtained from Cayman Chemical Company (INALCO, Milan, Italy). The reagent was prepared in phosphate buffered saline (PBS). The treatment was performed 1h before irradiation.

Reserpine, an ABCG2 inhibitor, was obtained from Sigma Aldrich (Milan, Italy). The treatment was administered to the cells 30 min before irradiation, at the concentration of 10µM.

Cell metabolic assay

PC3 cells were seeded in a 96-well plate at a density of 5x10^3 cells/well. The cell metabolic assay was performed 24 or 48h after irradiation. The cell proliferation was determined by the resazurin assay following the manufacturer's instructions (Sigma–Aldrich, Milan, Italy). The values were obtained using fluorometer (EnSpireTM 2300 Multilabel reader, PerkinElmer, Finland).

Western blot analysis

The extracted proteins (40 µg) were subjected to electrophoresis on 12% SDS–PAGE and transferred to a nitrocellulose membrane (70 V for 2 h). The filter was blocked for 1 h with PBS-0.01% Tween (Sigma–Aldrich, Milan, Italy) containing 5% dry non-fat-milk, and then incubated, at 4 °C overnight, with the primary antibodies, rabbit polyclonal anti-RKIP, (G38, Cell Signaling, Merck Millipore, Darmstadt, Germany) diluted 1:1000; rabbit polyclonal anti-NF-κB p65 (C-20, sc-372 Santa Cruz Biotechnology, Santa Cruz, CA), diluted 1:1000; rabbit polyclonal anti-iNOS antibody (NOS2, sc-651 Santa Cruz Biotechnology, Santa Cruz, CA), diluted 1:200; mouse monoclonal anti-E-cadherin (610182 BD Biosciences) diluted 1:2500; mouse monoclonal anti-vimentin (VI-RE/1 sc 517721 Santa Cruz Biotechnology, Santa Cruz, CA) diluted 1:1000; rabbit polyclonal anti-YY1 (C-20, sc-

281 Santa Cruz Biotechnology, Santa Cruz, CA) diluted 1:1000; rabbit anti-ABCG2 (B-25 sc-130933 Santa Cruz Biotechnology, Santa Cruz, CA) diluited 1:500; rabbit polyclonal anti-PARP (9542, Cell Signalling, Danvers, MA) diluted 1:1000; rabbit polyclonal anti-Akt (9272 Cell Signaling technology, Danvers, MA) diluited 1:1000 and rabbit polyclonal anti-phospho-Akt (4058, Cell Signaling technology, Danvers, MA) diluited 1:1000 The expression of β-actin, used as an internal control, was detected with a mouse monoclonal anti β-actin (Ab-1, CP01, Calbiochem, Merck Millipore, Darmstadt, Germany), diluted 1:10,000. The filters were incubated for 1 h with the secondary antibodies with either anti-rabbit IgG diluted 1:4000 (Calbiochem, Merck Millipore, Darmstadt, Germany) or anti-mouse IgM, diluted 1:5000 (Calbiochem, Merck Millipore, Darmstadt, Germany), or anti-mouse IgG diluted 1:4000 (Calbiochem, Merck Millipore, Darmstadt, Germany). Each secondary antibody was coupled to horseradish peroxidase (HPR). For the detection of the proteins, we used ECL (enhanced chemiluminescence) reagents (Super Signal®West PICO, and Super Signal®West FEMTO, ThermoFisher Scientific Pierce, Rockford, USA). The exposure length depended on the antibodies used and was usually between 30 s and 5 min. The protein levels were quantified by Image Quant TL Version 2003 software (Amersham).

Fluorimetric determination of nitric oxide with DAF-FM diacetate

PC3 cells were seeded in a 6-well plate at the density of 6×10^5 cells/well. The day after, the cells were treated with different doses of Pb*a*. This indirect assay to measure NO is based on DAF-FM diacetate (4-amino-5-methylamino-2',7'-difluorofluorescein diacetate) (D-23844, Molecular Probes, Invitrogen, Milan, Italy). It diffuses into cells and tissue where non-specific esterases hydrolyze the diacetate residues thereby trapping DAF within the intracellular space. NO-derived nitrosating agents such as N_2O_3 nitrosate DAF to yield a highly fluorescent product, DAF triazole. This compound has some important advantages compared to 4,5-diaminofluorescein diacetate (DAF-2 diacetate), which is considered the most common indicator for nitric oxide (Kojima H et al. 1998)

A 5 mM stock solution of DAF-FM diacetate (MW = 496) in DMSO was made. The cells, after Pb*a*/PDT treatment, were incubated with 10 µM of diluted DAF-FM diacetate for 30

min at 37 °C. The cells were then washed with PBS to remove excess probe and replaced with fresh PBS and incubated for an additional 15 min to allow complete de-esterification of the intracellular diacetates. The cells were then trypsinized and recovered in PBS. The NO level was measured by FACS (FACScan, Becton Dickinson, San Jose, CA). The signal was detected by the FL1 channel in log scale. The samples were analyzed with the FLUOJO software (Tri Star, Inc., Ashland, OR).

Induction of resistance to Pba/PDT treatment

PC3 cells were seeded at day 0, at a density of $5x10^5$ cells in a 30 mm Petri dish. After 48h they were treated with 40 nM (low-dose) Pb*a*/PDT and after two days they were harvested and reseeded at the same concentration ($5x10^4$ cells). The final population received a total of 8 cycles of PDT. The initial population, not subjected to PDT, was called not treated cells (NT).

The cellular population submitted to four and eight PDT treatments was called IV and VIII treatment, respectively. Each experimental assay was performed 24 h after the last PDT treatment.

FACS analysis of cell cycle

For the cell cycle analyses the cells after a repeated treatment, were harvested by trypsinization and fixed for 1 h at 4°C in 70% ethanol in PBS. After PBS washing, the cells were stained with 0.05 mg/ml propidium iodide in the presence of 0.1 mg/ml RNase A in PBS (30 min at room temperature). The samples were analyzed by FACScan flow cytometer (Becton-Dickinson, San Jose CA) (FL 2 channel). A minimum of $1x10^5$cells for each sample were acquired in list mode and analyzed with FLUOJO software (Tri Star, Inc., Ashland, OR).

Clonogenic assay

After a repeated treatment, PC3 cells were seeded at a density of $5×10^3$ cells in a 60 mm petri dish. After 18 days, the colonies were formed, fixed and stained with 2.5%

methylene blue in 50% ethanol. The images were obtained by Gel DOC 2000 Bio-Rad (Milan, Italy).

Sorting of $CD44^+CD24^+$ cells and cultures of spheroids

After repeated treatment $1x10^6$ cells were re-suspended with 100 µl of PBS, incubated with 3 µl of CD44-PE and CD24-FITH antibodies (Invitrogen) in the dark at 4°C for 15 min; After that the cells were washed twice and resuspended in PBS and kept in the dark until subsequent analysis on FACS (Salvatori L et al.2012). Selected cells ($CD44^+CD24^+$) were seeded in 6-well cell-repel tissue culture plate (Eppendorf) using RPMI medium. To avoid cell damage by centrifugation, 1 ml of fresh medium was added weekly. To have a negative control also the cells characterized like a $CD44^+CD24^-$ population were seeded in the same condition. Sorting experiments were performed in collaboration with Dr Daniela Cesselli, Department of Medical and Biological Sciences of the University of Udine.

Fluorimetric determination of ABCG2 expression:

The tumorspheres obtained after sorting were harvested and washed with PBS. The cells were permeabilized using the buffer cytofix cytoperm™ (BD biosciences). Then the cells were incubated with the primary antibody anti-ABCG2 (B-25 sc-130933 Santa Cruz Biotechnology, Santa Cruz, CA). After incubation of 30 min in the dark at room temperature, the cell are washed and incubated with the secondary antibody Alexa fluo anti-rabbit IgG (invitrogen) diluted 1:500 for 30 min in the dark at room temperature. Finally the cells were washed and resuspended with 200 µl PBS and analyzed by FACS.

Flow cytometry uptake after treatment with ABCG2 inhibitor:

The cells were seeded at the density of 6×10^5 cells/well. The day after they were incubated in complete medium with each photosensitizer (5 µM m-THPP, Pb*a* or DRPDT2) with or without 10 µM reserpine (an ABCG2 inhibitor) for 30 min in the dark with 5% CO_2 air, at 37 °C. After an incubation in PBS-free fresh medium, with or without 10 µM reserpine; for 1h, the cells were detached from the plate, washed, recovered in PBS. The

PS uptake was measured by FACS and analyzed with the FLUOJO software (Tri Star, Inc., Ashland, OR).

4 RESULTS AND DISCUSSION

4.1 Effect of Pba/PDT on prostate cancer cell lines LNCaP and PC3.

In this study we evaluated the effect of photodynamic treatment with Pheophorbide *a* (Pb*a*), a chlorophyll derivate, in two type of prostate cancer cell lines PC3 and LNCaP. PC3 cell line is composed by heterogeneous cells, some of them growing up in suspension and the others in adhesion; PC3 cells differ from LNCaP cells because they show (a) an elevated metastatic capability (Chaiswing L et al.2011); (b) an increased expression of CD44 stemness marker (Chaiswing L et al.2011); (c) an increased antioxidant capacity, correlated to resistance and aggressiveness (Chaiswing L et al.2011;Tai S et al. 2011). Moreover LNCaP cell line, is considered a less aggressive tumor cell type. The cells grow up in adhesion, they are androgen-dependent, and consequently androgen withdrawal inhibits their growth (Tai S et al. 2011).

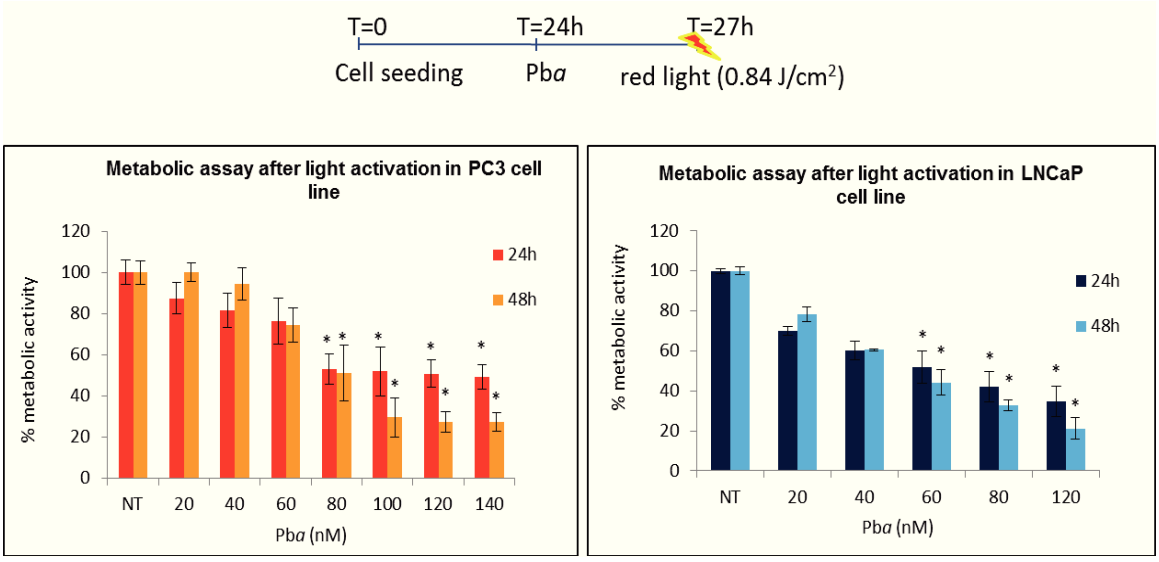

Figure 1. Metabolic activity in PC3 and LNCaP cells after Pba/PDT treatment. *The cells were treated 24h after seeding for 3h and light irradiated (0.84 J/cm2). The Histograms represent the values of % metabolic activity in both PC3 and LNCaP cell lines, performed by the resazurin assay, 24 and 48 h after light irradiation and expressed as T/C x 100. T and C are the absorbance of treated and not treated cells. The values are the mean ± SD of four independent experiments. A standard t-test versus control was performed (P < 0.01)*

Photodynamic treatment with Pb*a* (Pb*a*/PDT) was performed 24h after cell seeding. The cells were treated with the PS for 3h in the dark and then irradiated using an halogen lamp with a red filter (considering that Pb*a* absorption peak was measured at~670 nm), at the fluence of 0.84 J/cm^2. The metabolic activity of both cell lines, at 24h and 48h after irradiation is reported in Figure 1. The efficacy of the treatment is dose-dependent with an estimated dose of IC_{50} of 60nM for LNCaP and 80nM for PC3 cells. Both PC3 and LNCaP cells, treated with high dose of Pb*a*/PDT (Pb*a*/PDT ≥ IC_{50}), showed a cell growth arrest; whereas, with a low-dose (Pb*a*/PDT < IC_{50}) they showed, at 24h, a slight cell growth arrest, and at 48h a cell recurrence, in agreement with previous observations in Hela, HepG2 and B78-H1 tumor cells (Rapozzi V et al. 2009; Rapozzi V et al. 2013).

It is also important to underline that Pb*a*/PDT treatment, in both cell lines, didn't show toxicity in the dark (Figure 2).

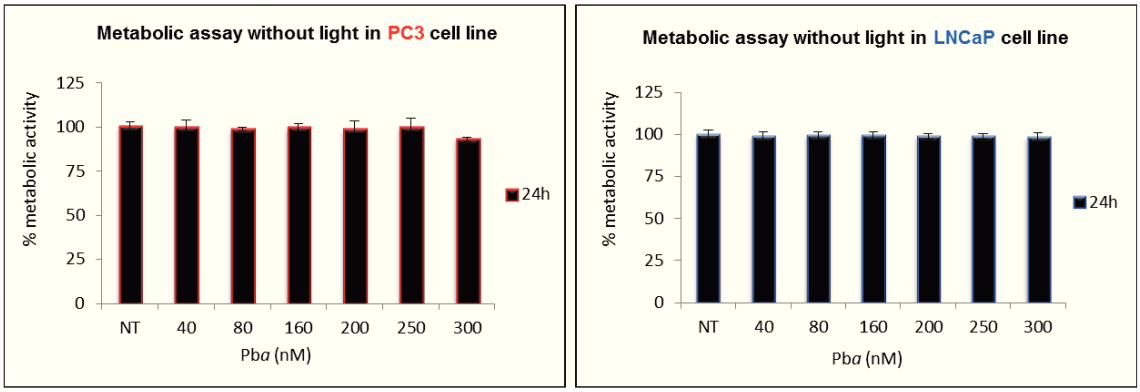

Figure 2. Metabolic assay in the dark*. PC3 and LNCaP cells, plated at density of 5×10^{3}cells/well in a 96-well plate, were treated with different doses of Pba. 24h after treatment the cells were analyzed by resazurin assay. The values "% Metabolic activity" are defined by T/C x 100, where T and C are the fluorescence of treated and not treated cells, respectively. The values are the mean±SD of three independent experiments. The x-axis report the (nM) concentration of Pba*

4.2 Nitric oxide induction after Pba/PDT treatment

In previous studies we highlighted, in B78H1 murine amelanotic melanoma cells, the role of nitric oxide in Pb*a*/PDT (Rapozzi V et al.2013). This molecule, indeed, has a dual effect according to its concentration: generated at high rates it is cytotoxic, at low rates it has a cytoprotective role. At the first, we measured the NO levels in both photostressed PC3

and LNCaP cells. NO in the cells is producted by the nitric oxide synthase (NOS) enzymes so, we measured the protein levels of inducible NOS (iNOS) after Pb*a*/PDT treatment. The Western blot analysis (Figure 3A), performed 16h after Pb*a*/PDT, showed a dose-dependent increase of iNOS protein amount. We measured also the NO levels using a fluorophore (DAF-FM). After cellular uptake, DAF-FM is hydrolyzed to DAF that can be nitrosated by NO by-products to yield a fluorescent compound detected by FACS. Figure 3B shows the fluorescence intensity in PC3 and LNCaP cells after Pb*a*/PDT treatment. The fluorescence signal, which indirectly represents NO-byproducts, is increased in a concentration-dependent manner in both cell lines. These data confirmed the NO induction after PDT and are in agreement with other studies (Gupta et al. 1998; Bhowmick R et al. 2009; Bhowmick et al. 2013).

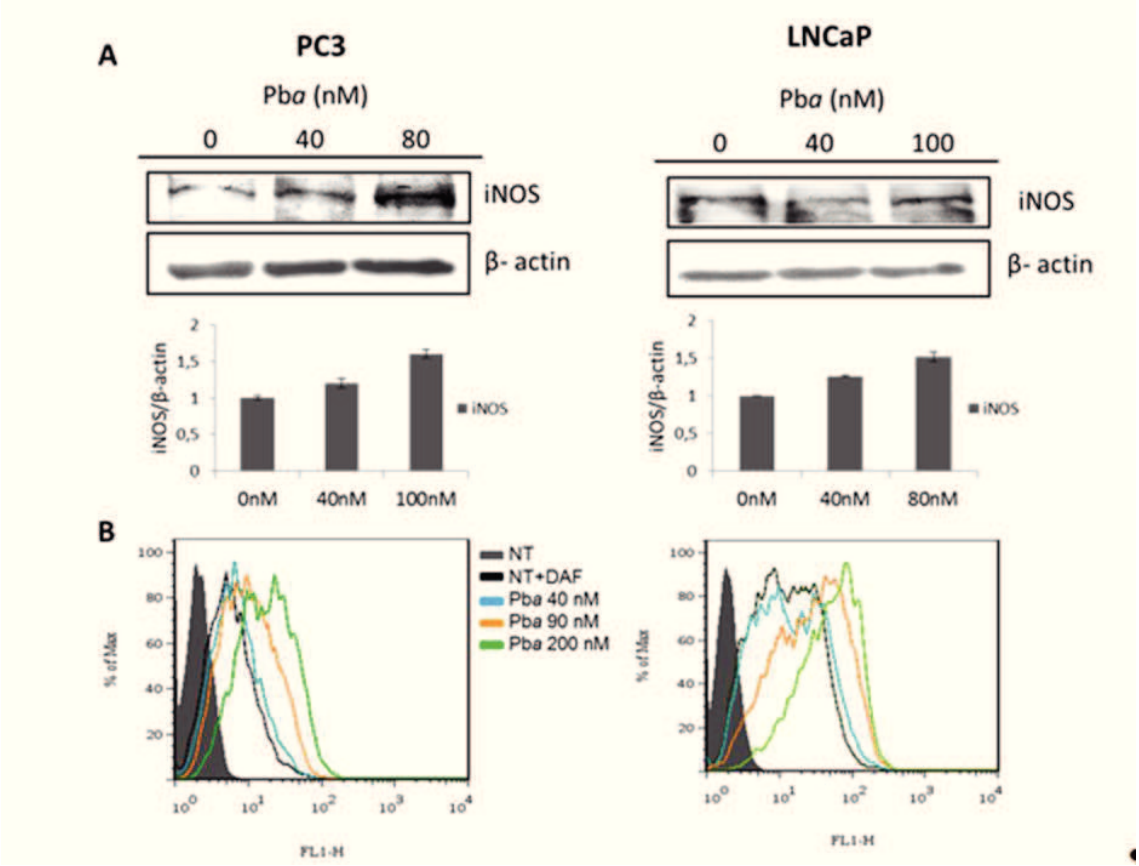

Figure 3. Determination of NO levels induced by Pba/PDT treatment in PC3 and LNCaP cells. ***A.*** *Expression of iNOS protein level by immunoblot analysis. The PC3 and LNCaP cells were treated with different concentrations of Pba (0, 40, 80 nM). iNOS band intensity was determined densitometrically, normalized to β-actin and not treated cells (0 nM) for each sample. Protein lysates were analyzed 16h after irradiation* ***B****.*

*The graphs report the mean fluorescence of NO/byproducts after Pb*a*/PDT treatments in both cell lines. The values were obtained by the DAF reaction and measured by FACS.*

4.3 Effect of Pba/PDT treatment in the NF-κB /YY1/RKIP loop

Several studies have reported that the cellular response to PDT involves the NF-κB pathway (Matroule JY et al. 2006; Rapozzi V et al 2011). It has been demonstrated that after a non-optimal PDT treatment, exists a mechanism relating to cell recurrence. This process involves the stimulation of NF-κB pathways induced by ROS (Matroule JY et al. 2006) and NO (scheme 1) (Rapozzi V et al. 2011). Furthermore, It has been shown that through NF-κB stimulation, NO is able to modulate downstream genes such as the pro-survival and pro-metastatic genes, YY1 and Snail. Moreover, it has been demonstrated that these genes are able to modulate the pro-apoptotic and metastasis suppressor gene product Raf-1 kinases inhibitor protein (RKIP). The activated RKIP is able to induce cell growth arrest acting both on Raf-1/MEK/ERK (Deiss K et al. 2012) and on NF-κB survival pathways (Bonavida B et al.2011). The modulation of NF-κB by RKIP, includes this protein in a dysregulated loop NF-κB /YY1/Snail/RKIP that is involved in cell survival and metastatic process. The western blot analysis, reported in Figure 4, showed that a high-dose of Pb*a*/PDT treatment, reduced NF-κB and YY1 protein levels and consequently, it increased the levels of RKIP protein, in both cell lines (Figure 4A and B). On the other hand, low NO rates induced by a low-dose of Pb*a*/PDT treatment reduced RKIP levels, leading to cell growth. This data can, in part, explain the cell recurrence observed in the metabolic assay 48h after Pb*a*/PDT in both PC3 and LNCaP cell lines (Figure 2). Akt is one of the activators of NF-κB via phosphorylation-activation of IKK (Bhowmick R et al. 2013) and since it can be indirectly modulated by NF-κB through Snail/PTEN (Scheme1) (Lin K et al. 2010), we measured its protein levels after Pb*a*/PDT treatment. Figure 4C showed the reduction of active Akt (P-Akt) after a high dose of Pb*a*/PDT treatment in PC3 cells. On the whole, these findings confirmed the importance of nitric oxide induced by Pb*a*/PDT treatment and that high NO levels can induce cell growth arrest, inhibiting the NF-κB/YY1/RKIP loop; moreover, they suggested that when present in low rates, NO plays a cytoprotective role.

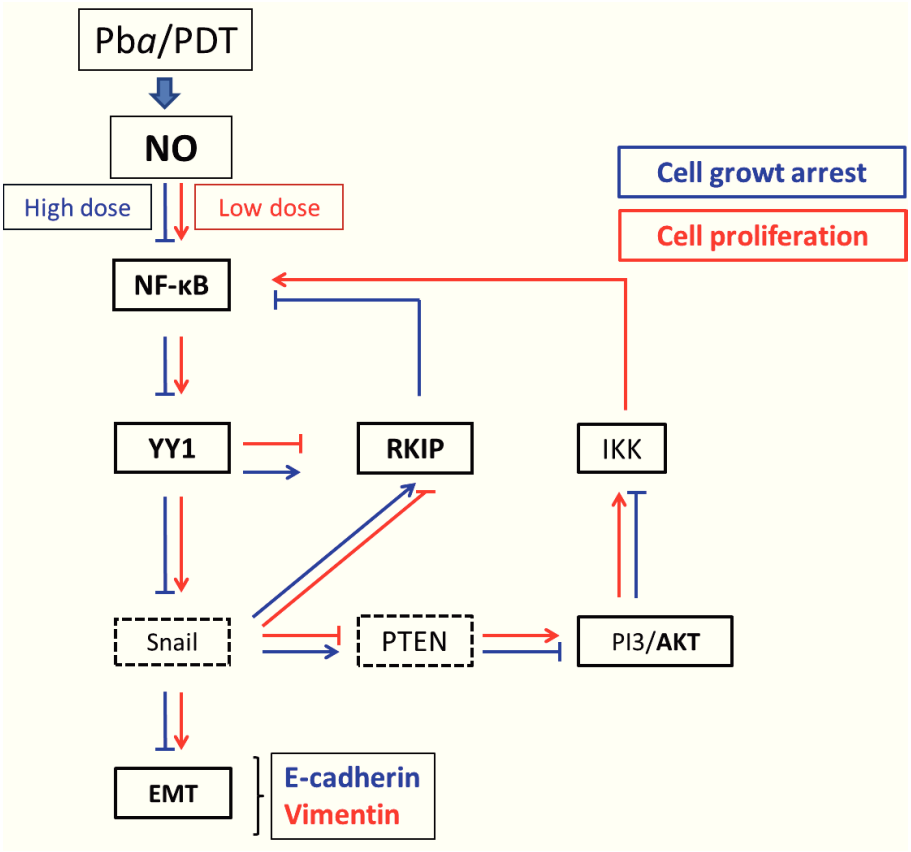

Scheme 1. Role of NO induced by Pba/PDT treatment on the NF-κB /YY1/RKIP loop and in the modulation of pro-survival pathways and on EMT. *Pba/PDT, in dependence by the dose (low in red and high in blue), modulates the NF-κB expression. NF-κB regulates downstream genes YY1 and Snail, that are strictly correlated. Both YY1 and Snail modulate the expression of pro-apoptotic RKIP. The inhibition of RKIP results in the minimal inhibition of NF-κB and activation of YY1 and Snail. The activation of YY1 and Snail induce the activation of pro-survival pathways and EMT. Likewise Snail modulates the metastasis suppressor phosphate and tensin homologue (PTEN). The suppression of PTEN results in the maintenance of the PI3/Akt activated pathway that cross-talks with the NF-κB pathway. These dysregulated gene products in the circuit result in the induction of cell survival and of EMT (Bonavida B t al. 2011)*

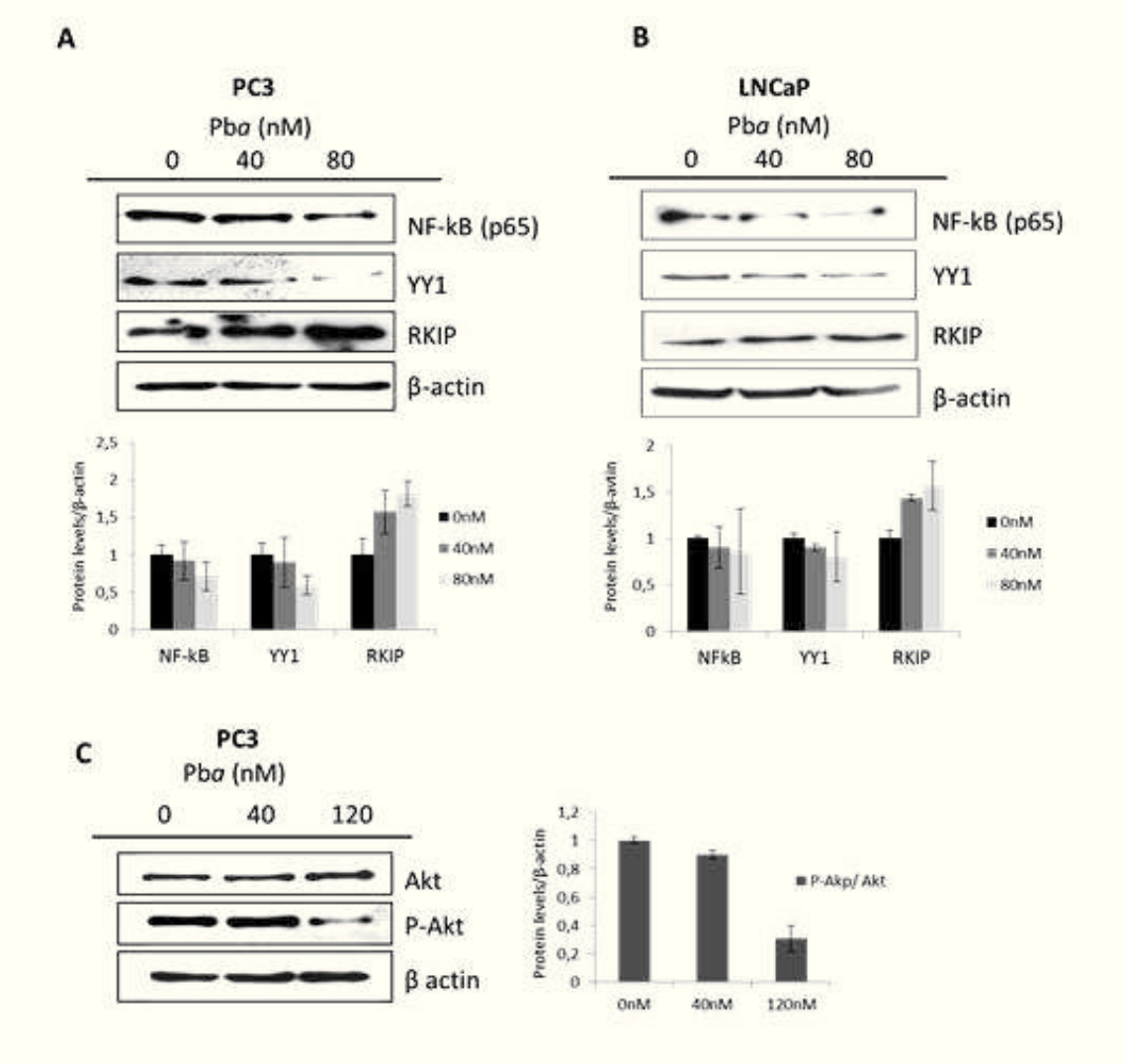

Figure 4. Effect of Pba/PDT treatment on the NF-κB /YY1/RKIP loop*. Western blot analysis of gene products of the NF-κB /YY1/RKIP in PC3 cells (A); LNCaP cells(B) and gene product pAKT/AKT in PC3 cells (C). The cells were treated with increasing doses of Pba. 0 represents the not treated cells. The protein lysates were analyzed 24h after irradiation.*

4.4 Effect of Pba/PDT treatment on Epithelial to Mesenchymal Transition

EMT is a multi-step phenomenon whereby epithelial cells lose their characteristics and acquire a more motile mesenchymal phenotype (Sánchez-Tilló E et al. 2012). This phenomenon is tightly correlated with metastasis development, indeed through it the cell loses the capability to adhere to basal membrane. One of the more important proteins involved in cell adhesion is E-cadherin. Down-regulation of E-cadherin is a critical initial

step in EMT, because of the disruption of adherent junctions that mediate cell-cell adhesion. The loss of E-cadherin can be the result of the induction of Snail, that acts directly on its modulation (Julien S et al. 2007), or through the activation of NF-κB/YY1/RKIP loop (Bonavida B et al. 2011). Western blot analysis, in PC3 cell line, showed that the high dose of Pb*a*/PDT treatment induced an increase of E-cadherin expression and a reduction of the mesenchymal protein vimentin expression (Figure 5). These findings suggest that the high level of NO induced by high dose of Pb*a*/PDT, through the NF-κB /YY1/RKIP loop inhibition, is able to inhibit EMT.

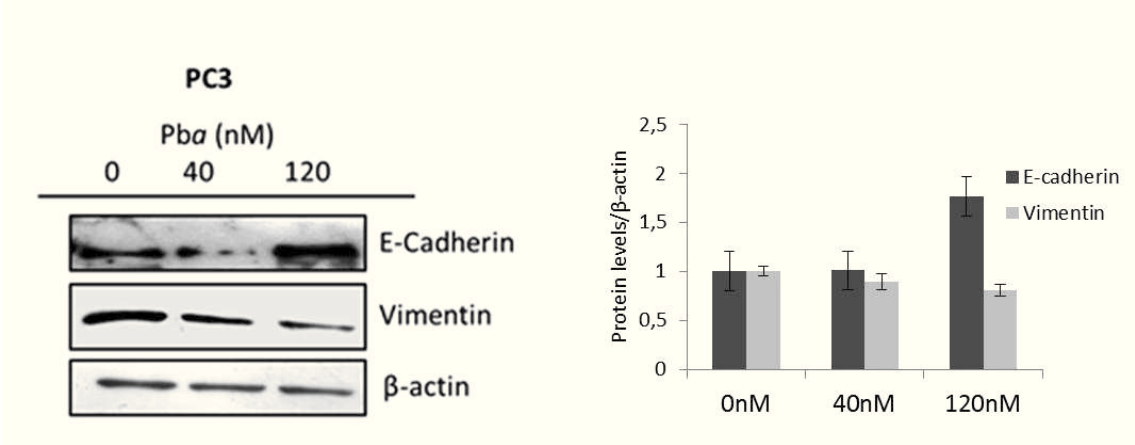

Figure 5. Effect of Pba/PDT treatment on epithelial to mesenchymal transition in PC3 cell line. *Western blot analysis of epithelial E-cadherin and of mesenchymal vimentin. The cells were treated with increasing doses of Pba. 0 represents the not treated cells. The toltal protein lysates were analyzed 24h after irradiation.*

4.5 Effect of a repeated low-dose Pba/PDT treatment in PC3 cell line

Since that the high dose of Pb*a*/PDT treatment induces the completely arrest of cell growth and EMT inhibition, we wanted to evaluate if a pro-survival mechanism can be activated by low-dose of Pb*a*/PDT treatment. In particular, we evaluated what happens after a repeated low-dose Pb*a*/PDT treatment. We focused our attention on PC3 because it is the metastatic cell line. As a low-dose Pb*a*/PDT we chose a treatment with 40 nM Pb*a*, which induced 5-10% of cell growth inhibition 24h after light irradiation and recovery after 48h. We envisaged two possibilities: the repeated treatment might result in a cumulative effect, causing a tumor growth arrest; alternatively, the repeated treatment

could cause a stimulation of cell proliferation and so a sort of resistance to treatment, linked to the development of a more aggressive population (Milla LN et al. 2011). To perform this experiment we decided to change the treatment scheme using the following method: 2 days after seeding, the PC3 cells were treated with Pb*a*/PDT. After an additional 2 days, the cells were harvested, reseeded and treated as above. The treatment lasted ~ 5 weeks. To follow the cell changes throughout the experiment, the cells were examined after the fourth (IV) and eighth (VIII) treatment (Scheme 2). The cells were healthy and had a normal cell cycle profile as determined by FACS analysis (Figure 6)

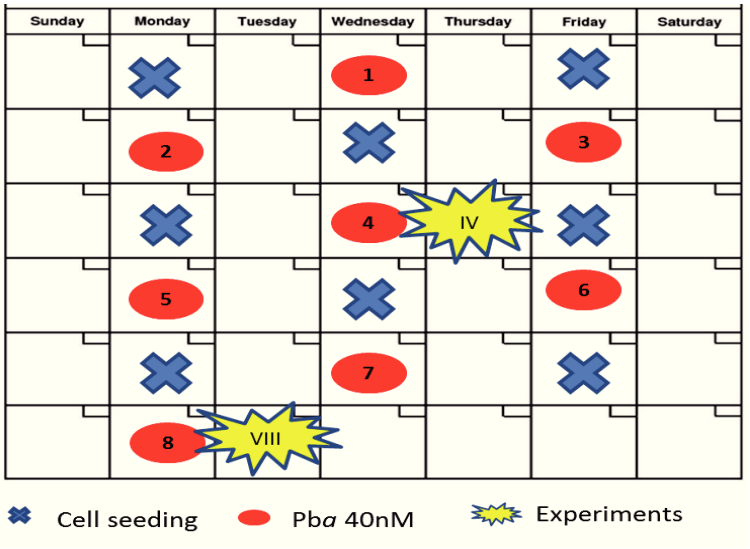

Scheme 2. Schematic panel of repeated treatment. *PC3 cells were seeded at day 0 at a density of 5 x 10* ^{5} *cells ina 6-well plate, after 48h they were submitted to PDT treatment (3h with a low-dose of Pba/PDT (40 nM) and then light irradiated). After n additional 48 h the cells were harvested and seeded as above. This procedure was repeated four or eight times, when the cells were harvested and processed for different experiments.*

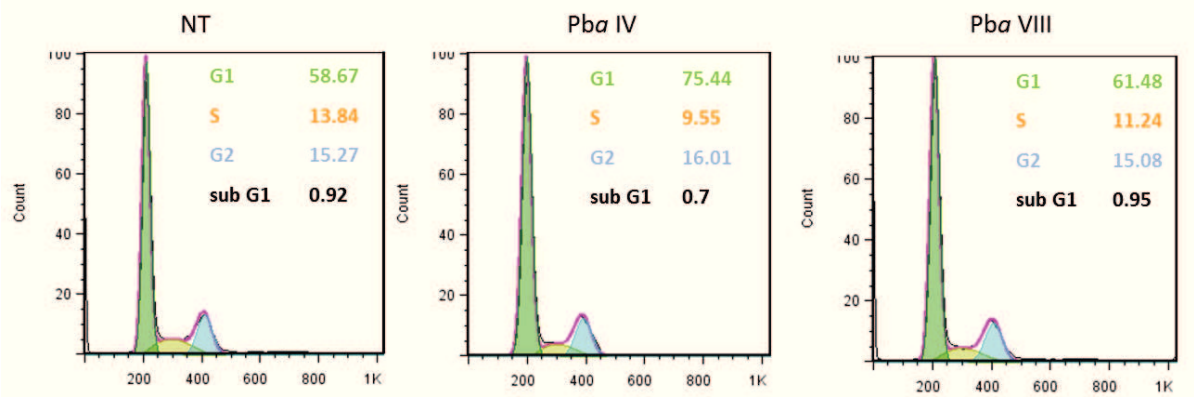

Figure 6. ***Effect of a repeated low-dose Pba/PDT treatment on cell cycle progression****. Cell cycle phase distribution. Graphs show the frequencies of the, G_1, S, G_2/M and sub-G_1 phases after the fourth (Pba IV) and eighth (Pba VIII) Pba/PDT treatment.*

To investigate if a repeated low-dose Pb*a*/PDT treatment stimulated cell proliferation, we performed a clonogenic assay as described in methods. PC3 cells were harvested after the IV and the VIII low-dose Pb*a*/PDT treatment and seeded (500 cells) in a 30 mm Petri dish. After 18 days, the colonies were formed. It was evident that by proceeding with the treatment, the number and size of the colonies increased (Figure 7). This finding clearly showed the stimulation of cell proliferation after a repeated low-dose Pb*a*/PDT treatment. This result indicated that a repeated low-dose Pb*a*/PDT treatment didn't result in a cumulative effect leading to tumor growth arrest.

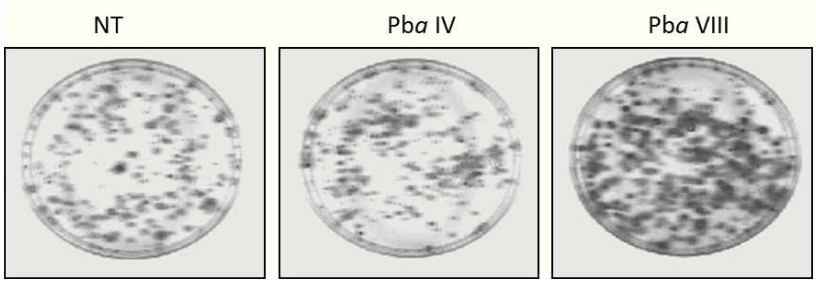

Figure 7. Clonogenic assay on PC3 cells after repeated low-dose Pba/PDT treatment. *After the IV and VIII Pba/PDT treatment, 500 cells from each group were seeded in 60 mm petri dishes. After 18 days the colonies were formed, fixed and stained with 2.5 % methylene blue in 50% ethanol. The images were obtained with Gel Doc 2000 Bio-Rad. The experiment has been performed in triplicate.*

4.6 A repeated low-dose Pba/PDT treatment induces EMT activation through NF-κB /YY1/RKIP loop

We compared the protein lysates obtained after the IV and VIII treatment in order to follow the proceeding of the experiment. The western blot analysis in Figure 8 showed the expression of the gene products involved in the loop during the repeated treatment. There was an increase of the pro-survival proteins NF-κB (p65) and YY1. The enhances of both factors supported a pro-survival response. In agreement with these findings we observed a decrease of the expression of the pro-apoptotic gene product RKIP.

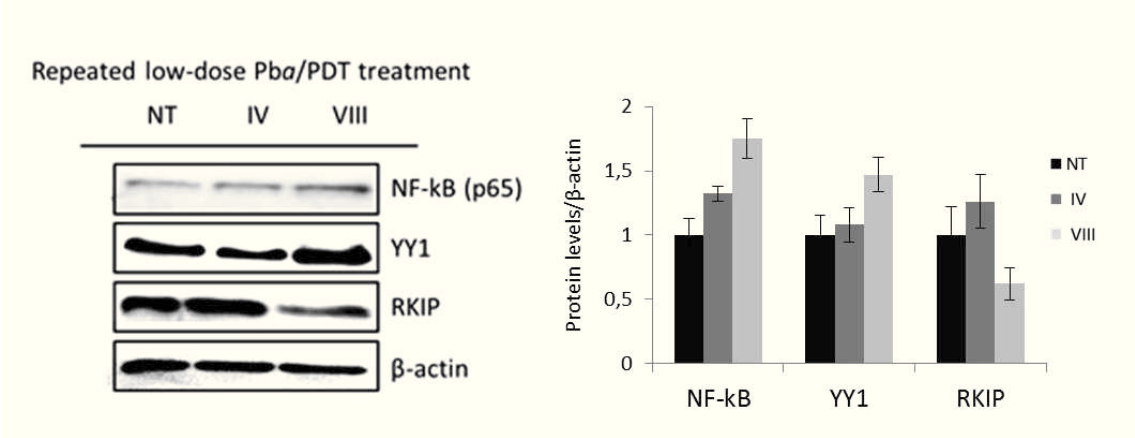

Figure 8. Effect of a repeated low-dose Pba/PDT treatment on NF-κB /YY1/RKIP loop. *Western blot analysis for NF-κB, YY1, RKIP. PC3 cells were: NT, not treated; IV, treated with 40nM Pba/PDT for 4 times ; VIII, treated with 40nM Pba/PDT for 8 times. Total protein lysates were recovered 24h after the last treatment.*

As the loss of RKIP function has been associated with metastasis in an increasing number of solid tumors (Escara-Wilke J et al. 2012), this result suggested that a repeated low-dose Pb*a*/PDT treatment in PC3 cells activated the NF-κB /YY1/RKIP loop and induced the stimulation of cell proliferation and EMT activation. A critical feature of EMT is the downregulation of E-cadherin, a protein involved in cell adhesion. Western blot analysis showed a decrease of the E-cadherin adhesion protein and an increase of the mesenchymal protein vimentin, leading to the loss of epithelial characteristics that coincides with the acquisition of motility and invasiveness (Figure 9) (Van Der Pluijin G 2011).

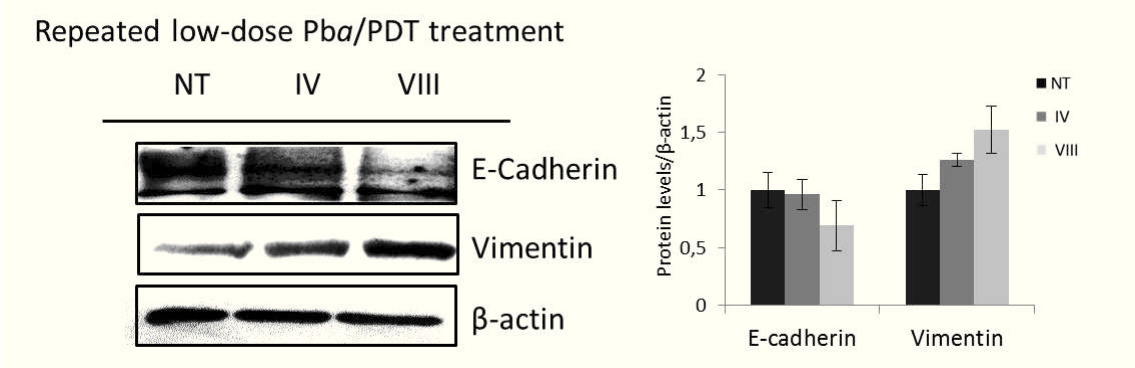

Figure 9. EMT induction after a repeated low-dose Pba/PDT treatment in PC3 cell line. *Western blot analysis of E-cadherin and vimentin. PC3 cells were NT, not treated; IV, treated with 40nM Pba for 4 times and VIII, treated with 40nM Pba for 8 times.*

Moreover, we observed an increase of phosphorylated Akt/Akt (p-Akt/Akt) (Figure 10). The increase of both p-Akt and NF-κB suggested that active Akt could induce NF-κB and consequently EMT, in keeping with the previous study of Julien et al. (Julien S et al. 2007).

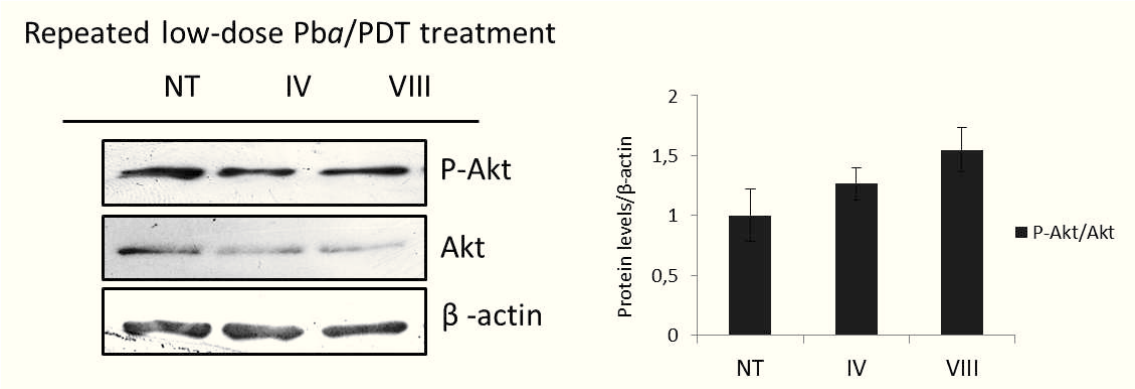

Figure 10. Activation of EMT and cell survival through activation of Akt pathway *Western blot analysis of total Akt (Akt) and active Akt (P-Akt). PC3 cells were NT, not treated; IV, treated with 40nM Pba for 4 times and VIII, treated with 40nM Pba for 8 times.*

4.7 A repeated low-dose Pba/PDT treatment induces the formation of a more aggressive population.

We have demonstrated that a repeated low-dose Pb*a*/PDT treatment, through the activation of NF-κB YY1/RKIP loop, stimulated EMT activation. Several studies showed that EMT program can promote cells self-renewal capability and the therapy resistance (Polyak K et al. 2009; Van Der Pluijin G 2011; Zhou W et al. 2014). According to these

considerations we wanted to understand if a repeated low-dose Pb*a*/PDT treatment can cause the increase of a more aggressive population. To evaluate the presence of this population we used two typical surface markers for cancer stem cells (Salvatori L et al. 2012): CD44 and CD24. In collaboration with Dr Daniela Cesselli (DMSB, University of Udine, Italy) we performed a cell sorting of PC3 cells after a repeted low-dose Pb*a*/PDT treatment and the Figure 11 reported the percentage of $CD44^{+}CD24^{+}$ population . It is evident that after this type of treatment the more aggressive population was increased.

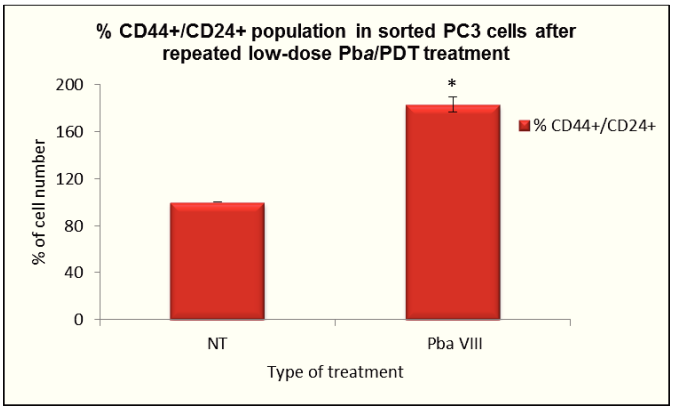

Figure 11. Increase of $CD44^{+}CD24^{+}$ population after a repeated low-dose Pba/PDT treatment in PC3 cell. *After a repeated Pba/PDT treatment PC3 cells were sorted and an increase of $CD44^{+}CD24^{+}$ population was detected. The histogram represent the percentage of positive $CD44^{+}CD24^{+}$ cells expressed as T/C x 100. T and C are the treated and not treated cells. The values are the mean ± SD of three independent experiments. A standard t-test versus control was performed ($P < 0.05$)*

Considering that most of PC3 cell are normally positive for CD44, and that CD44 is used to isolate CSC cells (Tai S et al. 2011), we compared two population: $CD44^{+}CD24^{+}$ and CD44+/CD24-. In order to confirm that the $CD44^{+}CD24^{+}$ was effectively the more aggressive population, we tested its capability to form tumorspheres (Gupta PB et al. 2009). We plated the cells in a particular non-adherent plate. In Figure 12, is possible to observe that $CD44^{+}CD24^{-}$ cells, 1 week after seeding, were died, while $CD44^{+}CD24^{+}$ population were aggregated to form tumorspheres, a peculiarity of CSC (Gupta PB et al. 2009; Pfeiffer MJ et al. 2010).

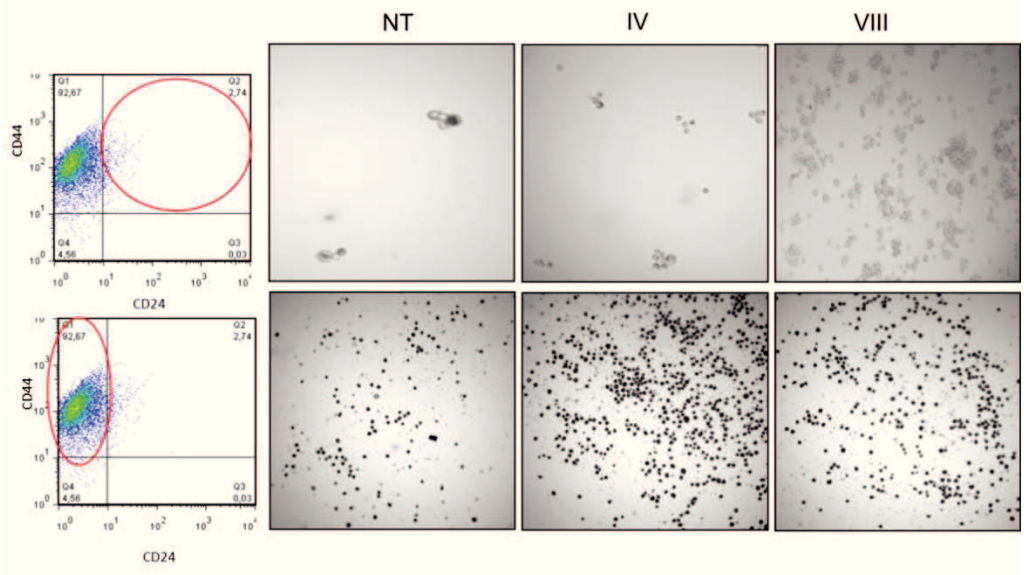

Figure 12. Tumorspheres formation. *After a repeated low-dose Pba/PDT treatment the PC3 cells were sorted and two population were isolated (CD44$^+$24$^+$ and CD44$^+$ CD24$^-$). The cell were again plated in a cell-repell 6-well plate and after 1 week the tumorspheres were visible only in the plate with CD44$^+$CD24$^+$ cells. Pictures were taken by epiluminescent microscope.*

Cancer stem cells are also characterized by an increased drug resistance (Pfeiffer MJ et al. 2010). It has been demonstrated that CSCs are more resistant to drug therapy than normal cells and for this reason this population could be responsible for cancer recurrence (Li Y et al. 2012). An important stemness marker, that is also correlated to the capability of CSC to escape from cancer therapy, is ABCG2 (Kim M et al. 2002; Zhang L et al. 2012). In our experiments, the CD44$^+$CD24$^+$ population showed an increase of ABCG2 expression confirming the stemness features of this population (Figure 13 A and B).

ABCG2 is an efflux pump involved in toxics elimination (Selbo PK et al. 2012) and it is tightly correlated to resistance to photodynamic therapy (Casas A et al. 2011; Morgan J et al. 2010) because it is involved in the efflux of the most common PSs, including Pb*a* (Selbo PK et al. 2012). The repeated low-dose Pb*a*/PDT treatment in PC3 cells induced an increase of ABCG2 expression (Figure 13B) and these cells resulted also more resistant to a single Pb*a*/PDT treatment. The histogram of the metabolic activity in Figure 13C, in fact, showed that after 8 treatments (red column), PC3 cells were more resistant to the single acute Pb*a*/PDT treatment (40nM and 80nM), compared to normal cells (Grey column). All these findings demonstrated that after a repeated low-dose Pb*a*/PDT treatment a more

aggressive population was formed ($CD44^{+}CD24^{+}$). These cells showed an higher expression of ABCG2 than normal cells and they resulted more resistant to Pb*a*/PDT treatment.

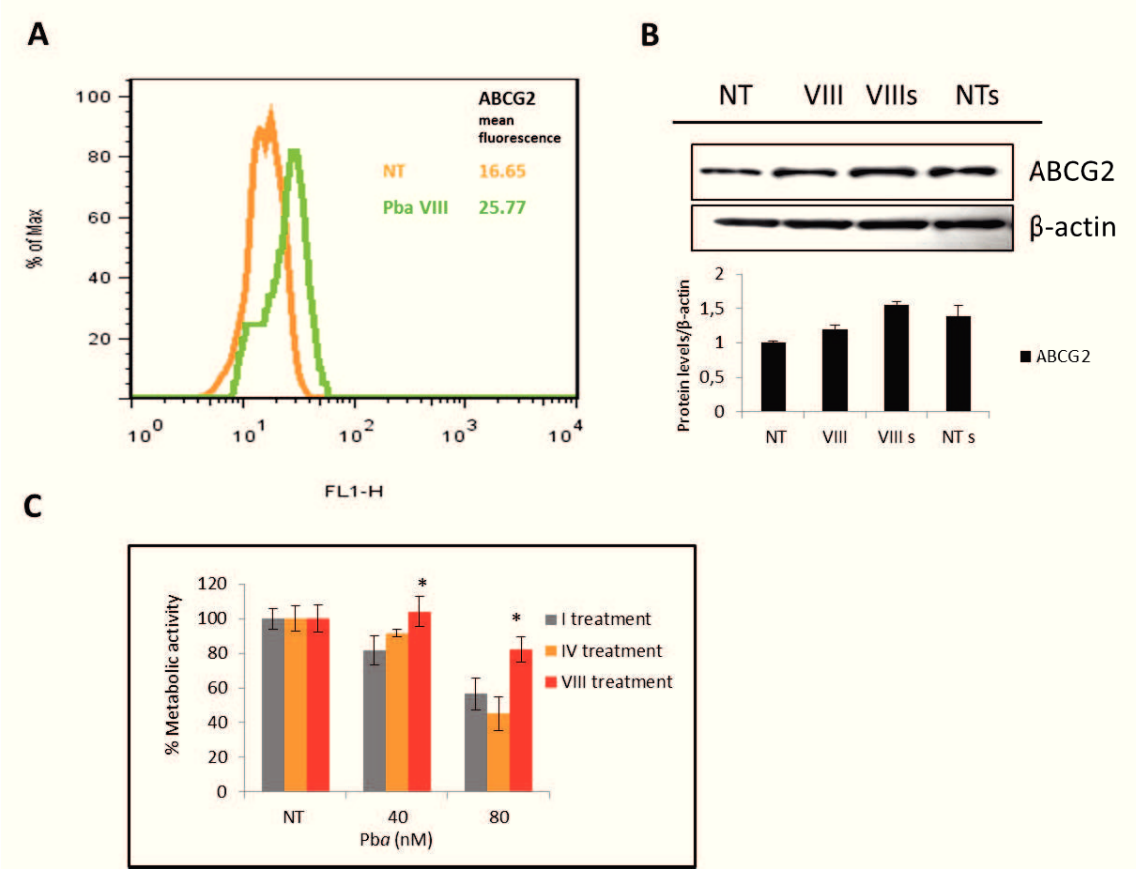

Figure 13.A. FACS analysis of ABCG2 expression *PC3 cells repeatedly treated were incubated with anti-ABCG2 and then incubated with the fluorescent secondary antibody and detected by FACS. The values were expressed as mean fluorescence. An increase of ABCG2 expression in PC3 cells repeatedly treated was detected.* ***B. Western blot analysis of ABCG2 expression.*** *PC3 cells were: NT, not treated; VIII, treated with 40nM Pba for 8 times; VIII s, sorted after 8 Pba/PDT treatments; NT s, sorted and not treated. Total protein lysates were recovered* ***C. Resistance to Pba/PDT treatment in PC3 cells repeatedly treated with a low-dose of Pba/PDT.*** *PC3 cells repeatedly treated four (IV) and eight (VIII) times were again treated with (40 or 80 nM) Pba/PDT. The Histograms represent the values of % metabolic activity A standard t-test versus control was performed ($P < 0.05$)*

4.8 Role of nitric oxide in the response of PC3 cells to a repeated low-dose Pba/PDT treatment

As it already reported, we observed that Pb*a*/PDT treatment in PC3 cells stimulated the expression of iNOS in a dose dependent way (Figure 3). In order to understand the role of NO in the repeated low-dose Pb*a*/PDT treatment, we measured iNOS levels. In Figure 14 the western blot analysis showed a mild increase of iNOS expression and, as a consequence, a mild increase of NO levels that is correlated to induction of prosurvival pathways (Bhowmick R et al. 2013), and to EMT activation (Bonavida B et al. 2011).

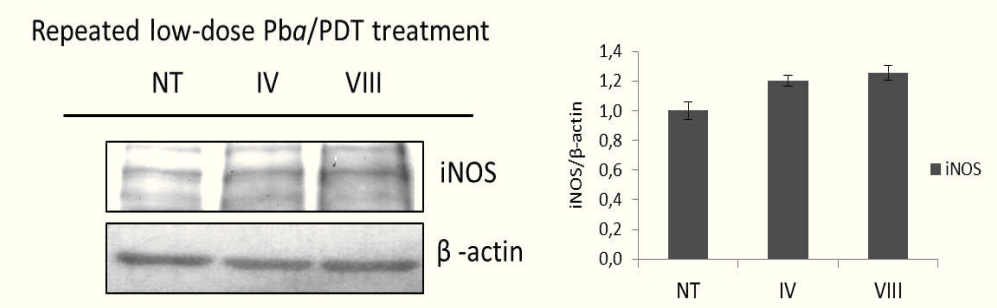

Figure 14. Mild iNOS activation after repeated low-dose Pba/PDT treatment. *Western blot analysis of iNOS protein expression during a repeated low-dose Pba/PDT treatment. The protein lysates were analyzed 16 h after the IV and VIII treatment. iNOS band intensity was determined densitometrically, normalized to β-actin and to not treated cells (NT) for each sample.*

In order to confirm the influence of NO in a repeated low-dose Pb*a*/PDT treatment we used a non-selective iNOS inhibitor L-NAME in combination with Pb*a*/PDT. L-NAME (1mM) was added to the cells 1h before light irradiation (Figure 15A). After the repeated combined L-NAME+Pb*a*/PDT treatment, as shown in the histogram of Figure 15B, a decrease of iNOS expression was found. This finding confirmed that Pb*a*/PDT can up-regulate the NO levels after light activation.

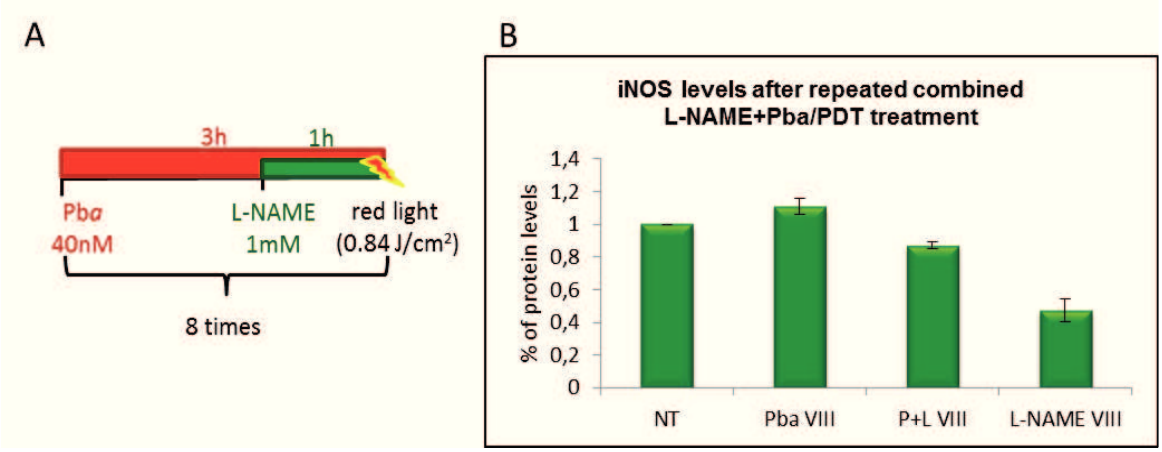

Figure 15.A. Combined treatment scheme. *PC3 cells were treated with 40nM of Pba for 3h in the dark; 1h before irradiation was added 1mM L-NAME. The cells were irradiated with red light at the fluence of 0.84 J/cm^2; this treatment scheme was repeated eight times, after the cell were harvested and used for the experiments.* ***B. Reduction of iNOS induced by L-NAME****. PC3 cells were divided in 4 groups: NT, not treated cells; Pba VIII, cells treated with Pba (40 nM) eight times, P+L VIII, cells treated eight times with a combined repeated treatment L-NAME+Pba/PDT; L VIII, cells treated with L-NAME (1mM) eight times. The protein lysates were analyzed 16 h after the last treatment.*

In order to determinate if NO carries out a cytoprotective role after a repeated low-dose Pb*a*/PDT treatment, we evaluated the following assays: (i) the cell cycle by FACS, ii) the clonogenic capacity, iii) the protein levels of the gene products involved in the NF-κB/YY1/RKIP loop and in EMT and iv) the analysis of the CSC population. The Figure 16A highlighted that PC3 cells repeatedly treated with L-NAME+Pb*a*/PDT, presented a strong reduction in the number of colonies compared with each single treatment; moreover, cell cycle analysis showed an increase of the G2/M and sub-G1 phases, indicating cell growth arrest (Figure 16B) (Di Paola RS 2002).

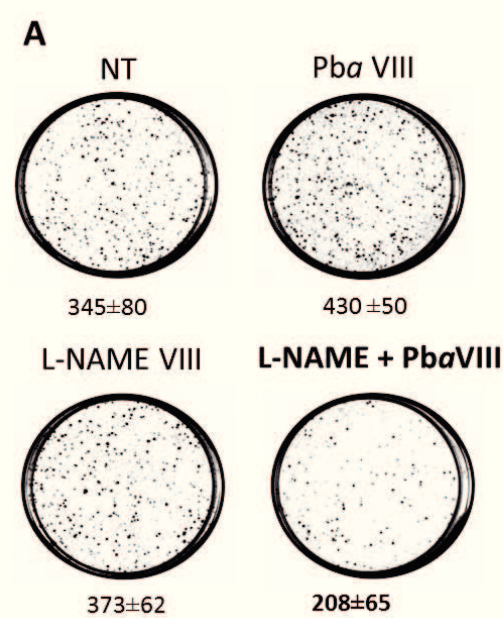

B

Treatment	G1	S	G2/M	SubG1
NT	68.5	7.5	8.2	0.4
Pb*a* VIII	66.29	9.61	7.5	0.5
L-NAME	66.27	8.73	7.9	0.6
L-NAME+Pb*a*	68.98	1.52	**23.35**	**2.32**

Figure.16. Role of NO induced by a repeated low-dose Pba/PDT treatment. A. On colony formation. *PC3 cells were divided in 4 groups: NT, not treated cells; Pba VIII, cells treated eight times with repeated low-dose Pba/PDT treatment; L-NAME VIII, cells treated eight times with 1 mM L-NAME and L-NAME+Pba VIII, cells treated eight times with a combined low-dose Pba/PDT + L-NAME treatment. After the last treatment, 500 cells from each group, were seeded in 60 mm Petri plate. After 18 days the colonies were formed, fixed and stained with 2.5 % methylene blue in 50% ethanol. The images were obtained with Gel Doc 2000 Bio-Rad. The number of colonies (>50 cells) is reported below each plate. The experiment has been performed in triplicate.* ***B. On cell cycle****. The table show occupancy of the, G_1, S_1 G_2/M and sub-G_1phases.*

The repeated combined L-NAME+Pb*a*/PDT treatment decreased the expressions of p-Akt, NF-κB and YY1 and induced a strong expression of RKIP, in comparison with the repeated treatment with Pb*a* alone, suggesting a reduction of cell growth (Figure 17). The inhibition of NF-κB /YY1/RKIP loop is correlated to EMT inhibition. PC3 cells treated repeatedly with L-NAME+Pb*a*/PDT resulted in a high level of E-cadherin expression and a concomitant strong reduction of vimentin and p-AKT, suggesting EMT inhibition (Figure 17).

EMT phenotype is also considered a characteristic of more aggressive population (Singh A et al. 2010). Previously we observed that the repeated low-dose Pb*a*/PDT treatment induced an increase of this more aggressive population (Figure 11-18), but the repeated combined L-NAME+Pb*a*/PDT induced its reduction: Figure 18 shows a decreased amount

of $CD44^{+}CD24^{+}$ population in cells repeatedly treated with L-NAME+Pb*a*/PDT respect to those obtained after a repeated low-dose Pb*a*/PDT treatment. Co-treated PC3 cells showed a percentage similar to the not treated cells.

These findings confirmed the role of NO in PDT and demonstrated that the administration of low-dose Pb*a*/PDT in PC3 cells induced a continuous low level of NO that could activate cell proliferation pathways, EMT and could induce the development of a more aggressive population.

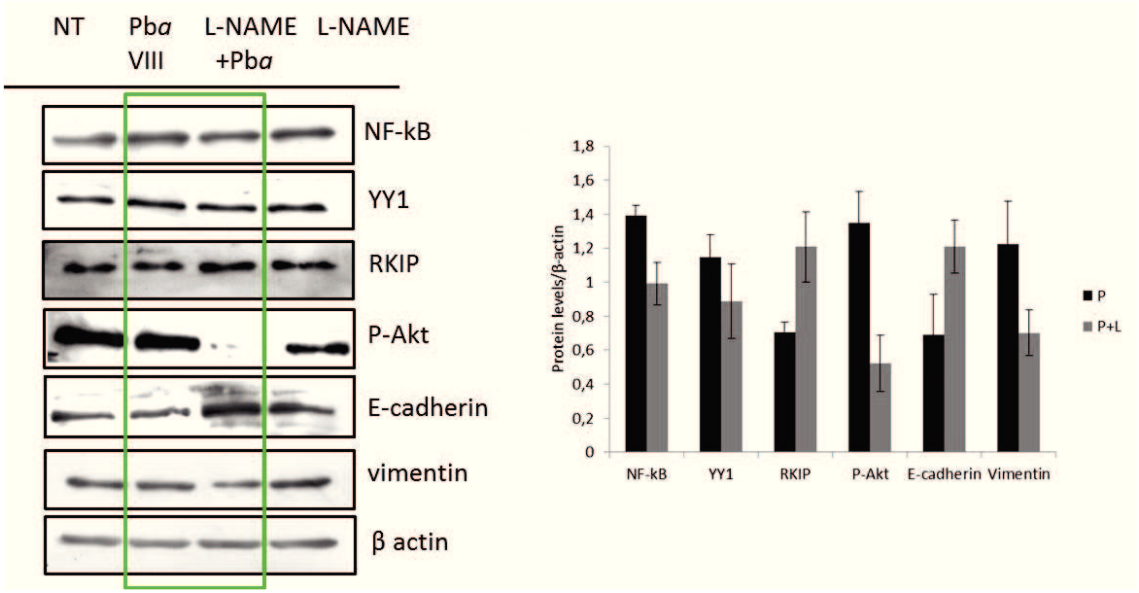

Figure 17. Effect of a repeated combined L-NAME+Pba/PDT treatment on NF-κB YY1/RKIP loop and on EMT. *PC3 cells were treated with a combined repeated low-dose L-NAME (1 mM)+Pba/PDT treatment. The protein lysates were analyzed 24 h after the last treatment.*

	% of more aggressive population CD44+/CD24+
NT	4%
Pb*a* VIII	11%
Pb*a*+L-NAME VIII	**5%**
L-NAME VIII	5%

Figure 18 Effect of a repeated combined L-NAME+Pba/PDT treatment on the development of the more aggressive population. *Percentage of $CD44^{+}CD24^{+}$ cell population, analyzed by FACS. PC3 cells were divided*

in 4 groups: NT, not treated cells; Pba VIII, cells treated eight times with repeated low-dose Pba/PDT treatment; L-NAME VIII, cells treated eight times with 1 mM L-NAME and L-NAME+Pba VIII, cells treated eight times with a combined low-dose L-NAME+Pba/PDT treatment.

4.9 Involvement of the structure of the PS in the resistance to photodynamic therapy

The structure of the PS is believed to be a key point in the development of resistance, being probably related to its subcellular localization and to the possibility of PS to be a substrate for efflux pumps, involved in multy-drug resistance (Casas A et al. 2011). In this field an important role is conferred to ABCG2; as mentioned before in relation of the structure, several PSs have been reported to be substrates of ABCG2, included Pb*a* (Selbo PK et al. 2012). Since we have demonstrated that a repeated low-dose Pb*a*/PDT treatment induced the development of a more aggressive and resistant population and an increase of ABCG2 efflux pump (Figure 13 A), we wanted to demonstrate the importance of the structure of the PS, comparing two PSs: Pb*a*, substrate for ABCG2 and meso-tetra(hydroxyphenil)porphyrin (m-THPP), not substrate for ABCG2 (Selbo PK et al. 2012).

In order to compare the effect obtained with Pb*a*/PDT in PC3 cells, we performed a repeated treatment with a low-dose of m-THPP. After the repeated low-dose m-THPP/PDT treatment, we evaluated: i) the clonogenic capability, ii) the EMT induction, iii) the development of a more aggressive population and iv) the resistance to the treatment.

A repeated low-dose m-THPP/PDT treatment induced the arrest of cell cycle and a reduction of the colony formation.

For the repeated low-dose m-THPP/PDT treatment we used the dose of 5nM that induced a 5-10% of cell growth arrest at 24h but induced a cell recurrence at 48h. This behavior is comparable to that obtained with the dose of 40nM Pb*a.* After eight m-THPP/PDT treatments, the cell cycle analysis showed a decrease of G1 and an increase of sub-G1, correlated with apoptosis activation (Di Paola RS 2002)(Figure 19B). In agreement with this result, the clonogenic assay showed a decrease of the number of the colonies after a

repeated low-dose m-THPP/PDT treatment (Figure 19A). These data suggested that m-THPP, not substrate for ABCG2, is more effective in terms of phototoxicity respect to Pb*a*/PDT.

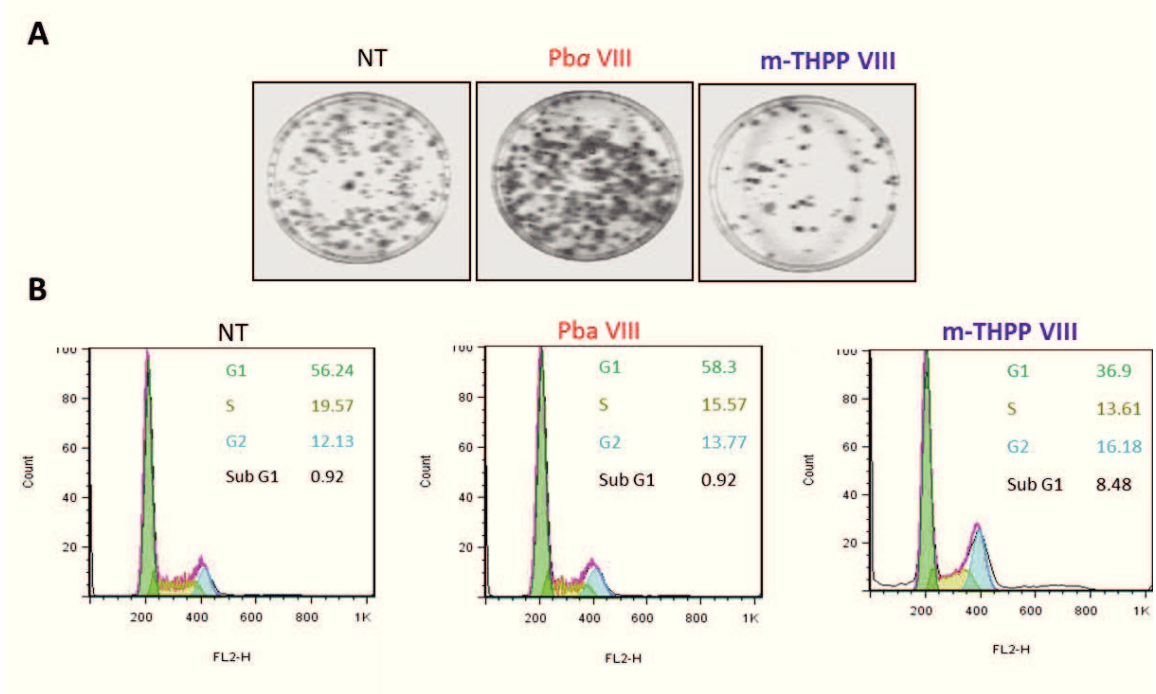

Figure 19. Different effects obtained in PC3 cells repeatedly treated with a low-dose of Pba/PDT or m-THPP/PDT. A. On clonogenic assay*. After the last treatment, 500 cells from each group, were seeded in a 60 mm petri plate. After 18 days the colonies were formed, fixed and stained with 2.5 % methylene blue in 50% ethanol. The images were obtained with Gel Doc 2000 Bio-Rad.* ***B. On cell cycle.*** *After the last treatment PC3 cells were divided in three groups: NT, not treated; Pba VIII, treated eight times with a low-dose of Pba/PDT and m-THPP VIII, treated eight times with a low-dose of m-THPP. The table in each graph show occupancy of G_1, S, G_2/M and the sub-G_1,phases.*

A repeated low-dose m-THPP/PDT treatment induced arrest of cell proliferation and EMT inhibition.

In addition to clonogenic assay and FACS analysis we evaluated the expression of the metastatic suppressor RKIP gene, that resulted in an increase expression after low-dose m-THPP/PDT treatment. Considering that a decrease of RKIP is correlated with EMT induction, the repeated low-dose m-THPP/PDT treatment showed a EMT inhibition (an increase of E-cadherin and a reduction of vimentin) (Figure 20).

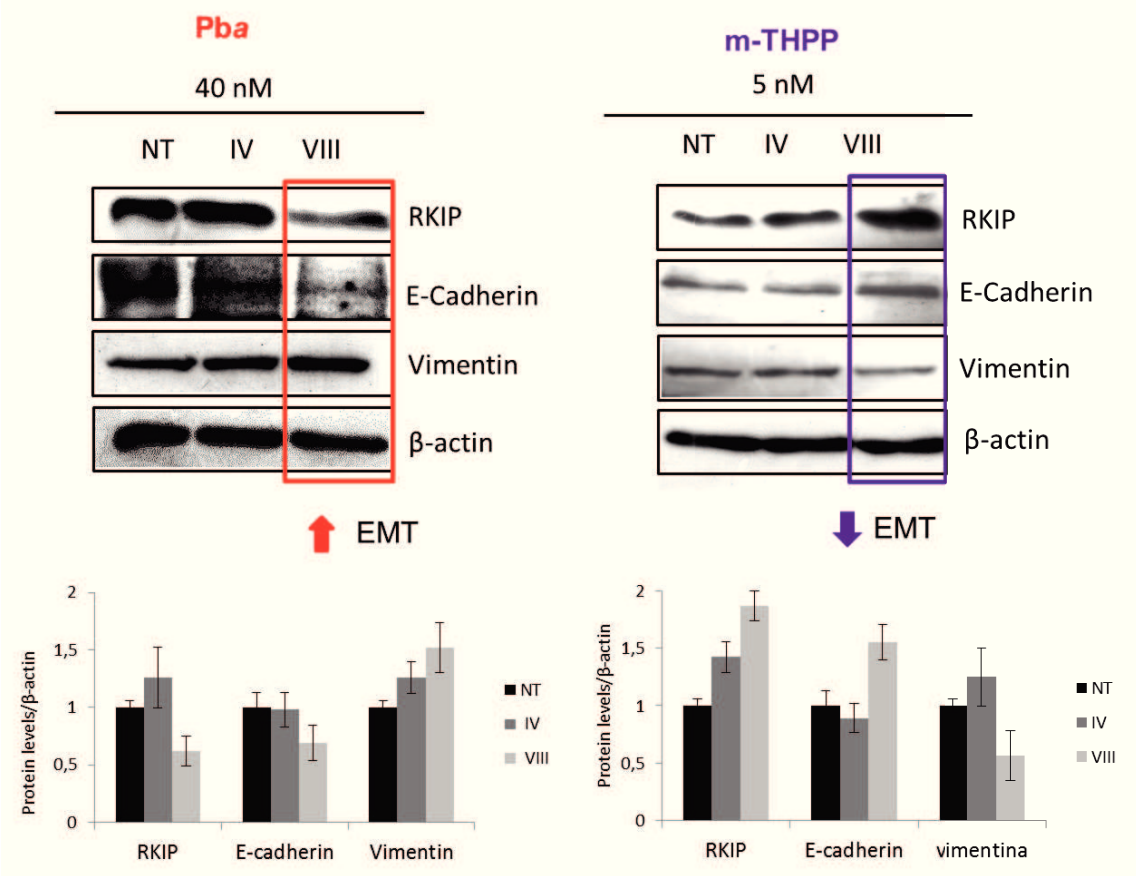

Figure 20. Different effects obtained in PC3 cells repeatedly treated with a low-dose of Pba/PDT or a low-dose of m-THPP/PDT in EMT activation. *Western blot analysis for RKIP,E-cadherin, vimentin. NT, PC3 cells not treated; IV, PC3 cells treated with Pba or m-THPP four times and VIII,PC3 cells treated for 8 times with Pba or m-THPP. Total protein lysates were recovered 24h after the last treatment.*

A repeated low-dose m-THPP/PDT treatment does not increase the more aggressive population

The percentage of PC3 sub-population $CD44^{+}CD24^{+}$, after a repeated low-dose m-THPP/PDT treatment showed no changes in comparison to not treated PC3 cells (Figure 21).

	NT	Pba VIII	m-THPP VIII
CD44+/CD24+	3.29%	6.13%	3.40%

Figure 21. Different effects obtained in PC3 cells repeatedly treated with a low-dose of Pba/PDT or a low-dose m-THPP/PDT in the development of the $CD44^{+}CD24^{+}$ population. *PC3 cells were repeatedly treated*

with low-dose of Pba/PDT (Pba VIII) and with low-dose of m-THPP (m-THPP VII) eight times. The percentage of $CD44^{+}CD24^{+}$ were analyzed by FACS and reported in the table.

A repeated low-dose m-THPP/PDT treatment does not induce resistance to PDT

The histogram in Figure 22, showed that after a repeated low-dose m-THPP/PDT treatment, the sensitivity of PC3 cells to a new acute m-THPP/PDT treatment (purple column) is the same of that observed in parental PC3 cells (grey column). This result suggested the importance of the PS structure in the development of resistance to PDT treatment.

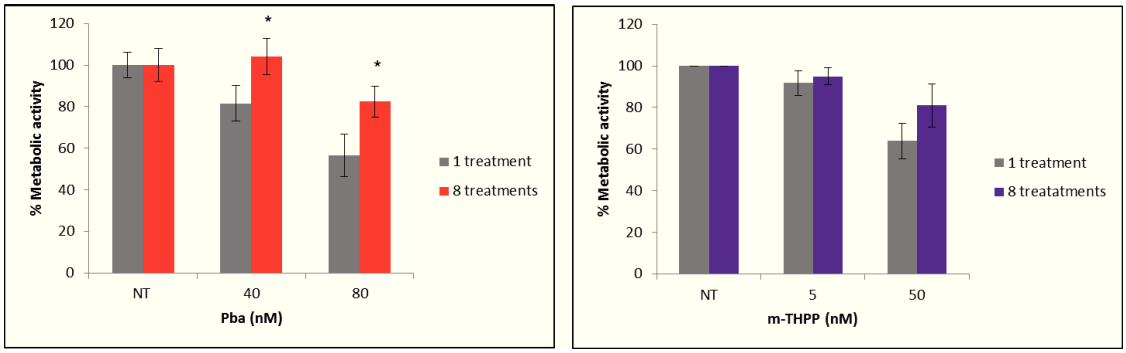

Figure 22 Different effects obtained in PC3 cells repeatedly treated with a low-dose of Pba/PDT or a low-dose of m-THPP/PDT in resistance. *PC3 cells obtained after eight treatments with a low-dose of Pba (red) or m-THPP (purple) were treated with Pba/PDT (40nM and 80nM) and with m-THPP (5nM and 50nM). The Histograms represent the values of % metabolic activity. A standard t-test versus control was performed ($P < 0.05$)*

4.10 Role of nitric oxide in improving the effectiveness of PDT

To increase the efficacy of PDT, we have proposed a combined treatment with an NO donor. We used in conjunction with Pb*a*, DETANONOate (DETA/NO), a molecule that spontaneously releases in the cytoplasm 2 mol of NO per mole of compound (Devis KM et al. 2001). We found, indeed, that the combination of the PS with an NO donor resulted in a significant modulation of the NF-κB /YY1/Snail/RKIP loop towards the expression of the pro-apoptotic RKIP and the inhibition of anti-apoptotic NF-κB and Snail gene products. The clinical relevance of increasing the RKIP expression by NO correlated with a favorable

clinical outcome resulting in tumor regression and in inhibition of metastatic spread (Huerta-Yepez S .et al. 2011).

The dual treatment with DETA/NO and mPEG-Pb*a*/PDT (Rapozzi V et al. 2011) was administered in C57BL/6 mice inoculated s.c. with the B78-H1 murine amelanotic melanoma. The results obtained showed that the use of an NO donor significantly increased the anti-tumor efficacy of PDT. Noteworthy, the group of mice treated with mPEG-Pb*a* and DETA/NO showed a significant delay of tumor growth compared to the not treated group. Furthermore, the Kaplan-Meier survival analyses showed a difference of the median survival times between the mice treated with DETA/NO + mPEG-Pb*a* (59 days) and the mice treated with mPEG-Pb*a*/PDT alone (52.5 days) (Rapozzi V et al. 2013).

The data obtained both in vitro and in vivo with the combined treatment of an NO donor and PDT (Rapozzi V et al. 2013) are significant and open new horizons for the optimization of photodynamic treatment.

4.11 New therapeutic strategies with nitric oxide and PDT.

The effect of the combined treatment DETA/NO+Pb*a*/PDT in an *in vivo* application may be more complex than its effects *in vitro*, due essentially to a systemic effect of the NO donor and especially to its lack of organ or tissue specificity. Therefore, it is exceedingly challenging to selectively deliver NO to a target compartment, preventing changes of vascular dynamics that result in systemic hypotension (Shan SQ et al. 1997). An alternative approach is to deliver NO via the site specific activation of a pro-drug, which minimizes adverse drug reactions.

In collaboration with Dr. Greta Varchi (ISOF-CNR, Bologna, Italy), we synthesized a new compound named DRPDT2 (DR2) (Figure 23A). This is a conjugate between Pb*a* and an NO donor that allows a controlled NO release in the tumor at the time of irradiation of the PS. The NO release happens through a photo-rearrangement upon controlled light irradiation (Figure 23B). The combination between singlet oxygen ($^1O_2$), reactive oxygen species (ROS) and NO should culminate in synergistic cytotoxicity, increasing the efficacy of PDT used alone.

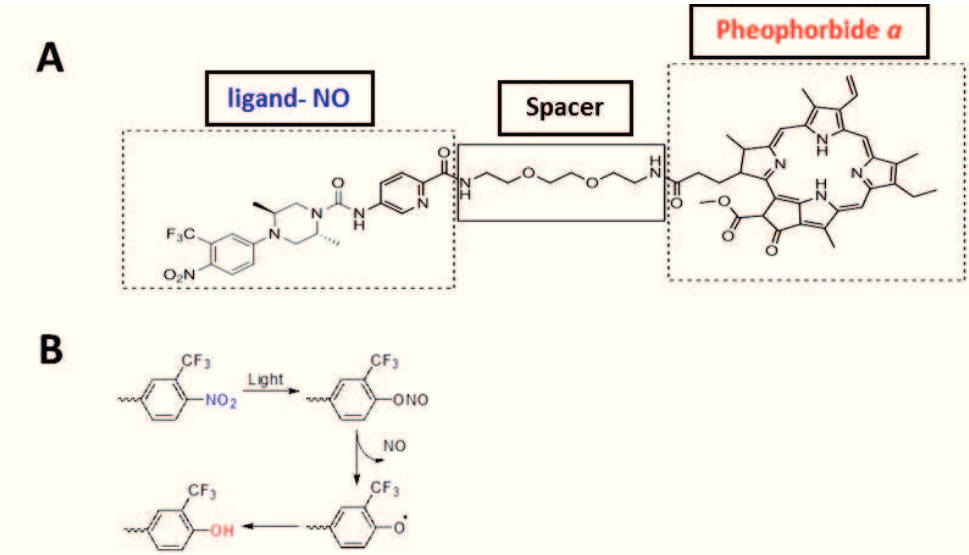

Figure 23.A. Chemical structure of DRPDT2. B. Light-induced NO-releasing mechanism of nitrobenzene compounds

Another important characteristic of this compound is its ability to bind androgen receptor even when low amount of AR (data not published yet) was expressed as it occurs in PC3 cells. We compared the efficacy of Pb*a*/PDT and DR2/PDT treatment in term of the same quantity of Pb*a*, in this way, the differences obtained by treatments were due to the different NO production/induction. PC3 cells were treated with Pb*a* and with DR2 for 6h in the dark in order to permit the complete uptake of DR2. After drug incubation, the cells were irradiated with white light in order to permit both the Pb*a* activation (670nm) and the NO release (400nm) by DR2 molecule. In Figure 24 it has been reported the metabolic activity 24h after irradiation. It is possible to observe that at the concentration of 40nM the effect of DR2 is better than the effect of Pb*a* and this molecule induces an arrest of cell growth comparable to that obtained with the high dose of Pb*a*/PDT treatment (> 80nM).

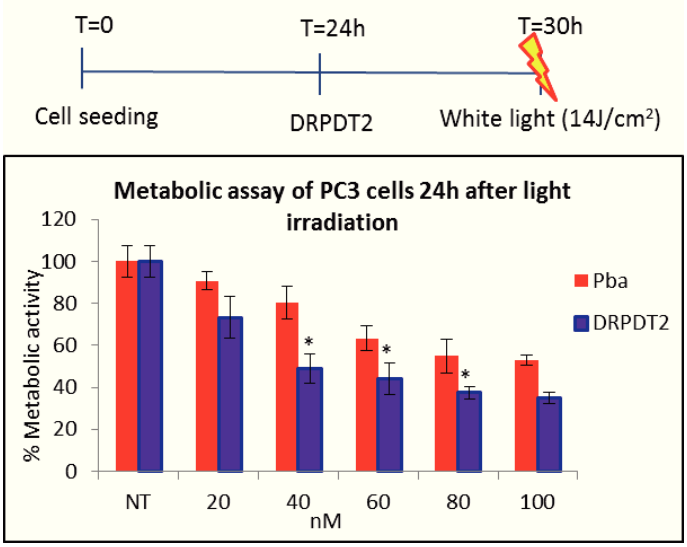

Figure 24. Comparison of metabolic activity in PC3 cells after Pba/PDT and DR2/PDT treatment. *Effects of Pba and DR2/PDT treatments on metabolic activity in PC3 cells. 24h after seeding the cells were treated for 6h in the dark and then light irradiated with white lamp (14 J/cm2). The Histogram represents the values of % metabolic activity, performed by the resazurin assay, 24 after light irradiation and expressed as T/C x 100. T and C are the absorbance of treated and not treated cells. The values are the mean ± SD of three independent experiments. A standard t-test versus control was performed (P < 0.05).*

The cell growth arrest after DR2/PDT treatment was confirmed by the protein expression of the NF-κB /YY1/RKIP loop. The western blot analysis showed the reduction of NF-κB and YY1 gene products and a strong increase of RKIP gene product after treatment with DR2/PDT (40nM). Moreover, the increase of the epithelial protein E-cadherin expression suggested an inhibition of EMT and invasiveness. Opposite behaviors were observed in Pb*a*/PDT treated PC3 cells (Figure 25).

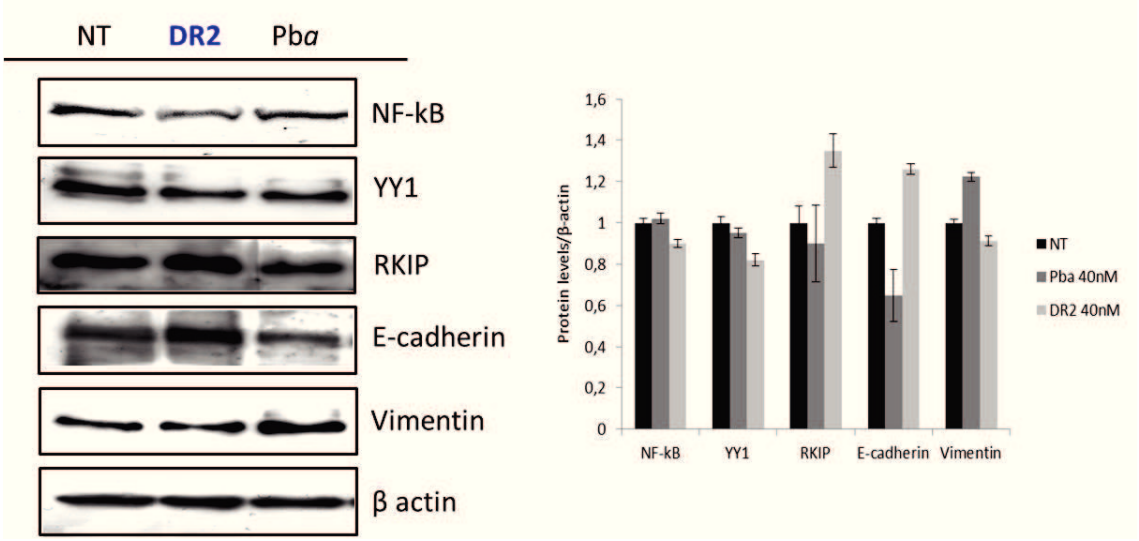

Figure 25. Effect of DR2/PDT treatment on NF-κB /YY1/RKIP loop and on EMT. *The protein lysates were analyzed 24h after light irradiation.*

In the conjugate DR2, the high level of NO simultaneously produced by both NO photo-release and Pb*a* excitation, induced an inhibition of NF-κB /YY1/RKIP loop correlated to EMT inhibition. To evaluate the kind of cell death we performed an annexin V/PI assay. The PC3 cells treated with 40nM of Pb*a*/PDT showed only a slight increase of cells stained with annexin and PI, indicating a weak apoptosis activation (Chen S et al. 2008; Yoo JO et al. 2011) (Figure 26B). On the other hand, PC3 cells treated with DR2/PDT showed an evident increase of the same population. More in detail, the positivity of these cells to both annexin V and PI suggested that the cell death is correlated to tardive apoptosis or to necrosis (Chen S et al. 2008; Yoo JO et al. 2011). This data was confirmed by the western blot analysis of PARP in which the cleavage resulted less evident respect to that obtained after Pb*a*/PDT treatment, suggesting again a necrotic cell death (He J et al. 1998) (Figure 26A). All together these data again underline the role of NO in PDT but also suggest a relation between the structure of the PS and the type of cell death. Changes in the subcellular localization and in the amount of PS really activated into the cell, can influence the type of cell death (Castano AP et al. 2005).

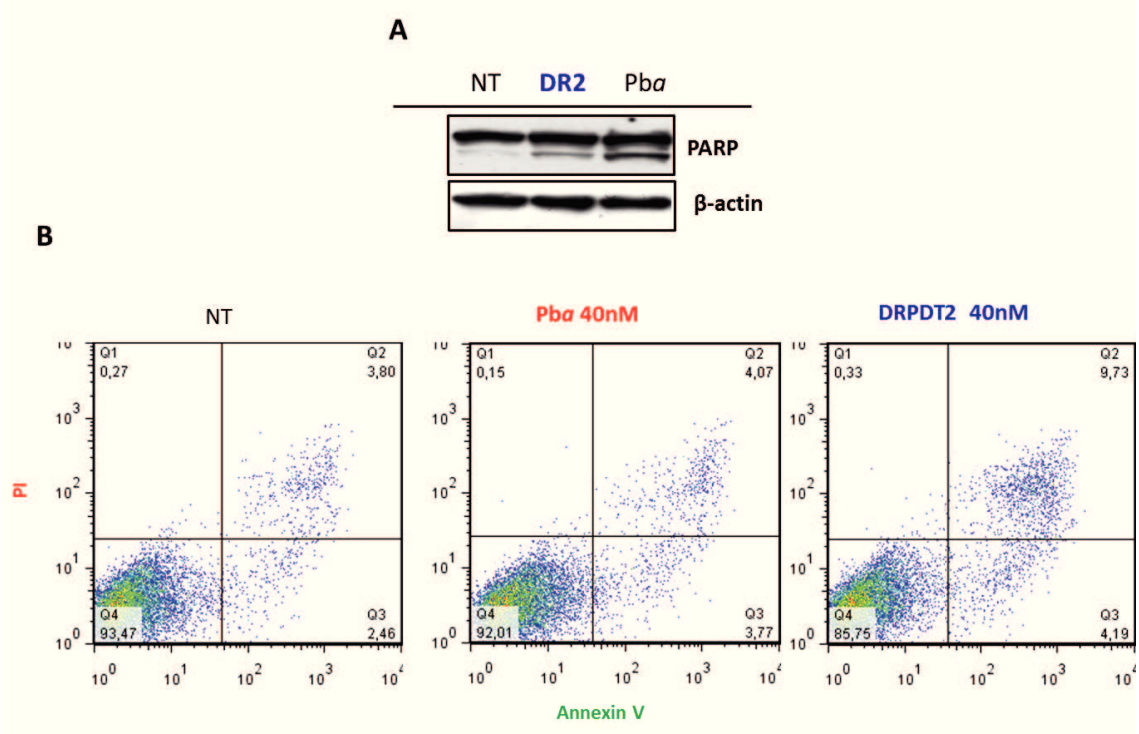

Figure 26. Cell death analysis. A. PARP-1 cleavage assay *PC3 cells were treated with the dose of 40nM of DR2 and Pba. The western blot show the cleavage of PARP-1.* ***B. Annexin V/Propidium iodide assay.*** *PC3 cells were treated with Pba or DR2 at the same concentration The assay was performed 24h after irradiation.*

Considering the importance of the structure of the PS in relation to PDT resistance, we evaluated if DR2 is a substrate for ABCG2 efflux pump. First of all, we chose a cell line, A549 (human lung adenocarcinoma epithelial cell line), that express ABCG2 (Robey RW et al. 2009) in a higher quantity than PC3 cells (Figure 27A). Robey et al. (Robey RW et al. 2005) described a functional assay for ABCG2 that involves the use of a fluorescent ABCG2 substrate (Pb*a*) and an ABCG2 inhibitor (reserpine) (Ingram WJ et al.2013). The cells were incubated with 5µM of Pb*a* or DR2 in the presence or absence of 10uM of reserpine for 30 min. Subsequently the cells were washed and incubated for 1h in a PS-free medium in presence of the ABCG2 inhibitor (Robey RW et al. 2005; Robey RW et al. 2009). The graphs in Figure 27B showed that using Pb*a*, a ABCG2 substrate, the use of reserpine increased its accumulation (blue line). Using DR2 there was no shift of the peak suggesting that this molecule is not a substrate for this efflux pump (Robey et al.2004; Robey RW et al. 2005; Selbo PK et al. 2012). Since this molecule has a high affinity for

androgen receptor (AR), it could be possible that the link with the AR increases the accumulation of this new conjugate into the cell. These considerations could in part explain the results obtained about cell death: the long-lasting permanence of DR2 into the cell could be linked to an higher oxidative damage (ROS+NO) leading to necrosis. Moreover, considering that AR is expressed also in the majority androgen-independent prostate cancer or hormone-refractory prostate cancer (Heinlein CA et al.2004) and that DR2 showed high affinity for the AR (unpublished data), this conjugate could be a new therapeutic drug for these tumors.

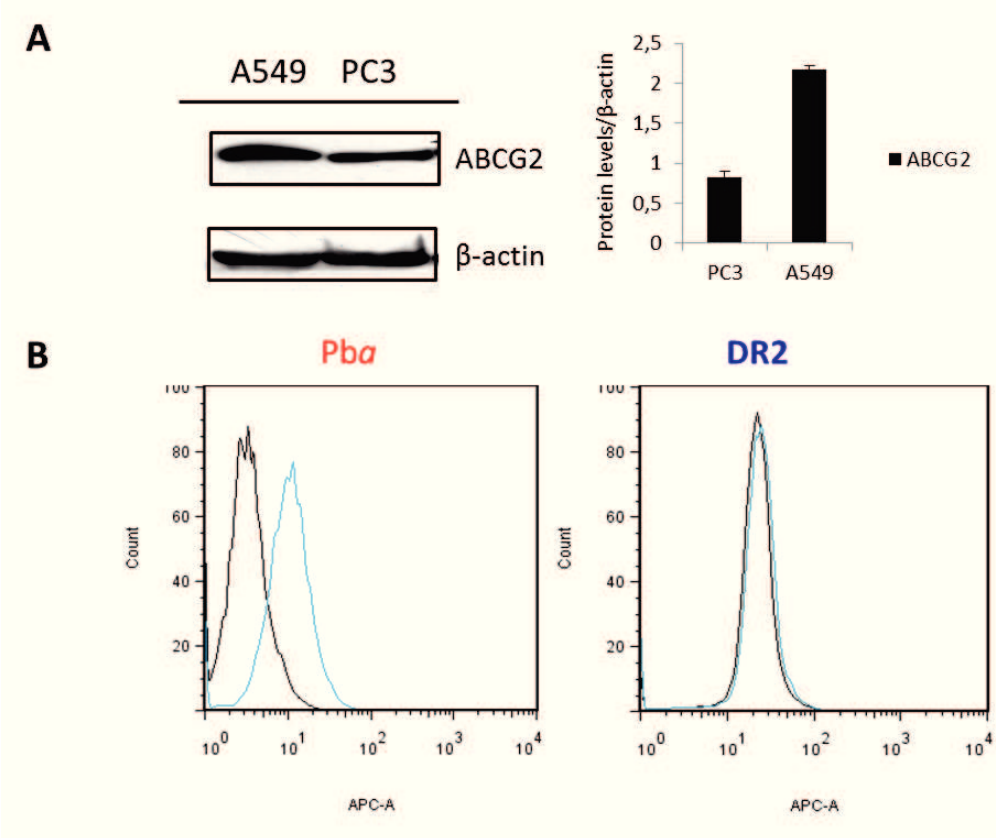

Figure 23. A. ABCG2 expression in PC3 and A549 cell lines*. ABCG2 band intensity was determined densitometrically and normalized to β-actin****. B Functional assay for ABCG2.*** *The A549 cells were incubated with 5 µM of Pba or DR2 in the presence or absence of 10 µM of reserpine for 30 min. Subsequently the cells were washed and incubated for 1h in a PS-free medium in presence of the ABCG2 inhibitor. PS uptake was analyzed by FACS.*

5 CONCLUSIONS

Photodynamic therapy employs a photosensitizer (PS), the molecular oxygen and a visible light to produce reactive oxygen species (ROS) that can selectively destroy tumor cells. It is always more evident that the non-optimal PDT treatment leaves a significant number of surviving cells that causes tumor recurrence. The study of the molecular pathways involved in the tumor response to PDT treatment is important to propose new and effective strategies to improve this therapy.

The aim of this work has been to study the response of cancer cells to photodynamic therapy with Pheophorbide *a* (Pb*a*), focusing our attention on the NF-κB /YY1/RKIP loop, normally dysregulated in cancer (Lin K et al.2010). Through the induction of NO after PDT this loop can be modulated in a dose dependent way, influencing the outcome of the therapy.

The high NO level generated by a high-dose of Pb*a*/PDT treatment induces an inhibition of the pro-survival genes involved in this loop, leading to cell death. On the other hand, studying more in detail the effect of a repeated low-dose Pb*a*/PDT treatment, we have demonstrated, for the first time, that the chronic low-dose of NO induced by PDT, acting through the NF-κB /YY1/RKIP loop, can modulate pivotal aspects of tumor recurrence: cell survival, EMT, resistance and, indirectly, the development of a more aggressive population (CSC).

With the intent of increase the efficacy of PDT we have proposed the use of a NO-donor (DETANONOate, DETA/NO) in combination with Pb*a*/PDT (Rapozzi V et al. 2013). The results obtained showed that the use of an NO donor can increase the anti-tumor efficacy of PDT. In order to reduce the systemic effects of NO, observed in our *in vivo* studies we have synthesized in collaboration with Dr Greta Varchi (ISOF-CNR, Bologna, Italy), a new PDT-NO conjugate, DRPDT2, that in addition to oxidative damage produced by PDT, releases the NO only during light irradiation. The use of this new compound permits to regulate the NO flux, taking advantages of NO and excluding its side effects.

Another important aspect that we are analyzing is the importance of the structure of the PS in PDT. We have demonstrated, using m-THPP and Pb*a,* that the choice of a PS that isn't substrate for ABCG2 efflux pump, may prevent the development of a more aggressive cell phenotype and it can permit a more effective PDT. The study of the relationship between the structure of PS, its subcellular target and its involvement in MDR development is important in the development of new strategies to increase PDT efficacy.

6 REFERENCES

Agostinis P, Berg K, Cengel KA, Foster TH, Girotti AW, Gollnick SO, Hahn SM, Hamblin MR, Juzeniene A, Kessel D, Korbelik M, Moan J, Mroz P, Nowis D, Piette J, Wilson BC, Golab J. Photodynamic therapy of cancer: an update. *CA Cancer J Clin. 2011;61:250-81. Review.*

Allison RR, Moghissi K. Photodynamic Therapy (PDT): PDT Mechanisms. *Clin Endosc. 2013;46:24-9.*

Beckman JS. Peroxynitrite versus hydroxyl radical: the role of nitric oxide in superoxide-dependent cerebral injury. *Ann N Y Acad Sci. 1994 738:69-75.*

Benov L. Photodynamic Therapy: Current Status and Future Directions. *Med Princ Pract. 2014.1:14-28.*

Beshir AB, Ren G, Magpusao AN, Barone LM, Yeung KC, Fenteany G. Raf kinase inhibitor protein suppresses nuclear factor-κB-dependent cancer cell invasion through negative regulation of matrix metalloproteinase expression. *Cancer Lett*. 2010;299:137-49.

Bhowmick R, Girotti AW. Signaling events in apoptotic photokilling of 5-aminolevulinic acid-treated tumor cells: inhibitory effects of nitric oxide. *Free Radic Biol Med.* 2009;47:731-40*.*

Bhowmick R, Girotti AW Rapid upregulation of cytoprotective nitric oxide in breast tumor cells subjected to a photodynamic therapy-like oxidative challenge. *Photochem Photobiol*. 2011;87:378-86.

Bhowmick R, Girotti AW. Cytoprotective signaling associated with nitric oxide upregulation in tumor cells subjected to photodynamic therapy-like oxidative stress*. Free Radic Biol Med. 2013;57:39-48.*

Bhowmick R, Girotti AW. Pro-survival and pro-growth effects of stress-induced nitric oxide in a prostate cancer photodynamic therapy model. *Cancer Lett. 2014 1343:115-22.*

Bonavida B, Baritaki S Dual role of NO donors in the reversal of tumor cell resistance and EMT: Downregulation of the NF-κB/Snail/YY1/RKIP circuitry. *Nitric Oxide.* 2011;24:1-7.

Bonavida B, Baritaki S. The novel role of Yin Yang 1 in the regulation of epithelial to mesenchymal transition in cancer via the dysregulated NF-κB/Snail/YY1/RKIP/PTEN Circuitry *Crit Rev Oncog.* 2011;16:211-26.

Burke AJ, Sullivan FJ, Giles FJ, Glynn SA. The yin and yang of nitric oxide in cancer progression. *Carcinogenesis 2013 34; 503-12.*

Casas A, Sanz-Rodriguez F, Di Venosa G, Rodriguez L, Mamone L, Blázquez A, Jaén P, Batlle A, Stockert JC, Juarranz A Disorganisation of cytoskeleton in cells resistant to photodynamic treatment with decreased metastatic phenotype. *Cancer Lett.* 2008;270:56-65.

Casas A, Di Venosa G, Hasan T, Al Batlle. Mechanisms of resistance to photodynamic therapy. *Curr Med Chem. 2011;18:2486-515. Review.*

CastanoAP, Demidova TN, Hamblin MR. Mechanisms in photodynamic therapy: part one-photosensitizers, photochemistry and cellular localization. *Photodiagnosis Photodyn. Ther. 2004;1:279-293.*

Castano AP, Demidova TN, Hamblin MR. Mechanisms in photodynamic therapy: part two-cellular signaling, cell metabolism and modes of cell death. Photodiagnosis P*hotodyn Ther. 2005;2:1-23.*

Castellano G, Torrisi E, Ligresti G, Malaponte G, Militello L, Russo AE, McCubrey JA, Canevari S, Libra M. The involvement of the transcription factor Yin Yang 1 in cancer development and progression. *Cell Cycle. 2009;8:1367-72.*

Chaiswing L, Zhong W, Oberley TD Distinct redox profiles of selected human prostate carcinoma cell lines: implications for rational design of redox therapy. *Cancers (Basel). 2011;3:3557-84.*

Chen S, Cheng AC, Wang MS, Peng X. Detection of apoptosis induced by new type gosling viral enteritis virus in vitro through fluorescein annexin V-FITC/PI double labeling. World *J Gastroenterol. 2008;14:2174-8.*

Chua HL, Bhat-Nakshatri P, Clare SE, Morimiya A, Badve S, Nakshatri H. NF-kappaB represses E-cadherin expression and enhances epithelial to mesenchymal transition of mammary epithelial cells: potential involvement of ZEB-1 and ZEB-2. *Oncogene. 2007;26:711-24.*

Croker AK, Goodale D, Chu J, Postenka C, Hedley BD, Hess DA, Allan AL. High aldehyde dehydrogenase and expression of cancer stem cell markers selects for breast cancer cells with enhanced malignant and metastatic ability. *J Cell Mol Med. 2009;13:2236-52.*

Cruz MH, Sidén A, Calaf GM, Delwar ZM, Yakisich JS. The stemness phenotype model. *ISRN Oncol. 2012;2012:392647.*

Dalbasti T, Cagli S, Kilinc E, Oktar N, Ozsoz M. Online electrochemical monitoring of nitric oxide during photodynamic therapy. *Nitric Oxide. 2002 7:301–305*

Davies KM, Wink DA, Saavedra JE, Keefer LK. Chemistry of the diazeniumdiolates. 2. Kinetics and mechanism of dissociation to nitric oxide in aqueous solution*. J. Am. Chem. Soc. 2001;123:5473-81.*

Deiss K, Kisker C, Lohse MJ, Lorenz K. Raf kinase inhibitor protein (RKIP) dimer formation controls its target switch from Raf1 to G protein-coupled receptor kinase (GRK) 2. *J Biol Chem. 2012;287:23407-17.*

Dewaele M, Maes H, Agostinis P. ROS-mediated mechanisms of autophagy stimulation and their relevance in cancer therapy. *Autophagy. 2010;6:838-54.*

Di Di Paola RS. **Paola RS**. To Arrest or Not To G2-M Cell-Cycle Arrest*. Clin Cancer Res 2002;8:3311-3314.*

Di Venosa G, Rodriguez L, Mamone L, Gándara L, Rossetti MV, Batlle A, Casas A. Changes in actin and E-cadherin expression induced by 5-aminolevulinic acid photodynamic therapy in normal and Ras-transfected human mammary cell lines*. J Photochem Photobiol B. 2012*;106:47-52.

Dougherty TJ, Gomer CJ, Henderson BW, Jori G, Kessel D, Korbelik M, Moan J, Peng Q. Photodynamic therapy*. J Natl Cancer Inst. 1998;17;90:889-905.review.*

Escara-Wilke J, Yeung K, Keller ET. Raf kinase inhibitor protein (RKIP) in cancer. *Cancer Metastasis Rev. 2012 ;31:615-20. review.*

Fan X, Liu S, Su F, Pan Q, Lin T. Effective enrichment of prostate cancer stem cells from spheres in a suspension culture system*. Urol Oncol. 2012;30:314-8*

Ferrario A, von Tiehl KF, Rucker N, Schwarz MA, Gill PS, Gomer CJ. Antiangiogenic treatment enhances photodynamic therapy responsiveness in a mouse mammary carcinoma. *Cancer Res. 2000;60:4066-9.*

Ferrario A, Von Tiehl K, Wong S, Luna M, Gomer CJ. Cyclooxygenase-2 inhibitor treatment enhances photodynamic therapy-mediated tumor response. *Cancer Res. 2002;62:3956-61.*

Ferrario A, Chantrain CF, von Tiehl K, Buckley S, Rucker N, Shalinsky DR, Shimada H, DeClerck YA, Gomer *CJ*. The matrix metalloproteinase inhibitor prinomastat enhances photodynamic therapy responsiveness in a mouse tumor model. *Cancer Res. 2004;64:2328-32.*

Ferrario A, Fisher AM, Rucker N, Gomer CJ. Celecoxib and NS-398 enhance photodynamic therapy by increasing in vitro apoptosis and decreasing in vivo inflammatory and angiogenic factors. *Cancer Res. 2005;65:9473-8*

Ferrario A, Rucker N, Wong S, Luna M, Gomer CJ Survivin, a member of the inhibitor of apoptosis family, is induced by photodynamic therapy and is a target for improving treatment response. *Cancer Res. 2007;67:4989-95.*

Fukumura D, Kashiwagi S, Jain RK. The role of nitric oxide in tumour progression. *Nat Rev Cancer. 2006; 6:521-34. Review.*

Gomer CJ, Ferrario A, Luna M, Rucker N, Wong S. Photodynamic therapy: combined modality approaches targeting the tumor microenvironment. *Lasers Surg Med. 2006;38:516-21. Review.*

Gomes ER, Almeida RD, Carvalho AP, Duarte CB. Nitric oxide modulates tumor cell death induced by photodynamic therapy through a cGMP-dependent mechanism. *Photochem Photobiol. 2002;76:423-30.*

Gordon S, Akopyan G., Garban H., Bonavida B. Transcription factor YY1: structure, function, and therapeutic implications in cancer biology. *Oncogene 2006;25:1125-42.*

Gupta PB, Chaffer CL, Weinberg RA. Cancer stem cells: mirage or reality? *Nat Med. 2009;15:1010-2. Review.*

Gupta PB, Onder TT, Jiang G, Tao K, Kuperwasser C, Weinberg RA, Lander ES. Identification of selective inhibitors of cancer stem cells by high-throughput screening. *Cell. 2009;138:645-59.*

Gupta S, Ahmad N, Mukhtar H. Involvement of nitric oxide during phthalocyanine (Pc4) photodynamic therapy-mediated apoptosis. *Cancer Res. 1998;58:1785-8.*

Hamblin MR, Hasan T. Photodynamic therapy: a new antimicrobial approach to infectious disease? *Photochem Photobiol Sci. 2004; 3:436-50.*

Hanlon JG, Adams K, Rainbow A, Gupta R, Singh G. Induction of HSP60 by Photofrin-mediated photodynamic therapy. *J Photochem Photobiol B. 2001;64:55–61.*

He J, Whitacre CM, Xue LY, Berger NA, Oleinick NL. Protease activation and cleavage of poly(ADP-ribose) polymerase: an integral part of apoptosis in response to photodynamic treatment. *Cancer Res. 1998;58:940-6.*

Heinlein CA, Chang C. Androgen receptor in prostate cancer. *Endocr Rev. 2004,25:273-308. Review.*

Huerta-Yepez S, Yoon NK, Hernandez-Cueto A, Mah V, Rivera-Pazos CM, Chatterjee D, Vega MI, Maresh EL, Horvath S, Chia D, Bonavida B, Goodglick L. Expression of phosphorylated raf kinase inhibitor protein (pRKIP) is a predictor of lung cancer survival. *BMC Cancer. 2011;11:259-267.*

Ingram WJ, Crowther LM, Little EB, Freeman R, Harliwong I, Veleva D, Hassall TE, Remke M, Taylor MD, Hallahan AR. ABC transporter activity linked to radiation resistance and molecular subtype in pediatric medulloblastoma. *Exp Hematol Oncol. 2013;2:26.*

Inguscio V, Panzarini E, Dini L. Autophagy Contributes to the Death/Survival Balance in Cancer PhotoDynamic Therapy *Cells. 2012; 1: 464–491.*

Ishikawa T, Nakagawa H, Hagiya Y, Nonoguchi N, Miyatake S, Kuroiwa T. Key Role of Human ABC Transporter ABCG2 in Photodynamic Therapy and Photodynamic Diagnosis. *Adv Pharmacol Sci. 2010;2010:587306.*

Jing Y, Han Z, Zhang S, Liu Y, Wei L. Epithelial-Mesenchymal Transition in tumor microenvironment. *Cell Biosci. 2011;1:29.*

Jori G, Fabris C, Soncin M, Ferro S, Coppellotti O, Dei D, Fantetti L, Chiti G, Roncucci G. Photodynamic therapy in the treatment of microbial infections: basic principles and perspective applications. *Lasers Surg Med. 2006;38:468-81. Review.*

Julien S, Puig I, Caretti E, Bonaventure J, Nelles L, van Roy F, Dargemont C, de Herreros AG, Bellacosa A, Larue L. Activation of NF-kappaB by Akt upregulates Snail expression and induces epithelium mesenchyme transition. *Oncogene. 2007;26:7445-56.*

Kashyap V, Bonavida B. Role of YY1 in the pathogenesis of prostate cancer and correlation with bioinformatic data sets of gene expression*. Genes Cancer. 2014;5:71-83.Review.*

Kennedy JC, Pottier RH, Pross DC. Photodynamic therapy with endogenous protoporphyrin IX: basic principles and present clinical experience *J Photochem Photobiol B. 1990;136:891-97.*

Kim M, Turnquist H, Jackson J, Sgagias M, Yan Y, Gong M, Dean M, Sharp JG, Cowan K. The multidrug resistance transporter ABCG2 (breast cancer resistance protein 1) effluxes Hoechst 33342 and is overexpressed in hematopoietic stem cells. *Clin Cancer Res. 2002;8:22-8.*

Kim YS, Yi BR, Kim NH, Choi KC. Role of the epithelial-mesenchymal transition and its effects on embryonic stem cells *Exp Mol Med. 2014;46:e108. Review.*

Kojima H, Sakurai K, Kikuchi K, Kawahara S, Kirino Y, Nagoshi H, Hirata Y, Nagano T. Development of a fluorescent indicator for nitric oxide based on the fluorescein chromophore. *Chem Pharm Bull. 1998;46:373-5.*

Korbelik M, Parkins CS, Shibuya H, Cecic I, Stratford MR, Chaplin DJ Nitric oxide production by tumour tissue: impact on the response to photodynamic therapy*. Br J Cancer. 2000;82:1835-43.*

Krishnamurthy P, Schuetz JD. Role of ABCG2/BCRP in biology and medicine**.** *Annu Rev Pharmacol Toxicol. 2006;46:381-410. Review.*

Kunju LP, Cookingham C, Toy KA, Chen W, Sabel MS, Kleer CG. EZH2 and ALDH-1 mark breast epithelium at risk for breast cancer development. *Mod Pathol. 2011;24:786-93.*

Li Y, Laterra J. Cancer stem cells: distinct entities or dynamically regulated phenotypes? *Cancer Res. 2012;72:576-80. Review.*

Lin K, Baritaki S, Militello L, Malaponte G, Bevelacqua Y, Bonavida B. The Role of B-RAF Mutations in Melanoma and the Induction of EMT via Dysregulation of the NF-κB/Snail/RKIP/PTEN Circuit. *Genes Cancer. 2010;1:409-420.*

Lu Y, Ma W, Mao J, Yu X, Hou Z, Fan S, Song B, Wang H, Li J, Kang L, Liu P3, Liu Q, Li Salinomycin exerts anticancer effects on human breast carcinoma MCF-7 cancer stem cells via modulation of Hedgehog signaling. *Chem Biol Interact. 201; 228:100-7.*

Mani SA, Guo W, Liao MJ, Eaton EN, Ayyanan A, Zhou AY, Brooks M, Reinhard F, Zhang CC, Shipitsin M, Campbell LL, Polyak K, Brisken C, Yang J, Weinberg RA. The epithelial-mesenchymal transition generates cells with properties of stem cells. *Cell. 2008;133:704-15.*

Mao Q, Unadkat JD. Role of the Breast Cancer Resistance Protein (BCRP/ABCG2) in Drug Transport-an update**.** *AAPS J. 17:65-82.*

Marhaba R, Zöller M. CD44 in cancer progression: adhesion, migration and growth regulation*. J Mol Histol. 2004;35:211-31. Review.*

Matroule JY, Volanti C, Piette J. NF-kappaB in photodynamic therapy: discrepancies of a master regulator. *Photochem Photobiol. 2006;82:1241-6. Review.*

Milla LN, Cogno IS, Rodríguez ME, Sanz-Rodríguez F, Zamarrón A, Gilaberte Y, Carrasco E, Rivarola VA, Juarranz A. Isolation and characterization of squamous carcinoma cells resistant to photodynamic therapy. *J Cell Biochem. 2011;112:2266-78.*

Mo W, Zhang JT. Human ABCG2: structure, function, and its role in multidrug resistance. *Int J Biochem Mol Biol. 2012;3:1-27.*

Moan J. Porphyrin photosensitization and phototherapy *Photochem Photobiol. 1986;43:681-90. Review.*

Moor AC. Signaling pathways in cell death and survival after photodynamic therapy.*J Photochem Photobiol B. 2000;57:1-13. Review.*

Morel AP, Lièvre M, Thomas C, Hinkal G, Ansieau S, Puisieux A. Generation of breast cancer stem cells through epithelial-mesenchymal transition. *PLoS One. 2008;3:e2888.*

Morgan J, Jackson JD, Zheng X, Pandey SK, Pandey RK. Substrate affinity of photosensitizers derived from chlorophyll-a: the ABCG2 transporter affects the phototoxic response of side population stem cell-like cancer cells to photodynamic therapy. *Mol Pharm. 2010;7:1789-04.*

Murphy MP. Nitric oxide and cell death. *Biochim Biophys Acta. 1999 ;1411:401-14. Review.*

Nagano O, Murakami D, Hartmann D, De Strooper B, Saftig P, Iwatsubo T, Nakajima M, Shinohara M, Saya H. Cell-matrix interaction via CD44 is independently regulated by different metalloproteinases activated in response to extracellular Ca(2+) influx and PKC activation*. J Cell Biol. 2004;165:893-902.*

Nieto MA. The snail superfamily of zinc-finger transcription factors*. Nat Rev Mol Cell Biol. 2002;3:155-66. Review.*

Nowis D, Makowski M, Stokłosa T, Legat M, Issat T, Gołab J. Direct tumor damage mechanisms of photodynamic therapy*. Acta Biochim Pol. 2005;52:339-52.*

Ochsner M. Photophysical and photobiological processes in the photodynamic therapy of tumours. *J Photochem Photobiol B. 1997 ;39:1-18. Review.*

Pfeiffer MJ, Schalken JA. Stem cell characteristics in prostate cancer cell lines. *Eur Urol. 2010;57:246-54.*

Piette J, Volanti C, Vantieghem A, Matroule JY, Habraken Y, Agostinis P. Cell death and growth arrest in response to photodynamic therapy with membrane-bound photosensitizers. *Biochem Pharmacol. 2003;66:1651-9. Review.*

Plaetzer K, Krammer B, Berlanda J, Berr F, Kiesslich T. Photophysics and photochemistry of photodynamic therapy: fundamental aspects. *Lasers Med Sci. 2009;24:259-68. Review.*

Polyak K, Weinberg RA. Transitions between epithelial and mesenchymal states: acquisition of malignant and stem cell traits. *Nat Rev Cancer. 2009;9:265-73. Review.*

Porro A, Chrochemore C, Cambuli F, Iraci N, Contestabile A, Perini G. Nitric oxide control of MYCN expression and multi drug resistance genes in tumours of neural origin. *Curr Pharm Des. 2010;16:431-9.*

Rapozzi V, Miculan M, Xodo LE. Evidence that photoactivated pheophorbide a causes in human cancer cells a photodynamic effect involving lipid peroxidation *Cancer Biol Ther. 2009;8:1318-27.*

Rapozzi V, Umezawa K, Xodo LE. Role of NF-κB/Snail/RKIP loop in the response of tumor cells to photodynamic therapy. *Lasers Surg Med. 2011;43:575-85.*

Rapozzi V, Della Pietra E, Zorzet S, Zacchigna M, Bonavida B, Xodo LE Nitric oxide-mediated activity in anti-cancer photodynamic therapy. *Nitric Oxide. 2013;30:26-35*

Reeves KJ, Reed MW, Brown NJ. Is nitric oxide important in photodynamic therapy? *J Photochem Photobiol B. 2009;95:141-7.*

Repetto O, De Paoli P, De Re V, Canzonieri V, Cannizzaro R. Levels of Soluble E-Cadherin in Breast, Gastric, and Colorectal Cancers. *Biomed Res Int. 2014;2014:408047.*

Robertson CA, Evans DH, Abrahamse H. Photodynamic therapy (PDT): a short review on cellular mechanisms and cancer research applications for PDT. *J Photochem Photobiol B. 2009;96:1-8.*

Robey RW, Steadman K, Polgar O, Morisaki K, Blayney M, Mistry P, Bates SE. Pheophorbide a is a specific probe for ABCG2 function and inhibition. *Cancer Res. 2004;64:1242*-6.

Robey RW, Steadman K, Polgar O, Bates SE. ABCG2-mediated transport of photosensitizer: potential impact on photodynamic therapy *Cancer Biol.Ther. 2005;4:187-194.*

Robey RW, Obrzut T, Shukla S, Polgar O, Macalou S, Bahr JC, Di Pietro A, Ambudkar SV, Bates SE. Becatecarin (rebeccamycin analog, NSC 655649) is a transport substrate and induces expression of the ATP-binding cassette transporter, ABCG2, in lung carcinoma cells. *Cancer Chemother Pharmacol. 2009;64:575-83.*

Salvatori L, Caporuscio F, Verdina A, Starace G, Crispi S, Nicotra MR, Russo A, Calogero RA, Morgante E, Natali PG, Russo MA, Petrangeli E. Cell-to-cell signaling influences the fate of prostate cancer stem cells and their potential to generate more aggressive tumors. *PLoS One. 2012;7:e31467.*

Milla Sanabria L, Rodríguez ME, Cogno IS, Rumie Vittar NB, Pansa MF, Lamberti MJ, Rivarola VA. Direct and indirect photodynamic therapy effects on the cellular and molecular components of the tumor microenvironment. *Biochim Biophys Acta. 2013;1835:36-45. Review.*

Sánchez-Tilló E, Liu Y, de Barrios O, Siles L, Fanlo L, Cuatrecasas M, Darling DS, Dean DC, Castells A, Postigo A. EMT-activating transcription factors in cancer: beyond EMT and tumor invasiveness. *Cell Mol Life Sci. 2012;69:3429-56. Review*

Schmidt HHH and Walter U NO at work. *Cell.1994 78: 919–925*

Selbo PK, Weyergang A, Eng MS, Bostad M, Mælandsmo GM, Høgset A, Berg K. Strongly amphiphilic photosensitizers are not substrates of the cancer stem cell marker ABCG2 and provides specific and efficient light-triggered drug delivery of an EGFR-targeted cytotoxic drug. *J Control Release. 2012;159:197-203.*

Shan SQ, Rosner GL, Braun RD, Hahn J, Pearce C, Dewhirst MW. Effects of diethylamine/nitric oxide on blood perfusion and oxygenation in the R3230Ac mammary carcinoma. *Br. J. Cancer. 1997;76:429-437.*

Singh A, Settleman J. EMT, cancer stem cells and drug resistance: an emerging axis of evil in the war on cancer. *Oncogene 2010;29:4741-51. Review.*

Singh S, Gupta AK. Nitric oxide: role in tumour biology and iNOS/NO-based anticancer therapies. *Cancer Chemother Pharmacol. 2011;67:1211-24. Review.*

Solban N, Selbo PK, Sinha AK, Chang SK, Hasan T. Mechanistic investigation and implications of photodynamic therapy induction of vascular endothelial growth factor in prostate cancer *Cancer Res. 2006;66:5633-40.*

Tai S, Sun Y, Squires JM, Zhang H, Oh WK, Liang CZ, Huang J. PC3 is a cell line characteristic of prostatic small cell carcinoma*. Prostate. 2011;71:1668-79.*

Tejedo JR, Tapia-Limonchi R, Mora-Castilla S, Cahuana GM, Hmadcha A, Martin F, Bedoya FJ, Soria B. Low concentrations of nitric oxide delay the differentiation of embryonic stem cells and promote their survival. *Cell Death Dis. 2010;1:e80.*

Triesscheijn M, Baas P, Schellens JH, Stewart FA. Photodynamic therapy in oncology. *Oncologist. 2006;11:1034-44. Review.*

Van der Pluijm G. Epithelial plasticity, cancer stem cells and bone metastasis formation. *Bone. 2011;48:37-43. Review.*

Verma S, Watt GM, Mai Z, Hasan *T.* Strategies for enhanced photodynamic therapy effects. *Photochem Photobiol. 2007;83:996-1005.*

Volanti C, Matroule JY, Piette J. Involvement of oxidative stress in NF-kappaB activation in endothelial cells treated by photodynamic therapy. *Photochem Photobiol. 2002;75:36-45.*

Volanti C, Hendrickx N, Van Lint J, Matroule JY, Agostinis P, Piette J. Distinct transduction mechanisms of cyclooxygenase 2 gene activation in tumour cells after photodynamic therapy. *Oncogene. 2005;24:2981-91.*

Wang H, Hertlein E, Bakkar N, Sun H, Acharyya S, Wang J, Carathers M, Davuluri R, Guttridge DC. NF-kappaB regulation of YY1 inhibits skeletal myogenesis through transcriptional silencing of myofibrillar genes*. Mol Cell Biol. 2007;27:4374-87.*

Wang Y, Ma J, Shen H, Wang C, Sun Y, Howell SB, Lin X. Reactive oxygen species promote ovarian cancer progression via the HIF-1α/LOX/E-cadherin pathway. *Oncol Rep. 2014;32:2150-8*

Wilson BC, Patterson MS. The physics, biophysics and technology of photodynamic therapy. *Phys Med Biol. 2008 7;53:R61-109. Review.*

Wink DA, Vodovotz Y, Laval J, Laval F, Dewhirst MW, Mitchell JB. The multifaceted roles of nitric oxide in cancer. *Carcinogenesis. 1998;19:711-21*.

Wu Y, Deng J, Rychahou PG, Qiu S, Evers BM, Zhou BP. Stabilization of snail by NF-kappaB is required for inflammation-induced cell migration and invasion. *Cancer Cell. 2009;15:416-28.*

Xue ZX, Zheng JH, Zheng ZQ, Cai JL, Ye XH, Wang C, Sun WJ, Zhou X, Lu MD, Li PH, Cai ZZ. Latexin inhibits the proliferation of CD133+ miapaca-2 pancreatic cancer stem-like cells. *World J Surg Oncol. 2014;12:404*

Yoo JO, Lim YC, Kim YM, Ha KS. Differential cytotoxic responses to low- and high-dose photodynamic therapy in human gastric and bladder cancer cells. *J Cell Biochem. 2011* ;112:3061-71

Yoon I, Li JZ, Shim YK. Advance in photosensitizers and light delivery for photodynamic therapy. *Clin Endosc. 2013 ;46:7-23.*

Zhang L, Jiao M, Li L, Wu D, Wu K, Li X, Zhu G, Dang Q, Wang X, Hsieh JT, He D. Tumorspheres derived from prostate cancer cells possess chemoresistant and cancer stem cell properties. *J Cancer Res Clin Oncol. 2012;138:675-86.*

Zhou J, Brüne B. NO and transcriptional regulation: from signaling to death. *Toxicology. 2005 15;208:223-33. Review.*

Zhou W, Lv R, Qi W, Wu D, Xu Y, Liu W, Mou Y, Wang L. Snail contributes to the maintenance of stem cell-like phenotype cells in human pancreatic cancer. *PLoS One. 2014;9:e87409.*

Zhuang S, Kochevar IE. Singlet oxygen-induced activation of Akt/protein kinase B is independent of growth factor receptors**.** *Photochem Photobiol. 2003;78:361–371*

7 LIST OF PAPERS

Rapozzi V, Della Pietra E, Zorzet S, Zacchigna M, Bonavida B, Xodo LE. Nitric oxide-mediated activity in anti-cancer photodynamic therapy. *Nitric Oxide. 2013;30:26-35.*

Rapozzi V, Zorzet S, Zacchigna M, Della Pietra E, Cogoi S, Xodo LE. Anticancer activity of cationic porphyrins in melanoma tumour-bearing mice and mechanistic in vitro studies. *Mol Cancer. 2014;13:75.*

Rapozzi V, Della Pietra E Photodynamic Therapy and Nitric Oxide, *In: Bonavida B (Ed) Nitric Oxide and Cancer: Pathogenesis and Therapy, Springer 2015*

Della Pietra E, Simonella F, Bonavida B, Xodo LE, Rapozzi V.
Repeated sub-optimal photodynamic treatments with pheophorbide a induce an epithelial mesenchymal transition in prostate cancer cells via nitric oxide. *Nitric Oxide. 2015. pii: S1089-8603(15)00022-1.doi: 10.1016/j.niox.2015.02.005*

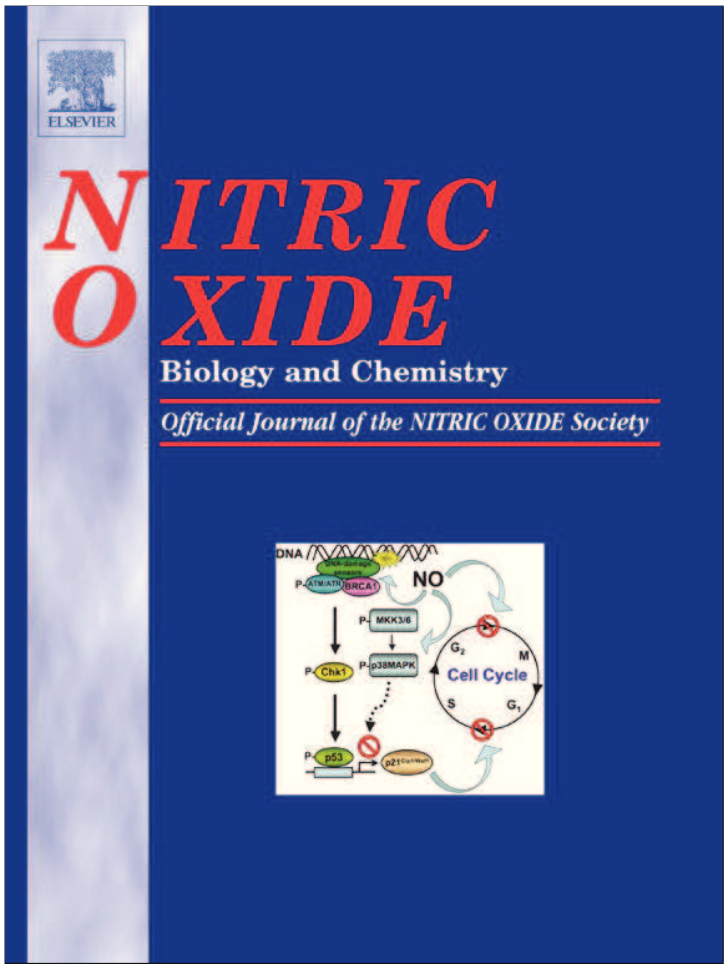

(This is a sample cover image for this issue. The actual cover is not yet available at this time.)

Nitric Oxide 30 (2013) 26–35

Contents lists available at SciVerse ScienceDirect

Nitric Oxide

journal homepage: www.elsevier.com/locate/yniox

Nitric oxide-mediated activity in anti-cancer photodynamic therapy

Valentina Rapozzi [a,*], Emilia Della Pietra [a], Sonia Zorzet [b], Marina Zacchigna [c], Benjamin Bonavida [d], Luigi Emilio Xodo [a]

[a] Department of Medical and Biological Sciences, School of Medicine, University of Udine, P.le Kolbe 4, 33100 Udine, Italy
[b] Department of Life Science, University of Trieste, Via Giorgieri 7-9, 34100 Trieste, Italy
[c] Department of Chemical and Pharmaceutical Sciences, University of Trieste, P.le Europa 1, 34100 Trieste, Italy
[d] Department of Microbiology, Immunology and Molecular Genetics, David Geffen School of Medicine, Jonsson Comprehensive Cancer Center, University of California Los Angeles, Los Angeles, CA 90095, USA

ARTICLE INFO

Article history:
Received 20 September 2012
Revised 8 January 2013
Available online 26 January 2013

Keywords:
Nitric oxide
Photodynamic therapy
Pheophorbide *a*
DETANONOate
B78-H1 amelanotic melanoma
C57BL/6 mice

ABSTRACT

Cell recurrence in cancer photodynamic therapy (PDT) is an important issue that is poorly understood. It is becoming clear that nitric oxide (NO) is a modulator of PDT. By acting on the NF-κB/Snail/RKIP survival/anti-apoptotic loop, NO can either stimulate or inhibit apoptosis. We found that pheophorbide *a*/PDT (Pb*a*/PDT) induces the release of NO in B78-H1 murine amelanotic melanoma cells in a concentration-dependent manner. Low-dose PDT induces low NO levels by stimulating the anti-apoptotic nature of the above loop, whereas high-dose PDT stimulates high NO levels inhibiting the loop and activating apoptosis. When B78-H1 cells are treated with low-dose Pb*a*/PDT and DETA/NO, an NO-donor, intracellular NO increases and cell growth is inhibited according to scratch-wound and clonogenic assays. Western blot analyses showed that the combined treatment reduces the expression of the anti-apoptotic NF-κB and Snail gene products and increases the expression of the pro-apoptotic RKIP gene product. The combined effect of Pb*a* and DETA/NO was also tested in C57BL/6 mice bearing a syngeneic B78-H1 melanoma. We used pegylated Pb*a* (mPEG-Pb*a*) due to its better pharmacokinetics compared to free Pb*a*. mPEG-Pb*a* (30 mg/Kg) and DETA/NO (0.4 mg/Kg) were i.p. injected either as a single molecule or in combination. After photoactivation at 660 nM (fluence of 193 J/cm^2), the combined treatment delays tumor growth more efficiently than each individual treatment ($p < 0.05$). Taken together, our results showed that the efficacy of PDT is strengthened when the photosensitizer is used in combination with an NO donor.

Introduction

Photodynamic therapy (PDT) is a therapeutic approach for the cure of different kinds of solid tumors. This therapy is based on the interaction of three different components: the photosensitizer, light and oxygen. This triad produces oxidatively-generated damage to the cells through the production of reactive oxygen species (ROS) and/or singlet oxygen ($^1O_2$). Cell death occurs by apoptosis, autophagy or necrosis and the outcome depends on the PDT dose and localization of the photosensitizer [1,2]. When PDT is not optimal to induce cell death, after an initial growth arrest, cancer cells recover by activating different signaling pathways [3]. Thus, new strategies to sensitize tumor cells to PDT are needed [4–8].

It has been found that nitric oxide (NO) is present in tumor tissues and that its level and persistence may affect tumor progression or tumor repression [9–11]. This discrepancy may be explained by the finding that high levels of NO exhibit a pro-oxidant cytotoxic effect whereas low levels of NO have been reported to be cytoprotective [12]. Furthermore, NO can act as a free radical-scavenging antioxidant [13]. The primary determinant for the role of NO is the surrounding redox environment. In fact, NO can react directly with metals or other highly reactive radicals (e.g., lipid radicals) or indirectly, after reaction with O_2 or $O_2^{\cdot}$, to give reactive nitrogen species such as N_2O_3, NO_2 and $ONOO^-$ (RNS), which can impair the functions of biomacromolecules [14,15].

The NO level in the tumor and microenvironment is known to directly influence the response of the tumor cells to PDT [16,17].

Abbreviations: ALA, 5-aminolevulinic acid; cPTIO, 2-(4-carboxyphenyl)-4,4,5,5-tetramethylimidazoline-1-oxyl-3-oxide; DAF-FM, 4-amino-5-methylamino-2′,7′-difluorofluorescein; DAF-2, 4,5-diaminofluorescein diacetate; DETA/NO, DETANONOate; DMSO, dimethylsulfoxide; EMT, epithelial mesenchymal transition; H_2O_2, hydrogen peroxide; L-NAME, L-N^G-nitroarginine methyl ester; L-NNA, N$^\omega$-nitro-L-arginine; MA, metabolic activation; mPEG-Pb*a*, methoxypolyethylene glycol-pheophorbide *a*; MTT, 3-[4,5-dimethylthiazol-2-yj]-2,5-diphenyl tetrazolium bromide; NO, nitric oxide; NO_2, nitrogen dioxide; N_2O_3, nitrogen trioxide; NOS, nitric oxide synthase; $^1O_2$, singlet oxygen; $O_2^{\cdot-}$, superoxide anion; $ONOO^-$, peroxynitrite; Pb*a*, pheophorbide *a*; PBS, phosphate buffered saline; PDT, photodynamic therapy; ROS, reactive oxygen species; SPNO, spermine NONOate; 1400W, N-[3-(aminomethyl)benzyl]acetamidine.

* Corresponding author. Fax: +39 0432 494301.
E-mail address: valentina.rapozzi@uniud.it (V. Rapozzi).

1089-8603/$ - see front matter © 2013 Elsevier Inc. All rights reserved.
http://dx.doi.org/10.1016/j.niox.2013.01.002

PDT influences the NO level, as the activated photosensitizer can induce the production of NO. Gupta et al. [18] reported, for the first time, an increase of NO following treatment of A431 tumor cells with phthalocyanine/PDT. The increase of NO correlated with an enhanced constitutive expression of nitric oxide synthase (NOS). This is probably due to the PDT activation of specific signal transduction pathways inducing transcription factors that transcribe the genes encoding NOS. Furthermore, activated inflammatory cells accumulated in PDT-treated tumors may be responsible for the release of NO [19–21].

The above considerations suggest that NO levels in both the tumors and microenvironment may considerably impact the curative result of PDT. Thus, we hypothesized that the anti-tumor efficacy of PDT may be increased through the use of an exogenous NO donor. In the present study, we used DETANONOate (DETA/NO), an NO donor belonging to the family of diazoniumdiolates (formerly NONOates) [22]. It has been reported that this molecule sensitizes tumor cells to apoptotic stimuli induced by both chemotherapeutic and immunotherapeutic drugs. In addition, DETA/NO inhibits the induction of the epithelial–mesenchymal transition (EMT) phenotype by modulating the NF-κB/Snail/RKIP loop [23,24].

A combined PDT-NO donor treatment is based on the following considerations: (i) the dual role of NO in tumor biology is controversial as its capacity to promote or inhibit tumor growth depends on NO concentration and its time-dependent regulation [25]; (ii) NO modulates the activity of the NF-κB pathway [26], a major survival/anti-apoptotic pathway often dysregulated in tumors, and downstream gene products such as pro-survival and the metastasis-induced gene *Snail* and the pro-apoptotic metastasis-suppressor gene *RKIP* [23,27]; (iii) Pheophorbide *a*/PDT (Pb*a*/PDT) induces the release of cellular NO according to the dose used [28]; and (iv) Pb*a*/PDT acts through the inhibition of the NF-κB pathway via NO release [28]. In this study, we investigated *in vitro* and *in vivo* the effects of B78-H1 amelanotic melanoma cells treated with Pb*a*, DETA/NO or a combination of the two drugs. *In vitro*, we have investigated the release of NO by an indirect assay, its cytotoxic activity and its effect on cell invasion (scratch-wound assay); *in vivo*, we investigated the inhibitory effect of Pb*a* in combination with DETA/NO in mice bearing a B78-H1 syngeneic tumor.

Materials and methods

Cell lines

B78-H1 amelanotic murine melanoma cells were initially provided by Professor Giulio Jori, Department of Biology, University of Padova. The cells were cultured in DMEM (high glucose) medium which contained 10% fetal bovine serum and antibiotics (penicillin 100 U/ml, streptomycin 100 μg/ml and glutamine 2 mM) (CELBIO, Milan, Italy). All experiments were performed using cells at the exponential growth phase.

Photodynamic treatment and reagents

Pheophorbide *a* (Pb*a*) ($C_{35}H_{36}N_4O_5$; MW 592.69) was purchased from Frontier Scientific Inc, Logan, UT. Pb*a* was dissolved in dimethylsulfoxide (DMSO) and conserved in aliquots of 0.5 mM at −80 °C. The stability in aqueous solution of Pb*a* was checked by measuring its UV–vis spectrum at weekly intervals. Cells were treated with Pb*a* in the dark for 3 h, then irradiated with a metal halogen lamp at an irradiance of 8 mW/cm^2 for 30 min (14 J/cm^2). On the basis of previous results, the IC_{50} value of Pb*a*/PDT at 24 h in our model is 250 nM, that we consider as high-dose of Pb*a*/PDT; we assumed the dose of 120 nM as low-dose Pb*a*/PDT [28].

For the animal experiments, we used mPEG-Pb*a* to increase the solubility and uptake of Pb*a*. The synthesis of mPEG-Pb*a* (mPEG M.W. = 5000 Da) (97% yield) was carried out following the procedures previously described [29].

The nitric oxide donors, (Z)-1-[N-(2-aminoethyl)-N(2-aminoethyl)amino] diazen-1-ium-1,2-diolate, DETANONOate (DETA/NO) and (Z)-1-[N-3-aminopropyl]-N-[4-(3-aminopropylammonio)butyl]-amino]diazen-1-ium-1,2-diolate, spermine NONOate (SPNO), the nitric oxide inhibitors, L-N^G-nitroarginine methyl ester (L-NAME), 1400 W and carboxy-PTIO (cPTIO), an NO scavenger, were obtained from Cayman Chemical Company (INALCO, Milan, Italy). The reagents were prepared in phosphate buffered saline (PBS) before cell treatment. In the combined treatments with NO donors and iNOS inhibitors we added to the samples the same amount of DMSO used for Pb*a*. The modality of each treatment is reported in the caption of the figures. In *in vivo* experiments with DETA/NO we used a dose of 0.4 mg /kg as reported in the literature [27,30].

Cell metabolic assay

B78-H1 cells were seeded in a 96-well plate at a density of 5×10^3 cells/well. The cell proliferation, in terms of metabolic activity, was determined by the MTT (3-[4,5-dimethylthiazol-2-yj]-2,5-diphenyl tetrazolium bromide) assay following the manufacturer's instructions (Sigma–Aldrich, Milan, Italy). The values were obtained by using the spectrofluorometer Spectra Max Gemini XS (Molecular Devices, Sunnyvale, CA).

To evaluate the combination of two treatments we used the mathematical method reported by Zuluaga et al. [31] : $1 = \frac{D_1}{ID_{X,1}} + \frac{D_2}{ID_{X,2}}$

whereas D_1 and D_2 represent the concentrations of each drug in the mixture, and $ID_{X,1}$ and $ID_{X,2}$ are the concentrations of each drug that result in X% of the inhibition when given alone. When the right side of the equation (equal to the combination index (CI)) is less than 1, then synergism is indicated [31].

The scratch wound assay

Cells were seeded in a 6-well plate at a density of 6×10^5 cells/well and grown for another 24 h to 80% confluence. A denuded area was created across the diameter of the dish by a yellow tip. After treatment with drugs and light activation, the cells were washed with PBS and further incubated in a complete medium. At different times after incubation, pictures were taken with an epiluminescent microscope Leica DMI6000B (Leica Microsystem, Heidelberg, Germany) at a magnification of 10× to evaluate the migration distance. The scratch wound assay provides distinct advantages, namely: (i) the assay can be performed in any readily available plate configuration; (ii) the cells move in a defined direction, i.e., to close the wound; (iii) the movement and morphology of the cells can be followed in real time and images obtained throughout the experiment, thereby, permitting velocity measurements and also discriminating between cell migration and cell proliferation [32].

Clonogenic assay

After the PDT treatments, B78-H1 cells were seeded at a density of 5×10^3 cells in 60 mm Petri dish. After one week, the colonies were formed, fixed and stained with 2.5% methylene blue in 50% ethanol. The images were obtained by Gel DOC 2000 Bio-Rad (Milan, Italy).

Apo-ONE caspase-3/7 homogeneous assay

The Apo-ONE casapase-3/7 homogeneous assay (Promega, Milano, Italy) was used to measure the activity of caspase 3 and caspase 7. Following the manufacturer's instructions, the cells were grown in an 96-well plate at a density of 5×10^3 cells/well, and exposed to different treatments (Pb*a*, DETA/NO and combined). The assay was performed 20 h following light activation. To each well containing 25 μl of sample, 25 μl of homogeneous caspase-3/7 reagent was added (diluted 1:100 with buffer). The plate was incubated for 30 min at room temperature before measuring the fluorescence at 521 nm on a fluorescence microplate reader (Spectra Max Gemini XS, Molecular Device, Senyvale, CA) (Ex 499 nm; Em 521 nm).

Fluorimetric determination of NO with DAF-FM diacetate

B78-H1 cells were plated in a 6-well plate at a cell density of 5×10^5 cells/well. The day after, the cells were treated under different experimental conditions, described in the captions of the figures. This indirect assay to measure NO is based on DAF-FM diacetate (4-amino-5-methylamino-2′,7′-difluorofluorescein diacetate) (D-23844, Molecular Probes, Invitrogen, Milan, Italy). It diffuses into cells and tissue where non-specific esterases hydrolyze the diacetate residues thereby trapping DAF within the intracellular space. NO-derived nitrosating agents such as N_2O_3 nitrosate DAF to yield a highly fluorescent product, DAF triazole. Developed by Kojima and collaboratores [33,34], this compound has some important advantages compare to 4,5-diaminofluorescein diacetate (DAF-2 diacetate), which is the most common indicator for nitric oxide [33,34]. The spectra of the nitric oxide adduct of DAF-FM are independent of pH above pH 5.5 [35]. Moreover, the nitric oxide adduct of DAF-FM is significantly more photostable than that of DAF-2 [35], which means additional time for imaging. Finally, DAF-FM is more sensitive for NO than DAF-2 (NO detection limit for DAF-FM is ~3 nM [35], for DAF-2 is ~5 nM [34]).

A 5 mM stock solution of DAF-FM diacetate (MW = 496) in DMSO was made. The cells, after Pb*a*/PDT treatment, were incubated with 10 μM of diluted DAF-FM diacetate for 30 min at 37 °C in a phenol-red free medium DMEM (Biowhittaker LONZA, Milan, Italy) without serum. Cells were then washed with PBS to remove excess probe and replaced with fresh PBS and incubated for an additional 15 min to allow complete de-esterification of the intracellular diacetates. The cells were then trypsinized from the plate, recovered in PBS and measured by FACS (FACScan, Becton Dickinson, San Jose, CA). The signal was detected by the FL1 channel in log scale. The samples were analyzed with the CellQuest program (BD Biosciences).

Preparation of protein extracts

Total protein extract was obtained from cells plated in a 6-well plate at a density of 5×10^5 cells/well. After treatment, as described in the figure legends, the cells were washed twice with ice-cold PBS, scraped in 100 μl of Laemmli buffer (0.5 mol tris–HCl/L, pH 6.8; glycerol, 10% sodium dodecyl sulfate, β-mercaptoethanol, and 0.05% bromophenol blue) and centrifuged for 15 min at 15,000*g* at 4 °C. Supernatants were immediately frozen at −80 °C. Protein concentration was determined by the Markwell assay [36].

Western blotting analysis

The extracted proteins (30 μg) were subjected to electrophoresis on 12% SDS–PAGE and transferred to a nitrocellulose membrane 70 V for 2 h. The filter was blocked for 1 h with PBS-0.01% Tween (Sigma–Aldrich, Milan, Italy) containing 5% dry non-fat-milk, and then incubated, at 4 °C overnight, with the primary antibodies, rabbit monoclonal anti-Snail (C15D3, Cell Signaling, Merck Millipore, Darmstadt, Germany) diluted 1:1000, rabbit polyclonal anti-RKIP, (G38, Cell Signaling, Merck Millipore, Darmstadt, Germany) diluted 1:1000; rabbit polyclonal anti-NF-κB p65 (C-20, sc-372 Santa Cruz Biotechnology, Santa Cruz, CA), diluted 1:1000; rabbit polyclonal anti-iNOS antibody (NOS2, sc-651 Santa Cruz Biotechnology, Santa Cruz, CA), was used as a solution of 1:200. The expression of β-actin, used as an internal control, was detected with a mouse monoclonal anti β-actin (Ab-1, CP01, Calbiochem, Merck Millipore, Darmstadt, Germany), diluted 1:10,000. The filters were incubated for 1 h with the secondary antibodies with either anti-rabbit IgG diluted 1:5000 (Calbiochem, Merck Millipore, Darmstadt, Germany) or anti-mouse IgM, diluted 1:5000 (Calbiochem, Merck Millipore, Darmstadt, Germany). Each secondary antibody was coupled to horseradish peroxidase (HPR). For the detection of the proteins, we used ECL (enhanced chemiluminescence) reagents (Super Signal®West PICO, and Super Signal®West FEMTO, ThermoFisher Scientific Pierce, Rockford, USA). The exposure length depended on the antibodies used and was usually between 30 s and 5 min. The protein levels were quantified by Image Quant TL Version 2003 software (Amersham).

In vivo activity of mPEG-Pba/PDT + DETANONOate

Female 6-week old C57BL/6 mice were obtained from Harlan-Nossan (Italy) and were maintained in a conventional animal house for two weeks. The procedures involving animals and their care were conducted in accordance with the National Institutes of Health Guide for the Care and the Use of Laboratory Animals and were approved by the Institutional Animal Care Committee at the University of Trieste (approval number of the Italian Ministry of Health 6/2011-B). In particular, every effort was put to avoid unnecessary pain to the animals. The mice, weighing 20 g, were implanted into the upper flank by subcutaneously injection with 2×10^6 B78-H1 amelanotic melanoma cells harvested from cell cultures.

Fourteen days after the tumors reached a size of 6–8 mm (along the largest diameter) the mice were randomized into groups (a minimum of five mice for each group) and injected intraperitoneally (i.p.) with DETA/NO 0.4 mg/Kg, and after 2 h they were injected ip with 30 mg/Kg of the photosensitizer mPEG-Pb*a* solubilized in saline solution-DMSO (9 + 1v/v). Four hour after injection of the photosensitizer, a time which allows its accumulation in the tumor, the mice were anesthetized with Zoletil® + Xylazine (15 mg/kg + 15 mg/kg; i.p.), the tumor area shaved and irradiated with a laser BWN-660-60E (B&WTEK, Inc, Newark, DE) at 660 nm with a fluence rate of 193 J/cm^2. The treatment was repeated three times (once a week).

The animals were examined every two days for changes in weight, appearance of side effects or signs of sickness. The tumor growth was determined every 2–3 days up to 22 days following treatment by caliper measurements of two orthogonal axes. The tumor volume was calculated according to volume = $\pi/6 \cdot a^2 b$ where a is the shorter axis and b the larger (cm) (the tumor density was assumed to be equal to one). Survival time was calculated as the duration of the animal's life span from the inoculation of tumor cells until death.

Statistical analysis

The primary growth tumor analyses were performed by the Graph Pad PRISM. Tabled values are group means ± SE (standard error). Data were subjected to the appropriate factorial ANOVAs assessing significance against an alfa-level $p < 0.05$. When the indi-

vidual effect of the treatments and the interaction between the independent variables in a 2 × 2 ANOVA was significant, the data were subjected to *post hoc* Tukey test for significance of the differences in the mean values. All analyses were performed using standard procedures implemented in the Systat package (SYSTAT Inc., Evanston, IL). The survival analysis was performed using the Kaplan-Meier curve (SPSS 11.0 for Windows 2000 software), and the *p* values were calculated by long-rank test.

Results

Effects of DETA/NO, Pba/PDT or DETA/NO + Pba/PDT on B78-H1 murine amelanotic melanoma cells

We recently reported that NF-κB is down-regulated in B78-H1 amelanotic melanoma cells treated with a high-dose Pb*a*/PDT (i.e., with 250 nM Pb*a*, corresponding to the IC_{50} dose). We thus hypothesized that the effect was due to the photosensitizer inducing the production of a relatively high level of nitric oxide (NO). To corroborate this hypothesis, we measured the levels of the protein iNOS induced by Pb*a*/PDT as well as the release of NO/byproducts by FACS (Supplementary data, S1). To this end, NO was measured by using DAF-FM, as it is more specific then DAF-2. It should be taken into account that these fluorimentric assays have some limitations, for instance DAF-2 can be enzymatically converted not only to the triazol nitrosation product but also to other fluorescent molecules [37].

Fig. 1 shows a concentration-dependent increase of iNOS in B78-H1 cells treated with different doses of Pb*a*/PDT. The iNOS level was measured 5 h after light irradiation: the time point at which we observed a high iNOS expression induced by Pb*a*/PDT (data not shown). We found that a low-dose Pb*a*/PDT (Pb*a* concentration < IC_{50}, 120 nM), inducing the formation in the cells of a lower NO amount, results in cell recurrence and in the increase of the expression of antiapoptotic NF-κB and Snail gene products of the NF-κB/Snail/RKIP loop [28]. Since the amount of NO correlates with the type of cell response to PDT, we examined the effect of a nitric oxide donor (DETA/NO) on cell recurrence in B78-H1 cells. Fig. 2A shows that the treatment of B78-H1 cells with DETA/NO inhibits the metabolic activity (MA) in a concentration-dependent manner and this effect was directly proportional to the release of NO/byproducts in the cells (Fig. 2B). To assess the effect of a combined DETA/NO + Pb*a*/PDT treatment, we chose for each effector molecule a concentration that inhibited cell growth by ~30%: 0.25 mM DETA/NO and 120 nM Pb*a*. The combined treatment was carried out as follows: B78-H1 amelanotic melanoma cells were first treated with 0.25 mM DETA/NO for 3 h and then with 120 nM Pb*a* for further 3 h. Following the two treatments, the cells were irradiated with light at a fluence of 14 J/cm^2. Since we have found that the release of NO by DETA/NO is constant up to 6 h (Supplementary data, S2), at the time point of PDT light irradiation, the cells contained a maximum level of NO. Fig. 3 shows that the level of NO/byproducts in the cells treated with a single effector molecule, DETA/NO or Pb*a*, was slightly higher than the level of NO in the untreated cells. However, when the cells were treated simultaneously with 0.25 mM DETA/NO and 120 nM Pb*a*, a synergistic effect was obtained in the release of NO/byproducts, that reached a level of 30.12 MFI units, significantly higher than that obtained with DETA/NO (MFI 9.55) or Pb*a* (MFI 18.68).

The MA of B78-H1 cells treated with DETA/NO, Pb*a*/PDT or with both effector molecules was determined by the MTT assay. The results reported in Fig. 4A showed that, in comparison to untreated cells, each single treatment with DETA/NO or Pb*a* reduced the MA to 67% and 75% of the control (untreated cells), respectively, while the combined treatment caused a stronger inhibition to 30% of the control. The combined treatment produced a synergistic effect characterized by a combination index CI <1 (Section 2), according to Zuluaga et al. [31].

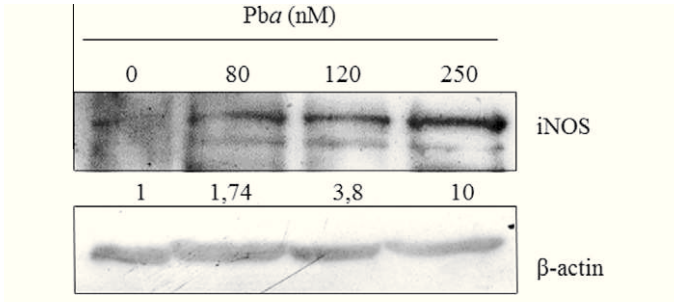

Fig. 1. iNOS protein determination by immunoblot analysis. B78-H1 cells were Pb*a*/PDT treated, by using different concentrations of Pb*a* (80, 120, 250 nM). The protein lysates were analyzed 5 h after irradiation. The iNOS band intensity was determined densitometrically, normalized to β-actin and untreated cells (0 nM Pb*a*) for each sample.

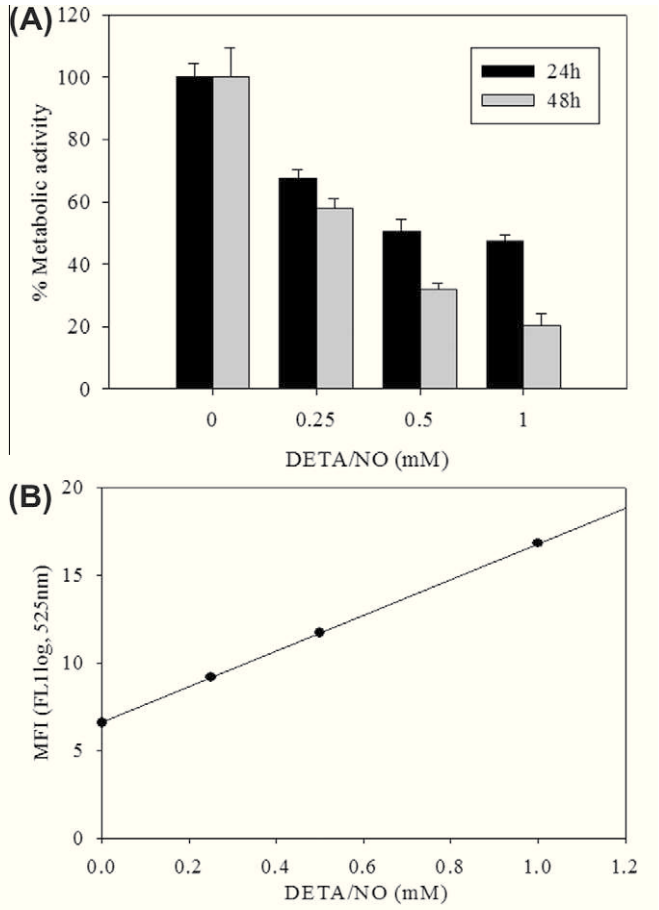

Fig. 2. Effect of different concentrations of DETA/NO on B78-H1 cells. (A) Cell metabolic assay performed by the MTT assay following treatment with different concentrations of DETANONOate (DETA/NO). B78-H1 cells were plated at a density of 5 × 10^3 cells in a 96-well plate. 24 h later, the cells were treated with DETA/NO at different concentrations. After 24 and 48 h the MTT assay was performed. (B) NO fluorescence measurements by flow cytometry in cells treated with different concentrations of DETA/NO. B78-H1 cells were plated at a density of 5 × 10^5 cells/well in a 6-well plate. They were treated with DETA/NO (0–1 mM), and after 6 h they were incubated for 30 min with DAF-FM diacetate and were then processed by flow cytometry analysis to measure the levels of nitric oxide. The graph reports the values of Mean Fluorescence Intensity (MFI), measured by FACS (FLI log, 525 nM), in relation to increasing concentrations of DETA/NO. The correlation coefficient *r* is 1 indicating a linear correlation between the concentration and the fluorescence emission.

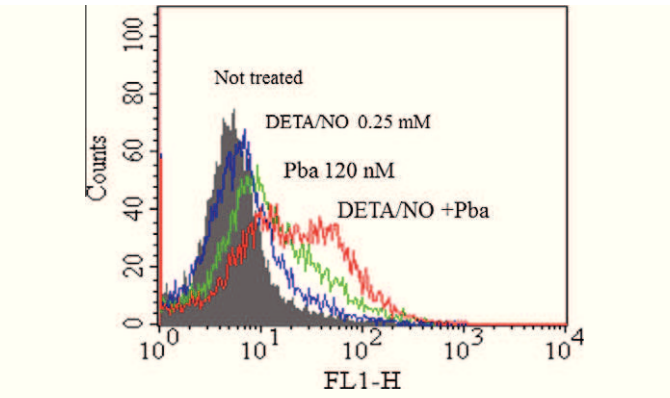

Fig. 3. Fluorescence measurements of DETA/NO, Pb*a* and combination by flow cytometry. B78-H1 cells were plated at a density of 5×10^5 cells/well in a 6-well plate. The treatments were divided into four groups: Not treated, cells treated only with light (Mean Fluorescence Intensity (MFI) = 3.84); DETA/NO, cells treated with 0.25 mM DETANONOate for 6 h and then with light (MFI = 10.23); Pb*a*, cells treated with 120 nM pheophorbide *a* for 3 h and then with light (MFI = 34.69); and DETA/NO + Pb*a*, cells treated for 3 h with 0.25 mM DETA/NO, then with 120 mM Pb*a* and after 3 h they were treated with light (MFI = 106.92). After light activation, the cells were incubated for 30 min with DAF-FM diacetate and then were processed by flow cytometry analysis.

The proliferative response, of B78-H1 cells treated with Pb*a* or DETA/NO was assessed also by the scratch-wound assay. Following the experiment in real time by a microscope, this assay permits to study the morphology and movement of the cells, and allowed to distinguish between cell migration and cell proliferation [32]. Moreover, the assay visualizes the capacity of the cells to grow under different treatment conditions. It is based on the assumption that a denuded area created in a cell plate, where the cells are 80% confluent, will be quickly healed. But if proliferation and/or migration is inhibited by the effector molecules, the cells will lose their healing capacity and the area will remain denuded. Fig. 4B and C shows a representative experiment. It can be seen that untreated cells are able to heal the wound in 48 h, due to the fact that these cells proliferate. When the cells were treated with either Pb*a* (120 nM) or DETA/NO (0.25 mM) only, they were able to grow with a sufficient rate to cover the denuded area. However, when a combined DETA/NO + Pb*a*/PDT treatment was performed, the cells did not heal the wound, and indicated the effectiveness of the combined treatment to inhibit cell growth.

Contribution of endogenous NO species produced by the cells treated with Pba or a combination of Pba and DETA/NO on metabolic activity

It has been reported that tumors containing low levels of endogenous NO respond to PDT better than tumors with higher

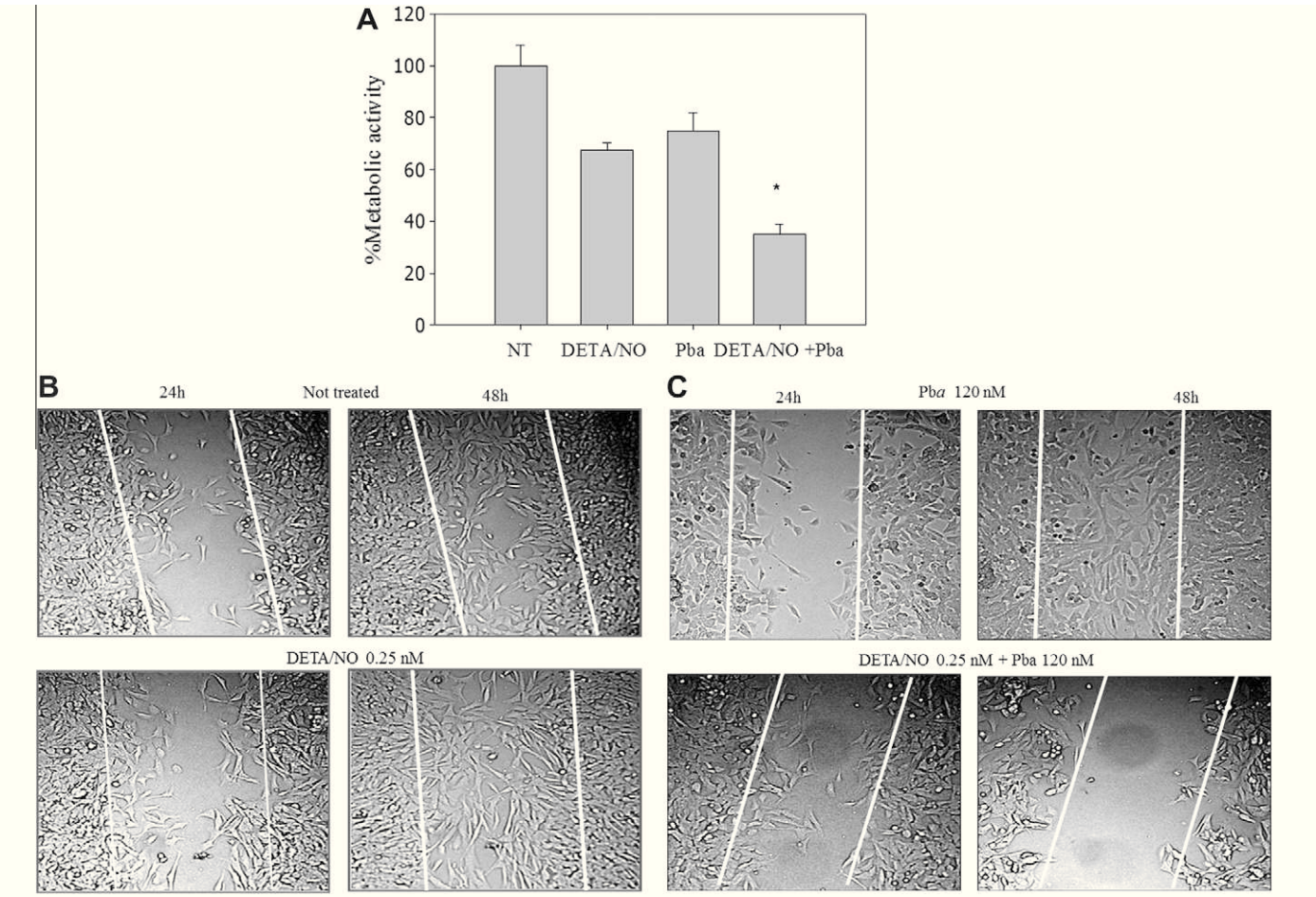

Fig. 4. Effect of treatments with DETA/NO, Pb*a*, and combination on B78-H1 cells. (A) Cell metabolic assay. B78-H1 cells were plated at a density of 5×10^3 cells/well in a 96-well plate. After attachment, the cells were divided into four groups as indicated in the legend of Fig. 2. 24 h after photo-activation, the cells were assayed by the MTT assay. The data are expressed as a mean ± SD of four independent experiments. The combined treatment results were statistically different from the other groups (standard *t*-test $^*p < 0.01$). (B) The scratch wound assay. B78-H1 cells were plated at a density of 5×10^5 cells/well in a 6-well plate. Immediately after light activation, a denudated area was done across the diameter of the dish with a yellow tip. The cells were washed with PBS and further incubated in a complete medium. At different times (24 and 48 h after light activation) pictures were taken by an epiluminescent microscope (at a magnification of 10×) to evaluate the migration of the cells.

NO levels [16,38]. In agreement, a recent study by Bhowmick et al. [39,40] showed that the COH-BR1 breast tumor was cured more efficiently with ALA/PDT when the photosensitizer was used in the presence of an inhibitor of nitric oxide synthase (L-NAME or L-NNA).

As the activity of nitric oxide synthase is normally upregulated in melanoma cell lines [41], we evaluated the effect of L-NAME, an iNOS inhibitor, in B78-H1 cells. The aim was to reduce endogenous NO in the cells before a low-dose Pb*a*/PDT treatment (Supplementary data, S3). The cells were treated with 120 nM Pb*a* for 2 h and then with 1 mM L-NAME for 1 h. At the end of the treatment, the cells were irradiated with light (14 J/cm^2). The effect on MA of the cells was determined 24 and 48 h following irradiation. The results showed that 24 h following the combined treatment, the MA was reduced to 60% of the control (untreated cells) ($p < 0.01$), whereas the single treatments produced a weaker effect (75% of the control) (Fig. 5A and B). A possible explanation of the mechanism of action of L-NAME + Pb*a* is that L-NAME, by inhibiting iNOS, reduces the consumption of O_2 so that more oxygen would be available for its reduction to ROS by Pb*a*.

The effect of L-NAME is limited in time. At 48 h following the dual treatment we observed cell recurrence with both the single and combined treatments, indicating that the cells respond to the treatment by activating survival pathways. As L-NAME is an aspecific iNOS inhibitor, we evaluated in B78-H1 cells the effects of 1400 W, a specific iNOS inhibitor, and carboxy-PTIO (cPTIO), a scavenger of nitric oxide. We observed by both the clonogenic and MTT assays that these molecules did not affect the proliferation and MA (*Supplementary* data, S4).

In the present study, we have assumed that, independently from the level of endogenous NO, the PDT activity is strengthened when a high release of NO occurs at the moment of irradiation, as this effector molecule will divert the anti-apoptotic NF-κB/Snail/RKIP loop toward apoptosis. Indeed, when we treated B78-H1 cells with DETA/NO (see scheme in Fig. 5A) and Pb*a*/PDT, the combined treatment significantly inhibited cell growth (MA <40%) at both at 24 and 48 h following treatment (Fig. 5C). The efficacy of the combined DETA/NO + Pb*a*/PDT treatment was also observed with a clonogenic assay where we found that B78-H1 cells did not recover (Fig. 5D), while L-NAME + Pb*a*/PDT treated cells did.

In order to validate these findings obtained with DETA/NO, we used another NO donor, spermine NONOate (SPNO), which is characterized by a shorter half life (30 min at 37 °C, pH 7.4) than DETA/NO (20 h) and the results were similar to those observed with DETA/NO (Supplementary data, S5).

Effect of DETA/NO, Pba/PDT and DETA/NO + Pba/PDT on the NF-κB/Snail/RKIP loop

In a previous study we have found that the level of cellular NO species modulates the NF-κB/Snail/RKIP loop, whose activity controls cell recurrence [28]. Thus, we analyzed the expression of NF-κB (p65), Snail and RKIP in cell lysates of B78-H1 cells treated with DETA/NO (0.25 mM), Pb*a* (120 nM) or DETA/NO (0.25 mM) + Pb*a* (120 nM). Cell lysates were obtained 24 h after irradiation (14 J/cm^2) of the cells. The treatment with only DETA/NO downregulated the expression of the antiapoptotic NF-κB (p65) and Snail gene products, whereas it upregulated the proapoptotic expression of RKIP. The treatment with Pb*a* had no effect on RKIP, in keeping with the fact that the cells after low-dose Pb*a*/PDT are found in a recovering phase at 48 h from treatment. However, the combined treatment of Pb*a* + DETA/NO resulted in a significant downregulation of both NF-κB (p65) and Snail and upregulation of RKIP (Fig. 6A).

Previous findings demonstrated that the overexpression of RKIP sensitizes resistant tumor cells to apoptosis induced by drugs [42,43]. Based on these findings, we measured the levels of caspases 3/7 in treated B79-H1 cells. The results reported in Fig. 6B show that treatment with DETA/NO only had no effect on caspase activation, in agreement with the literature data indicating that this NO-donor activates apoptosis through a caspase-independent way [44]. The Pb*a*/PDT treatment caused a 2-fold increase of caspases 3/7, as previously reported by us [45] and other laboratories [46]. However, a significantly stronger caspase activation was observed when the cells were co-treated with DETA/NO and Pb*a*. The caspase levels were 3.5-fold higher than those of untreated cells ($p < 0.01$).

Effects of DETA/NO, Pba and DETA/NO- Pba in mice bearing a syngeneic B78-H1 tumor

To test *in vivo* the efficacy of PDT combined with an NO donor, we used C57BL/6 mice transplanted with syngeneic B78-H1 amelanotic melanoma cells subcutaneously. As photosensitizer, we used pegylated Pb*a* (mPEG-Pb*a*) due to its superior pharmaco-distribution compared to free Pb*a* (Pb*a* and mPEG-Pb*a* have the same PDT activity [47]. When the tumor size reached 6–8 mm (along the largest diameter), the mice were treated intraperitoneally with DETA/NO (0.4 mg/Kg) and 2 h later with mPEG-Pb*a* (30 mg/Kg). Four hours after delivery, the mice were irradiated with a 660 nm-laser at 193 J/cm^2. According to our previous pharmaco-distribution data, when the mice were irradiated, mPEG-Pb*a* was present in the tumor mass [47]. We assumed that DETA/NO, being a small molecule, was also present in the tumor [27,30]. The treatment was carried out three times at days 1, 7 and 14. Following the first treatment, tumor growth was measured every 2 days with a caliper. In Fig. 7A, we report the tumor mass (mg) as a function of time (days) of the mice groups treated with the different effector molecules. It can be seen that, in comparison to untreated mice, both mPEG-Pb*a* and DETA/NO + mPEG-Pb*a* promoted a statistically significant delay of tumor growth 7 days after the first treatment ($p < 0.05$). Moreover, the growth inhibition became statistically more evident from day 13 ($p < 0.001$). The combined treatment appeared statistically different from mPEG-Pb*a* only treatment after the third administration (at day 20 $p = 0.04$; day 22 $p = 0.006$) (Fig. 7A). Although it slightly reduces tumor growth, DETA/NO did not produce a statistically significant effect. In Fig. 7B we report the median survival times (MST) obtained according to a Kaplan-Meir statistical analysis. The control untreated group shows a MST of 40 days; the DETA/NO group, 44 days; the mPEG-Pb*a* group, 52.5 days; and the combined DETA/NO + mPEG-Pb*a* group, 59 days. Compared to the control group (untreated), both mPEG-Pb*a* ($p < 0.0062$) and DETA/NO + mPEG-Pb*a*/PDT ($p < 0.0026$) groups of treated mice showed a statistically significant longer survival.

Discussion

The main objective of this study was to evaluate the anti-tumor effect of an NO donor on Pb*a*/PDT applied to B78-H1 amelanotic melanoma cells *in vitro* as well as *in vivo* in C57BL/6 mice. Although photoactivated Pb*a* is an efficient inducer of cell death by apoptosis and/or necrosis [45,47], tumor cells often respond to PDT by activating rescuing pathways leading to cell recurrence and tumor survival, in particular under non-optimal PDT conditions, i.e. when either the photosensitizer or oxygen or light is limiting. To investigate the mechanism of cell recurrence, we focused on the photoactivation process which involves the production of both ROS [48,49] and RNS [18,50]. It is known that PDT stimulates the expression of inducible nitric oxide synthase (iNOS) [18] which increases the intracellular level of NO. We found that Pb*a*, through the induction

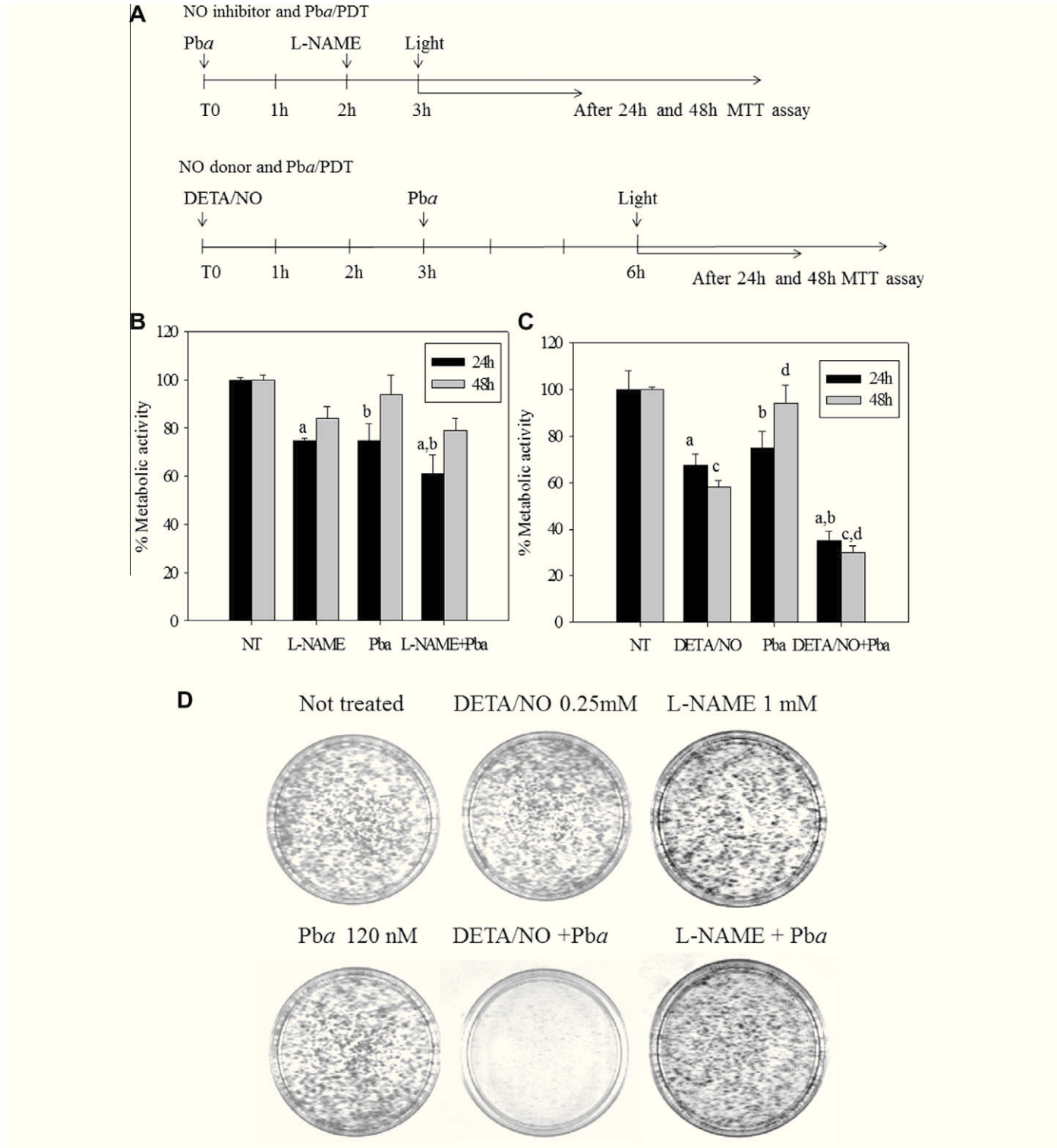

Fig. 5. Effect of different cell treatments on the metabolic activity of B78-H1 cells. (A) Schematic panels of cell treatments. Treatment with the NO-inhibitor L-NAME: 24 h after plating, the cells were treated at time 0 with Pb*a* (120 nM), after 2 h with L-NAME (1 mM), and 1 h later the cells were light irradiated. Treatment with the NO donor DETA/NO: 24 h after plating, the cells were treated with DETA/NO (0.25 mM), after 3 h with Pb*a* (120 nM) and 3 h later the cells were light irradiated. (B) Cell metabolic activity performed by the MTT assay following treatments with L-NAME, Pb*a*, and combination on B78-H1 cells, 24 and 48 h after light activation. NT: Not treated cells; L-NAME: cells treated with L-NAME 1 mM 1 h before irradiated; Pba: cells treated 3 h with 120 nM Pb*a* and then irradiated; L-NAME + Pba: cells treated with Pb*a* after 2 h with L-NAME and then after 1 h irradiated. The values "% Metabolic activity", expressed as T/C × 100, where T and C are the absorbance of treated and untreated cells, respectively, are the mean ± SD of three independent experiments. Treatments evidenced with the same letter (a and b) are significantly different, standard *t*-tests ($p < 0.01$). (C) Proliferation assay performed by the MTT assay following treatments with DETA/NO, Pb*a*, and combination on B78-H1 cells at 24–48 h after light activation. NT: not treated cells; DETA/NO: cells treated with 0.25 mM DETA/NO (6 h before light); Pba: cells treated with 120 nM Pb*a* (3 h before light); DETA/NO + Pba: cells treated with 0.25 mM DETA/NO and after 3 h with 120 nM Pb*a* (3 h before light). The values "% Metabolic activity", expressed as T/C × 100, where T and C are the absorbance of treated and untreated cells, respectively, are the mean ± SD of three independent experiments. Treatments evidenced with the same letter (a–d) are significantly different, standard *t*-tests ($p < 0.01$). (D) Clonogenic assay. After PDT treatments, the cells were plated at a density of 5×10^3 cells/60-mm petri plate. After 1 week the colonies were formed, fixed and stained with 2.5% methylene blue in 50% ethanol. The images were obtained with Gel DOC 2000 Bio-Rad.

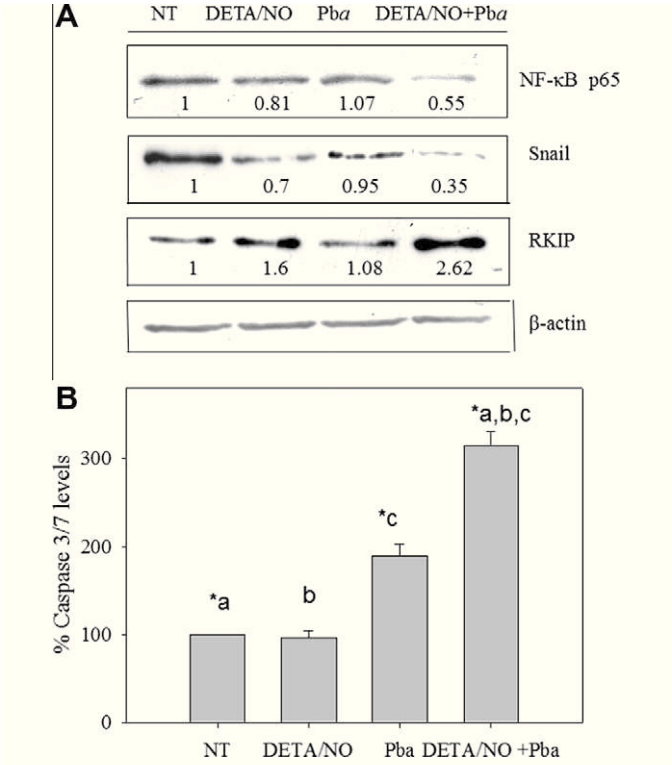

Fig. 6. Analyses by western blot and caspases activation. (A) Western blot analysis for NF-κB, Snail, RKIP, and actin. B78-H1 cells were left untreated, NT, (lane 1), treated with 0.25 mM DETA/NO (lane 2), 120 nM Pb*a*/PDT (lane 3), or with 0.25 mM DETA/NO + 120 nM Pb*a* 3h before light. Total protein lysates were recovered 24 h after light-activation. The protein band intensities were determined densitometrically, normalized to β-actin and untreated cells (NT). (B) Activation of caspases 3/7. The values are the mean ± SD of three independent experiments expressed as T/C × 100, where T is the fluorescence of treated cells and C the fluorescence (given in RFUs by the microplater reader) of untreated cells. Standard *t*-tests of each single treatment versus control ($^{*}p < 0.01$) and of combined treatment versus each single treatment ($^{a,b,c}p < 0.01$) were performed.

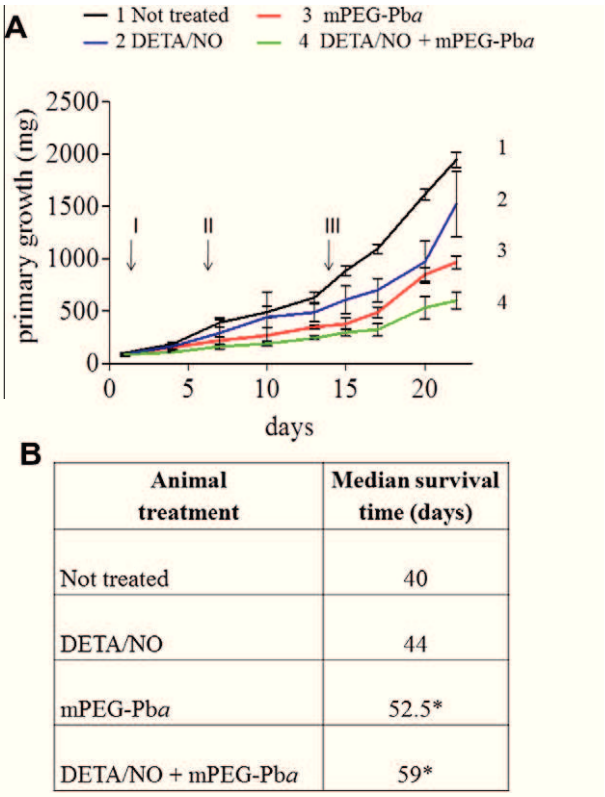

B

Animal treatment	Median survival time (days)
Not treated	40
DETA/NO	44
mPEG-Pb*a*	52.5*
DETA/NO + mPEG-Pb*a*	59*

Fig. 7. Effect of various treatments *in vivo* in mice bearing melanoma. (A) This figure represents the primary tumor growth (mg) in groups of five mice each: Not treated, mice treated only with light (193 J/cm^2); DETA/NO, mice treated with DETA/NO (0.4 mg/Kg) i.p. 6 h before light and then irradiated; mPEG-Pb*a*, mice treated i.p. with mPEG-Pba (30 mg/Kg) and after 4 h with light; DETA/NO + mPEG-Pb*a*, mice treated i.p. with DETA/NO, 2 h after with i.p. mPEG/Pb*a* and 4 h later with light; the same treatments were repeated three times: once a week (1, 7, 14 days). The groups treated with mPEG-Pba and combined treatment DETA/NO + mPEG-Pb*a* were statistically different from the not treated group (from 7 day $p < 0.05$; in the interval 13–22 days $p < 0.001$, 2 × 2 ANOVA and Tukey tests); the DETA/NO + mPEG-Pb*a* and mPEG-Pb*a* groups became statistically different at 20 day, $p = 0.04$ and 22 day = 0.006. (B) Survival of mice bearing B78-H1 melanoma and treated as above by Kaplan–Meier analyses. The mPEG-Pb*a* group and the combined treatment group were statistically different (*) from not treated group ($p = 0.0062$ and 0.0026, respectively, long-rank test).

of iNOS, inhibits the NF-κB/Snail/RKIP survival/anti-apoptotic loop [28], that controls pathways leading to apoptosis or cell recurrence [23,24,27]. On the basis of these considerations, to minimize cell recurrence occurring under low-dose PDT conditions, we used the photosensitizer in combination with an NO-donor, i.e., an effector molecule capable to generate NO inside the target cell. As a proof of principle, we used in conjunction with Pb*a*, DETA/NO, a molecule that spontaneously releases in the cytoplasm 2 mol of NO per mole of compound [51]. Nitric oxide is a small hydrophobic molecule capable of mediating a multitude of reactions [52]. It can act as an anti-oxidant against several reactive oxygen species such as hydrogen peroxide (H_2O_2) and the superoxide anion ($O_2^{\cdot -}$) [53] or as a cytotoxic agent. NO can form peroxynitrite ($ONOO^-$), a highly oxidizing and nitrating reactive nitrogen species [54], that, depending of its concentration, may trigger free radical (chain) peroxidation reactions that exacerbate the overall damage. Moreover, through the S-nitrosylation of the cysteine residues within proteins and peptides, NO can play a significant role in signal transductions [55]. For these properties, an NO donor may be a promising enhancer for cancer therapy [56,57].

The role of NO in PDT is not yet fully understood. However, our data suggest that the response of the cells to PDT depends on endogenous NO [16,58] as well as on PDT-induced NO [18]. Recent studies showed that photosensitizer-induced NO seems to be cytoprotective [18,39,40], in agreement with what we have observed with low-dose Pb*a*/PDT. It has been reported that low NO levels show a cytoprotective effect due to trapping lipid-derived radicals generated by one-electron turnover of primary LOOHs [59]. Furthermore, to rationalize the cytoprotective effect, it has been proposed that moderate levels of NO may: (i) inhibit caspases by S-nitrosylation [60]; (ii) induce downregulation of pro-apoptotic Bax and upregulation of anti-apoptotic Bcl-xL [40]; and (iii) induce cytoprotective heme oxygenase-1 [39].

Our results suggest that NO may also act through its modulation of the NF-κB/Snail/RKIP loop. As low-dose PDT elicits prosurvival/growth by upregulating the activation of NF-κB and Snail and by inhibiting the anti-proliferative expression of RKIP, a strategy to prevent cell recurrence would be to significantly increase NO in the target cells, by using a specific NO donor. High levels of NO, in fact, resulted in the inhibition of NF-κB through S-nitrosylation of p65 [27,61] and the increase of RKIP [27]. We found, indeed, that the combination of the photosensitizer with an NO donor results in a significant modulation of the NF-κB/Snail/RKIP loop towards the expression of the pro-apoptotic RKIP and the inhibition of anti-apoptotic NF-κB and Snail gene products. The clinical relevance of increasing the RKIP expression by NO correlates with a favorable clinical outcome in terms of tumor progression reduction and metastatic spread [62].

The dual treatment with an NO donor and Pb*a* has been tested in B78-H1 cells in culture and transplanted in C57BL/6 mice. To our knowledge, we demonstrate *in vivo* for the first time the anti-tumor efficacy of a photosensitizer (Pb*a*) delivered with an NO donor (DETA/NOate). The results obtained showed that the use of an NO donor significantly increased the anti-tumor efficacy of PDT. In fact, the group of mice treated with mPEG-Pb*a* and DETA/NO showed a significant delay of tumor growth compared to the untreated group. Treatment with Pb*a* alone also produced a retardation of tumor growth, but to a lower extent when compared to the combined treatment: after the third week, the curves relative to the two treatments statistically diverged ($p < 0.05$). Furthermore, the Kaplan-Meier survival analysis showed a difference of the median survival times between the mice treated with DETA/NO + mPEG-Pb*a*/PDT (59 days) and the mice treated with mPEG-Pb*a*/PDT alone (52.5 days).

In conclusion, considering that the effect of the combined treatment observed *in vivo* may be more complex than its effects *in vitro,* our data suggest that NO (and byproducts) plays an important role in the cytotoxic activity of Pb*a*/PDT used in combination with an NO donor. We are currently investigating the use of a molecular construct, i.e. a conjugate between a photosensitizer and an NO donor that allows a controlled release of NO in the tumor at the time of irradiation of the photosensitizer.

Conflicts of interest

The authors declare no conflict of interest.

Acknowledgments

This work has been carried out with the financial support of PRIN 2009, FVG 2009. The assistance of the Jonnson Comprehensive Cancer Center at UCLA is acknowledged.

Appendix A. Supplementary data

Supplementary data associated with this article can be found, in the online version, at http://dx.doi.org/10.1016/j.niox.2013.01.002.

References

[1] T.J. Dougherty, C.J. Gomer, B.W. Henderson, G. Jori, D. Kessel, M. Korbelik, J. Moan, Q. Peng, Photodynamic therapy, J. Natl. Cancer Inst. 90 (1998) 889–905.
[2] P. Agostinis, K. Berg, K.A. Cengel, T.H. Foster, A.W. Girotti, S.O. Gollnick, S.M. Hahn, M.R. Hamblin, A. Juzeniene, D. Kessel, M. Korbelik, J. Moan, P. Mroz, D. Nowis, J. Piette, B.C. Wilson, J. Golab, Photodynamic therapy of cancer: an update, CA Cancer J. Clin. 4 (2011) 250–281.
[3] C.J. Gomer, A. Ferrario, M. Luna, N. Rucker, S. Wong, Photodynamic therapy: combined modality approaches targeting the tumor microenvironment, Lasers Surg. Med. 38 (2006) 516–521.
[4] A. Ferrario, K. von Tiehl, S. Wong, M. Luna, C.J. Gomer, Cyclooxygenase-2 inhibitor treatment enhances photodynamic therapy mediated tumor response, Cancer Res. 62 (2002) 3956–3961.
[5] A. Ferrario, C.F. Chantrain, K.F. von Thiel, S. Buckley, N. Rucker, D.R. Shalinsky, H. Shimada, Y.A. DeClerck, C.J. Gomer, The matrix metalloproteinase inhibitor prinomastat enhances photodynamic therapy responsiveness in a mouse tumor model, Cancer Res. 64 (2004) 2328–2332.
[6] A. Ferrario, N. Rucker, S. Wong, M. Luna, C.J. Gomer, Survivin, a member of the inhibitor of apoptosis family, is induced by photodynamic therapy and is a target for improving treatment response, Cancer Res. 67 (2007) 4989–4995.
[7] I. Coupienne, S. Bontems, M. Dewaele, N. Rubio, Y. Habraken, S. Fulda, P. Agostinis, J. Piette, NF-kappaB inhibition improves the sensitivity of human glioblastoma cells to 5-aminolevulinic acid-based photodynamic therapy, Biochem. Pharmacol. 8 (2011) 606–616.
[8] A.P. Castano, P. Mroz, M.R. Hamblin, Photodynamic therapy and anti-tumour immunity, Nat. Rev. Cancer 6 (2006) 535–545.
[9] P.K. Lala, C. Chakraborty, Role of nitric oxide in carcinogenesis and tumour progression, Lancet Oncol. 3 (2001) 149–156.
[10] D. Hirst, T. Robson, Targeting nitric oxide for cancer therapy, J. Pharm. Pharmacol. 59 (2007) 3–13.
[11] S. Mocellin, V. Bronte, D. Nitti, Nitric oxide, a double-edged sword in cancer biology: searching for therapeutic opportunities, Med. Res. Rev. 27 (2007) 317–352.
[12] D.A. Wink, J.B. Mitchell, Chemical biology of nitric oxide: insights into the regulatory, cytotoxic, and cytoprotective mechanisms of nitric oxide, Free Radic. Biol. Med. 25 (1998) 434–456.
[13] S.R. Moncada, R.M.J. Palmer, E.A. Higgs, Nitric oxide: physiology, pathophysiology, and pharmacology, Pharmacol. Rev. 43 (1991) 109–143.
[14] S.D. Cline, J.N. Riggins, S. Tornaletti, L.J. Marnett, P.C. Hanawalt, Malondialdehyde adducts in DNA-arrest transcription by T7 RNA polymerase and mammalian RNA polymerasse II, Proc. Natl. Acad. Sci. USA 101 (2004) 7275–7280.
[15] J.D. West, J.C. Duncan, S.T. Amarnath, V. Schneider, C. Rizzo, C.J. Brash, L.J. Marnett, Induction of apoptosis in colorectal carcinoma cells treated with 4-hydroxy-2-nonenal and structurally related aldehydic products of lipid peroxidation, Chem. Res. Toxicol. 17 (2004) 453–462.
[16] M. Korbelik, C.S. Parkins, H. Shibuya, I. Cecic, M.R. Stratford, D.J. Chaplin, Nitric oxide production by tumour tissue: impact on the response to photodynamic therapy, Br. J. Cancer 82 (2000) 1835–1843.
[17] K.J. Reeves, M.W.R. Reed, N.J. Brown, Is nitric oxide important in photodynamic therapy?, J Photochem. Photobiol. B 95 (2009) 141–147.
[18] S. Gupta, N. Ahmad, H. Mukhtar, Involvment of nitric oxide during phthalocyanine (Pc4) photodynamic therapy-mediated apoptosis, Cancer Res. 58 (1998) 1785–1788.
[19] T.B. McCall, N.K. Boughton-Smith, R.M. Palmer, B.J. Whittle, S. Mocada, Synthesis of nitric oxide from L-arginine by neutrophils. Release and interaction with superoxide anion, Biochem. J. 261 (1989) 293–296.
[20] J. Mehta, D.L. Lawson, F.A. Nicolini, M.H. Ross, D.W. Player, Effects of activated polymorphonuclear leukocytes on vascular smooth muscle tone, Am. J. Physiol. 261 (1991) H327–H334.
[21] T.J. Evans, L.D.K. Buttery, A. Carpenter, D.R. Springall, J.M. Polak, J. Cohen, Cytokine-treated human neutrophils contain inducible nitric oxide synthase that produces nitration of ingested bacteria, Proc. Natl. Acad. Sci. USA 93 (1996) 9553–9558.
[22] L.K. Keefer, R.W. Nims, K.M. Davies, D.A. Wink, NONOates (1-substituted diazen-1-ium-1,2-diolates) as nirtric oxide donors: convenient nitric oxide dosage form, Methods Enzymol. 268 (1996) 281–293.
[23] B. Bonavida, S. Baritaki, S. Huerta-Yepez, M.I. Vega, D. Chatterjee, K. Yeung, Novel therapeutic applications of nitric oxide donors in cancer: roles in chemo- and immunosensitization to apoptosis and inhibition of metastases, Nitric Oxide 19 (2008) 152–157.
[24] B. Bonavida, S. Baritaki, Dual role of NO donors in the reversal of tumor cell resistance and EMT: downregulation of the NF-κB/Snail/YY1/RKIP circuitry, Nitric Oxide 24 (2011) 1–7.
[25] D. Fukumura, S. Kashiwagi, R.K. Jain, The role of nitric oxide in tumor progression, Nat. Rev. Cancer 6 (2006) 521–534.
[26] N.L. Reynaert, K. Ckless, S.H. Korn, N. Vos, A.S. Guala, E.F. Wouters, A. van der Vliet, Y.M. Janssen-Heininger, Nitric oxide represses inhibitory kappaB kinase through S-nitrosylation, Proc. Natl. Acad. Sci. USA 101 (2004) 8945–8950.
[27] S. Baritaki, S. Huerta-Yepez, A. Sahakyan, I. Karagiannides, K. Bakirtzi, A. Jazirehi, B. Bonavida, Mechanisms of nitric oxide-mediated inhibition of EMT in cancer: inhibition of the metastasis-inducer Snail and induction of the metastasis-suppressor RKIP, Cell Cycle 9 (2010) 4931–4940.
[28] V. Rapozzi, K. Umezawa, L.E. Xodo, Role of NF-κB/Snail/RKIP loop in the response of tumor cells to photodynamic therapy, Lasers Surg. Med. 43 (2011) 575–585.
[29] G.M. Bonora, P. Campaner, S. Drioli, Synthesis of selectively end-modified high-molecular weight polyethylenglycole, Lett. Org. Chem. 3 (2006) 773–779.
[30] X. Gao, D. Saha, P. Kapur, T. Anthony, E.H. Livingston, S. Huerta, Radiosensitization of HT-29 cells and xenografts by the nitric oxide donor DETANONOate, J. Surg. Oncol. 100 (2009) 149–158.
[31] M.F. Zuluaga, N. Lange, Combination of photodynamic therapy with anti-cancer agents, Curr. Med. Chem. 15 (2008) 1655–1673.
[32] A. Vogt, Advances in two-dimensional cell migration assay technologies, Eur. Pharm. Rev. 5 (2010) 26–29.
[33] H. Kojima, K. Sakurai, K. Kikuchi, S. Kawahara, Y. Kirino, H. Nagashi, Y. Hirata, T. Nagano, Development of a fluorescent indicator for nitric oxide based on the fluorescein chromophore, Chem. Pharm. Biol. 46 (1998) 373–375.
[34] H. Kojima, N. Nakatsubo, K. Kikuchi, S. Kawahara, Y. Kirino, H. Nagashi, Y. Hirata, T. Nagano, Detection and imaging of nitric oxide with novel fluorescent indicators: diaminofluoresceins, Anal. Chem. 70 (1998) 2446–2453.
[35] H. Koijma, Y. Urano, K. kikuchi, T. Higuchi, Y. Hirata, T. Nagano, Fluorescent indicators for imaging nitric oxide production, Angew. Chem., Int. Ed. 38 (1999) 3209–3212.
[36] M.A.K. Markwell, S.M. Haas, L.L. Bieber, N.E. Tolbert, A modification of the Lowry procedure to simplify protein determination in membrane and lipoprotein samples, Anal. Biochem. 87 (1978) 206–210.
[37] S. Rumer, M. Krischke, A. Fekete, M.J. Mueller, W.M. Kaiser, DAF-fluorescence without NO: elicitor treated tobacco cells produce fluorescing DAF-derivatives not related to DAF-2 triazol, Nitric Oxide 27 (2012) 123–135.
[38] M. Niziolek, W. Korytowski, A.W. Girotti, Nitric oxide-induced resistance to lethal photooxidative damage in a breast tumor cell line, Free Radic. Biol. Med. 40 (2006) 1323–1331.
[39] R. Bhowmick, A.W. Girotti, Signaling events in apoptotic photokilling of 5-aminolevulinic acid-treated tumor cells: inhibitory effects of nitric oxide, Free Radic. Biol. Med. 47 (2009) 731–740.

[40] R. Bhowmick, A.W. Girotti, Cytoprotective induction of nitric oxide synthase in a cellular model of 5-aminolevulinic acid-based photodynamic therapy, Free Radic. Biol. Med. 48 (2010) 1296–1301.
[41] M. Joshi, J. Strandhoy, W.L. White, Nitric oxide synthase activity is up-regulated in melanoma cell lines: a potential mechanism for metastases formation, Melanoma Res. 6 (1996) 121–126.
[42] S. Baritaki, A. Katsman, D. Chatterjee, K.C. Yeung, D.A. Spandidos, B. Bonavida, Regulation of tumor cell sensitivity to TRAIL-induced apoptosis by the metastatic suppressor Raf kinase inhibitor protein via Yin Yang 1 inhibition and death receptor 5 up-regulation, J. Immunol. 179 (2007) 5441–5453.
[43] F. Al-Mulla, M.S. Bitar, J. Feng, S. Park, K.C. Yeung, A new model for raf kinase inhibitory protein induced chemotherapeutic resistance, PLoS ONE 7 (2012) e29532 (Epub 2012 Jan 18).
[44] S. Huerta, G. Baay-Guzman, C.R. Gonzales-Bonilla, E.H. Livingston, S. Huerta-Yepez, B. Bonavida, *In vitro* and *in vivo* sensitization of SW620 metastatic colon cancer cells to CDDP-induced apoptosis by the nitric oxide donor DETANONOate: involvement of AIF, Nitric Oxide 20 (2009) 182–194.
[45] V. Rapozzi, M. Miculan, L.E. Xodo, Evidence that photoactivated pheophorbide a causes in human cancer cells a photodynamic effect involving lipid peroxidation, Cancer Biol. Ther. 8 (2009) 1318–1327.
[46] P.M.K. Tang, J.Y.W. Chan, S.W.N. Au, S.K. Kong, S.K.W. Tsui, M.M.Y. Waye, T.C. Mak, W.P. Fong, K.P. Fung, Pheophorbide *a*, an active compound isolated from *Scutellaria barbata*, possesses photodynamic activities by inducing apoptosis in human hepatocellular carcinoma, Cancer Biol. Ther. 5 (2006) 1111–1116.
[47] V. Rapozzi, M. Zacchigna, S. Biffi, C. Garrovo, F. Cateni, M. Stebel, S. Zorzet, G.M. Bonora, S. Drioli, L.E. Xodo, Conjugated PDT drug: photosensitizing activity and tissue distribution of PEGylated pheophorbide *a*, Cancer Biol. Ther. 10 (2010) 471–482.
[48] B.W. Henderson, T.J. Dougherty, How does photodynamic therapy work?, Photochem Photobiol. 55 (1992) 145–157.
[49] E. Buytaert, M. Dewaele, P. Agostinis, Molecular effectors of multiple cell death pathways initiated by photodynamic therapy, Biochim. Biophys. Acta 1776 (2007) 86–107.
[50] G. Di Venosa, C. Perotti, H. Fukuda, A. Batlle, A. Casas, Sensitivity to ALA–PDT of cell lines with different nitric oxide production and resistance to NO cytotoxicity, J. Photochem. Photobiol. B 80 (2005) 195–202.
[51] K.M. Davies, D.A. Wink, J.E. Saavedra, L.K. Keefer, Chemistry of the diazeniumdiolates. 2. Kinetics and mechanism of dissociation to nitric oxide in aqueous solution, J. Am. Chem. Soc. 123 (2001) 5473–5481.
[52] G.A. Blaise, D. Gauvin, M. Cangal, S. Authier, Nitric oxide, cell signaling and cell death, Toxicology 208 (2005) 177–192.
[53] D. Benz, P. Cadet, K. Mantione, W. Zhu, G. Stefano, Tonal nitric oxide and health – a free radical and a scavenger of free radicals, Med. Sci. Monit. 8 (2002) RA1–RA4.
[54] N. Tuteja, M. Chandra, R. Tuteja, M.K. Misra, Nitric oxide as a unique bioactive signaling messenger in physiology and pathophysiology, J. Biomed. Biotechnol. 2004 (2004) 227–237.
[55] D.T. Hess, A. Matsumoto, S.O. Kim, H.E. Marshall, J.S. Stanler, Protein S-nitrosylation: purview and parameters, Nat. Rev. Mol. Cell Biol. 6 (2005) 150–166.
[56] M. Cortier, L. Leon, N. Sassi, C. Paul, J.F. Jeannin, A. Bettaieb, Nitric oxide is a promising enhancer for cancer therapy, in: B. Bonavida (Ed.), Nitric Oxide and Cancer Prognosis, Prevention and Therapy, Human Press, New York, 2010, pp. 253–263.
[57] T. Efferth, Role of nitric oxide for modulation of cancer therapy resistance, in: B. Bonavida (Ed.), Nitric Oxide and Cancer Prognosis, Prevention and Therapy, Human Press, New York, 2010, pp. 265–282.
[58] K.J. Reeves, M.W. Reed, N.J. Brown, The role of nitric oxide in the treatment of tumours with aminolaevulinic acid-induced photodynamic therapy, J. Photochem. Photobiol. B 101 (2010) 224–232.
[59] M. Niziolek, W. Korytowski, A.W. Girotti, Chain-breaking antioxidant and cytoprotective action of nitric oxide on photodynamically stressed tumor cells, Photochem. Photobiol. 78 (2003) 262–270.
[60] C. Li, G.N. Wogan, Nitric oxide as a modulator of apoptosis, Cancer Lett. 226 (2005) 1–15.
[61] Z.T. Kelleher, A. Matsumoto, J.S. Stamler, H.E. Marshall, NOS2 regulation of NF-κB by S-nitrosylation of p65, J. Biol. Chem. 282 (2007) 30667–30672.
[62] S. Huerta-Yepez, N.K. Yoon, A. Hernandez-Cueto, V. Mah, C.M. Rivera-Pazos, D. Chatterjee, M.I. Vega, E.L. Maresh, S. Horvath, D. Chia, B. Bonavida, L. Goodglick, Expression of phosphorylated raf kinase inhibitor protein (pRKIP) is a predictor of lung cancer survival, BMC Cancer 11 (2011) 259–267.

Rapozzi et al. Molecular Cancer 2014, 13:75
http://www.molecular-cancer.com/content/13/1/75

MOLECULAR CANCER

RESEARCH Open Access

Anticancer activity of cationic porphyrins in melanoma tumour-bearing mice and mechanistic *in vitro* studies

Valentina Rapozzi[1†], Sonia Zorzet[2†], Marina Zacchigna[3†], Emilia Della Pietra[1], Susanna Cogoi[1] and Luigi E Xodo[1*]

Abstract

Background: Porphyrin TMPyP4 (P4) and its $C_{14}H_{28}$-alkyl derivative (C14) are G-quadruplex binders and singlet oxygen ($^1O_2$) generators. In contrast, TMPyP2 (P2) produces $^1O_2$ but it is not a G-quadruplex binder. As their photosensitizing activity is currently undefined, we report in this study their efficacy against a melanoma skin tumour and describe an *in vitro* mechanistic study which gives insights into their anticancer activity.

Methods: Uptake and antiproliferative activity of photoactivated P2, P4 and C14 have been investigated in murine melanoma B78-H1 cells by FACS, clonogenic and migration assays. Apoptosis was investigated by PARP-1 cleavage and annexin-propidium iodide assays. Biodistribution and *in vivo* anticancer activity were tested in melanoma tumour-bearing mice. Porphyrin binding and photocleavage of G-rich mRNA regions were investigated by electrophoresis and RT-PCR. Porphyrin effect on ERK pathway was explored by Western blots.

Results: Thanks to its higher lipophylicity C14 was taken up by murine melanoma B78-H1 cells up to 30-fold more efficiently than P4. When photoactivated (7.2 J/cm^2) in B78-H1 melanoma cells, P4 and C14, but not control P2, caused a strong inhibition of metabolic activity, clonogenic growth and cell migration. Biodistribution studies on melanoma tumour-bearing mice showed that P4 and C14 localize in the tumour. Upon irradiation (660 nm, 193 J/cm^2), P4 and C14 retarded tumour growth and increased the median survival time of the treated mice by ~50% ($P < 0.01$ by ANOVA), whereas porphyrin P2 did not. The light-dependent mechanism mediated by P4 and C14 is likely due to the binding to and photocleavage of G-rich quadruplex-forming sequences within the 5′-untranslated regions of the mitogenic ras genes. This causes a decrease of RAS protein and inhibition of downstream ERK pathway, which stimulates proliferation. Annexin V/propidium iodide and PARP-1 cleavage assays showed that the porphyrins arrested tumour growth by apoptosis and necrosis. C14 also showed an intrinsic light-independent anticancer activity, as recently reported for G4-RNA binders.

Conclusions: Porphyrins P4 and C14 impair the clonogenic growth and migration of B78-H1 melanoma cells and inhibit melanoma tumour growth *in vivo*. Evidence is provided that C14 acts through light-dependent (mRNA photocleavage) and light-independent (translation inhibition) mechanisms.

Keywords: Melanoma B78-H1 cells, Cationic porphyrins, Biodistribution, C57/BL6 mice, Ras genes, G4-RNA, ERK pathway

* Correspondence: luigi.xodo@uniud.it
†Equal contributors
[1]Department of Medical and Biological Sciences, School of Medicine, P.le Kolbe 4, 33100 Udine, Italy
Full list of author information is available at the end of the article

Background

Photodynamic therapy (PDT) is a rapidly expanding therapeutic modality for the treatment of a number of diseases including cancer [1-3]. PDT employs a photosensitizer which, upon irradiation, produces singlet oxygen ($^1O_2$) that damages cells [4,5]. One major objective of PDT is the search of new photosensitizers with high water solubility, low dark cytotoxycity, high capacity to penetrate the plasma membrane and generate $^1O_2$, and an ability to interact with specific cellular targets [6-8]. In previous studies from our laboratory we synthesized expanded porphyrins, composed of a macrocycle of five pyrroles, that exhibit a photodynamic activity in cancer cells at micromolar concentrations, either as free molecules or complexed to Zn or Lu [9,10]. In addition, we examined squaraines [11] and pheophorbide *a* [12-15], a chlorophyll derivative with a tetrapyrrolic macrocycle which is active at a nanomolar concentration range, comparable to that of verteporfin and temoporfin: two well-known photosensitizers used in clinic [16,17]. However, like many other photosensitizers, pheophorbide *a* is not very soluble in water, and this reduces PDT efficacy. A group of potential photosensitizers that are completely soluble in water are the cationic porphyrins TMPyP2 (called P2), with four 2-methypyridyl groups, and TMPyP4 (called P4), with four 4-methylpyridyl groups (Figure 1A). Porphyrin P4 has been extensively studied for its capacity to bind to an unusual nucleic acid conformation called G-quadruplex, formed by DNA and RNA sequences composed of blocks of guanines [18-21]. DNA and RNA G-quadruplexes (G4-DNA and G4-RNA) are stabilized by the stacking upon each other of at least two G-tetrads (a planar arrangement of four guanines each forming two Hoogsteen hydrogen bonds with the neighboring bases) and by alkali metal ions (Na^+ or K^+) that coordinate to O6 of guanines and lie in the central cavity of the structure [22]. Over the last decade G4-DNA and G4–RNA have attracted interest of several researchers providing growing evidence that these quadruplexes are involved in the regulation of gene expression. Compared to double-stranded DNA, single-stranded RNA is unconstrained and thus prone to fold into complex secondary/tertiary structures containing double-stranded and G-quadruplex elements. A bioinformatic study by Huppert et al. [23] revealed that

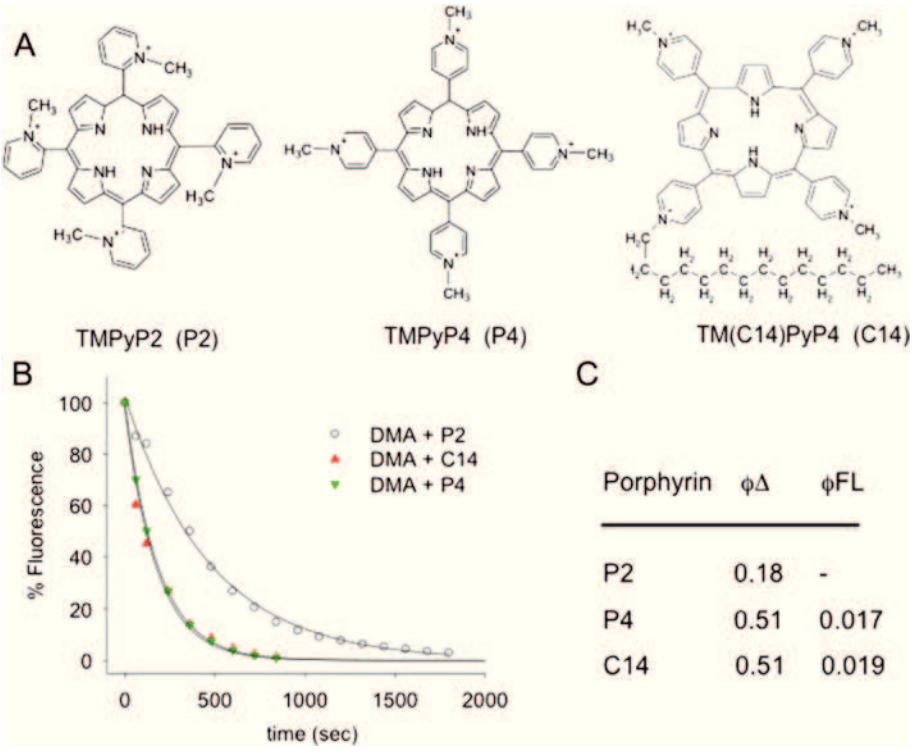

Figure 1 Structure and physical properties of the cationic porhyrins. (A) Structure of cationic porphyrins 5,10,15,20-tetra(N-methyl-4-pyridyl) porphin (TMPyP4 or P4); 5,10,15,20-tetra(N-methyl-2-pyridyl)porphin (TMPyP2 or P2) and 5,10,15-tri(N-methyl-4-pyridyl)20(N-$C_{14}H_{29}$)-4-pyridyl) porphin (C14); **(B)** DMA assay to determine the singlet oxygen quantum yield of porphyrins P2, P4 and C14. Full lines are the best-fit of experimental points to first order decay equation y = exp(-kt). Irradiation was performed with 60 mW lamp. Fluorescence quantum yield data are from [34]; **(C)** Singlet oxygen and fluorescence quantum yield values.

about 3000 5′-UTR of the human transcriptome contains one or more G-quadruplex motifs. This brought the authors to the conclusion that these tertiary structures should regulate translation. They also demonstrated that an RNA quadruplex-forming sequence within the 5′-UTR of the *NRAS* transcript inhibited translation *in vitro* [24]. Ever since, there has been a growing literature on the possible functions of RNA G-quadruplexes [25-27]. As G4-RNA can indeed inhibit translation, the use of small molecules to inhibit the function of mRNA looks quite attractive [28].

In our study we focus on bifunctional G4 RNA-interacting agents, *i.e.* molecules capable not only to bind to RNA G-quadruplexes with a high affinity but also to generate singlet oxygen ($^1O_2$) upon irradiation. In most human cancers the RAS-MEK-ERK pathway that controls proliferation is hyperactive [29,30]. The activator of this pathway is protein RAS which is expressed by the ras genes (*KRAS, NRAS* and *HRAS*). These genes are characterized by the presence in the 5′ end of mRNA of a guanine rich untranslated region (5′-UTR) containing quadruplex-forming motifs which can serve as targets for small molecules with photosensitizing properties. Of particular interest is *KRAS*, as it contains a 192-nt 5′-UTR with 45% guanines that can fold into a cluster of G4-RNA structures and is in principle capable of providing multiple binding sites for cationic porphyrins [18-21]. The 5′-UTR of *NRAS* also harbors a G-rich motif forming a very stable G-quadruplex structure.

Against this background we have hypothesized a new strategy to down-regulate in cancer cells the mitogenic RAS/MEK/ERK pathway [31]. We reasoned that the porphyrins delivered to the cells should bind to mRNA, in particular at G-rich quadruplex-forming sequences in the 5′-UTRs of the ras genes. Upon irradiation, the porphyrins mediate a photoprocess leading to the degradation of mRNA, inhibition of ERK pathway and cell proliferation. This therapeutic approach has been tested in murine amelanotic melanoma B78-H1 cells both *in vitro* (cell cultures) and *in vivo* (B78-H1 melanoma cells transplanted in C57/BL6 mice). B78-H1 melanoma cells derive from the B16 clone and have an activated RAS/MEK/ERK pathway [32]. As bifunctional photosensitizing agents we tested the cationic porphyrins tetra-meso (N-methyl-4-pyridyl) porphine (called P4) and C14-alkyl derivative tri-meso(N-methyl-4-pyridyl), meso(N-tetradecyl-4-pyridyl) porphine (called C14). As a control, we used the positional isomer tetra-meso(N-methyl-2-pyridyl) porphine (called P2), which does not bind to G4-RNA. In the following we demonstrate that the cationic porphyrins C14 and P4 strongly inhibit the growth of melanoma cells both in vitro and in vivo. This anticancer effect correlates with the capacity of these porphyrins to bind to the G-rich region of mitogenic ras genes.

Results and discussion

Singlet oxygen generation by porphyrins C14, P4 and P2

The structures of porphyrins C14, P4 and P2 are shown in Figure 1A. Due to their cationic charges they are very soluble in aqueous solutions and obey the Lambert-Beer law over a wide concentration range (not shown). Their capacity to generate $^1O_2$ was examined by the 9,10-dimethylantracene (DMA) photobleaching assay [33]. DMA is a fluorescent dye [$\lambda_{ex} = 375$ nm, $\lambda_{em} = 436$ nm] that reacts selectively with $^1O_2$ to form a non-fluorescent endoperoxide derivative. An equimolar solution of DMA and porphyrin (10 μM each) was irradiated with a lamp (60 mW) for different periods of time up to 1000 s and the residual fluorescence was recorded between 380 and 550 nm. The residual fluorescence was plotted as a function of time and the experimental curve was best-fitted to a first order decay equation $y = \exp(-k \cdot t)$ where k (s^{-1}) is the rate constant and t the time(s) (Figure 1B). We obtained $k = 0.0058 \pm 0.0004$ s^{-1} for P4 and C14 and $k = 0.0021 \pm 0.0006$ $s^{-1}$for P2. Considering that the quantum yield of singlet oxygen generation (ϕΔ) of P4 was reported to be 0.51 [34], we found that the ϕΔ of C14 and P2 were respectively 0.51 and 0.18 (Figure 1C). It is worth noting that porphyrin P2, being non planar due to steric clashes between the 2-methyl-pyridyl groups and the 3-pyrrol hydrogens, shows a lower ϕΔ.

Cellular uptake and phototoxicity of the cationic porphyrins

The uptake of the cationic porphyrins by melanoma B78-H1 cells has been investigated by FACS, taking advantage of the fact that the porphyrins emit red fluorescence when they are excited at 488 nm. Figure 2A shows a typical FACS analysis of B78-H1 cells treated with 10 μM porphyrins for 2, 4, 8 and 24 h. As observed with human Panc-1 cells [31], C14 is taken up by melanoma cells more efficiently than P2 or P4. After an incubation of 24 h, the fluorescence of the cells treated with C14 is 25 and 50-fold higher than that observed with P4 and P2, respectively. The data show that the addition to P4 of the lipophilic chain significantly enhances the cellular uptake.

The photoactivity of the porphyrins in B78-H1 cells (24 h after delivery) has been evaluated by resazurin assays (Figure 2B). Without irradiation the porphyrins are not cytotoxic (not shown), but when they are irradiated with a halogen lamp at a fluence of 7.2 J/cm^2, C14 and P4 decrease the metabolic activity of the cells, at concentrations < 1 μM, while P2 shows some bioactivity only at concentrations > 20 μM. A dose-response assay is shown in Figure 2B. From these plots we estimated IC_{50} values of about 10 and 200 nM for C14 and P4 and 30 μM for P2. These values correlate with the different uptake of the three porphyrins.

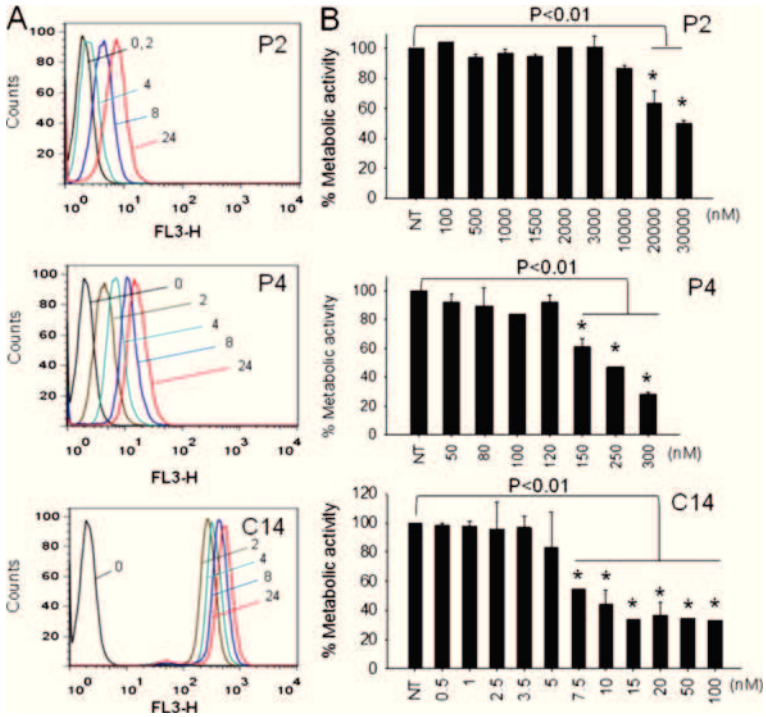

Figure 2 Uptake and metabolic activity of the cationic porphyrins. (A) FACS analyses of B78-H1 cells treated with 10 μM porphyrin. The fluorescence associated to the cells (Ex 420 nm, Em 650–720 nm), was detected at 2, 4, 8 and 24 h after drug delivery; **(B)** % Metabolic activity of B78-H1 cells treated with increasing amounts of porphyrin. 24 h after porphyrin delivery the cells have been irradiated with a halogen lamp at the fluence of 7.2 J/cm^2. A resazurin assay was carried out 24 h after irradiation. Experiments have been performed in triplicate, a Student T-test is reported * = P < 0.01.

The impact of the photoactivated porphyrins on the clonogenic growth of B78-H1 melanoma cells was also examined (Figure 3A). The cells treated with the porphyrins were seeded in plates and after an incubation of 7 days the colonies were stained with methylene blue. The data show that the untreated cells formed colonies uniformly distributed in the plate (control). In contrast, the cells treated with P4 and light (7.2 J/cm^2) showed ~30% reduction in the number of colonies, while C14/light completely arrested the clonogenic growth. In contrast, porphyrin P2/light did not have any inhibitory effect on colony formation.

As a next step, the inhibition of proliferation and migration of B78-H1 cells caused by the cationic porphyrins was assessed by the scratch-wound healing assay. This assay is based on the assumption that a denuded area created in a plate (80% confluent) will quickly heal thanks to proliferating and migrating cells. But as soon as proliferation and migration are inhibited by the effector molecules, the cells will lose their healing capacity and the area will remain denuded. Figure 3B reports a typical experiment showing that B78-H1 cells untreated or treated with P2 and light are able to heal the wound in 24 h. Instead, when the cells are treated with an IC$_{50}$ dose of P4 or C14 and light, they are not able to grow and migrate with a sufficient rate to cover the denuded area.

Having established that photoactivated P4 and C14 arrest proliferation, we asked if this effect was due to apoptosis. An early event occurring in apoptosis is the translocation of phosphatidylserine from the inner to the outer leaflet of the plasma membrane, thus exposing it to the external cell environment. Annexin V, a phosphatidylserine recognizing protein labeled with FITC, can be used to detect this event by FACS. Early apoptosis and late apoptosis/necrosis can be distinguished by using annexin V and propidium iodide (PI) together (Figure 4A). The percentage of apoptotic/necrotic cells is reported in Table 1. It can be seen that C14 (10 nM) strongly induces apoptosis (43%) and necrosis (38%) in the melanoma B78-H1 cells, whereas P4 (250 nM) appears less efficient in triggering apoptosis (26%) and necrosis (11%). The treatment with P4 produces, however, a larger amount of cell debris than with C14 (18% against 9%). From this experiment we concluded that C14 and P4 promoted in melanoma cells both apoptosis and necrosis and not only necrosis as previously found with fibrosarcoma cells [35].

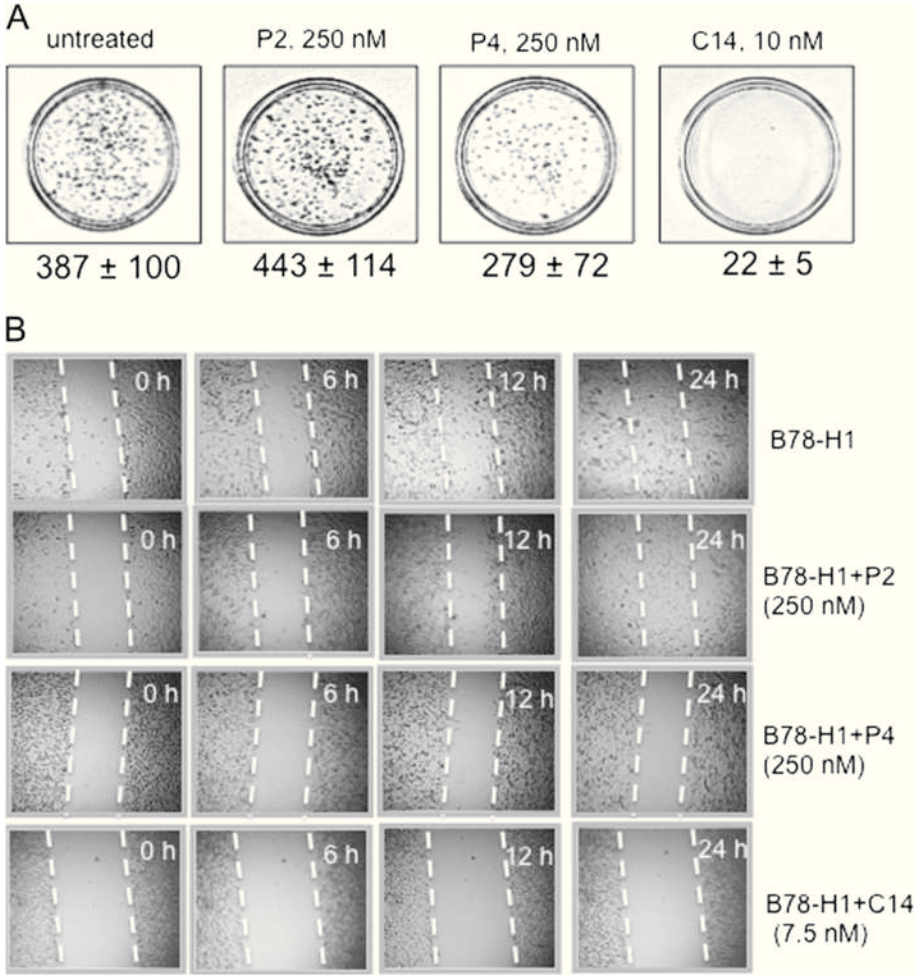

Figure 3 Clonogenic and scratch-wound assays. (A) Clongenic growth of B78-H1 cells treated with porphyrin at concentration near the IC_{50}: C14 (10 nM), P4 (250 nM). The cells have been treated with porphyrin /light and let to grow for one week. The colonies formed have been fixed, stained with methylene blue and counted. The number of colonies (>50 cells) is reported below each plate. The experiment has been perfomed in duplicate; **(B)** Scratch-wound assay of B78-H1 cells plated at density of 6×10^5 cells/well in a 6-well plate. After attachment, the cells were treated with 7.5 nM C14, 250 nM P2 and P4. A denudated area was created across the diameter of the dish with a yellow tip. Cells were washed with PBS and further incubated in complete medium. After light irradiation (7.2 J/cm^2), pictures were taken by an epiluminescent microscope (at 10-fold magnification) to evaluate the migration of the cells. The experiment has been perfomed in duplicate.

To confirm the presence of apoptosis in B78-H1 cells treated with the porphyrins, we measured by immunoblotting the cleavage of poly-(ADP ribose)-polymerase (PARP-1) by caspases, as this is considered one of the best markers for apoptosis [36]. In keeping with annexin/PI, Figure 4B shows that P4 and C14 induced the cleavage of PARP-1, while P2 did not. The extent of cleavage is proportional to the percentage of apoptotic cells found by FACS. Indeed, the cells treated with C14 showed 43% apoptosis and ~50% PARP-1 cleavage, while those treated with P4 had 26% apoptosis and ~10% PARP-1 cleavage.

Given the strong impact on clonogenic growth and mobility caused by P4 and C14 in B78-H1 melanoma cells, we asked whether these molecules are also able to inhibit the growth of a B78-H1 melanoma tumour subcutaneously transplanted in mouse. To address this question, we first had to know how the porphyrins distribute in the mouse body, in order to determine the time point at which the porphyrins show a high accumulation in the tumour after delivery.

Biodistribution of the cationic porhyrins

The time-dependent distribution of P2, P4 and C14 after injection in the peritoneum (i.p.) of female C57/BL6 mice bearing a subcutaneous B78-H1 melanoma tumour of about 6–8 mm was examined as previously described

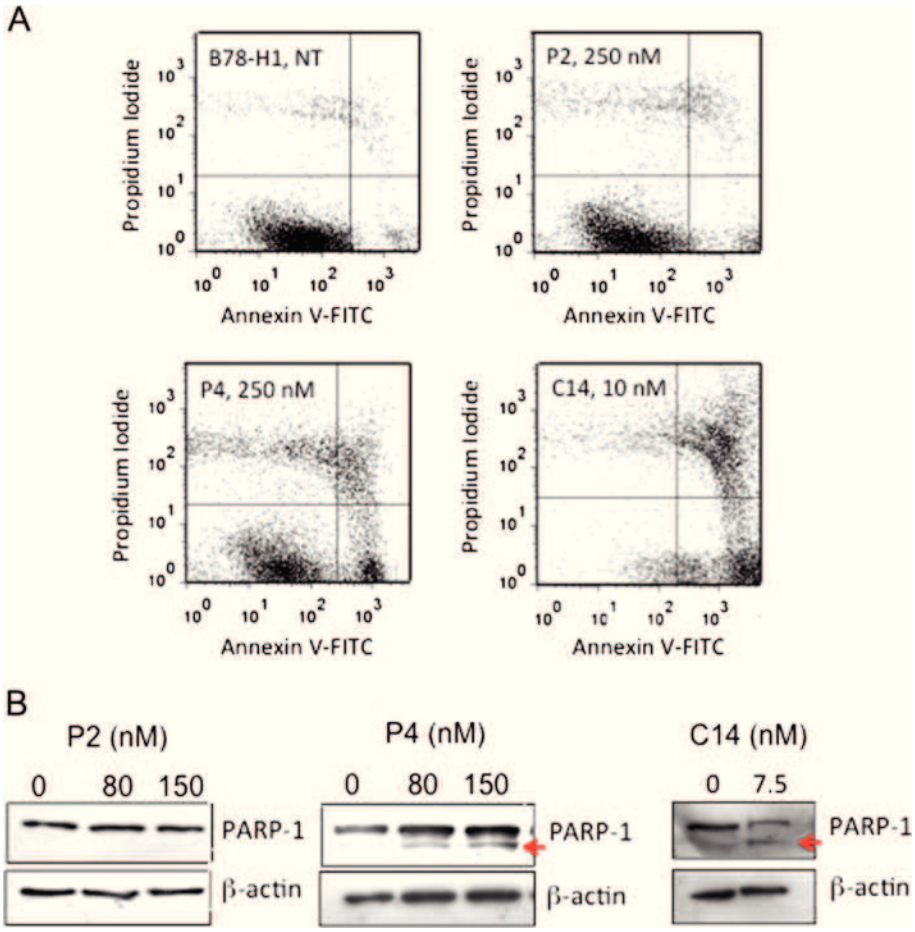

Figure 4 Annexin V-propidium iodide and PARP-1 cleavage assays. (A) Annexin V-propidium iodide assay of B78-H1 cells treated with 250 nM P2 or P4 and 10 nM C14. The proportion of cell population in apoptosis and necrosis is reported in Table 1. Before the FACS analysis the cells have been treated with porphyrin and light (7.2 J/cm^2). The experiment has been performed in triplicate; **(B)** Levels of PARP-1 and β-actin in B78-H1 cells untreated or treated with 80 and 150 nM P2 and P4, 7.5 nM C14. The Western blots show the cleavage of PARP-1.

[37]. Porphyrins P2 and P4 were injected (and not treated with light) at a concentration of 30 mg/Kg, while C14, due to its higher cytoxicity, was used at a concentration of 9 mg/Kg. For each molecule three animals were sacrificed at each time point: 1, 3, 6, 9 and 24 h post-injection. The amount of porphyrin recovered from the various organs was measured as described in Materials and Methods and the percentage of injected dose per gram of organ (% ID/g) was determined and reported in Figure 5. At 1, 3 and 6 h post-injection, the porphyrins were detected in all the organs, except in the brain. It is noteworthy that the amount of injected dose in the tumour is higher than in normal tissues, except liver and kidneys. Surprisingly, P4 showed a higher tumour accumulation than C14 (at 9 h after delivery % ID/g P4 ~ 2.5 *versus* % ID/g C14 ~ 0.9). It is possible that the alkyl group reduces the capacity of C14 to diffuse from the peritoneus. Indeed, the presence of C14 in the intestine is greater than that of P4, at 3, 6 and 9 h post injection. The amount of P2 in the organs is relatively low, and this correlates with the low cellular uptake of this molecule.

Table 1 Percentage of normal, apoptotic and necrotic B78-H1 cells treated with P2, P4 or C14

Porphyrin	% N T[§]	% Ap C[§]	% Ne C[§]	% Debris
NT	91	4	2	3
P2[&]	77	11	5	7
P4[&]	45	26	11	18
C14[&]	10	43	38	9

[&]P2 and P4 used at 250 nM, C14 used at 10 nM; [§]NT = untreated cells; Ap C = apoptotic cells; Ne C = necrotic cells.

The presence of C14 and P4 in liver, duodenum and blood (not shown) up to 3 h post-injection suggests that the porphyrins are recycled via the enterohepatic pathway, but at higher time points, the urinary output

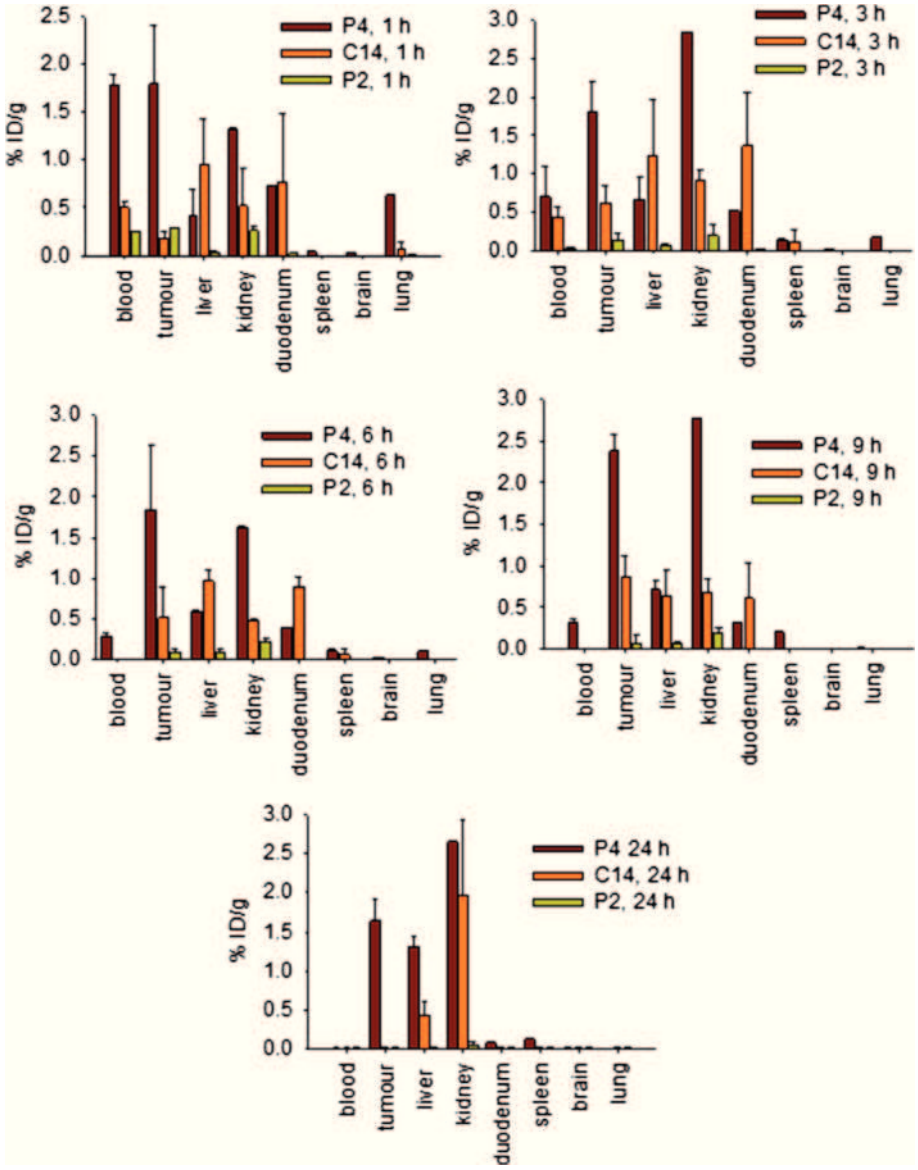

Figure 5 Biodistribution of cationic porphyrins. Biodistribution of the porphyrins in various organs, after i.p. injection in C57/BL6 mice, bearing a subcutaneous melanoma tumour, at the concentration of 30 mg/Kg P2 and P4 and 9 mg/Kg C14 (the mice were not irradiatiated). Ordinate reports the percentage of injected dose (% ID). Distributions at 1, 3, 6, 9 and 24 h post injection are shown. Each bar is the average of 3 values (3 mice).

prevails over the bile-gut recycling. Furthermore, the fact that the porphyrines are practically not found in the spleen, suggests that their elimination through the reticolo-endothelial system is limited, contrarily to what has been observed with more hydrophobic photosensitizers [38].

Porphyrins P4 and C14 reduce tumour growth and increase the mouse median survival time

To evaluate *in vivo* the anticancer property of P2, P4 and C14, C57/BL6 mice with a subcutaneous B78-H1 melanoma tumour of about 6–8 mm were randomized into groups of 8 animals each (the animals were prepared as reported in Materials and Methods). In Figure 6A we report the results obtained with P2 and P4. Group 1 was untreated, groups 2 and 3 were i.p. injected with P2 (30 mg/Kg) and P4 (30 mg/Kg), respectively, groups 4 and 5 were injected with P2 (30 mg/Kg), P4 (30 Kg/mg) then irradiated at the Q-1 band (620–690 nm) with a diode laser at 660 ± 5 nm (fluence of 193 J/cm^2), i.e. in the optical therapeutic window where light is harmless and shows its maximum depth of tissue penetration, as previously described [37,39] (Additional file 1: Figure S1).

Irradiation was carried out ~7 h after delivery, when the molecules showed a significant accumulation in the tumour. We performed three porphyrin-light treatments,

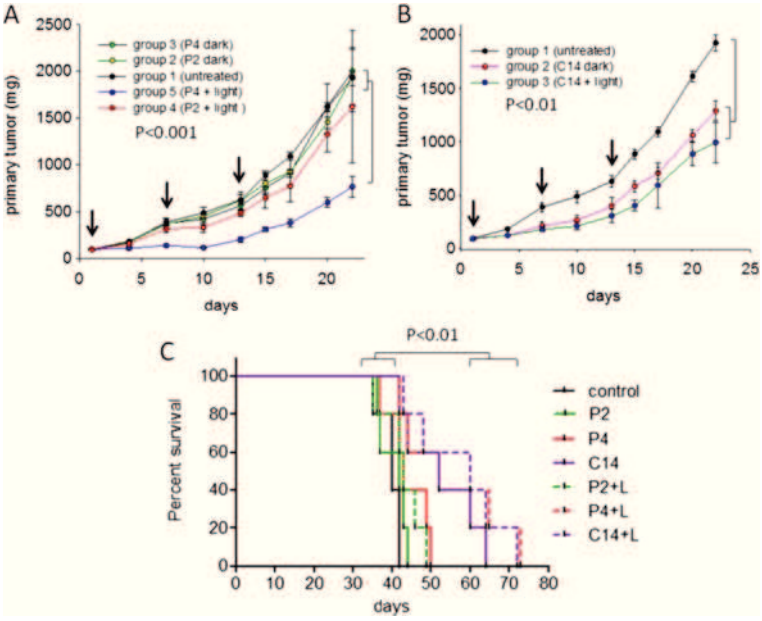

Figure 6 Effect of porphyrins on melanoma tumour-bearing mice. (A) The mice with a melanoma tumour of about 8 mm were randomized in 5 groups, each of 8 mice. Group 1 was untreated. Groups 2 and 3 were treated with 30 mg/Kg of P2 and P4; groups 4 and 5 were treated with P2 and P4 (30 mg/Kg) then irradiated with a laser at 660 ± 5 nm (193 J/cm^2), 9 h after delivery; **(B)** The mice were treated as follows. Group 1, untreated; group 2, treated with 3 mg/Kg of C14; group 3, treated with 3 mg/Kg C14 and irradiated. Three treatments have been carried out: at days 1, 7 and 14. A statistical analysis by ANOVA is reported. Each point of the curves is the average of 8 values (8 mice); **(C)** Kaplan-Meir showing the median survival time of the treated mice compared to untreated (control) or mice treated with the porphyrin but not irradiated.

at days 1, 7 and 14. The melanoma tumour grew with its typical aggressiveness in the untreated mice (control), and the mice showed a median survival time (*m.s.t.*) of about 43 days (Figure 6C). The treatment with P2 and P4 without irradiation did not delay tumour growth and did not increase the *m.s.t.* compared to control (Figure 6A,C). In contrast, when the tumour was irradiated with the laser, a significant delay in tumour growth was obtained with P4, but not with P2, in keeping with the scarce uptake and photosensitizing property of P2. As a further control, we measured the rate of tumour growth when the mice were irradiated in the absence of porphyrin, but no effect was observed (not shown). The impact of P4 on tumour growth was significant after the second treatment (day 7) compared to both the untreated group ($P < 0.001$ by ANOVA) and the group treated with P4 without irradiation ($P < 0.01$). The Kaplan-Maier survival curves showed that treatment with P4 and light increased the *m.s.t.* by ~ 50% compared to the untreated group (from 40 to 60 days) or the group treated with P2 and light (from 42 to 60 days) ($P < 0.01$). In Figure 6B we show the behaviour of C14. Porphyrin C14, at the concentration of 3 mg/Kg, inhibited tumour growth and increased the *m.s.t.*, as does P4 at 30 mg/Kg (Figure 6B,C). However, contrarily to P4, porphyrin C14 affected somewhat tumour growth, even in the absence of irradiation. After the second PDT-treatment (day 7), tumour growth in the groups treated with C14/dark and C14/light was lower than in the untreated group ($P < 0.05$ and $P < 0.01$, respectively). The dual effect of C14 appears more evident when the survival curves are examined. Compared to the untreated group, C14 with and without irradiation increased the median survival time from 40 to 60 and 52 days, respectively ($P < 0.01$ for both groups). The likely mechanism by which C14-dark reduces tumour growth will be discussed in the next sections.

In summary, photoactivated C14 and P4 showed a remarkable capacity to delay tumour growth in a melanoma mouse model and to increase the survival of the treated mice. Since the cationic porphyrins have a high affinity for RNA G-rich sequences folded into G-quadruplex structures [31], we interrogated whether the antitumour activity of the porphyrins correlates with their binding to RNA.

The cationic porphyrins bind to G-rich quadruplex-forming sequences of mRNA

Previous studies have shown that mitochondria are major intracellular targets for hydrophobic photosensitizers, while cationic P4 seems to locate in the lysosomes [35]. So

far however, research on PDT did not focus on nucleic acids as targets for photosensitizers. Considering that P4 and C14 accumulate in the cytoplasm and are cationic in nature, they should interact with negatively charged mRNA. There is a vast literature on porphyrin P4's capacity to bind to DNA, in particular at G-rich quadruplex-forming sequences occurring in the promoters of the genes and at the ends of the chromosomes [40-47]. It seems therefore reasonable to assume that if a quadruplex structure is extruded by genomic G-rich sequences, these structures should form more easily by unconstrained single-stranded mRNA. We thus hypothesized that cationic porphyrins could bind to G4-RNA structures formed by mRNA. Considering that in all stages of melanoma the key signaling cascade stimulating proliferation is the RAS/MEK/ERK pathway [48], we focused on the ras genes that encode for protein RAS: the pathway activator [49]. The ras genes show a high homology and their transcripts are composed of six exons of which the exon at the 5′-end is untranslated (5′-UTR) [50]. The 5′-UTR of *KRAS* has a guanine content of 44% and five quadruplex-forming sequences [31] (Figure 7A). Also *NRAS* [24] and *HRAS* include in their 5′-UTR G-rich sequences that can fold into G4-RNA structures (Additional file 2: Figure S2). Quadruplex formation by mRNA sequences can easily be detected by circular dichroism (CD). Typical CD spectra at various temperatures for the *KRAS* sequence that we called utr-2 are shown in Figure 7B. The spectra clearly show that utr-2 forms a parallel quadruplex with a T_M of 54°C in 100 mM KCl [51]. In Table 2 we report the melting data for some quadruplex-forming sequences of the ras genes. These folded RNA structures are strong targets for cationic porphyrins. Indeed, upon binding to the G4-RNA, the porphyrin's Soret band undergoes strong hypochromic and bathochromic effects (Figure 7C). Analyzing the data with a simple binding equation (Sigma plot 11.0), we found that the interaction between C14 and utr-2 G4-RNA is characterized by a K_D of ~ 5×10^{-7} M.

The porphyrins mediate the photocleavage of mRNA

Next, we asked if mRNA is indeed degraded by the photoactivated porphyrins. To address this question we used three ^{32}P-radiolabelled RNA fragments adopting one of the possible conformations present in mRNA: G4-RNA, duplex and single-stranded RNA. The three radiolabelled RNA substrates were incubated with

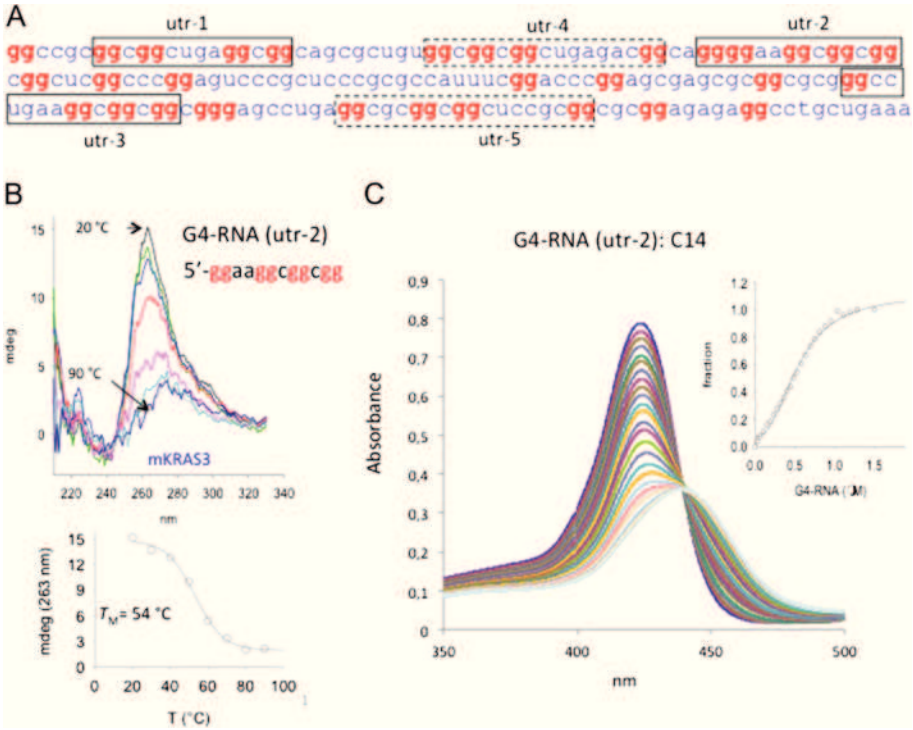

Figure 7 G4-RNA formation within 5′-UTR of ras mRNAs. (A) Sequence of 5′-UTR in the murine *KRAS* mRNA. The quadruplex-forming sequences (QFS) utr-1, utr-2, utr-3, utr-4 and utr-5 are boxed (strong QFS, full line; weak QFS broken line); **(B)** Typical CD spectra at various temperatures (from 20 to 90°C) of sequence utr2. Spectra have been collected at 20–30–40–50–60–70–80–90°C, using RNA 10 μM RNA, 50 mM Tris-HCl, pH 7.4, 100 mM KCl. The ordinate reports the CD values in mdeg. Graph below shows the CD-melting curve of the utr-2 G-quadruplex; **(C)** UV-vis titration of porphyrin C14 (6 μM) with quadruplex utr-2. Inset shows the fraction of bound C14 as a function of G4-RNA. The experimental points have been best fitted to a standard binding equation (Sigma Plot 11.0).

Table 2 Circular dichroism data of 5′-UTR sequences in mKRAS and mNRAS

	Sequence5′ → 3′	T_M[°C]	CD	KCl (mM)]
NRAS	GGGGGCGGGGCGGGGCUGGACUGGG	74	Parallel	20
KRAS [utr1]	GGCGGCUGAGGCGG	68	Parallel	100
KRAS [utr2]	GGAAGGCGGCGG	54	Parallel	100
KRAS [utr3]	GGCCUGAAGGCGGCGG	61	Parallel	100

porphyrin P2, P4 or C14 at r = 1, 3 and 6 (r = [porphyrin]/[RNA]) and irradiated with a halogen light at a fluence of 7.2 J/cm^2. The extent of photocleavage was quantified and reported as histograms in Figure 8A. In the absence of irradiation the porphyrins, even at r = 6, did not promote any degradation (lane 2). Irradiation, in the absence of porphyrin, did not affect RNA either (lane 14). In contrast, when the samples were irradiated in the presence of the porphyrins, a photochemical process leading to RNA degradation took place. The highest cleavage is observed with the G4-RNA substrate (*KRAS* utr-2 at r = 3 and 6) (lanes 4 and 5), in keeping with the fact that P4 and C14 show a higher affinity for the quadruplexes than the duplex or single-stranded substrates [31].

Finally, we checked if the level of cellular mRNA is actually reduced by the photoactivated porphyrins. By quantitative RT-PCR, we found that 1 h after irradiation P2 did not appreciably decrease the level of ras transcript, while 15 or 30 nM C14 reduced *KRAS* mRNA by ~50% compared to the control (cells tretead with porphyrin but non irradiated). Porphyrin P4 also reduced the mRNA but only at the highest concentration (500 nM) (Figure 8B). These data are in keeping with those obtained in Panc-1 cells and support our hypothesis that the cationic porphyrins target mRNA [31].

C14 exhibits also an intrinsic light-independent anticancer activity

Several studies have hypothesized that the formation of secondary or tertiary structures within the 5′-UTR of mRNAs may have important functions in the regulation of translation [25]. Since Balasubramanian and coworkers have demonstrated that an RNA-forming sequence located in *NRAS* mRNA inhibited translation *in vitro*, there has been a growing interest in G4-RNA in the 5′-UTR of mRNA [24]. To interfere with the translation process, small molecules binding to G4-RNA in 5′-UTR of mRNA have been used [28]. By stabilizing G4-RNA, these ligands should impair the assembly and/or scanning of the 43S ribosomal complex along mRNA. For example, quinolone dicarboxamide derivatives and bisquinolinum compounds showed translational inhibition [52,53]. The finding that C14 without irradiation slows down tumour growth and increases the median survival time by 35% (from 40 to 52 days) may be rationalized in terms of translation inhibition. Due to its high cellular uptake, C14 accumulates in the cytoplasm more than P4. Its binding to G4-RNA in the 5′-UTR of ras mRNA (*KRAS* and *NRAS*) may inhibit the translation process. Indeed, when we measured by immunoblotting the level of total protein RAS in B78-H1 cells treated with 1 or 5 μM P2, P4 and C14 (in the absence of light), we found that the protein was significantly reduced by 5 μM C14, but not by P2 and P4 (Figure 9A). The drop of RAS protein caused by C14 in the dark is likely to be the cause of the observed decline of tumour growth and increase of survival. Further investigation is necessary for more insight into this point.

Photoactivated P4 and C14 inhibit the ERK pathway and NF-kB

Our data showed that photoactivated P4 and C14 inhibit the metabolic activity and the clonogenic growth of melanoma B78-H1 cells by apoptosis and necrosis. We therefore asked how this process is activated. Evidence that the RAS/MEK/ERK signaling pathway plays a central role in melanoma has been reported [54,55]. Protein RAS initiates sequential phosphorylations leading to P-ERK which, in turn, activates downstream proteins enhancing proliferation and survival. About 90% of melanoma tumours carries a high level of P-ERK [55]. Indeed, we found that P-ERK in B78-H1 cells is aberrantly high, though the ras genes are not mutated (Additional file 3: Figure S3). This suggests that the ERK signaling pathway can also be activated by perturbations of components upstream of RAS [56]. Previous studies have demonstrated that P-ERK induces the expression of various cytokines and chemokines that are activators of NF-κB [57,58]. In earlier work we found that in melanoma B78-H1 cells NF-κB controls apoptosis via a loop involving anti-apoptotic Snail and pro-apoptotic RKIP [59]. When B78-H1 cells are treated with porphyrin P4 or C14 and then irradiated, the resulting down-regulation RAS expression is accompanied by a significant decrease of the P-ERK and NF-κB (Figure 9B). A decrease of NF-κB in B78-H1 cells brings about a repression of anti-apoptotic Snail and an activation of pro-apoptotic RKIP [59]. Apoptosis is thus activated, as documented

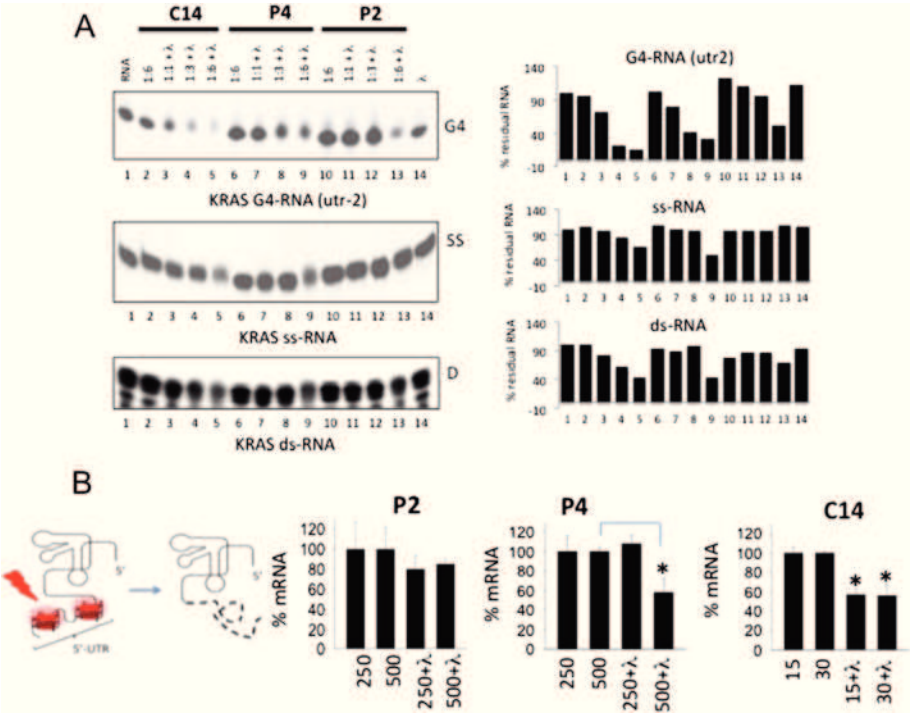

Figure 8 Photoactivated porphyrins degrade mRNA. (A) Photocleavage of RNA fragments from *KRAS* mRNA in three different conformations: quaduplex utr-2; single stranded (ss-RNA) and double stranded (ds-RNA) after treatment with porphyrin P2, P4 or C14 at ratios 1:1, 1:3 and 1:6 and light (7.2 J/cm^2). The histograms show the percentage of clevage. Untreated RNA (lane 1), RNA treated with porphyrin only (lane 2), RNA treated with light only (lane 14), RNA treated with both porphyrin and light (lanes 3–13); **(B)** Quantitative RT-PCR showing the level of *KRAS* mRNA in B78-H1 cells after treated with porphyrin P2, P4 (250 and 500 nM) and C14 (15 and 30 nM) and light (7.2J/cm2). RT-PCR analysis performed 1 h after irradiation. The experiment has been carried out in triplicate.

by PARP-1 cleavage and annexin V/PI assays. Considering the role of NF-κB in the tumourigenesis of melanoma, combined treatments with cationic porphyrin/light and NF-κB inhibitors should be effective against melanoma [60].

Conclusions

In summary, we have documented that tetracationic, *meso*-substituted porphyrins P4 and C14 are effective photosensitizers for the photodynamic treatment of melanoma. A previous study reported that P4 and C14 internalize in human fibrosarcoma cells by endocytosis, causing cell death by necrosis [35]. In melanoma B78-H1 cells, photoactivated P4 and C14 behave in a more complex way, as they cause cell death by apoptosis and necrosis. Our data suggest that an intracellular target of the porphyrins is mRNA, in particular the G-rich quadruplex-forming sequences located in the 5′-UTR of the mitogenic ras genes. Although we cannot rule out that these molecules can also bind to other gene transcripts, the cationic porphyrins are particularly active in cancer cells showing a RAS/MEK/ERK dependence, such as B78-H1 (Additional file 3: Figure S3) and Panc-1 [31,61] cells. Evidence that the porphyrins tightly bind to the G-rich quadruplex-forming sequences in the *KRAS* transcripts is provided. Due to their capacity to generate singlet oxygen upon irradiation, P4 and C14 photocleave *KRAS* mRNA, thus reducing the level of protein RAS and the activation of downstream RAS/MEK/ERK and NF-κB pathways. This photodynamic action against the ras transcripts is likely to be responsible of the inhibitory effects on cell growth seen *in vitro* and on tumour growth seen *in vivo*. In priciple, this strategy has the advantage of minimizing undesired secondary effects, as the photoprocess mediated by the porphyrins leading to the degradation of mRNA takes place only in the irradiated tumour. The data reported are promising, however, to fully understand the mechanism of tumour suppression *in vivo,* further studies are necessary.

As for the two active porphyrins, we found that C14 is a stronger anticancer drug than P4 as it: (i) internalizes in the melanoma cells more than P4; (ii) inhibits the clonogenic growth more than P4; (iii) acts through a light-dependent mechanism (photocleavage of mRNA) as well as a light-independent mechanism (blockade of translation through the stabilization of G4-RNA at the 5′-UTR

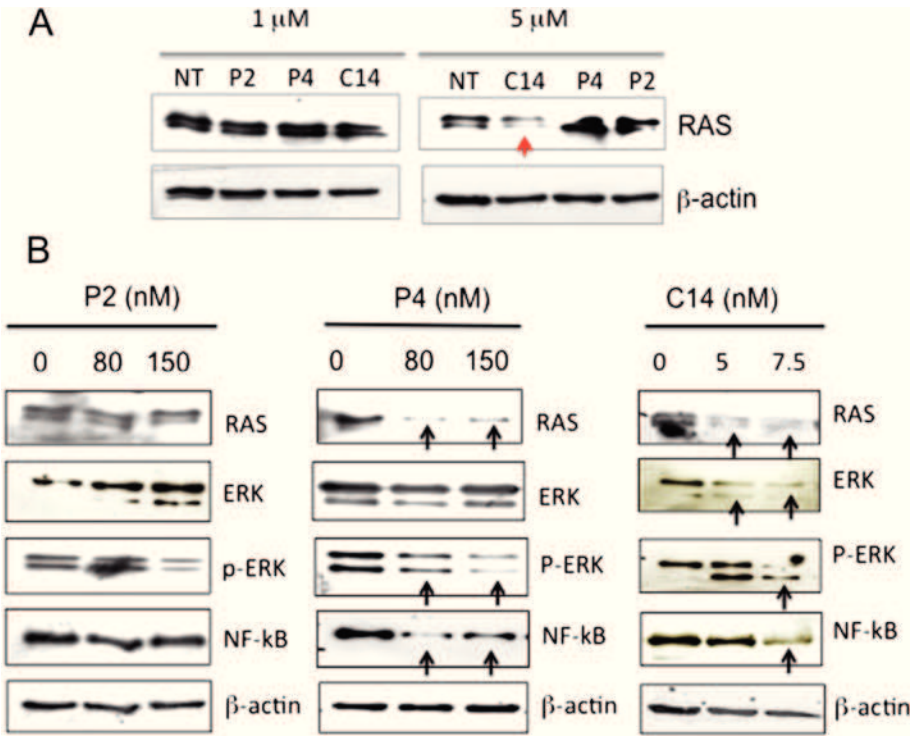

Figure 9 Effect of porphyrins on protein RAS and ERK pathway. (A) Immunoblots showing the expression level of protein RAS in melanoma B78-H1 cells 24 h after treatment with porphyrins P2, P4 and C14 (1 and 5 μM) without irradiation. C14 at 5 μM reduces the level of protein RAS through a light-independent mechanism; **(B)** Immunoblots showing the levels of RAS, ERK, P-ERK, NF-κB and β-actin in untreated or porphyrin/light treated B78-H1 cells, 24 h after light treatment.

of the ras genes). Indeed, C14 at 3 mg/Kg produces in vivo the same effect as P4 does at 30 mg/Kg. By improving the biodistribution of C14, for instance by incorporating the molecule in nanoparticles to exploit their enhanced permeability and retention (EPR) effect, this cationic porphyrin may have a great potential in the cure of melanoma skin tumours.

Methods

Porphyrins and oligonucleotides

Porphyrin tri-meso (N-methyl-4-pyridyl), meso (N-tetradecyl-4-pyridyl) porphine (TMPyP4-C14) was obtained from Frontier Scientific Inc, Logan, UT, U.S.A, while tetra-meso (N-methyl-4-pyridyl) porphine (TMPyP4) and tetra-meso (N-methyl-2-pyridyl) porphine (TMPyP2) were purchased from Porphyrins Systems (Lubeck, Germany). They have been dissolved in water and conserved in aliquots of 0.5 mM at −80°C. The stability in aqueous solution of the porphyrins was checked by measuring its UV-Vis spectrum at intervals of days. The RNA oligoribonucleotides, HPLC purified, have been purchased from Microsynth (CH). The samples were conserved at −80°C in 100 μM aliquots in water.

UV spectroscopy and circular dichroism

UV-vis spectra have been obtained with a Jasco V-530 UV/VIS spectrophotometer. CD spectra have been collected with a JASCO J-600 spectropolarimeter equipped with a thermostatted cell holder. RNA samples in 50 mM Tris-HCl, pH 7.4, 100 mM KCl were 10 μM. The spectra were recorded in 0.5 cm quartz cuvette at increasing temperature. Ordinate is expressed in mdeg.

Cell culture, metabolic activity assay and PDT treatment

In this study we used murine amelanotic melanoma B78-H1 cells. The cells were maintained in exponential growth in Dulbecco's modified eagle's medium containing 100 U/ml penicillin, 100 mg/ml streptomycin, 20 mM L-glutamine and 10% fetal bovine serum (Euroclone, Milano, Italy). The cells were seeded in a 96-well plate at a density of 5×10^3 cells/well. The following day they have been treated with the porphyrins in the dark and after 24 h, irradiated with metal halogen lamp with an irradiation of 8 mW/cm^2 for 15 min (fluence 7.2 J/cm^2). 24 h after irradiation the metabolic activity was determined by the resazurin assay following the manufacturer's instructions (Sigma–Aldrich, Milan, Italy). The fluorescence

was measured with a spectrofluorometer Spectra Max GeminiXS (Molecular Devices, Sunnyvale, CA). The data are presented as the percentage of metabolic activity compared to untreated cells. The data are the average of at least three independent experiments.

The protocol for PDT was the same for each type of experiment. B78-H1 cells have been plated, the day after the cells have been treated with porhyrins. Then, after 24 h the cells have been irradiated with the halogen lamp (fluence 7.2 J/cm^2). As P2 is an isomer of P4 and does not produce any effect on the cells, this molecule was used at the same dose of P4, as a negative control.

Clonogenic assay

B78-H1 cells have been treated with porphyrin/light and seeded in 60 mm Petri dish, at a density of 5×10^3 cells. After one week of growth, the colonies were fixed and stained with 2.5% methylene blue in 50% ethanol for 10 min. The images were obtained by Gel DOC 2000 Bio-Rad (Milan, Italy). The stained colonies (>50 cells) have been counted by an Image Scanner equipped with Image Quant TL software (Amersham Biosciences). The experiment was performed in duplicate.

Annexin V-propidium iodide assay

Apoptosis was assessed by annexin V, a protein that binds to phosphatidylserine (PS) residues, which are exposed on the cell surface of apoptotic cells. B78-H1 cells were seeded in a 6-well plate at density of 5×10^5 cells/well. After one day, the cells were treated with P2, P4 or C14 for 24 h and irradiated for 15 min with a halogen lamp (7.2 J/cm^2). After light activation, cells were washed with PBS, trypsinized, and pelleted. Pellets were suspended in 100 μL Hepes buffer added with 2 μL of annexin V and 2 μL of propidium iodide, PI (annexin-V FLUOS Staining kit, Roche, Penzberg, Germany) and incubated for 10 min at 25°C in the dark. Cells were immediately analyzed by FACS (Becton-Dickinson, San Jose, United States). A minimum of 10^4 cells *per* sample were acquired in list mode and analyzed using Cell Quest software. The cell population was analyzed by FSC light and SSC light. The signal was detected by FL1 (annexin V-FITC) and FL-2 (PI). The dual parameter dot plots combining annexin V-FITC and PI fluorescence show the vial cell population in the lower left quadrant, the early apoptotic cells in the lower right quadrant, and the late apoptotic or necrotic cells in the upper right quadrant.

The scratch-wound assay

The cells were seeded in a 6-well plate at a density of 6×10^5 cells/well and grown for 24 h to 80% confluence. A denuded area was created across the diameter of the dish by a yellow tip. After treatment with the porphyrin and light, the cells were washed with PBS and further incubated in a complete medium. Pictures were taken with an epiluminescent microscope Leica DMI6000B (Leica Microsystem, Heidelberg, Germany) at a 10-fold magnification to evaluate cell growth and migration [62].

Immunoblotting analysis

Total protein lysates (30 μg), obtained 24 h after porphyrin/light treatment (see above), were run on 12% SDS-PAGE and blotted to a nitrocellulose membrane 70 V for 2 h. The membrane was treated for 1 h with PBS-0.01% Tween (Sigma-Aldrich, Milan, Italy) containing 5% dry non-fat-milk and incubated overnight at 4°C with the primary antibodies: mouse monoclonal c-KRAS Oncogene, (Cell Signaling, Merck Millipore, Darmstadt, Germany) diluted 1:40, rabbit polyclonal anti-NF-κB p65 (C-20, sc-372 Santa Cruz Biotechnology, Santa Cruz, CA), diluted 1:1000; rabbit polyclonal anti-ERK (p44/42 MAPK, 9102, Cell Signalling, Danvers MA) diluted 1:1000; rabbit polyclonal anti-P-ERK (phospho-p 44/42 MAPK, 9101Cell Signalling, Danvers MA) diluted 1:1000; rabbit polyclonal anti-PARP (9542, Cell Signalling, Danvers MA) diluted 1:1000. β-Actin was used as an internal control. It was detected with a mouse monoclonal anti β-actin (Ab-1, CP01, Calbiochem, Merck Millipore, Darmstadt, Germany), diluted 1:10000. The membranes were incubated for 1 h with a secondary antibodies, either anti-rabbit IgG diluted 1:5000 (Calbiochem, Merck Millipore, Darmstadt, Germany) or anti-mouse IgM, diluted 1:5000 (Calbiochem, Merck Millipore, Darmstadt, Germany). Each secondary antibody was coupled to horseradish peroxidase (HPR). For the detection of the proteins, we used ECL (enhanced chemiluminescence) reagents (Super Signal®West PICO, and Super Signal®West FEMTO, Thermo Fisher Scientific Pierce, Rockford, USA). The exposure depended on the type of antibody and varied between 30 seconds to 5 min. The protein levels were quantified by Image Quant TL Version 2003 software (Amersham).

RNA extraction and quantitative RT-PCR

B78-H1 cells have been plated in a 96-well plate (25000 cells/well). After 24 h, the cells have been treated for further 24 h with C14 (15 and 30 nM), P4 and P2 (250 and 500 nM). For each porphyrin concentration, we prepared 6 samples: three have been irradiated (15 min, halogen lamp, fluence 7.2 J/cm^2) and 3 were not. 1 h following irradiation, total RNA was extracted from each sample with 20 μl of iScript™ RT-qPCR Sample Preparation Reagent (Bio-Rad).

For cDNA synthesis mixtures containing 1.25 μl of RNA, 1× buffer, 0.01 M DTT (Invitrogen, Milan, Italy),

1.6 μM primer dT (MWG Biotech, Ebersberg, Germany; d(T)16), 1.6 μM Random examers (Microsynth), 0.4 mM of each dNTP (Euroclone, Pavia, Italy), 0.6 units/μl RNase OUT, and 8 units/μl of Maloney murine leukemia virus reverse transcriptase (Invitrogen, Milan, Italy) were prepared and incubated for 1 h at 37°C. Real-time PCR reactions were performed with 1× Kapa Sybr Fast qPCR kit (Kapa Biosystems), 100–250 nM of each primer, 1 μl of reverse transcription reaction. The PCR cycle was: 3 min at 95°C, 40 cycles 10 s at 95°C, 30 s at 60°C for KRAS and 65°C for hypoxanthine-guanine phosphoribosyltransferase (HPRT) and β2-microglobulin (β2M) with CFX 96 real-time PCR controlled by Bio-Rad CFX Manager 3.0 (Bio-Rad). The sequences of primers used for amplifications are: for KRAS (Accession n. BC 010202) mKRAS for 5′-GCTCAGGAGTTAGCAAGGAG bases 570-89 and mKRAS back 5′-GTATTCACATAACTGTAC ACCTTG 730-753 (200nM); for β2M (NM_009735) mβ2M for 5′-GTCTCACTGACCGGCCTGTATG 91-112 and mβ2M rev 5′-CCCGTTCTTCAGCATTTGGATTTC 220-43 (100nM); for HPRT (NM_013556) mHPRT for 5′-GTGTTGGATACAGGCCAGACTTTG 599-622 and mHPRT rev 5′-ATCAACAGGACTCCTCGTATTTGC 765-88 (250nM). KRAS expression is normalized with HPRT and β2M.

Photocleavage experiment

^{32}P-labelled RNA fragments in quadruplex, duplex or single-strand conformations have been incubated overnight in 50 mM Tris HCl, pH 7.5, 100 mM KCl, 4°C. Mixture of 5 nM RNA and porphyrin (1:1; 1:2; 1:6) were incubated for 2 h at room temperature, then irradiated with the halogen lamp for 20 minutes. After irradiation the samples were denaturated and run in a 20% acrylamide gel, 7 M urea and 1 × TBE, at 55°C. The gels were dried and exposed to autoradiography.

Organ extraction and porphyrin biodistribution in mice with a B78-H1 tumour

The amount of porphyrin in the various organs was determined using the method of Villanueva and Jori [37]. The molecules were solubilized in saline solution and administered by intraperitoneal injection (i.p.) at the mice (P2 and P4, 30 mg/kg; C14, 9 mg/kg). The animals were sacrificed by cervical dislocation at different time points after administration (1, 3, 6, 9 and 24 h) (three mice for each time point). The organs (brain, kidney, duodenum, spleen, lung, liver, tumour and blood) were collected and homogenized in MeOH:DMSO (4:1 v/v). The homogenates were centrifuged and the amount of P2, P4 or C14 present in the supernatant was measured by fluorescence (Ex. 420 nm, Em. 450 to 750 nm). We did not observe any interference from other compounds present in the extracts. The amount of porphyrin in the various organs was determined by means of a calibration curve, which was obtained by plotting the fluorescence intensity against porphyrin concentration, using standard calibration porphyrin solutions. The curve was linear in the range from 0 to 2 μg/100 mg tissue with a correlation coefficient $r^2 = 0.9994$. Blood samples were taken from the left ventricle and centrifuged at 3000 g for 10 min to separate the plasma and stored at −80°C. Serum samples were diluted with defined volumes of 2% SDS so that the absorbance of cationic porphyrins at 423 nm was lower than 0.1 and analysed at the spectrofluorimeter. The porphyrin amounts were determined by interpolation on a standard curve plotted with known amounts of cationic porphyrins in 2% SDS, and reported in terms of mg/mg tissue or mg/ml of serum. The assay was highly reproducible with errors <8%.

Antitumour activity of the cationic porphyrins

Female 6-week old C57/BL6 mice were obtained from Harlan-Nossan (Italy) and were maintained in a conventional animal house for 2 weeks. All procedures with animals were carried out in accordance with the National Health Institute Guide for the Care and Use of Laboratory Animals and approved by the Institutional Animal Care Committee at the University of Trieste (approval number given by the Italian Ministry of Health: 6/2011-B). In particular every effort was made to avoid unnecessary pain to the animals. The mice, weighing 20 g, were implanted into the upper flank by subcutaneously injection with 2×10^6 B78-H1 amelanotic melanoma cells harvested from a cell culture. After 2 weeks the tumours reached a size of 6–8 mm (along the largest diameter) and the mice were randomized into groups of 8 mice each and injected intraperitoneally with the porphyrins (P2 and P4, 30 mg/Kg; C14, 3 mg/Kg). About 7 h after injection, when the porphyrins were present in the tumour in significant amounts, the mice were anesthetized with Zoletil® + Xylazine (15 mg/kg + 5 mg/kg; i.p.), shaved in the tumour area and irradiated with a laser BWN-660-60E [B&WTEK, Inc, Newark, DE, USA] at 660 ± 5 nm, fluence of 193 J/cm^2. Three porphyrin/light treatments have been carried out at days 1, 7 and 14. The mice were examined every 2 days for changes in weight, appearance of side effects or signs of sickness. The size of the tumour was measured every 2–3 days by a caliper. The mass (mg) of the tumour was calculated assuming a tumour density of 1 and a tumour volume given by $\pi/6 \cdot a^2 \cdot b$ where a and b are the shorter and larger axes (cm), respectively. The median survival time is defined as the animal's life spanning from the inoculation of tumour cells till death.

Singlet oxygen quantum yield of the cationic porphyrins determined by DMA

The quantum yield ($\phi\Delta$) of $^1O_2$ generation by the photoexcited triplet state of the porphyrins was measured by 9,10-dimethyl-anthracene (DMA). Upon reacting with $^1O_2$, DMA is transformed in the non-fluorescent 9,10-endoperoxide. As this reaction occurs with a high degree of specificity and with 100% chemical quenching of the fluorescence [33], the amount of DMA modified by the photoactivated porphyirn is a quantitative estimate of singlet oxygen generation. In a typical experiment 1 ml DMA (10 μM) was added to 1 ml porphyrin (10 μM) in a quartz cuvette and the resulting solution irradiated with a lamp (60 mW) for increasing times, under gentle magnetic stirring. In a typical experiment a solution containing DMA and porphyrin (1:1, 10 μM) was irradiated for different periods of time after which the residual fluorescence was recorded between 380 and 550 nm. The residual fluorescence was best-fitted to a first order decay equation $y = \exp(-k \cdot t)$ where k (s^{-1}) is the rate constant and t the time [s]. We obtained k for for P4, C14 and P2. Considering that the quantum yield of singlet oxygen generation ($\phi\Delta$) of P4 was reported to be 0.51 [34], the singlet oxygen quantum yield was obtained by the relation:

$$k(P4) : k(\text{porhyrin}) = \phi\Delta(P4) : \phi\Delta(\text{porhyrin})$$

where k (P4) and k (porphyrin) are determined experimentally.

Statistical analysis

The primary growth tumour analyses were performed by the Graph Pad PRISM. Tabled values are group means ± SE (standard error). Data were subjected to the appropriate factorial ANOVAs assessing significance against an alfa-level $p < 0.05$. When the individual effect of the treatments and the interaction between the independent variables in a 2×2 ANOVA was significant, the data were subjected to *post hoc* Tukey test for significance of the differences in the mean values. All analyses were performed using standard procedures implemented in the Systat package (SYSTAT Inc., Evanston, IL). The survival analysis was performed using the Kaplan-Meier curve (SPSS 11.0 for Windows 2000 software), and the P values were calculated by long-rank test.

Additional files

Additional file 1: Figure S1. Dimethylanthracene assay shows singlet oxygen production by the cationic porphyrins irradiated with a laser at 660 nm.

Additional file 2: Figure S2. G4-RNA formation in the 5'-UTR of KRAS and NRAS mRNAs.

Additional file 3: Figure S3. Melanoma B78-H1 cells are characterized by a hyperactive RAS/MEK/ERK pathway.

Abbreviations

$^1O_2$: Singlet oxygen; DMA: 9-10-dimethyl-anthracene; [$\phi\Delta$]: Quantum yield; PDT: Photodynamic therapy; C14: Tri-meso(N-methyl-4-pyridyl)- meso (N-tetradecyl-4-pyridyl) porphine; TMPyP4 (or P4): Meso-tetrakis (N-methyl-4-pyridyl) porphine; TMPyP2 (or P2): Meso-tetrakis (N-methyl-2-pyridyl) porphine; PI: Propidium iodide; PARP-1: Poly-[ADP ribose]-polymerase; CD: Circular dichroism.

Competing interests

The authors declare that they have no competing interests.

Authors' contributions

VR, SZ, MZ, SC participated in the design of the experiments; VR performed the cell cultured experiments and partecipated to the in vivo experiments; SZ and MZ performed the in vivo experiments; ED carried out western blots, SC performed RT-PCR, photocleavage and CD experiments; LX conceived the study and wrote the manuscript; VR, MZ and SC contributed to the final drafting of the manuscript. All authors read and approved the final manuscript.

Acknowledgements

This work has been carried out with the financial support of AIRC (Italian Association for Cancer Research), Project code 10546 (2010-13).

Author details

[1]Department of Medical and Biological Sciences, School of Medicine, P.le Kolbe 4, 33100 Udine, Italy. [2]Department of Life Science, University of Trieste, Via Giorgieri 7-9, 34100 Trieste, Italy. [3]Department of Chemical and Pharmaceutical Sciences, University of Trieste, P.le Europa 1, Trieste 34100, Italy.

Received: 26 September 2013 Accepted: 20 March 2014
Published: 1 April 2014

References

1. Dolmans DE, Fukumura D, Jain RK: **Photodynamic therapy for cancer.** *Nat Rev Cancer* 2003, **3:**380–387.
2. Castano AP, Mroz P, Hamblin MR: **Photodynamic therapy and anti-tumour immunity.** *Nat Rev Cancer* 2006, **6:**535–545.
3. Dougherty TJ, Gomer CJ, Henderson BW, Jori G, Kessel D, Korbelik M, Moan J, Peng Q: **Photodynamic therapy.** *J Natl Cancer Inst* 1998, **90:**889–905.
4. Miller JB: **Photodynamic therapy: the sensitization of cancer cells to light.** *J Chem Educ* 1999, **76:**592–594.
5. Pervaiz S: **Reactive oxygen-dependent production of novel photochemotherapeutic agents.** *FASEB J* 2001, **15:**612–617.
6. Josefsen LB, Boyle RW: **Photodynamic therapy and the development of metal-based photosensitizers.** *Metal-Based Drugs* 2008, **2008:**1–24.
7. Castano AP, Demidova TN, Hamblin MR: **Mechanisms in photodynamic therapy: part one-photosensitizers, photochemistry and cellular localization.** *Photodiagn Photodyn Ther* 2004, **1:**279–293.
8. Castano AP, Demidova TN, Hamblin MR: **Mechanisms in photodynamic therapy: part three-photosensitizers pharmacokinetics, biodistribution, tumour localization and modes of tumour destruction.** *Photodiagn Photodyn Ther* 2005, **2:**91–106.
9. Comuzzi C, Cogoi S, Overhand M, Van der Marel GA, Overkleeft HS, Xodo LE: **Synthesis and biological evaluation of new pentaphyrin macrocycles for photodynamic therapy.** *J Med Chem* 2006, **49:**196–204.
10. Ballico M, Rapozzi V, Xodo LE, Comuzzi C: **Metallation of pentaphyrin with Lu[III] dramatically increases reactive-oxygen species production and cell phototoxicity.** *Eur J Med Chem* 2011, **46:**712–720.
11. Rapozzi V, Beverina L, Salice P, Pagani GA, Camerin M, Xodo LE: **Photooxidation and phototoxicity of pi-extended squaraines.** *J Med Chem* 2010, **53:**2188–2196.
12. Rapozzi V, Zacchigna M, Biffi S, Garrovo C, Cateni F, Stebel M, Zorzet S, Bonora GM, Drioli S, Xodo LE: **Conjugated PDT drug: photosensitizing activity and tissue distribution of PEGylated pheophorbide *a*.** *Cancer Biol Ther* 2010, **10:**471–482.
13. Rapozzi V, Miculan M, Xodo LE: **Evidence that photoactivated pheophorbide *a* causes in human cancer cells a photodynamic effect involving lipid peroxidation.** *Cancer Biol Ther* 2009, **8:**1318–1327.

14. Rapozzi V, Zorzet S, Zacchigna M, Drioli S, Xodo LE: **The PDT activity of free and pegylated pheophorbide *a* against an amelanotic melanoma transplanted in C57/BL6 mice.** *Invest New Drugs* 2013, **31:**192–199.
15. Xodo LE, Rapozzi V, Zacchigna M, Drioli S, Zorzet S: **The chlorophyll catabolite pheophorbide *a* as a photosensitizer for the photodynamic therapy.** *Curr Med Chem* 2012, **19:**799–807.
16. Senge MO, Brandt JC: **Temoporfin Foscan®, 5,10,15,20-tetra[m-hydroxyphenyl]chlorin]-a second-generation photosensitizer.** *Photochem Photobiol* 2011, **87:**1240–1246.
17. Chan WM, Lim TH, Pece A, Silva R, Yoshimura N: **Verteporfin PDT for non-standard indications-a review of current literature.** *Graefes Arch Clin Exp Ophthalmol* 2010, **248:**613–626.
18. Hurley LH, Von Hoff DD, Siddiqui-Jain A, Yang D: **Drug targeting of the c-MYC promoter to repress gene expression via a G-quadruplex silencer element.** *Semin Oncol* 2006, **33:**498–512.
19. Han H, Langley DR, Rangan A, Hurley LH: **Selective interactions of cationic porphyrins with G-quadruplex structures.** *J Am Chem Soc* 2001, **123:**8902–8913.
20. Mikami-Terao Y, Akiyama M, Yuza Y, Yanagisawa T, Yamada O, Yamada H: **Antitumour activity of G-quadruplex-interactive agent TMPyP4 in K562 leukemic cells.** *Cancer Lett* 2008, **261:**226–234.
21. Morris MJ, Wingate KL, Silwal J, Leeper TC, Basu S: **The porphyrin TmPyP4 unfolds the extremely stable G-quadruplex in MT3-MMP mRNA and alleviates its repressive effect to enhance translation in eukaryotic cells.** *Nucleic Acids Res* 2012, **40:**4137–4145.
22. Parkinson GN, Lee MP, Neidle S: **Crystal structure of parallel quadruplexes from human telomeric DNA.** *Nature* 2002, **417:**876–880.
23. Huppert JL, Bugaut A, Kumari S, Balasubramanian S: **G-quadruplexes: the beginning and end of UTRs.** *Nucleic Acids Res* 2008, **36:**6260–6268.
24. Kumari S, Bugaut A, Huppert JL, Balasubramanian S: **An RNA G-quadruplex in the 5′ UTR of the NRAS proto-oncogene modulates translation.** *Nat Chem Biol* 2007, **3:**218–221.
25. Bugaut A, Balasubramanian S: **5′-UTR RNA G-quadruplexes: translation regulation and targeting.** *Nucleic Acids Res* 2012, **40:**4727–4741.
26. Lammich S, Kamp F, Wagner J, Nuscher B, Zilow S, Ludwig AK, Willem M, Haass C: **Translational repression of the disintegrin and metalloprotease ADAM10 by a stable G-quadruplex secondary structure in its 5′-untranslated region.** *J Biol Chem* 2011, **286:**45063–45072.
27. Weng HY, Huang HL, Zhao PP, Zhou H, Qu LH: **Translational repression of cyclin D3 by a stable G-quadruplex in its 5′ UTR: implications for cell cycle regulation.** *RNA Biol* 2012, **9:**1099–1100.
28. Bugaut A, Rodriguez R, Kumari S, Hsu ST, Balasubramanian S: **Small molecule-mediated inhibition of translation by targeting a native RNA G-quadruplex.** *Org Biomol Chem* 2010, **8:**2771–2776.
29. Santarpia L, Lippman SM, El-Naggar AK: **Targeting the MAPK-RAS-RAF signaling pathway in cancer therapy.** *Expert Opin Ther Targets* 2012, **16:**103–119.
30. Sebolt-Leopold JS, Herrera R: **Targeting the mitogen-activated protein kinase cascade to treat cancer.** *Nat Rev Cancer* 2004, **4:**937–947.
31. Faudale M, Cogoi S, Xodo LE: **Photoactivated cationic alkyl-substituted porphyrin binding to g4-RNA in the 5′-UTR of KRAS oncogene represses translation.** *Chem Commun (Camb)* 2012, **48:**874–876.
32. Ye Y, Wang H, Chu JH, Chou GX, Yu ZL: **Activation of p38 MAPK pathway contributes to the melanogenic property of apigenin in B16 cells.** *Exp Dermatol* 2011, **20:**755–757.
33. Gross E, Ehrenberg B, Johnson FM: **Singlet oxygen generation by porphyrins and the kinetics of 9,10-dimethylanthracene photosensitization in liposomes.** *Photochem Photobiol* 1993, **57:**808–813.
34. Reddi E, Ceccon M, Valduga G, Jori G, Bommer JC, Elisei F, Latterini L, Mazzucato U: **Photophysical properties and antibacterial activity of meso-substituted cationic porphyrins.** *Photochem Photobiol* 2002, **75:**462–470.
35. Ricchelli F, Franchi L, Miotto G, Borsetto L, Gobbo S, Nikolov P, Bommer JC, Reddi E: **Meso-substituted tetra-cationic porphyrins photosensitize the death of human fibrosarcoma cells via lysosomal cells via lysosomal targeting.** *Int J Biochem Cell Biol* 2005, **37:**306–319.
36. O'Brien MA, Moravec RA, Riss TL: **Poly (ADP-ribose) polymerase cleavage monitored in situ in apoptotic cells.** *Biotechniques* 2001, **30:**886–891.
37. Villanueva A, Jori G: **Pharmacokinetic and tumour-photosensitizing properties of the cationic porphyrinmeso-tetra(4 N-methylpyridyl)porphine.** *Cancer Lett* 1993, **73:**59–64.
38. Jori G: **Photodynamic therapy: basic and preclinical aspects.** In *Organic Photochemistry and photobiology.* Edited by Horspool W. Boca Raton, FL: CRC Press; 2004:146-1-10.
39. Villanueva A, Caggiari L, Jori G, Milanesi C: **Morphological aspects of an experimental tumour photosensitized with a meso-substituted cationic porphyrin.** *J Photochem Photobiol B* 1994, **23:**49–56.
40. Eddy J, Maizels N: **Gene function correlates with potential for G4 DNA formation in the human genome.** *Nucleic Acids Res* 2006, **34:**3887–3896.
41. Biffi G, Tannahill D, McCafferty J, Balasubramanian S: **Quantitative visualization of DNA G-quadruplex structures in human cells.** *Nat Chem* 2013, **5:**182–186.
42. Siddiqui-Jain A, Grand CL, Bearss DJ, Hurley LH: **Direct evidence for a G-quadruplex in a promoter region and its targeting with a small molecule to repress c-MYC transcription.** *Proc Natl Acad Sci USA* 2002, **99:**11593–11598.
43. McLuckie KI, Waller ZA, Sanders DA, Alves D, Rodriguez R, Dash J, McKenzie GJ, Venkitaraman AR, Balasubramanian S: **G-quadruplex-binding benzo[a] phenoxazines down-regulate c-KIT expression in human gastric carcinoma cells.** *J Am Chem Soc* 2011, **133:**2658–2663.
44. Cogoi S, Xodo LE: **G-quadruplex formation within the promoter of the KRAS proto-oncogene and its effect on transcription.** *Nucleic Acids Res* 2006, **34:**2536–2549.
45. Cogoi S, Paramasivam M, Spolaore B, Xodo LE: **Structural polymorphism within a regulatory element of the human KRAS promoter: formation of G4-DNA recognized by nuclear proteins.** *Nucleic Acids Res* 2008, **36:**3765–3780.
46. Cogoi S, Paramasivam M, Membrino A, Yokoyama KK, Xodo LE: **The KRAS promoter responds to Myc-associated zinc finger and poly(ADP-ribose) polymerase 1 proteins, which recognize a critical quadruplex-forming G4-element.** *J Biol Chem* 2010, **285:**22003–22016.
47. Membrino A, Cogoi S, Pedersen EB, Xodo LE: **G4-DNA formation in the HRAS promoter and rational design of decoy oligonucleotides for cancer therapy.** *PLoS One* 2011, **6:**1–15.
48. Oba J, Nakahara T, Abe T, Hagihara A, Moroi Y, Furue M: **Expression of c-Kit, p-ERK and cyclin D1 in malignant melanoma: an immunohistochemical study and analysis of prognostic value.** *J Dermatol Sci* 2011, **62:**116–123.
49. Leon J, Guerrero I, Pellicer A: **Differential expression of the ras gene family in mice.** *Mol Cell Biol* 1987, **7:**1535–1540.
50. Castellano E, Santos E: **Functional specificity of ras isoforms: so similar but so different.** *Genes Cancer* 2011, **2:**216–231.
51. Paramasivan S, Rujan I, Bolton PH: **Circular dichroism of quadruplex DNAs: applications to structure, cation effects and ligand binding.** *Methods* 2007, **43:**324–331.
52. Gomez D, Guedin A, Mergny JL, Salles B, Riou JF, Teulade-Fichou MP, Calsou P: **A G-quadruplex structure within the 5′-UTR of TRF-2 mRNA represses translation in human cells.** *Nucleic Acids Res* 2010, **38:**7187–7198.
53. Halder K, Largy E, Benzler M, Teulade-Fichou MP, Hartig JS: **Efficient suppression of gene expression by targeting the 5′-UTR based RNA quadruplexes with bisquinolinum compounds.** *Chembiochem* 2011, **12:**1663–1668.
54. Zhuang L, Lee CS, Scolyer RA, McCarthy SW, Palmer AA, Zhang XD, Thompson JF, Bron LP, Hersey P: **Activation of the extracellular signal regulated kinase (ERK) pathway in human melanoma.** *J Clin Pathol* 2005, **58:**1163–1169.
55. Cohen C, Zavala-Pompa A, Sequeira JH, Shoji M, Sexton DG, Cotsonis G, Cerimele F, Govindarajan B, Macaron N, Arbiser JL: **Mitogen-actived protein kinase activation is an early event in melanoma progression.** *Clin Cancer Res* 2002, **8:**3728–3733.
56. Hynes NE, Lane HA: **ERBB receptors and cancer: the complexity of targeted inhibitors.** *Nat Rev Cancer* 2005, **5:**341–354.
57. Finco TS, Westwick JK, Norris JL, Beg AA, Der CJ, Baldwin AS: **Oncogeic Ha-Ras-induced signalling activates NF-kB transcriptional activity, which is required for cellular transformation.** *J Biol Chem* 1997, **272:**24113–24116.
58. Lin G, Tang Z, Ye Y-B, Chen Q: **NF-kB activity is downregulated by KRAS knockdown in SW620 cells via the RAS-ERK-IkBa pathway.** *Oncology Rep* 2012, **27:**1727–1734.
59. Rapozzi V, Umezawa K, Xodo LE: **Role of NF-κB/Snail/RKIP loop in the response of tumour cells to photodynamic therapy.** *Lasers Surg Med* 2011, **43:**575–585.

60. Ueda Y, Richmond A: **NF-κB activation in melanoma.** *Pigment Cell Res* 2006, **19:**112–124.
61. Matsuda K, Idezawa T, You XJ, Kothari NH, Fan H, Korc M: **Multiple mitogenic pathways in pancreatic cancer cells are blocked by a truncated epidermal growth factor receptor.** *Cancer Res* 2002, **62:**5611–5617.
62. Vogt A: **Advances in two-dimensional cell migration assay technologies.** *Eur Pharm Rev* 2010, **5:**26–29.

doi:10.1186/1476-4598-13-75
Cite this article as: Rapozzi *et al.*: Anticancer activity of cationic porphyrins in melanoma tumour-bearing mice and mechanistic *in vitro* studies. *Molecular Cancer* 2014 **13**:75.

Dear Author/Editor,

Here are the proofs of your chapter as well as the metadata sheets.

Metadata

- Please carefully proof read the metadata, above all the names and address.
- In case there were no abstracts for this book submitted with the manuscript, the first 10-15 lines of the first paragraph were taken. In case you want to replace these default abstracts, please submit new abstracts with your proof corrections.

Page proofs

- Please check the proofs and mark your corrections either by
  - entering your corrections online
    or
  - opening the PDF file in Adobe Acrobat and inserting your corrections using the tool "Comment and Markup"
    or
  - printing the file and marking corrections on hardcopy. Please mark all corrections in dark pen in the text and in the margin at least ¼" (6 mm) from the edge.
- You can upload your annotated PDF file or your corrected printout on our Proofing Website. In case you are not able to scan the printout , send us the corrected pages via fax.
- Please note that any changes at this stage are limited to typographical errors and serious errors of fact.
- If the figures were converted to black and white, please check that the quality of such figures is sufficient and that all references to color in any text discussing the figures is changed accordingly. If the quality of some figures is judged to be insufficient, please send an improved grayscale figure.

Metadata of the chapter that will be visualized online

Book Title		New Insights on Nitric Oxide and Cancer
Chapter Title		Photodynamic Therapy and Nitric Oxide
Copyright		Springer International Publishing Switzerland 2015
Corresponding Author	Prefix	Dr.
	Family name	**Rapozzi**
	Particle	
	Given name	**Valentina**
	Suffix	
	Division	Department of Medical and Biological Sciences
	Organization	University of Udine
	Address	P.le Kolbe 4, 33100 Udine, Italy
	Email	valentina.rapozzi@uniud.it
Author	Prefix	
	Family name	**Pietra**
	Particle	
	Given name	**Emilia Della**
	Suffix	
	Division	Department of Medical and Biological Sciences
	Organization	University of Udine
	Address	P.le Kolbe 4, 33100 Udine, Italy
	Email	valentina.rapozzi@uniud.it
Abstract		Photodynamic therapy (PDT) is a clinically approved, minimally invasive therapeutic treatment that exerts a selectively cytotoxic activity towards cancer cells. This technique involves administration of a photosensitizer followed by irradiation at a wavelength corresponding to its absorbance band. In the presence of oxygen, a cascade of stress oxidative reactions leads to direct tumor cell death, damage to the microvasculature and induction of a local inflammatory reaction. Clinical studies showed that PDT can be curative particularly in early-stage tumors. Moreover, with many cancers becoming resistant to treatment, PDT offers a mechanistically distinct alternative, mitigating chemoresistance but also synergizing with chemotherapy and molecularly targeted therapies. A well-known phrase of Tayyaba Hasan, one of the experts in PDT, stated “with PDT no matter what you do, if you are lucky, there is a prodeath response, simultaneously, there is a prosurvival molecular response, which mitigates the desidered outcome with PDT”. These opposing molecular responses represent the challenge for basic science researchers and clinicians to enhance the photodynamic-mediated chemicals. Noteworthy, one of the major effectors that modulate the efficacy of PDT is nitric oxide, whose role will be discussed in this chapter.
Keywords		Cancer - Conjugates - Molecular mechanisms - Nitric oxide - NO-PDT - Photodynamic therapy

Chapter 14
Photodynamic Therapy and Nitric Oxide

Emilia Della Pietra and Valentina Rapozzi

Abstract Photodynamic therapy (PDT) is a clinically approved, minimally invasive therapeutic treatment that exerts a selectively cytotoxic activity towards cancer cells. This technique involves administration of a photosensitizer followed by irradiation at a wavelength corresponding to its absorbance band. In the presence of oxygen, a cascade of stress oxidative reactions leads to direct tumor cell death, damage to the microvasculature and induction of a local inflammatory reaction. Clinical studies showed that PDT can be curative particularly in early-stage tumors. Moreover, with many cancers becoming resistant to treatment, PDT offers a mechanistically distinct alternative, mitigating chemoresistance but also synergizing with chemotherapy and molecularly targeted therapies. A well-known phrase of Tayyaba Hasan, one of the experts in PDT, stated "with PDT no matter what you do, if you are lucky, there is a prodeath response, simultaneously, there is a prosurvival molecular response, which mitigates the desidered outcome with PDT". These opposing molecular responses represent the challenge for basic science researchers and clinicians to enhance the photodynamic-mediated chemicals. Noteworthy, one of the major effectors that modulate the efficacy of PDT is nitric oxide, whose role will be discussed in this chapter.

Keywords Cancer · Conjugates · Molecular mechanisms · Nitric oxide · NO-PDT · Photodynamic therapy

V. Rapozzi (✉) · E. D. Pietra
Department of Medical and Biological Sciences,
University of Udine, P.le Kolbe 4, 33100 Udine, Italy
e-mail: valentina.rapozzi@uniud.it

B. Bonavida (ed.), *Nitric Oxide and Cancer: Pathogenesis and Therapy,*
DOI 10.1007/978-3-319-13611-0_14

Book ID: 319328_1_En ChapterID: 14 Dispatch Date: 29/01/2015 ProofNo: 1

Abbreviations

AIF	Apoptosis-inducing factor
ALA	5-aminolevulinic acid
cGMP	Cyclic guanosine monophosphate
COX-2	Cyclooxygenase:2
CPTIO	2-4-carboxyphenyl-4,4,5,5-tetramethylimidazoline-1-oxyl-3-oxide
DETA/NO	Diethylenetriamine NONOate
EMT	Epithelial mesenchymal transition
GSNO	S-nitrosoglutathione
HbO_2	Oxyhemoglobin
HIF-1α	Hypoxia:inducible factor 1α
$HO^{\bullet}$	Hydroxyl radical
H_2O_2	Hydrogen peroxide
HpD	Hematoporphyrin derivative
JNK	c-Jun NH2-terminal kinase
LDL	Low density protein
LED	Light emitting diode
L-NAME	L-NG-Nitroarginine Methyl Ester
MAPK	Mitogen-Activated Protein Kinase
MMP-9	Matrix metallopeptidase 9
MOMP	Mitochondria outer membrane permeabilization
NF-kB	Nuclear Factor-KappaB
NO	Nitric oxide
$^1O_2$	Singlet oxygen
$ONOO^-$	Peroxynitrite anion
Pb*a*	Pheophorbide *a*
PDT	Photodynamic therapy;
PS	Photosensitizer
RIP1	Receptor interacting protein 1
RKIP	Raf kinase inhibitor protein
ROS	Reactive oxygen species
RNS	Reactive nitrogen species
SNT	S-nitrosothiol
TNF-α	Tumor necrosis factor:alpha
YY1	Yin Yang 1
VEGF	Vascular endothelial growth factor.

Basic Components of Photodynamic Therapy

Photodynamic therapy (PDT) consists of three essential components—a photosensitizer (PS), light and oxygen [1, 2]. None of these is individually toxic, but altogether they initiate a photochemical reaction that culminates in the generation of a highly reactive product termed singlet oxygen ($^1O_2$) and/or reactive oxygen species

(ROS). Both oxidative products can rapidly cause significant toxicity leading to cell death. The anti-tumor effects of PDT can involve three inter-related mechanisms: direct cytotoxic effects on tumor cells, damage to the tumor vasculature, and induction of an inflammatory reaction that can induce the activation of systemic immunity. The "choice" among these mechanisms depends on the type and dose of the PS used, the dose-light interval, and the total light dose and its fluence rate (i.e. the number of particles that intersect a unit area in a given amount of time, typically measured in Watts per m^2).

The Photosensitizer

Most of the PSs used in cancer therapy possess a structure similar to a tetrapyrrole ring of the protoporphyrin contained in hemoglobin. The ideal photosensitizer would be a pure compound in order to permit quality control analysis with low manufacturing costs and good stability in storage. It should have a high absorption peak between 600 and 800 nm, because in this wavelength range the penetration of light into tissue is very high. In fact, PSs, such as chlorins, bacteriochlorins and phtalocyanines, that present a strong absorbance in the deep red, offer improvements in tumor control (Table 14.1). Moreover, good PSs should have relatively rapid clearance from normal tissues, thereby, minimizing phototoxic side-effects and no dark toxicity [3]. The optimal photosensitizer should not preclude the combined use of others types of treatment such as chemotherapy, surgery or radiation [4–6].

The first PS to be clinically employed for cancer therapy was a water-soluble mixture of phorphyrins called hematoporphyrin derivative (HpD), a purified form

Table 14.1 Properties of various photosensitizers and their applications in cancer

PS	Structure	Wavelenght (nm)	Cancer types
Photofrin	Porphyrin	630	Lung, esophagus, bile duct, bladder, brain, ovarian
ALA	Porphyrin	635	Skin, bladder, brain, esophagus
ALA esters	Porphyrin precursor	635	Skin, bladder
Foscan	Chlorin	652	Head and neck, lung, skin, bile duct
Verteporfin	Chlorin	690	Ophtalmic, pancreatic, skin
HPPH	Chlorin	665	Head and neck, esophagus, lung, skin, breast
Purlytin	Chlorin	660	Skin, breast
Taloporfin	Chlorin	660	Liver, colon, brain
Fotolon	Chlorine	660	Nasopharyngeal, sarcoma, brain
Silicon pthalocyanine	Phtalocyanine	675	Cutaneous T cell lymphoma
Padoporfin	Bacteriochlorin	762	Prostate
Motexafin lutetium	Texaphyrin	732	Breast

of which later it became known as Photofrin [1, 4, 7]. Even if Photofrin is still the most employed PS, the product has some disadvantages such as a long-lasting skin photosensitivity and a relatively low absorbance at 630 nm. There has been a significant work among medicinal chemists to discover second generation PSs that have an absorbance at the longer wavelengths. Thus, over a hundred compounds have been proposed as potentially useful for the treatment of cancer with PDT. The discovery that 5-aminolevulinic acid (ALA) was a biosynthetic precursor of the PS protoporphyrin IX [8] has led to many applications in which ALA or ALA-ester can be topically applied or administered orally. These are considered to be "pro-drugs" and are required to be converted to protoporhyrin to be active photosensitizers.

Normally, the PSs are very selective towards tumors. Many hypotheses have been suggested to justify the tumor-localizing properties in PDT [9]. These include the prevalence of leaky and twisted tumor blood vessels due to the neovascularization and the absence of lymphatic drainage known to enhanced permeability and retention (EPR) [10]. Some of the most successful compounds bind to low density proteins (LDL) suggesting that the overexpression of LDL receptors found on tumor cells could be important [11]. Targeting studies have demonstrated an increase of tumor uptake when the PSs were covalently attached to various molecules that present some affinity for neoplasia or to receptors expressed on specific tumors [12]. The purpose is to count on the ability of the targeting vehicle to control localization factors so that the PS can be chosen based on its photochemical properties. These vehicles include monoclonal antibodies, antibody fragments, peptides, proteins such as transferrin, epidermal growth factor, insulin, LDL, various carbohydrates, somatostatin, folic acid and many others.

Light Sources

A crucial role in PDT is to ascribe to light irradiation. Considering the different light wavelengths, it is known that blue light penetrates least efficiently through the tissue while red and infrared radiations penetrate more deeply. Even if the region between 600 and 1200 nm is called the optical window for tissues, light up to only about 800 nm can generate $^1O_2$, and in fact longer wavelengths have insufficient energy to initiate a photodynamic reaction [13]. There are other phenomena that limit PDT such as (i) the processes of reflection, refraction and scattering, during light propagation, that reduce the beam power and the penetration in the tissue [14–16]; and (ii) the light absorption by tissue chromophores such as water, oxyhemoglobin (HbO_2) and deoxyhemoglobin, melanin and cytochrome [6, 17], that reduce the PS activation.

Choice of the light source should be based on PS absorption (fluorescence excitation and action spectra), disease (location, size of lesions, accessibility, and tissue chartacteristics), cost and size. The fluence rate also affects the PDT response [18].

Different kinds of lamps can be used including halogen, fluorescent, tungsten or xenon lamps (inexpensive); lasers (more expensive) and light emitting diodes (LEDs) that have narrow spectral bandwidths and high fluence rates [19–20]. La-

sers can be coupled into fibers equipped with diffusing tips to treat tumors present in the urinary bladder and the digestive tract. It is also possible to implant a light source in solid organs deep in the body under image guidance. Inflatable balloons, covered on the inside with a strongly scattering material and formed to fit an organ, are also commercially available [21]. The choice of optimal combinations of PSs, light sources, and treatment parameters is crucial for successful PDT [15–22].

Photophysics and Photochemistry

Most of PSs in their energetically stable state (ground state) possess two electrons with opposite spins located in an energetically most favorable molecular orbital. Absorption of light leads to a transfer of one electron to a higher-energy orbital determining the excited state. In this form, the PS is very unstable and releases this surplus energy as fluorescence and/or heat. Otherwise, an excited PS may through an intersystem crossing to change into a more stable triplet state with inverted spin of one electron. The PS in the triplet state can either decay radiationlessly to the ground state or transfer its energy to molecular oxygen (O_2). This step leads to the formation of singlet oxygen ($^1O_2$), and the reaction is known as a Type II process [23]. In another case, the PS may react directly with an organic molecule in the cellular microenvironment, acquiring a hydrogen atom or an electron to form a radical. This reaction is known as a Type I process. Subsequent autoxidation of the reduced PS produces a superoxide anion radical ($O_2^{\bullet-}$). Dismutation or one-electron reduction of $O_2^{\bullet-}$ gives hydrogen peroxide (H_2O_2), which in turn can undergo one-electron reduction to a powerful and virtually indiscriminate oxidant-hydroxyl radical ($HO^{\bullet}$). ROS generation via the Type II process is much simpler than the Type I, and most PSs are believed to operate via the Type II mechanism (Fig. 14.1).

AQ1

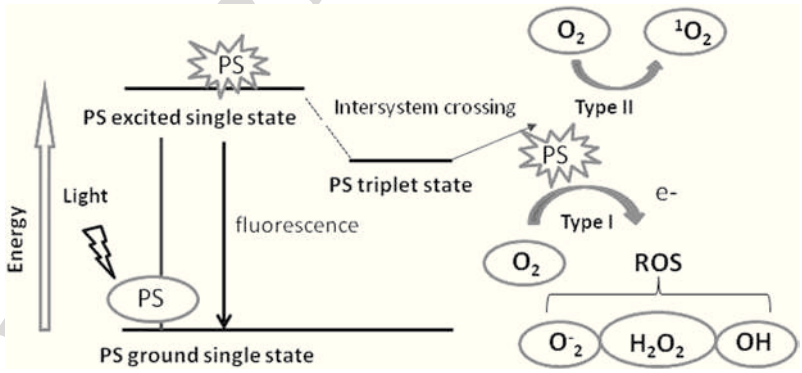

Fig. 14.1 Schematic illustration of photodynamic therapy including the Jablonski diagram. The PS initially absorbs a photon that excites it to the first excited singlet state and this can relax to the more long lived triplet state. This triplet PS can interact with molecular oxygen in two pathways, type I and type II, leading to the formation of reactive oxygen species (ROS) and singlet oxygen respectively [24].

Mechanisms of PDT-Mediated Cytotoxicity

PDT can evoke three main cell death pathways: apoptotic, necrotic, and autophagy-associated cell death determined by the subcellular localization of different PSs [25–26] (Fig. 14.2).

Apoptosis is generally the major cell death modality in PDT. When the PSs are associated to membrane mitochondria, the photodamage determines the release of Bcl-2 [27–29] that causes the mitochondria outer membrane permeabilization (MOMP) and the subsequent release of caspase activators such as cytochrome c and Smac/DIABLO, or other proapoptotic molecules, including the apoptosis- inducing factor (AIF) [30]. If the PSs are located on lysosome membrane, the rupture and leakage of cathepsins from photooxidation [31–32] induce Bid cleavage and MOMP [32]. The phototoxicity can involve other proteases, such as calpains, as well as nonapoptotic pathways [30]. Usually the inhibition or genetic deficiency of caspases can delay phototoxicity or shift the cell death modality toward necrotic cell death [33]. The molecular mechanisms of programmed necrosis are still unclear, but certain events including activation of receptor interacting protein 1 (RIP1) kinase, excessive mitochondrial ROS production, lysosomal damage, and intracellular Ca^{2+}overload have been involved [34–35]. Severe inner mithocondria photodamage or intracellular Ca^{2+} overload could promote mithochondrial permeability transition, an event that may favor the necrotic rather than the apoptotic-mediated phototoxicity [30, 36]. Autophagy is another cell death pathway since it can occur during in vitro tests involving PSs that are localized in the endoplasmatic reticulum

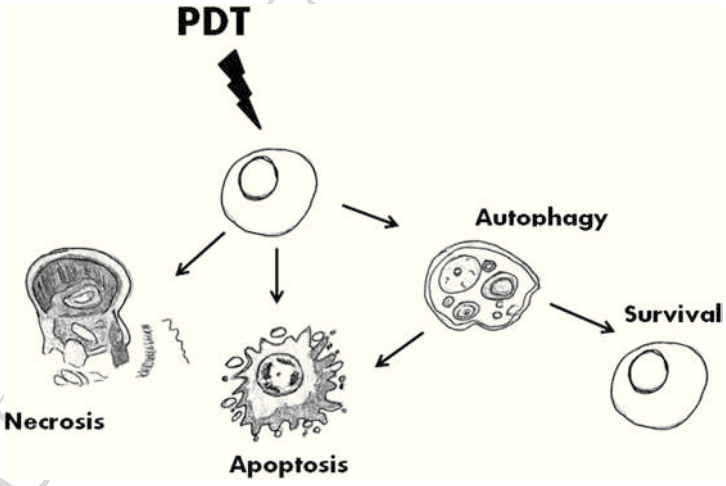

Fig. 14.2 Cell death pathways. Exposure to PDT leads to cellular damage that may result in cell death via different pathways.

(ER). This is a lysosomal pathway for the degradation and recycling of intracellular proteins and organelles. Autophagy can be stimulated by various stress signals including oxidative stress [37]. This process can have both a cytoprotective and a prodeath role after cancer chemotherapies, including those involving ROS as primary damaging agents [37]. Recent studies delineate autophagy as a mechanism to preserve cell viability after PDT [38].

PDT and the Microenvironment

It is important to know that PDT-mediated changes to the tumor microenvironment can modulate treatment responsiveness. The tumor microenvironment is made up of malignant cancer cells and connective tissue as well as a myriad of host cells including endothelial cells, pericytes, and inflammatory leukocytes (macrophages and neutrophils). Leukocytes are recruited into tumors and through the release of a lot of factors, stimulate the endothelium, and indirectly activate tumor vascularization. Also the neutrophil recruitment in tumors can be followed by VEGF and MMP-9 release with associated angiogenesis and invasion, respectively [39–40]. Moreover, tumor-associated macrophages exhibit a phenotype that favors tissue growth, angiogenesis, and tissue remodelling.

All the cellular factors associated with PDT, such as necrosis, apoptosis, and hypoxia, can function as stimuli within the tumor microenvironment. Likewise, PDT-induced hypoxia can lead to the transcriptional activation of VEGF via the HIF-1 pathway [41].

Several laboratories have also shown that PDT can induce the expression and/or activation of additional pro-angiogenic molecules including COX-2 and prostaglandins, TNF-, matrix metalloproteinases (MMPs), integrins, IL-6, and IL-8 within the tumor microevironment [41–47]. Preclinical investigations indicate that combining PDT with targeted therapies directed at attenuating the pro-survival actions of the tumor microenvironment can enhance the therapeutic potential of PDT [41–45].

Nitric Oxide and PDT

Nitric oxide (NO) is recognized as a major effector molecule in a diverse array of physiologic and pathologic processes. It is also evident that this radical, produced by many cells in the human body, not only controls important functions in tumor progression, but may have a major influence on the outcome of cancer therapies, in particular those dependent on oxygen and the generation of reactive oxygen species [1, 48–50] such as photodynamic therapy [48, 51–55].

AQ2

How NO Influences the PDT Antitumor Response?

1. During PDT

The endogenous tumor level of nitric oxide (NO) varies considerably in both human solid tumors [49, 56–59] and murine tumors [48–60]. As described above, the hallmark characteristics in the tumor microenvironment immediately following PDT treatment include tumor vasculature disruption, reduced blood flow, vascular occlusion with subsequent reperfusion injury, in addition to a marked infiltration of inflammatory cells [48]. NO is known to directly influence a number of these biological processes involved in PDT-induced anti-tumor effects. [48, 61]. It has, therefore, been suggested that the intrinsic level of tumor NO may be a determinant in the response to PDT [48, 62].

Both *in vitro* [53] and *in vivo* studies [48, 55] on several tumor models expressing different NO levels reported that a low production of NO makes tumors more sensitive to PDT, in contrast to high NO production. In tumors exhibiting high levels of NO, the vasculature events including vasoconstriction, ischaemia and hypoxia, in addition to the inflammatory reaction induced during PDT, may be reduced [51, 62]. This could result from the following effects of NO: (i) it acts as a potent vasodilator (ii) it prevents platelet aggregation and adhesion to the endothelium (iii) it suppresses the aggregation of accumulated inflammatory neutrophils (iv) it inhibits the expression of leukocyte adhesion molecules and, hence, the adhesion and extravasation of circulating leukocytes and (v) it averts mast cell degranulation [63–65]. On the other hand, elevated NO levels may maintain vessel dilation during PDT treatment, which can limit the decrease in tumor oxygenation and sustain in this way the oxygen-dependent generation of phototoxic damage [51]. Additionally, NO increases the vascular permeability and consequent vascular leakage, which are characteristic occurrences in PDT-treated vasculature (1). The NO-sensitive processes that unfold after termination of photodynamic light treatment include: (i) ischaemia-reperfusion injury, where NO can have a protective role resulting in increased tumor oxygenation (ii) apoptosis of tumor cells which can be stimulated by NO and (iii) development of the immune reaction against the treated tumor, whereby NO has immunoregulatory functions [1, 51].

2. Following PDT

Marked changes in tumor NO levels may be expected to occur after PDT. An increase in the generation of NO attributed to enhanced nitric-oxide synthase (NOS) expression has been observed following PDT using both silicon-phtalocyanine [66] and ALA [67]. Furthermore, the stimulation of cellular signal transduction pathways by PDT-oxidative stress leads to the activation of nuclear transcription factors [1], which may also result in the upregulation of genes encoding NOS. On the other hand, activated inflammatory cells accumulated in PDT-treated tumors may be responsible themselves for the release of NO [68–71].

Cytoprotective Role of NO in PDT

Depending on the concentration of NO present in the tumor (both endogenous and that induced by PDT), it is important to determine the underlying molecular pathways modulated by NO, with the aim to improve the efficacy of PDT. Once generated, NO combines with other oxidants to form reactive nitrogen species (RNS) which can damage a variety of cellular targets such as DNA and proteins that regulate various intracellular and intercellular signaling events, ultimately leading to apoptosis and mutagenesis [72] (Fig. 14.3).

When high levels of NO are present in a tumor, superoxide, generated by PDT, can react with an NO unpaired electron and form a peroxynitrite anion ($ONOO^-$) [69, 73–74]. This reaction inactivates the superoxide, hence, the neutrophils are subsequently not activated [75–77], diminishing the damage to the vasculature and surrounding tissue.

Tumors generating low levels of NO are much more sensitive to PDT than those containing high levels of NO, and the administration of NOS inhibitors together with PDT treatment enhances tumor regression [48, 52]. Administration of the NO inhibitors reduces the blood flow in the tumor, and this could explain the increase in PDT efficiency [48].

Several hypotheses have been raised to explain the mechanisms of protection induced by NO in the inhibition of apoptosis [72, 78–79]. NO can inhibit the activa-

Fig. 14.3 NO chemistry of biological significance. NO is synthesized endogenously from L-arginine, NADPH and oxygen. NO freely diffuses creating concentration gradients across subcellular compartments. Redox or additive reactions with constitutents of cellular microenvironment convert NO to a number of NO_x species, which in turn, dictate the biological effects of NO

tion of caspases directly by S-nitrosylation [80–81], or through a cyclic guanosine monophosphate (cGMP)-dependent mechanism, by activating protein kinase G (PKG) [82]. More recently, Girotti et al [83–84] demonstrated that the cytoprotective effect of nitric oxide in PDT is due not only to the cGMP involvement but also to the suppression of pro-apoptotic JNK and p38 MAPK activations.

NO Modulates Tumor Cell Death Induced by PDT Through the NF-κB/Snail/YY1/RKIP Loop

The NF-κB/Snail/YY1/RKIP loop is a pivotal molecular circuitry modulated by NO that controls the tumor progression [85]. Several studies have implicated the role of NO in the regulation of tumor cell behavior and have shown that NO either promotes or inhibits tumorigenesis [50, 86–87]. These conflicting findings have been resolved, in part, by the levels of NO used such that low levels promote tumor growth and higher levels inhibit tumor growth. The underlying mechanisms by which NO sensitizes tumor cells to apoptosis were shown to be regulated, in part, by NO-mediated inhibition of NF-κB survival/antiapoptotic pathways and downstream of NF-κB by inhibition of the pro-survival transcriprtion factors Snail and YY1. In addition, it has been shown [85] that NO induces the expression of the metastasis-suppressor/immunosureillance cancer gene product, Raf-1 kinase inhibitor protein (RKIP). Overexpression of RKIP mimics NO in tumor cell-induced sensitization to apoptosis. The induction of RKIP by NO was the result of the inhibition of the RKIP repressor, Snail, downstream of NF-κB. In the presence of a dysregulated NF-κB/Snail/YY1/RKIP circuitry in tumor cells, the treatment with NO modifies this loop in favor of the inhibition of tumor cell survival and the response to cytotoxic drugs. In addition, the NF-κB/Snail/YY1/RKIP loop consists of gene products that regulate the epithelial mesenchymal transition (EMT) and, thus, tumor metastasis [88] (Fig. 14.4).

Considering that PDT modulates NF-κB activity [89–90] and induces the NO release [66, 83, 91] we have focused our attention on the role of the NF-κB/Snail/YY1/RKIP loop in the tumor response to pheophorbide *a* (a chlorofill derivative, Pb*a*)/PDT. Although, in general, Pb*a*/PDT has been found to be an efficient inducer of cell death by apoptosis and/or necrosis [92–93], however, when the PS is not used at its optimal dose (<IC50), it can activate rescuing pathways, leading to tumor survival and recurrence. As the level of NO generated by a low-dose PDT is not sufficient to trigger apoptosis, we investigated how this limited NO release influenced the NF-κB/Snail/YY1/RKIP loop. We have observed that under low-dose Pb*a*/PDT conditions the expression of Snail is increased while the expression of RKIP is decreased: an expression pattern associated to the activation of anti-apoptotic and pro-survival pathways [90].

Moreover, with repeated treatments (8 times) of a low-dose Pb*a*/PDT in prostate cancer cell lines (PC3 and LNCaP), we have found that the NF-κB/YY1/RKIP

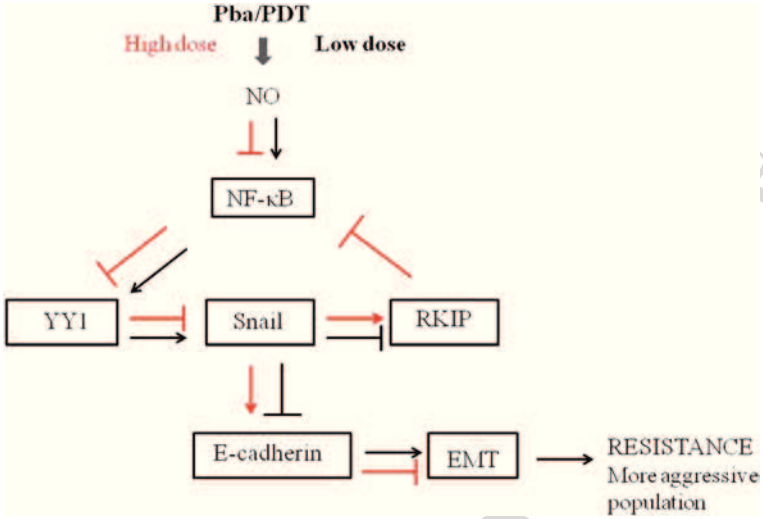

Fig. 14.4 A schematic diagram representing the effect of Pb*a*/PDT on the NF-κB/YY1/Snail/RKIP loop**.** Briefly, a low-dose PDT stimulates NF-κB and the pro-survival genes YY1 and Snail. The up-regulation of Snail results in the downregulation of the metastasis tumor suppressor RKIP. Snail is also correlated to EMT inducing a decrease of E-cadherin expression. Contrasting findings wese observed with a high-dose PDT

circuitry stimulates the EMT. In fact, we have observed a decreased expression of E-cadherin, the main transmembrane adhesion molecule responsible for cell-to-cell interactions and tissue organization in epithelial cells [94–95] and an increase of vimentin, a cytoskeletal component responsible for maintaining cell integrity. As a consequence, loss of E-cadherin expression is considered a crucial event on the disruption of cell-cell adhesion and cytoskeletal architecture and in the acquisition of an invasive phenotype in tumor cells [96]. In particular, in prostate carcinoma, a lower expression of E-cadherin has been associated with more advanced tumor stage and grade [97–98] and higher expression of vimentin is correlated with the invasive capacity [99]. Based on these findings, we have succeeded to isolate a rare cell subpopulation characterized by the CD24 + and CD44 + phenotypes [100–101]. This subpopulation within the tumor possesses the characteristics of self-renewal capacity, resistance to Pb*a*/PDT in comparison to normal PC3 cells and with tumorigenic ability (unpublished data). All of the above results, yet unpublished, indicate that repeated treatments with a suboptimal dose of PDT determine the presence of a subset cell population with properties of stem cells, that plays a vital role in the initiation, progression and recurrence of cancer [102]. With the administration of L-NAME, a non specific inhibitor of iNOS, in combination with Pb*a*/PDT, we highlighted the role of NO in this tumor progression, through the NK-κB/Snail/YY1/RKIP loop.

Role of Nitric Oxide in Improving the Effectiveness of PDT

NO has been found to be a pivotal factor in the chemosensitization of tumor cells to various chemotherapeutic drugs [72]. Regarding the involvement of NO in PDT, there are some parameters that must be considered in order to improve the efficacy of phototoxic treatment, such as the type of sensitizer (precursor or direct), the type of tumor (in terms of high or low levels of endogenous NO), the interval of time between the administration of the PS and the light exposure.

Many authors have reported that the use of NOS inhibitors (L-NAME, 1400 W) or a nitric oxide scavenger (CPTIO) improves the efficacy of ALA/PDT in tumors with high levels of NO [48, 53, 55, 84], indicating a cytoprotective role for NO. Also in our model, after repeated treatments with low-dose Pb*a*/PDT in PC3, we have observed the same cytoprotective behavior by NO (data unpublished). This effect might be due to trapping lipid-derived radicals generated by one-electron turnover of primary LOOHs [103]. Furthermore, it has been proposed that moderate levels of NO may inhibit caspases by S-nitrosylation [104], induce the downregulation of pro-apoptotic Bax and upregulates the anti-apoptotic Bcl-xL [105] and induce the cytoprotective heme oxygenase-1 [106].

To increase the efficacy of PDT, we have proposed a combined treatment with an NO donor. This treatment is based on the following considerations: (i) the dual role of NO in tumor biology is due to its capacity to promote or inhibit tumor growth dependent on the NO concentration [88] (ii) NO modulates the activity of the NF-κB pathway [107] (iii) Pb*a*/PDT induces the release of cellular NO according to the dose used [90] and (iv) Pb*a*/PDT, in a dose-dependent way, inhibits or stimulates the NF-κB/YY1/Snail/RKIP loop (90) leading to cell growth arrest or cell recurrence.

As a proof of principle, we used in conjunction with Pb*a*, DETANONOate (DETA/NO), a molecule that spontaneously releases in the cytoplasm 2 mol of NO per mole of compound [108]. We found, indeed, that the combination of the PS with an NO donor resulted in a significant modulation of the NF-κB/YY1/Snail/RKIP loop towards the expression of the pro-apoptotic RKIP and the inhibition of anti-apoptotic NF-κB and Snail gene products. The clinical relevance of increasing the RKIP expression by NO correlates with a favorable clinical outcome resulting in tumor regression and in inhibition of metastatic spread [109].

The dual treatment with DETA/NO and mPEG-Pb*a*/PDT [110] has been administered in C57BL/6 mice inoculated s.c. with the B78-H1 murine amelanotic melanoma. The results obtained showed that the use of an NO donor significantly increased the anti-tumor efficacy of PDT. Noteworthy, the group of mice treated with mPEG-Pb*a* and DETA/NO showed a significant delay of tumor growth compared to the untreated group. Furthermore, the Kaplan-Meier survival analyses showed a difference of the median survival times between the mice treated with DETA/NO + mPEG-Pb*a* (59 days) and the mice treated with mPEG-Pb*a*/PDT alone (52.5 days) [91].

The data obtained both *in vitro* and *in vivo* with the combined treatment of an NO donor and PDT [91] are significant and open new horizons for the optimization of photodynamic treatment.

New Therapeutic Strategies with Nitric Oxide and PDT

The effect of the combined treatment DETA/NO + Pb*a*/PDT in an *in vivo* application may be more complex than its effects *in vitro,* due essentially to a systemic effect of the NO donor and especially to its lack of organ or tissue specificity. Therefore, it is exceedingly challenging to selectively deliver NO to a target compartment, to prevent changes of vascular dynamics that result in systemic hypotension [111]. An alternative approach is to deliver NO via the site specific activation of a prodrug, which minimizes adverse drug reactions.

In collaboration with Dr. Greta Varchi, ISOF-CNR, Bologna, Italy, we have synthesized a new compound, named DRPDT2 (Fig. 14.5).

This is a conjugate between Pb*a* (as photosensitizer) and an NO donor that allows a controlled release of NO in the tumor at the time of irradiation of the photosensitizer. The combination between singlet oxygen ($^1O_2$), reactive oxygen species (ROS) and NO should culminate in synergistic cytotoxicity, increasing the efficacy of PDT used alone. Moreover, the linker between the two molecules is intended to increase specificity towards a particular target in prostate carcinoma. Preliminary results have demonstrated that DRPDT2 is a good PS in terms of no toxicity in the dark, easy and cheap synthesis and rapid clearance. It must be irradiated with a white light in order to activate both Pb*a* (λ = 670 nm) and the release of NO (λ = 400 nm). The DRPDT2 treatment performed *in vitro* with different lines of prostate cancer cells demonstrated a higher cytotoxic activity then Pb*a* treatment alone. Moreover, DRPDT2 acts through the NF-κB/YY1/Snail/RKIP loop causing an inhibition of NF-κB and, consequently, a strong upregulation of RKIP (unpublished data).

An alternative approach reported in the literature is to deliver NO via PDT: inert PS is activated by irradiation, followed by the decomposition of the excited elec-

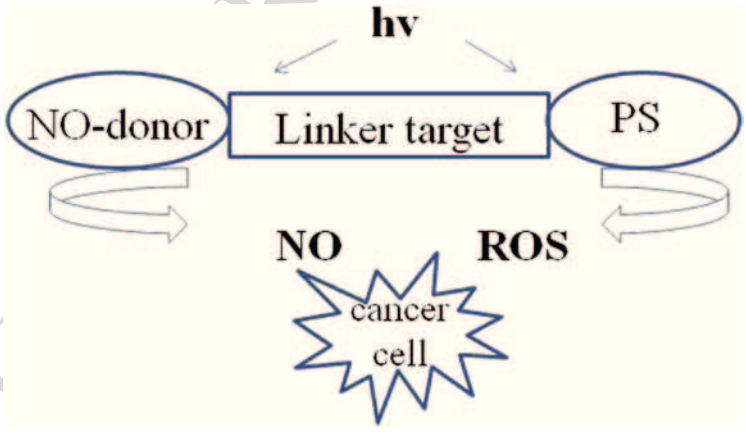

Fig. 14.5 Design of a PDT-NO conjugate. The conjugate is constituted by a an NO donor and a photosensitizer linked together through a linker that allows to increase the selectivity to the tumor cells. The light irradiation causes, at the same time, the release of units of NO and the activation of the PS

tronic state to release NO. This technique has been tested with thionitrites, also known as S-nitrosothiols (SNTs) of glutathione (GSH) forming S-nitrosoglutathione (GSNO) [112–113] and penicilamine [114], as well as photolabile metal-NO complexes [115–116]. Recently, an NO donor has been developed that combines thermal and chemical stabilities to increase the kinetics of NO release during photoactivation [117].

Conclusions and Future Directions

The ability to readily control the kinetics of NO release from these new conjugates, reported above, opens up a range of PDT applications [118]. In particular, regulation of the NO flux has the potential to provide therapies for hypoxia-reperfusion disorders and cardiovascular disease, while a higher exposure levels to these PDT agents could be used to selectively kill malignant cells. The use of these particular PDT-NO conjugates is desirable in cancer therapy to improve classical PDT, taking advantage of nitric oxide by excluding its harmful systemic effects.

Acknowledgements This work has been carried out with the financial support of AIRC (Italian Association for Cancer Research), Project code 10546 (2010-13). We also acknowledge Drs. Bonavida, Varchi and Xodo for their collaborative efforts.

No Conflict Statement No potential conflicts of interest were disclosed.

References

1. Dougherty TJ, Gomer CJ, Henderson BW, Jori G, Kessel D, Korbelik M, Moan J, Peng Q. Photodynamic therapy. J Natl Cancer Inst. 1998;90:889–905.
2. Dolmans DE, Fukumura D, Jain RK. Photodynamic therapy for cancer. Nat Rev Cancer. 2013;3:380–7.
3. Allison RR, Sibata CH. Oncologic photodynamic therapy photosensitizers: a clinical review. Photodiagnosis Photodyn Ther. 2010;7:61–75.
4. Triesscheijn M, Baas P, Schellens JH, Stewart FA. Photodynamic therapy in oncology. Oncologist. 2006;9:1034–44.
5. Plaetzer K, Krammer B, Berlanda J, Berr F, Kiesslich T. Photophysics and photochemistry of photodynamic therapy: fundamental aspects. Lasers Med Sci. 2009;24:259–68.
6. Agostinis P, Berg K, Cengel KA, Foster TH, Girotti AW, Gollnick SO, Hahn SM, Hamblin MR, Juzeniene A, Kessel D, Korbelik M, Moan J, Mroz P, Nowis D, Piette J, Wilson BC, Golab J. Photodynamic therapy of cancer: an update. CA Cancer J Clin. 2011;61:250–81.
7. Moan J Porphyrin photosensitization and phototherapy Photochem. Photobiol. 1986;43:681–90.
8. De Rosa FS Bentley MV. Photodynamic therapy of skin cancers: sensitizers, clinical studies and future directives. Pharm. Res. 2000;17:1447–55.
9. Hamblin MR, Newmann EL. On the mechanism of the tumour-localising effect in photodynamic therapy. J Photochem Photobiol B. 1994;23:3–8.

10. Iyer AK, Greish K, Seki T, Okazaki S, Fang J, Takeshita K, Maeda H. Polymeric micelles of zinc protoporhyrin for tumor targeted delivery based on EPR effect and singlet oxygen generation. J Drug Target. 2007;15:496–506.
11. Kessel D. The role of low-density lipoprotein in the biodistribution of photosensitizing agents. J Photochem Photobiol B. 1992;14:261–2.
12. Sibani SA, McCarron PA, Woolfson AD, Donnelly RF. Photosensitizer delivery for photodynamic therapy. Part 2: systemic carrier platforms. Expert Opin Drug Deliv. 2008;5:1241–54.
13. Juzeniene A, Nielsen KP, Moan J. Biophysical aspects of photodynamic therapy. J Environ Pathol Toxicol Oncol. 2006;25:7–28.
14. Nowis D, Makowski M, Stokłosa T, Legat M, Issat T, Gołab J. Direct tumor damage mechanisms of photodynamic therapy. Acta Biochim Pol. 2005;52:339–52.
15. Wilson BC, Patterson MS The physics, biophysics and technology of photodynamic therapy. Phys Med Biol. 2008;53:R61–R109.
16. Allison RR, Moghissi K. Photodynamic Therapy (PDT): PDT Mechanisms. Clin Endosc 2013;46:24–9.
17. Robertson CA, Evans DH, Abrahamse H. Photodynamic therapy (PDT): a short review on cellular mechanisms and cancer research applications for PDT. J Photochem Photobiol B. 2009;96:1–8.
18. Henderson BW, Busch TM, Snyder JW. Fluence rate as a modulator of PDT mechanisms. Lasers Surg Med. 2006;38:489–93.
19. Juzeniene A, Juzenas P, Ma LW, Iani V, Moan J. Effectiveness of different light sources for 5-aminolevulinic acid photodynamic therapy. Lasers Med Sci. 2004;19:139–49.
20. Szeimies RM, Morton CA, Sidoroff A, Braathen LR. Photodynamic therapy for non-melanoma skin cancer. Acta Derm Venerol. 2005;85:483–90.
21. Beyer W. Systems for light application and dosimetry in photodynamic therapy. J Photochem Photobiol B. 1996;36:153–6.
22. Platzer K, Krammer B, Berlanda J, Berr F, Kiesslich T. Photophysics and photochemistry of photodynamic therapy: fundamental aspects. Lasers Med Sci. 2009;24:259–68.
23. Foote CS. Mecganisms of photosensitized oxidation. There are several different types of photosensitized oxidation which may be important in biological systems. Science. 1968;162:963–70.
24. Dai T, Fuchs BB, Coleman JJ, Prates RA, Astrakas C, St Denis TG, Ribeiro MS, Mylonakis E, Hamblin MR, Tegos GP. Concepts and principles of photodynamic therapy as an alternative antifungal discovery platform. Front Microbiol. 2012;3:1–16.
25. Castano AP, Demidova TN, Hamblin MR. Mechanisms in photodynamic therapy: part two-cellular signaling, cell metabolism and modes of cell death. Photodiagnosis Photodyn Ther. 2005;2:1–23.
26. Ortel B, Shea CR, Calzavara-Pinton P. Molecular mechanisms of photodynamic therapy. Front Biosci. 2009;14:4157–72.
27. Kessel D, Castelli M. Evidence that bcl-2 is the target of three photosentizers that induce a rapid apoptotic response. Photochem Photobiol. 2001;74:318–22.
28. Xue LY, Chiu SM, Oleinick NL. Photochemical destruction of the Bcl-2 oncoprotein during photodynamic therapy with the phthalocyanine photosensitizer Pc4. Oncogene. 2001;20:3420–7.
29. Usuda J, Chiu SM, Murphy ES, Lam M, Niemimen AL, Oleinick NL. Domain-dependent photodamage to Bcl-2. A membrane anchorage region is needed to form the target of phthalocyanine photosensitization. J Biol Chem. 2003;278:2021–9.
30. Buytaert E, Dewaele M, Agostinis P. Molecular effectors of multiple cell death pathways initiated by photodynamic therapy. Biochim Biophys Acta. 2007;1776:86–107.
31. Berg K, Moan J. Lysosomes as photochemical targets. Int J Cancer. 1994;59:814–22.
32. Reiners JJ Jr, Caruso JA, Mathieu P, Chelladurai B, Yin XM, Kessel D. Release of cytochrome c and activation of pro-caspase-9 following lysosomal photodamage involves Bid cleavage. Cell Death Differ. 2002;9:934–44.

33. Kessel D. Relocalization of cationic porphyrins during photodynamic therapy. Photochem Photobiol Sci. 2002;1:837–40.
34. Vanlangenakker N, Vanden Berghe T, Krysko DV, Festjens N, Vandenabeele P. Molecular mechanisms and pathophysiology of necrotic cell death. Curr Mol Med. 2008;8:207–20.
35. Zong WX, Thompson CB. Necrotic death as a cell fate. Genes Dev. 2006;20:1–15.
36. Nakagawa T, Shimizu S, Watanabe T, Yamaguchi O, Otsu K, Yamagata H, Inohara H, Kubo T, Tsujimoto Y. Cyclophilin D-dependent mitochondrial permeability transition regulates some necrotic but non apoptotic cell death. Nature. 2005;434:652–8.
37. Dewaele M, Maes H, Agostinis P. ROS-mediated mechanisms of autophagy stimulation and their relevance in cancer therapy. Autophagy. 2010;6:838–54.
38. Reiners JJ Jr, Agostinis P, Berg K, Oleinick NL, Kessel D. Assessing autophagy in the context of photodynamic therapy. Autophagy. 2010;6:7–18.
39. Karin M. Cancer research in flames; tracking inflammation's role in promoting malignancy could lead to better treatments. Scientist. 2005;19:24–5.
40. Benelli R, Morini M, Carrozzino F, Ferrari N, Minghelli S, Santi L, Cassatella M, Noonan DM, Albini A. Neuthrophils as a key cellular target for angiostatin: implications for regulation of angiogenesis and inflammation. FASEB J. 2002;16:267–9.
41. Ferrario A, von Tiehl KF, Rucker N, Schwarz MA, Gill PS, Gomer CJ. Anti-angiogenic treatment enhances photodynamic therapy responsiveness in a mouse mammary carcinoma. Cancer Res. 2000;60:4066–9.
42. Ferrario A, von Tiehl KF, Wong S, Luna M, Gomer CJ. Cyclooxygenase-2 inhibitor treatment enhances photodynamic therapy-mediated tumor response. Cancer Res. 2002;62:3956–61.
43. Ferrario A, Fisher AM, Rucker N, Gomer CJ. Celecoxib and NS-398 enhance photodynamic therapy by increasing in vitro apoptosis and decreasing in vivo inflammatory and angiogenic factors. Cancer Res.2005;65:9473–9.
44. Ferrario A, Chantrain CF, von Tiehl KF, Buckley S, Rucker N, Shalinsky DR, Shimada H, DeClerck YA, Gomer CJ. The matrix metalloproteinase inhibitor Prinomastat enhances photodynamic therapy responsiveness in a mouse tumor model. Cancer Res. 2004;64:2328–32.
45. Ferrario A, Gomer CJ. Avastin enhances photodynamic therapy treatment of Kaposi's sarcoma in a mouse tumor model. J Environ Path Tox Oncol. 2006;25:251–9.
46. Gollnick SO, Evans SS, Baumann H, Owczarczak B, Maier P, Vaughan L, Wang WC, Unger E, Henderson BW. Role of cytokines in photodynamic therapy –induced local and systemic inflammation. Br J Cancer. 2003;88:1772–9.
47. Makowski M, Grzela T, Niderla J, Azarczyk M, Mroz P, Kopee M, Legat M, Strusinska K, Koziak K, Nowis D, Mrowka P, W, Nishikawa N, Uchida K, Yoshikawa K, Noguchi T, Miyaishi O, Shimozato K, Saga S, Matsumoto Y. Cyclooxygenase-2 is a possible target of treatment approach in conjunction with photodynamic therapy for various disorders in skin and oral cavity. Br J Dermatol. 2004;151:472–80.
48. Korbelik M, Parkins CS, Shibuya H, Cecic I, Stratford MR, Chaplin DJ. Nitric oxide production by tumor tissue: impact on the response to photodynamic therapy. Br J Cancer. 2000;82:1835–43.
49. Tozer GM, Everett SA. Nitric oxide in tumor biology and cancer therapy. Part 2: therapeutic implications. Clin Oncol. 1997;9:357–64.
50. Jenkins CD, Charles IG, Thomsen LL, Moss DW, Holmes LS, Baylis SA, Rhodes P, Westmore K, Emson PC, Moncada S. Roles of nitric oxide in tumor growth. Proc Nat Acad Sci USA. 1995;92:4392–6.
51. Korbelik M, Shibuya H, Cecic I. Relevance of nitric oxide to the response of tumours to photodynamic therapy. SPIE. 1998;3247:98–105.
52. Henderson B, Sitnik-Busch TM, Vaughan LA. Potentiation of photodynamic therapy antitumor activity in mice by nitric oxide synthase inhibition is fluence rate dependent. Photochem Photobiol. 1999;70:64–71.
53. Di Venosa G Perotti C Fukuda H Battle A Casas A. Sensitivity to ALA-PDT of cell lines with different nitric oxide production and resistance to NO cytotoxicity. J Photochem Photobiol B. 2005;80:195–202.

54. Yamamoto F, Ohgari Y, Yamaki N, Kitajima S, Shimokawa O, Matsui H, Taketani S. The role of nitric oxide in delta-aminolevulinic acid (ALA)-induced photosensitivity of cancerous cells. Biochem Biophys Res Commun. 2007;353:541–6.
55. Reeves KJ, Reed MWR, Brown NJ. The role of nitric oxide in the treatment of tumours with aminolevulinic acid-induced photodynamic therapy. J Photochem Photobiol B. 2010;101:224–32.
56. Thomsen LL, Lawton FG, Knowles RG, Beesley JE, Riveros-Moreno V, Moncada S. Nitric oxide synthase activity in human gynecological cancer. Cancer Res. 1994;54:1352–4.
57. Thomsen LL, Miles DW, Happerfield L, Bobrow LG, Knowles RG, Moncada S. Nitric oxide synthase activity in human cancer. Br J Cancer. 1995;72:41–4.
58. Cobbs CS, Brenman JE, Aldape KD, Bredt DS, Israel MA. Expression of nitric oxide synthase in human central nervous system tumors. Cancer Res. 1995;15:727–30.
59. Rosbe KW, Prazma J, Petrusz P, Mims W, Ball SS, Weissler MC. Immunohistochemical characterization of nitric oxide synthase activity in squamous cell carcinoma of the head and neck. Otolaryngol Head Neck Surg. 1995;113:541–9.
60. Parkins CS, Dennis MF, Stratford MR, Hill SA, Chaplin DJ. Ischemia reperfusion injury in tumors: the role of oxygen radicals and nitric oxide. Cancer Res. 1995;55:6026–9.
61. Reeves KJ, Reed MWR, Brown NJ. Is nitric oxide important in photodynamic therapy? J Photochem Photobiol. 2009;95:141–7.
62. Gilissen MJ, van de-Merbel-de Wit, Star WM, Koster JF, Sluiter W. Effect of photodynamic therapy on the endothelium-dependent relaxation of isolated rat aortas. Cancer Res. 1993;53:2548–52.
63. Schmidt HHH, Walker U. NO at work. Cell. 1994;78:919–25.
64. Vanhoutte PM. Endothelium and responsiveness of vascular smooth mucle. J Hypertens. 1987;5:S115–20.
65. Kubes P, Suzuki M, Granger DN. Nitric oxide: an endogenous modulator of leukocyte adhesion. Proc Natl Acad Sci USA. 1991;88:4651–5.
66. Gupta S, Ahmad N, Mukhtar H. Involvement of nitric oxide during phthalocyanine (Pc4) photodynamic therapy-mediated apoptosis. Cancer Res. 1998;58:1785–8.
67. Dalbasti T, Cagli S, Killnc E, Oktar N, Ozsoz M. Online electrochemical monitoring of nitric oxide during photodynamic therapy. Nitric Oxide. 2002;7:301–5.
68. Cecic I, Korbelik M. Mediators of peripheral blood neutrophilia induced by photodynamic therapy of solid tumors. Cancer Lett. 2002;183:43–51.
69. McCall TB, Boughton-Smith NK, Palmer RM, Whittle BJ, Moncada S. Synthesis of nitric oxide from L-arginine by neutrophils. Release and interaction with superoxide anion. Biochem J. 1989;261:293–6.
70. Mehta JL, Lawson DL, Nicolini FA, Ross MH, Player DW. Effects of activated polymophonuclear leukocytes on vascular smooth muscle tone. Am J Physiol. 1991;261:H327–34.
71. Evans TJ, Buttery LDK, Carpenter A, Springall DR, Polak JM, Cohen J. Cytokine-treated human neutrophils contain inducible nitric oxide synthase that produces nitration of ingested reeves bacteria. Proc Natl Acad Sci USA. 1996;93:9553–8.
72. Singh S, Gupta AK. Nitric oxide: role in tumour biology and iNOS/NO-based anticancer therapies. Cancer Chemother Pharmacol. 2011;67:1211–24.
73. Beckman JS, Beckman TW, Chen J, Marshall PA, Freeman BA. Apparent hydroxyl radical production by peroxinitrite: implications for endothelial injury from nitric oxide and superoxide. Proc Natl Acad Sci USA. 1990;87:1620–4.
74. Beckman JS, Crow JP. Pathological implications of nitric oxide, superoxide and peroxynitrite formation. Biochem Soc Trans. 1993;21:330–4.
75. Korbelik M, Parkins CS, Shibuya H, Cecic I, Stratford MR, Chaplin DJ. Nitric oxide production by tumour tissue: impact on the response to photodynamic therapy. Br J Cancer. 2002;82:1835–43.
76. Gaboury JP, Anderson DC, Kubes P. Molecular mechanisms involved in superoxide-induced leukocyte-endothelial cell interactions in vivo. Am J Physiol. 1994;266:H637–42.

77. Kurose I, Wolf R, Grisham MB, Granger DN. Modulation of ischemia/reperfusion-induced microvascular dysfunction by nitric oxide. Circ Res. 1994;74:376–82.
78. Liu L, Stamler JS. NO: an inhibitor of cell death. Cell Death Diff. 1999;6:937–42.
79. Melino G, Catani MV, Corazzari M, Guerrieri P, Bernassola F. Nitric oxide can inhibit apoptosis or switch it into necrosis. Cell Mol Life Sci. 2000;57:612–22.
80. Rossig L, Fichrlscherer B, Breitschopf K, Haendeler J, Zeither AM, Mulsch A, Dimmeler S. Nitric oxide inhibits caspase-3 by S-nitrosation in vivo. J Biol Chem. 1999;274:6823–6.
81. Dimmeler S, Haendeler J, Nehls M, Zeiher AM. Suppression of apoptosis by nitric oxide via inhibition of interleukin-1beta-converting enzyme (ICE)-like and cysteine protease protein (CPP)-32-like proteases. J Exp Med. 1997;185:601–7.
82. Gomes ER, Almeida RD, Carvalho AP, Duarte CB. Nitric oxide modulates tumor cell death induced by photodynamic therapy through a cGMP-dependent mechanism. Photochem Photobiol.2002;76:423–30.
83. Bhowmick R, Girotti AW. Cytoprotective signaling associated with nitric oxide upregulation in tumor cells subjected to photodynamic therapy-like oxidative stress. Free Radic Biol Med. 2013;57:39–48.
84. Bhowmick R, Girotti AW. Pro-survival and pro-growth effects of stress-induced nitric oxide in a prostate cancer photodynamic therapy model. Cancer Lett. 2014;343:115–22.
85. Baritaki S, Yeung K, Palladino M, Berenson J, Bonavida B. Pivotal roles of Snail inhibition and RKIP induction by the proteosoma inhibitor NPI-0052 in tumor cell chemosensitization. Cancer Res. 2009;69:8376–85.
86. Wink DA, Mitchell JB. Chemical biology of nitric oxide: insights into the regulatory, cytotoxic, and cytoprotective mechanisms of nitric oxide. Free Radic Bio Med. 1998;24:434–56.
87. Fukumura D, Kashiwagi S, Jain RK. The role of nitric oxide in tumor progression. Nat Rev Cancer. 2006;6:521–34.
88. Baritaki S, Huerta-Yepez S, Sahakyan A, Karagiannides I, Bakirtzi K, Jazirehi A, Bonavida B. Mechanisms of nitric oxide-mediated inhibition of EMT in cancer: inhibition of the metastasis-inducer Snail and induction of the metastasis-suppressor RKIP. Cell Cycle. 2010;9:4931–40.
89. Coupienne I, Fettweis G, Rubio N, Agostinis P, Piette J. NF-kappaB inhibition improves the sensitivity of human glioblastoma cells to 5-aminolevulinic acid-based photodynamic therapy. Biochem Pharmacol. 2011;81:606–16.
90. Rapozzi V, Umezawa K, Xodo LE. Role of NF-kB/Snail/RKIP loop in the response of tumor cells to photodynamic therapy. Lasers Surg Med. 2011;43:575–85.
91. Rapozzi V, Della Pietra E, Zorzet S, Zacchigna M, Bonavida B, Xodo LE. Nitric oxide-mediated activity in anti-cancer photodynamic therapy. Nitric Oxide. 2013;30:26–35.
92. Tang PMK, Chan JYM, Au SWN, Kong SK, Tsui SKW, Waye MMY, Mak TC, Fong WP, Fung KP. Pheophorbide *a*, an active compound isolated from *Scutellaria barbata*, possess photodynamic activities by inducing apoptosis in human hepatocellular carcinoma. Cancer Biol Ther. 2006;5:1111–6.
93. Rapozzi V, Miculan M, Xodo LE. Evidence that photoactivated pheophorbide *a* causes in human cancer cells a photodynamic effect involving lipid peroxidation. Cancer Biol Ther. 2009;8:1318–27.
94. Damsky CH, Richa J, Solter D, Knudsen K, Buck CA. Identification and purification of a cell surface glycoprotein mediating intercellular adhesion in embryonic and adult tissue. Cell 1983;34:455–66.
95. Takeichi M. Cadherin cell adhesion receptors as a morphogenic regulator. Science. 1991;251:1451–5.
96. Vleminckx K, Vakaet I Jr, Mareel M, Fiers W, van Roy F. Genetic manipulation of E-cadherin expression by epithelial tumor cells reveals an invasion suppressor role. Cell. 1991:66:107–19.
97. Umbas R, Isaac WB, Bringuier PP, Schaafsma HE, Karhaus HFM, Oosterhof GO, Debruyne FM, Schalken JA. Decreased E-cadherin expression is associated with poor prognosis in patients with prostate cancer. Cancer Res. 1994;54:3929–33.

98. De Marzo AM Knudsen B Chan-Tack K Epstein JI. E-cadherin expression as a marker of tumor aggressiveness in routinely processed radical prostatectomy specimens. Urology. 1999;53:707–13.
99. Lang SH, Hyde C, Reid IN, Hitchcock IS, Hart CA, Bryden AA, Villette JM, Stower MJ, Maitland NJ. Enhanced expression of vimentin in motile prostate cell lines and in poorly differentiated and metastatic prostate carcinoma. Prostate. 2002;52:253–63.
100. Salvatori L, Caporuscio F, Verdina A, Starace G, Crispi S, Nicotra MR, Russo AN, Calogero RA, Morgante E, Natali PG, Russo MA, Petrangeli E. Cell-to-cell signaling influences the fate of prostate cancer stem cells and their potential to generate more aggressive tumors. Plos One. 2012;7:e31467.
101. Whicha MS. Cancer stem cells and metastasis: lethal seeds. Clin Cancer Res. 2006;12:5606–7.
102. Mani SA, Guo W, Laio MJ, Eaton EN, Ayyanan A, Zhou AY, Brooks M, Reinhard F, Zhang CC, Shipitsin M, Campbell LL, Polyak K, Brisken C, Yang J, Weinberg RA. The epitheial-mesenchymal transition generates cells with properties of stem cells. Cell. 2008;133:704–15.
103. Niziolek M, Korytowski W, Girotti AW. Chaion-breaking antioxidant and cytoprotective action of nitric oxide on photodynamically stressed tumor cells. Photochem Photobiol 2003;78:262–70.
104. Li C, Wogan GN. Nitric oxide as a modulator of apoptosis. Cancer Lett. 2005;225:1–15.
105. Bhowmick R, Girotti AW. Cytoprotective induction of nitric oxide synthase in a cellular model of 5-aminolevulinic acid-based photodynamic therapy. Free Radic Biol Med. 2010;48:1296–301.
106. Bhowmick R, Girotti AW. Signaling events in apoptotic photokilling of 5-aminolevulinic acid-treated tumor cells: inibitory effects of nitric oxide. Free Radic Biol Med. 2009;47:731–40.
107. Reynaert NL, Ckless K, Korn SH, Vos N, Guala AS, Wouters EF, van der Vliet A, Janssen-Heininger YM. Nitric oxide represses inhibitory kappaB kinase through S-nitrosylation. Proc Natl Acad Sci USA. 2004;101:8945–50.
108. Davies KM, Wink DA, Saavedra JE, Keefer LK. Chemistry of the diazeniumdiolates. 2. Kinetics and mechanism of dissociation to nitric oxide in aqueous solution. J Am Chem Soc. 2001;208:5473–81.
109. Huerta-Yepez S, Yoon NK, Hernandez-Cueto A, Mah V, Rivera-Pazos CM, Chatterjee D, Vega MI, Maresh EL, Horvath S, Chia D, Bonavida B, Goodglick L. Expression of phosphorylated raf kinase inhibitor protein (pRKIP) is a predictor of lung cancer survival. BMC Cancer. 2011;11:259–67.
110. Rapozzi V, Zacchigna M, Biffi S, Garrovo C, Cateni F, Stebel M, Zorzet S, Bonora GM, Drioli S, Xodo LE. Conjugated PDT drug: photosensitizing activity and tissue distribution of PEGylated pheophorbide *a*. Cancer Biol.Ther. 2010;10:471–82.
111. Shan SQ, Rosner GL, Braun RD, Hahn J, Pearce C, Dewhirst MW. Effects of diethylamine/nitric oxide on blood perfusion and oxygenation in the R3230Ac mammary carcinoma. Br J Cancer. 1997;76:429–37.
112. Sexton DJ, Muruganandam A, McKenney DJ, Mutus B. Visible light photochemical release of nitric oxide from S-nitrosoglutathione: potential photochemotherapeutic applications. Photochem Photobiol. 1994;59:463–7.
113. Zhelyaskov VR, Gee KR, Godwin DW. Control of NO concentration in solutions of nitrosothiol compounds by light. Photochem Photobiol. 1998;67:282–8.
114. Singh RJ, Hogg N, Joseph J, Kalyanaraman B. Photosensitized decomposition of S-nitrosothiols and 2-methyl-2-nitrosopropane possible use for site-directed nitric-oxide production. FEBS Lett. 1995;360:47–51.
115. Carneiro ZA, de Moraes JC, Rodrigues FP, de Lima RG, Curti C, de Rocha ZN, Paulo M, Benhack LM, Tedesco AC, Formiga AL, da Silva RS. Phototoxic activity of a nitrosyl phtalocyanine ruthenium complex- a system capable of producing nitric oxide and singlet oxygen. J Inorg Biochem. 2011;105:1035–43.

116. Ostrowski AD, Deakin SJ, Azhar B, Miller TW, Franco N, Chemey MM, Lee AJ, Burstyn JN, Fukuto JM, Megson IL, Ford PC. Nitric oxide photogeneration from trans-Cr(cyclam)$(ONO)_2^+$ in a reducing environment. Activation of soluble guanylyl cyclase and arterial vasorelaxation. J Med Chem. 2010;53:715–22.
117. Giles NM, Kumari S, Gang BP, Yuen CWW, Billaud EMF, Giles GI. The molecular design of S-bitrosothiols as photodynamic agents for controlled nitric oxide release. Chem Biol Drug Des. 2012;80:471–8.
118. Lancaster JR Jr, Giles GI. Nitrogen monoxide (nitric oxide):bioinorganic chemistry. In: King RB, editor. Encyclopedia of inorganic chemistry, 2nd edn. Chichester: Wiley. 1994. pp. 1–21.

AQ4

Chapter 14: Author Query

AQ1. Figures 14.1 and 14.3 are low quality. Please provide better quality images.

AQ2. Please check heading levels.

AQ3. We have renumbered Scheme 14.1 and 14.2 to Figs. 14.4 and 14.5 respectively. Please check and confirm.

AQ4. We have updated the year of publication for reference: [118]. Please check and confirm

Nitric Oxide 45 (2015) 43–53

Contents lists available at ScienceDirect

Nitric Oxide

journal homepage: www.elsevier.com/locate/yniox

Repeated sub-optimal photodynamic treatments with pheophorbide *a* induce an epithelial mesenchymal transition in prostate cancer cells via nitric oxide

Emilia Della Pietra [a], Francesca Simonella [a], Benjamin Bonavida [b], Luigi Emilio Xodo [a], Valentina Rapozzi [a,*]

[a] Department of Medical and Biological Sciences, School of Medicine, University of Udine, Udine, Italy
[b] Department of Microbiology, Immunology and Molecular Genetics, David Geffen School of Medicine, Jonsson Comprehensive Cancer Center, University of California Los Angeles, Los Angeles, California 90095, USA

ARTICLE INFO

Article history:
Received 28 October 2014
Revised 31 December 2014
Accepted 12 February 2015
Available online 17 February 2015

Keywords:
Prostate cancer cells
Pheophorbide *a*
Photodynamic therapy
Epithelial–mesenchymal transition
Nitric oxide

ABSTRACT

Photodynamic therapy (PDT) is a clinically approved treatment that causes a selective cytotoxic effect in cancer cells. In addition to the production of singlet oxygen and reactive oxygen species, PDT can induce the release of nitric oxide (NO) by up-regulating nitric oxide synthases (NOS). Since non-optimal PDT often causes tumor recurrence, understanding the molecular pathways involved in the photoprocess is a challenging task for scientists. The present study has examined the response of the PC3 human metastatic prostate cancer cell line following repeated low-dose pheophorbide *a* treatments, mimicking non-optimal PDT treatment. The analysis was focused on the NF-kB/YY1/RKIP circuitry as it is (i) dysregulated in cancer cells, (ii) modulated by NO and (iii) correlated with the epithelial to mesenchymal transition (EMT). We hypothesized that a repeated treatment of non-optimal PDT induces low levels of NO that lead to cell growth and EMT via the regulation of the above circuitry. The expressions of gene products involved in the circuitry and in EMT were analyzed by western blot. The findings demonstrate the cytoprotective role of NO following non-optimal PDT treatments that was corroborated by the use of L-NAME, an inhibitor of NOS.

1. Introduction

Photodynamic therapy (PDT) is a clinically approved, minimally invasive therapeutic treatment that causes a selective cytotoxic effect against malignant cells. The procedure consists of the administration of a photosensitizer (PS) followed by irradiation at a wavelength falling within a PS absorbance band. In the presence of oxygen, a series of events lead to direct tumor cell death, damage to the microvasculature and induction of a local inflammatory reaction [1]. The success of this therapy depends on the type and dose of PS, the time between PS administration and light exposure, the light dose and the fluence rate [2]. Recent data suggest that PDT-mediating changes to the tumor microenvironment can modulate the responsiveness of the treatment. Preclinical investigations indicated that combining PDT with targeted therapies directed at attenuating the pro-survival actions of the tumor microenvironment can enhance the therapeutic potential of PDT [3].

Several reports support the role of nitric oxide (NO) in PDT, by considering both the endogenous level of NO in the tumor [4–6] and NO directly induced by the photoactivated photosensitizers [7–9]. NO is known to directly influence a number of biological processes involved in PDT-induced anti-tumor effects [10,11].

The biphasic role of NO in PDT seems to depend on a number of factors in the microenvironment, including the responsiveness of the tumor type, the redox state of the reaction, as well as the final intracellular concentration and the duration of intracellular exposure to nitric oxide [12–14]. Data in the literature indicated that low NO levels (<50 nM) enhance the survival, proliferation, and growth of tumor cells, by protecting the cells from apoptosis, whereas high NO levels (>300 nM) exhibit cytotoxic effects, by promoting DNA damage, protein dysfunctions, gene mutations and tumor cell death. Together, these effects may contribute to tumor regression [15,16].

Concerning a low level of NO induced by PDT, several hypotheses have been proposed in order to explain underlying mechanisms

Abbreviations: EMT, epithelial–mesenchymal transition; iNOS, inducible nitric oxide synthase; NO, nitric oxide; $^1O_2$, singlet oxygen; Pb*a*, pheophorbide *a*; PDT, photodynamic therapy; ROS, reactive oxygen species; WB, western blot.

* Corresponding author. Department of Medical and Biological Sciences, School of Medicine, University of Udine, P.le Kolbe 4, 33100 Udine, Italy. Fax: +39 0432 494301.
E-mail address: valentina.rapozzi@uniud.it (V. Rapozzi).

http://dx.doi.org/10.1016/j.niox.2015.02.005
1089-8603/

of inhibition of apoptosis induced by NO [17–21]. It has been reported that NO inhibits the activation of caspases directly by S-nitrosylation [22,23], by a cyclic guanosine monophosphate (cGMP)-dependent mechanism or by activating protein kinase G (PKG) [24]. Recently, Girotti and co-workers demonstrated that the cytoprotective role of NO in PDT is also due to the suppression of pro-apoptotic JNK and p38 MAPK activations [8,18]. We propose another important pathway involved in tumor progression that is susceptible to NO, namely, the dysregulation of the NF-kB/YY1/Snail/RKIP circuitry. In a murine amelanotic melanoma we have reported that, according to the dose of the pheophorbide *a*/PDT (Pb*a*/PDT) added to the cells, and consequently by the NO level induced by PDT, there were either progression or arrest of tumor growth, through the modulation of this circuitry [9,18].

A disagreement also exists on the role of NO in the regulation of steps that are involved in the metastatic process. Metastasis is initiated with the acquisition of invasive and migratory properties by the tumor cells: a process known as epithelial to mesenchymal transition (EMT). EMT is a target of several constitutively activated survival pathways including the NF-kB pathway [25–27]. NF-kB induces EMT via the regulation of the expression of multiple matrix proteases, adhesion molecules and both angiogenic and invasive factors [25,28–32].

Considering that (i) low NO concentrations have been reported to induce tumor cell migration and invasion [12,15]; (ii) PDT modulates the effect of NF-kB in a dose-dependent manner [18,33] through NO induction [9,18], (iii) NF-kB regulates downstream gene products such as YY1 [34], a hallmark for the initiation of EMT during development and cancer metastasis and (iv) YY1 is overexpressed in prostate cancer cells [35], we investigated if a repeated low-dose Pb*a*/PDT treatment can stimulate cell progression and induce EMT in a highly metastatic human prostate cancer cell line through the modulation of the NF-kB/YY1/RKIP circuitry.

2. Materials and methods

2.1. Cell culture

The human prostate cancer PC3 cells were cultured in RPMI medium which contained 10% fetal bovine serum and antibiotics (penicillin 100 U/ml, streptomycin 100 μg/ml and glutamine 2 mM) (CELBIO, Milan, Italy). Cells were maintained in a humidified atmosphere with 5% CO_2 air at 37 °C. All experiments were performed using cells in the exponential growth phase.

2.2. Photodynamic treatment and iNOS inhibitors

Pheophorbide *a* (Pb*a*) ($C_{35}H_{36}N_4O_5$; MW 592.69) was purchased from Frontier Scientific Inc., Logan, UT. Pb*a* was dissolved in dimethylsulfoxide (DMSO) and conserved in aliquots of 0.5 mM at –80 °C. The stability in solution of Pb*a* was checked by measuring its UV–vis spectrum at weekly intervals. Cells were treated with Pb*a* in the dark for 3 h, then irradiated with a metal halogen lamp with red filter for 7 min (0.84 J/cm^2). The IC_{50} value of Pb*a*/PDT at 24 h in our model is ~100 nM, that we consider as high dose of Pb*a*/PDT treatment; we assume that 40 nM is the low dose of Pb*a*/PDT treatment.

The iNOS inhibitors, L-N^G-nitroarginine methyl ester (L-NAME) and N-(3-aminomethyl)benzyl) acetamide (1400 W), were obtained from Cayman Chemical Company (INALCO, Milan, Italy). The reagents were prepared in phosphate buffered saline (PBS) before cell treatment. The treatment with each iNOS inhibitor (1 mM L-NAME or 10 μM 1400 W) was performed 1 h before light irradiation.

2.3. Procedure for a repeated low-dose Pb*a*/PDT treatment

PC3 cells were seeded at day 0, at a density of 5×10^5 cells in a 30 mm Petri dish. After 48 h they were treated with 40 nM (low-dose) Pb*a*/PDT and after two days they were harvested and re-seeded at the same concentration (500 cells). The final population received a total of 8 cycles of PDT. The initial population, not subjected to PDT, was non-treated cells (NT). The cellular population that was submitted to four and eight PDT treatments was called IV and VIII treatments, respectively. Each experimental assay was performed 24 h after the last PDT treatment.

2.4. Cell metabolic assay

PC3 cells were seeded in a 96-well plate at a density of 5×10^3 cells/well. After 24 h the cells were treated with Pb*a* for 3 h before light irradiation. The cell proliferation, in terms of metabolic activity, was determined by the resazurin assay following the manufacturer's instructions (Sigma–Aldrich, Milan, Italy). The values were obtained by using the spectrofluorometer (EnSpire™ 2300 Multilabel reader, PerkinElmer, Finland).

Pictures were taken with an epiluminescent microscope Leica DMI6000B (Leica Microsystem, Heidelberg, Germany) at a 40-fold magnification to evaluate cell growth and viability.

2.5. Cell cycle analysis by FACS

For the cell cycle analyses, the PC3 cells, after repeated treatments, were harvested by trypsinization and fixed in 70% ethanol for 1 h at 4 °C. After PBS washing, the cells were stained with 0.05 mg/ml propidium iodide in the presence of 0.1 mg/ml RNase A in PBS (30 min at room temperature). The samples were analyzed by a FACScan flow cytometer (Becton-Dickinson, San Jose CA). A minimum of 10,000 cells for each sample was acquired in list mode and analyzed with the FLUOJO software (Tri Star, Inc., Ashland, OR).

2.6. Clonogenic assay

After repeated treatments, PC3 cells were seeded at a density of 500 cells in a 60 mm Petri dish. After 18 days, the colonies were formed, fixed and stained with 2.5% methylene blue in 50% ethanol. The images were obtained by Gel DOC 2000 Bio-Rad (Milan, Italy).

2.7. Fluorometric determination of nitric oxide with DAF-FM diacetate

PC3 cells were seeded at a cell density of 6×10^5 cells/well in a 6-well plate. The day after, the cells were treated with different concentrations of Pb*a*. This indirect assay to measure NO is based on the DAF-FM diacetate (4-amino-5-methylamino-2′,7′-difluorofluorescein diacetate) (D-23844, Molecular Probes, Invitrogen, Milan, Italy) method. The DAF-FM diacetate diffuses into cells and tissue where non-specific esterases hydrolyze the diacetate residues thereby trapping DAF within the intracellular space. NO-derived nitrosating agents such as N_2O_3 nitrosate DAF to yield a highly fluorescent product, DAF triazole. This compound has some important advantages compared to 4,5-diaminofluorescein diacetate (DAF-2 diacetate), which is considered the most common indicator for nitric oxide.

A 5 mM stock solution of DAF-FM diacetate (MW = 496) was made in DMSO. The cells, after Pb*a*/PDT treatment, were incubated with 10 μM of diluted DAF-FM diacetate for 30 min at 37 °C. The cells were then washed with PBS to remove excess probe and replaced with fresh PBS and incubated for an additional 15 min to allow complete de-esterification of the intracellular diacetates. The cells were then trypsinized from the plate, recovered in PBS and measured by

FACS (FACScan, Becton Dickinson, San Jose, CA). The samples were analyzed with the FLUOJO software (Tri Star, Inc., Ashland, OR).

2.8. Western blot analysis

The protein extracts (40 μg), obtained from whole cell lysates, were subjected to electrophoresis on 12% SDS–PAGE and transferred to a nitrocellulose membrane 70 V for 2 h. The filter was blocked for 1 h with PBS–0.01% Tween (Sigma–Aldrich, Milan, Italy) containing 5% dry non-fat-milk, and then incubated, at 4 °C overnight, with the primary antibodies [rabbit polyclonal anti-RKIP (G38, Cell Signaling, Merck Millipore, Darmstadt, Germany) diluted 1:1000; rabbit polyclonal anti-NF-κB p65 (C-20, sc-372 Santa Cruz Biotechnology, Santa Cruz, CA), diluted 1:1000; rabbit polyclonal anti-iNOS antibody (NOS2, sc-651 Santa Cruz Biotechnology, Santa Cruz, CA), diluted 1:200; mouse monoclonal anti-E-cadherin (610182 BD Biosciences) diluted 1:2500; mouse monoclonal anti-vimentin (VIRE/1 sc 517721 Santa Cruz Biotechnology, Santa Cruz, CA) diluted 1:1000; rabbit polyclonal anti-YY1 (C-20, sc-281 Santa Cruz Biotechnology, Santa Cruz, CA) diluted 1:1000; rabbit polyclonal anti-Akt (#9272, Cell Signaling Technology), diluted 1:1000; rabbit monoclonal anti-phospho-Akt (#4058, Cell Signaling Technology), diluted 1:1000]. The expression of β-actin, used as an internal control, was detected with a mouse monoclonal anti β-actin (Ab-1, CP01, Calbiochem, Merck Millipore, Darmstadt, Germany), diluted 1:10,000. The filters were incubated for 1 h with the secondary antibodies [anti-rabbit IgG, diluted 1:4000 (Calbiochem, Merck Millipore, Darmstadt, Germany), anti-mouse IgM, diluted 1:5000 (Calbiochem, Merck Millipore, Darmstadt, Germany), anti mouse IgG diluted 1:4000 (Calbiochem, Merck Millipore, Darmstadt, Germany)]. Each secondary antibody was coupled to horseradish peroxidase (HPR). For the detection of the proteins, we used ECL (enhanced chemiluminescence) reagents (Super Signal®West PICO, and Super Signal®West FEMTO, ThermoFisher Scientific Pierce, Rockford, USA). The exposure length depended on the antibodies used and was usually between 30 s and 5 min. The protein levels were quantified by the Image Quant TL Version 2003 software (Amersham).

3. Results

3.1. Effect of Pba/PDT on prostate cancer cells

In our approach we have evaluated the efficacy of pheophorbide *a* (Pb*a*), a chlorophyll derivative, as a photosensitizer in PC3 human prostatic carcinoma cells. The Pb*a*/PDT treatment was performed as follows: the cells were seeded and after 24 h were treated with Pb*a* for 3 h in the dark. Thereafter, the cells were irradiated with a white halogen lamp equipped with a red filter, at a fluence of 0.84 J/cm^2 (Fig. 1 top). The percentage of metabolic activity after Pb*a*/PDT treatment of the PC3 carcinoma cells is shown in Fig. 1A. There was a concentration-dependent effect with an estimated IC_{50} of ~100 nM of Pb*a*. In the PC3 cells treated with a Pb*a* concentration <80 nM, we observed in the first 24 h a weak growth arrest and after 48 h a cell recovery, in comparison with the non-treated cells (Fig. 1B). This behavior in PC3 cells is in agreement with our previous observations of treatments with a low-dose Pb*a*/PDT applied to Hela, HepG2 [36] and B78-H1 tumor cells [9].

3.2. Effect of a repeated low-dose Pba/PDT treatment in PC3 cells

Since a sub-optimal Pb*a*/PDT concentration promotes cell recurrence in a short period of time in prostate cancer cells, we investigated the cell response following a repeated low-dose Pb*a*/PDT treatment. Two possibilities were envisaged: the repeated treatment may result in a cumulative effect that may cause an arrest of tumor cell growth. Alternatively, the repeated treatment may cause a stimulation of cell proliferation, a critical aspect of PDT, as cell recurrence could not only inhibit the therapeutic effect of the PDT treatment, but also could stimulate the tumor towards invasiveness and metastasis [3].

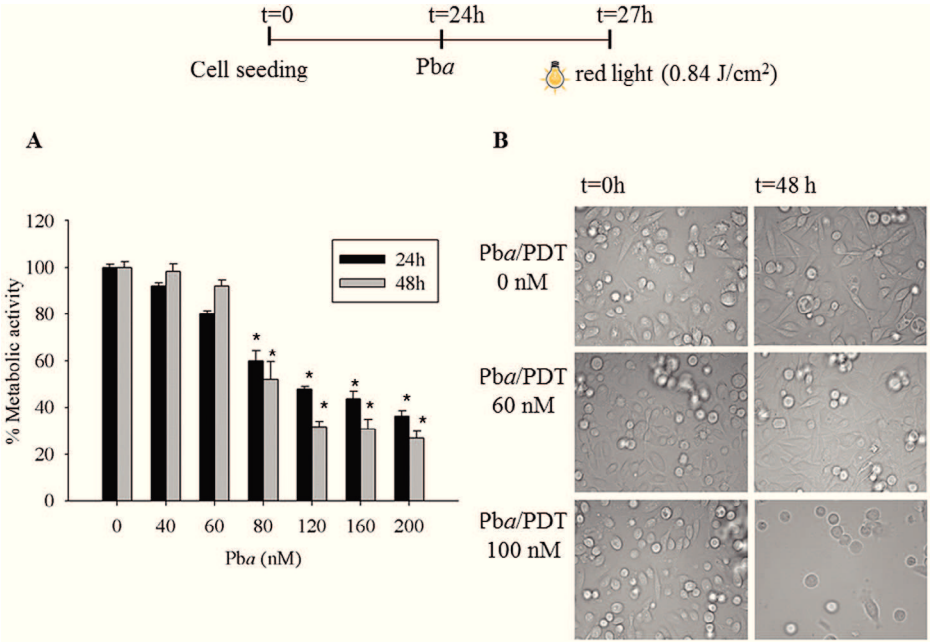

Fig. 1. Effect of Pb*a*/PDT treatment on the metabolic activity in PC3 prostate carcinoma cells. The schematic panel represents the experimental PDT procedure: PC3 cells were seeded at day 0 (t = 0), after 24 h they were treated with Pb*a* for 3 h and light irradiated (0.84 J/cm^2). (A) The histograms represent the values of % metabolic activity, performed by the resazurin assay, 24 and 48 h after light irradiation and expressed as T/C × 100. T and C are the absorbance of treated and non-treated cells. The values are the mean ± SD of four independent experiments. A standard t-test versus control was performed ($P < 0.01$). (B) (B) Phase-contrast micrographs of PC3 cells treated with 0, 60, or 100 nM Pb*a* soon and 48 h after light irradiation.

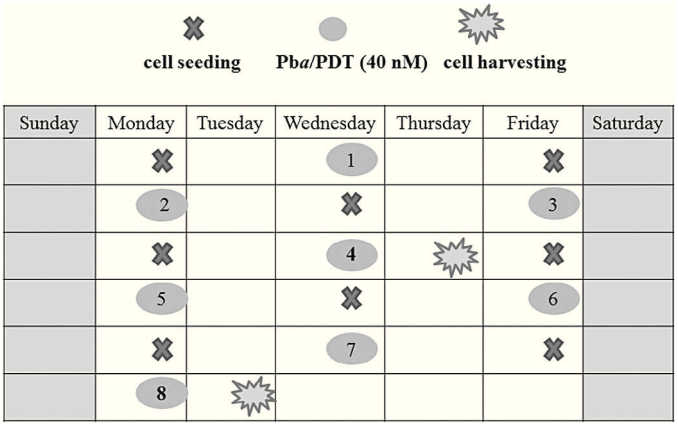

Scheme 1. Schematic panel of repeated treatment. PC3 cells were seeded at day 0 at a density of 5×10^5 cells in a 6-well plate, after 48 h they were submitted to PDT treatment (3 h with a low dose of Pb*a*/PDT (40 nM) and then light irradiated). After an additional 48 h the cells were harvested and re-seeded as above. This procedure was repeated four or eight times, when the cells were harvested and processed for different experiments. The symbols ✖, ●, and ✸ represent the cell seeding, Pb*a*/PDT treatment and cell harvesting respectively.

As a low-dose Pb*a*/PDT, we chose a treatment with 40 nM Pb*a*, which is capable to induce 5–10% cell growth inhibition 24 h after light irradiation and growth recovery after 48 h (Fig. 1). The schedule of the repeated treatment is shown in Scheme 1. The PC3 cells, 2 days after seeding, were treated with Pb*a*/PDT. After an additional 2 days, the cells were harvested and re-seeded and were treated as above. The treatment lasted ~5 weeks. To follow the cell changes throughout the experiment, the cells were examined after the fourth (IV) and eighth (VIII) treatment. The cells were healthy and had a normal cell cycle profile as determined by FACS analysis (Supplementary Fig. S1).

To investigate if a repeated low-dose Pb*a*/PDT treatment stimulated cell proliferation, we performed a clonogenic assay as described in methods (Fig. 2). PC3 cells were harvested after the IV and VIII low-dose Pb*a*/PDT treatments and seeded (500 cells) in a 30 mm Petri dish. After 18 days, the colonies that had developed were counted. It was evident that by proceeding with the treatment, the number and size

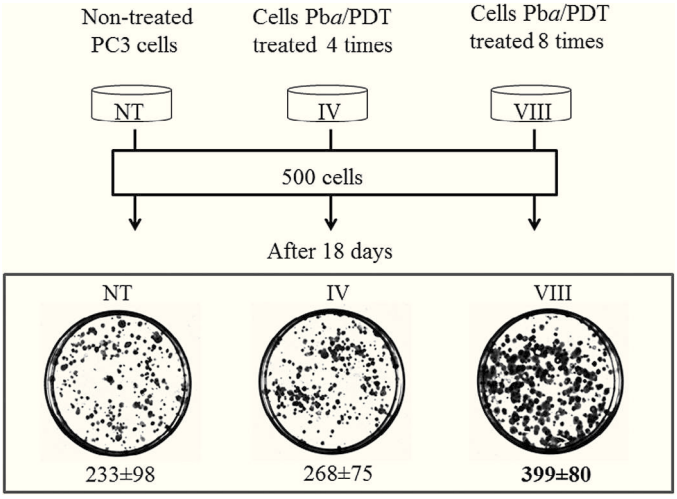

Fig. 2. Clonogenic assay after a repeated low-dose Pb*a*/PDT treatment. After the IV and the VIII Pb*a*/PDT repeated treatment, 500 cells from each group were seeded in 60 mm petri dishes. After 18 days the colonies were formed, fixed and stained with 2.5% methylene blue in 50% ethanol. The images were obtained with Gel Doc 2000 Bio-Rad. The number of colonies (>50 cells) is reported below each plate. The experiment has been performed in triplicate.

of the colonies increased (Fig. 2). This finding clearly showed the stimulation of cell proliferation after a repeated low-dose Pb*a*/PDT treatment. This result indicates that a repeated low-dose Pb*a*/PDT treatment does not result in a cumulative effect leading to tumor growth arrest. Importantly, this finding also suggests that a metronomic therapy with Pb*a* in prostate cancer cells is not recommended, in contrast with the treatment with 5 aminolevulinic acid ALA [37,38].

3.3. Induction of NO in PC3 cells treated with Pba/PDT

Reported experimental evidence supports the notion that, in addition to ROS and $^1O_2$, NO plays an important role in PDT [4,5,7]. We, therefore, monitored NO production in photo-stressed PC3 cells by using a fluorophore (DAF-FM). After cell uptake, DAF-FM is hydrolyzed to DAF that can be nitrosated by NO by-products to yield a fluorescent compound detected by FACS. Fig. 3A demonstrates the fluorescence intensity in PC3 cells after Pb*a*/PDT treatment. The fluorescence signal, which indirectly represents NO-byproducts, increased in a concentration-dependent manner in PC3 prostate cancer cells. To be sure that the increase of fluorescence obtained through the reaction between NO-byproducts and DAF is due to an increase of NO compared to the release of ROS after PDT treatment (Supplementary Fig. S2), we performed a Western blot analysis with Pb*a*/PDT-treated prostate carcinoma cells to determine the levels of protein iNOS. As shown in Fig. 3B, PC3 cells expressed a substantial increase of iNOS levels as a function of the Pb*a*/PDT concentration used. The iNOS levels were measured 16 h after light irradiation: i.e. the time point at which we observed a high iNOS expression induced by Pb*a*/PDT (data not shown). At the highest Pb*a*/PDT concentration (80 nM), the level of iNOS as determined densitometrically was 1.75 fold compared to control (non-treated cells).

To support that the increase of NO in PC3 cells was effectively due to its induction by Pb*a*/PDT, we repeated the Western blot and the FACS analysis on Pb*a* photostressed cells that were treated with an inhibitor of the iNOS synthase. We used L-NAME and 1400 W (a non specific and a specific iNOS inhibitor, respectively). They were added to Pb*a*-treated PC3 cell culture before light irradiation. Fig. 4A shows that both inhibitors reduced the protein iNOS expression. In addition to iNOS protein levels also the measurements of NO levels, reported in Fig. 4B and C, confirmed that iNOS inhibitor treatments mildly suppressed NO production demonstrating that pheophorbide *a* can upregulate, after light activation, the NO levels in prostate cancer cells. These data are in agreement with those obtained with two other photosensitizers: phtalocyanine (Pc4) in human epidermoid carcinoma A431 cells [7] and 5-aminolevulinic acid (ALA) both in COH-BR1 breast cancer cells [39] and PC3 cells [8].

3.4. Effect of a repeated low-dose Pba/PDT treatment on the NF-kB/YY1/RKIP circuitry in prostate cancer cells

It is known that activated NF-κB upregulates downstream anti-apoptotic gene products, including the metastasis inducer and anti-apoptotic Snail [40,41] and the resistance inducer and anti-apoptotic YY1 [35]. Furthermore, it has been reported that these gene products repress the expression of the metastatic suppressor Raf-1 kinase inhibitory protein (RKIP), belonging to the phosphatidylethanolamine-binding protein family [42]. In the active form, RKIP suppresses both the Raf-1/MEK/ERK and NF-kB survival pathways [43,44]. Since RKIP inhibits NF-kB [45], it is involved in a circuitry linking NF-kB, Snail and YY1 [Scheme 2]. We focused our attention on this particular NF-kB/Snail/YY1/RKIP circuitry [18] to investigate the molecular mechanism involved in the stimulation of tumor cell growth after a repeated low-dose Pb*a*/PDT treatment. As mentioned above, we compared the protein lysates obtained 24 h after the IV and the VIII treatments to follow the

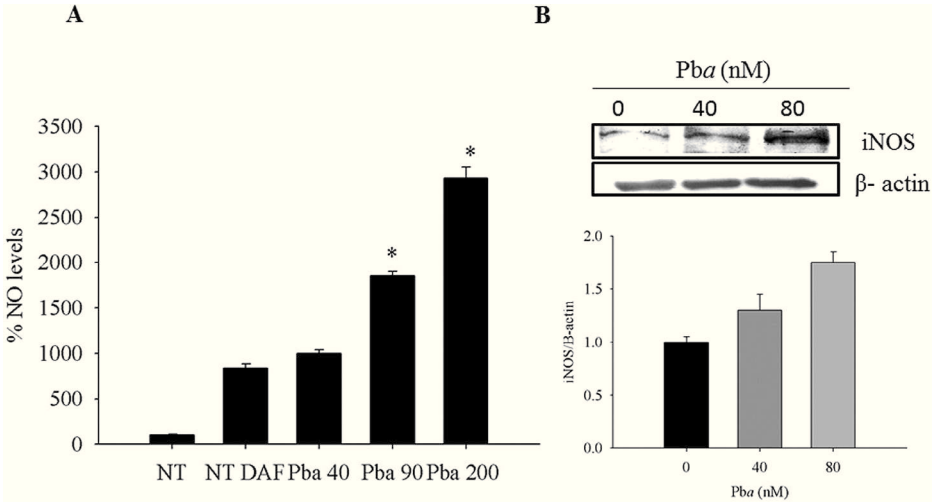

Fig. 3. Determination of NO levels induced by Pb*a*/PDT treatment in PC3 cells. (A) The histograms report the mean fluorescence of NO/by products (expressed in percent respect non-treated cells) after Pb*a*/PDT treatments. The values were obtained by the DAF-FM reaction and measured by FACS. The values are the mean ± SD of three independent experiments. A standard *t*-test versus control (NT DAF) was performed (* $P < 0.01$). (B) Expression of iNOS protein level by immunoblot analysis. PC3 cells were treated with different concentrations of Pb*a* (0, 40 and 80 nM). Protein lysates were analyzed 16 h after irradiation. The iNOS band intensity for each sample was determined densitometrically, normalized to β-actin and further normalized to the ratio of non-treated cells/β-actin, fixed to 1.

proceeding of the experiment. Western analysis in Fig. 5A shows the expression of the gene products involved in the circuitry. During the repeated treatment, there was an increase in the expressions of NF-kB (p65) and of YY1. The enhancement of both factors in PC3 cells suggested a pro-survival response to the repeated Pb*a*/PDT treatment. In agreement with this finding, we also observed a reduction of the expression of the pro-apoptotic RKIP gene product. As the loss of RKIP function has been associated with metastasis in an increasing number of solid tumors [46,47], this result suggested that repeated low-dose Pb*a*/PDT treatment in PC3 cells

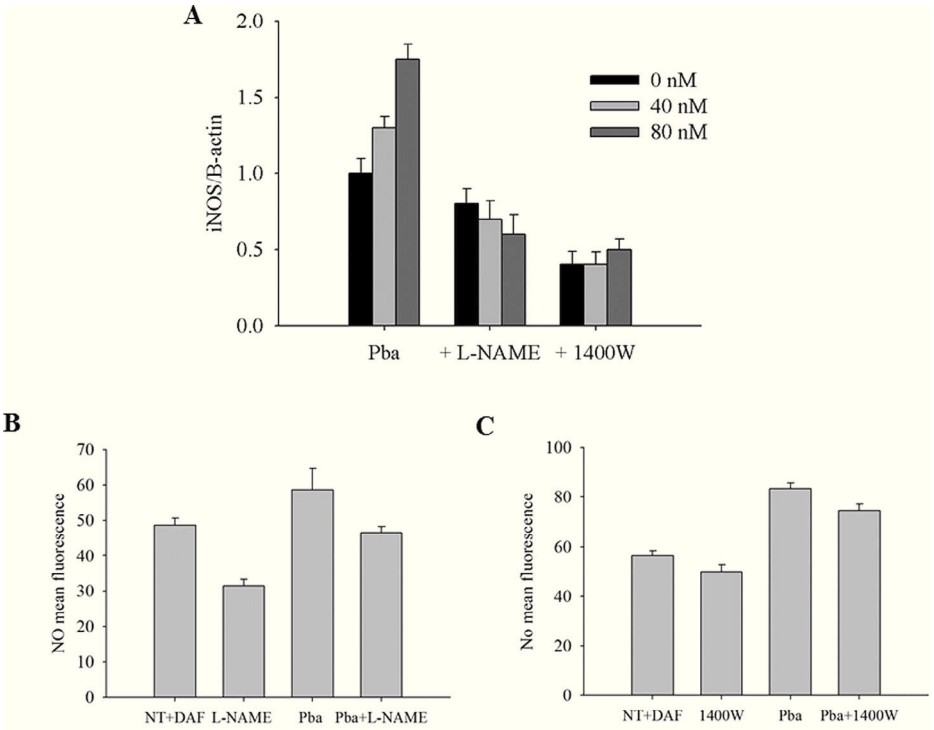

Fig. 4. (A) Expression of the iNOS protein level after a single combined treatment with Pb*a*/PDT and iNOS inhibitors. PC3 cells were divided into 3 groups: Pb*a*, cells treated with different dose of Pb*a* (0–40–80 nM) for 3 h in the dark and light irradiated; + L-NAME, cells treated with different doses of Pb*a* +1 mM L-NAME, 1 h before light irradiation; +1400 W, cells treated with different doses of Pb*a* +10 μM 1400 W, 1 h before light irradiation. All protein lysates were analyzed 16 h after irradiation. The histograms report the values of the iNOS band intensity determined densitometrically, normalized to β-actin and further normalized to the ratio of non-treated cells /β-actin, fixed to 1. (B) The histograms report the mean fluorescence of NO/by products in PC3 cells treated with Pb*a* 200 nM (3 h) and L-NAME 5 mM (1 h before light irradiation). The DAF-FM assay was performed 3 h after light irradiation. The values are the mean ± SD of two independent experiments. (C) The histograms report the mean fluorescence of NO/by products in PC3 cells treated with Pba 200 nM (3 h) and 1400 W 10 μM (1 h before light irradiation). The DAF-FM assay was performed soon after light irradiation. The values are the mean ± SD of two independent experiments.

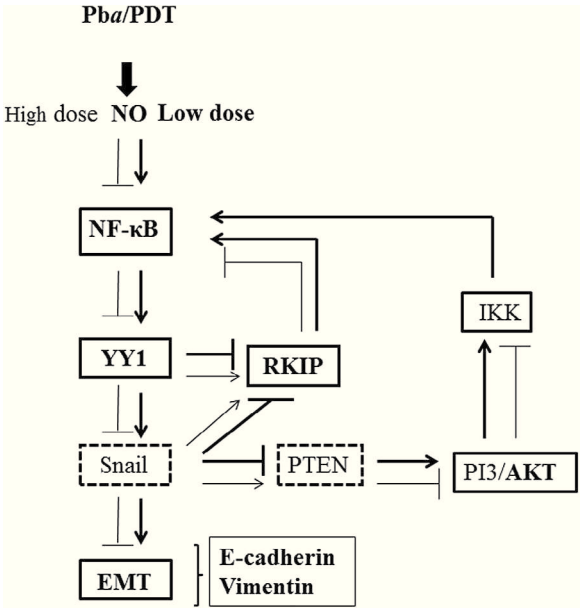

Scheme 2. The role of Pb*a*/PDT, through the induction of NO, on the regulation of EMT via NF-kB/YY1/Snail/RKIP/PTEN circuitry. Pb*a*/PDT, in dependence by the dose (low in light gray and high in bold), modulates the NF-kB expression. NF-kB regulates downstream genes such as YY1 and Snail that are strictly correlated. Both YY1 and Snail modulate the expression of pro-apoptotic RKIP. The inhibition of RKIP results in the minimal inhibition of NF-kB and activation of YY1 and Snail. The activation of YY1 and Snail induces the EMT. Likewise Snail modulates the metastasis suppressor phosphate and tensin homologue (PTEN). The suppression of PTEN results in the maintenance of the PI3/K-AKT activated pathway that cross-talks with the NF-kB pathway. These dysregulated gene products in the circuit result in the induction of EMT.

activated the NF-κB/YY1/RKIP circuitry and resulted in the stimulation of cell proliferation.

3.5. A repeated low-dose Pb*a*/PDT treatment induces EMT in PC3 cells

EMT is thought to play a fundamental role during the early steps of invasion and metastasis in carcinoma cells [48,49]. It allows the cells to dissociate from the epithelial tissue from which they originate and to migrate freely. A critical feature of EMT is the downregulation of E-cadherin, a protein involved in cell adhesion. E-cadherin acts *de facto* as a tumor suppressor by inhibiting invasion and metastasis, and it is frequently repressed or degraded during EMT transformation [50]. The loss of E-cadherin may result directly from the activation of its repressor Snail [40,51] or indirectly from the activation of AKT [52,53], which via NF-kB regulates the expression of E-cadherin [35]. The possible links between NF-kB, YY1, Snail, RKIP, AKT and EMT [35–54] are shown in Scheme 2.

The expressions of E-cadherin and vimentin after a repeated low-dose Pb*a*/PDT treatment are shown in Fig. 5B. There was a decrease of E-cadherin and an increase of vimentin: two variations that indicate the transition from the epithelial to the mesenchymal morphology, i.e. the early step of cell invasion. Moreover, there was an increase of phosphorylated AKT over non-phosphorylated AKT (pAKT/AKT) (Fig. 5C). The increase of both pAKT and NF-kB suggests that AKT can induce the activation of NF-kB and consequently EMT, in keeping with the previous studies by Julien et al. [55].

The above findings confirm that a repeated low-dose Pb*a*/PDT treatment in PC3 cells results in the stimulation of cell proliferation.

3.6. Role of NO in inducing EMT after a repeated low-dose Pb*a*/PDT treatment

A repeated low-dose Pb*a*/PDT treatment mildly stimulated the expression of iNOS (Fig. 6). Thus, we investigated the impact of NO on EMT. To address this point, we set up a new repeated treatment by combining Pb*a*/PDT with L-NAME, an iNOS inhibitor. L-NAME was added to the cells at 1 mM, 1 h before light irradiation (Scheme 3). The repeated combination of L-NAME + Pb*a*/PDT treatment decreased the iNOS expression as shown in the histogram of Fig. 7. On the basis of this finding, we evaluated: (i) the protein levels of the gene products involved in the NF-kB/YY1/RKIP circuitry and in EMT, (ii) the cell cycle by FACS and (iii) the clonogenic capacity. By immunoblotting, a strong inhibitory effect by L-NAME on the Pb*a* effect was observed. The repeated combined L-NAME and Pb*a*/PDT treatments decreased the expressions of both NF-kB and YY1 and induced a strong expression of RKIP, suggesting a reduction of cell growth (Fig. 8A). This result is in agreement with the findings of the clonogenic assay (Fig. 8B), which showed a strong reduction in the number of colonies in the cells treated with L-NAME and Pb*a*/PDT compared to each single treatment. Moreover, the analysis of the cell cycle of PC3 cells repeatedly treated with L-NAME and Pb*a*/PDT showed an increase of the G2/M and subG1 phases, indicating cell growth arrest (Table 1) [56].

Considering the expression of the proteins involved in EMT (Fig. 9A), PC3 cells treated repeatedly with L-NAME and Pb*a*/PDT resulted in a high level of E-cadherin expression and a concomitant strong reduction of vimentin and p-AKT (Fig. 9B), suggesting the inhibition of EMT.

The data obtained by the repeated combined treatment of the iNOS inhibitor and Pb*a*/PDT confirmed the role of NO in PDT and underlining, for the first time, a result of the administration of low-dose Pb*a*/PDT in PC3 prostate cancer cells; thus implying a continuous low level of NO can induce cell proliferation and EMT.

4. Discussion

Photodynamic therapy is an oncologic treatment for different types of tumors not only superficial (skin, cutaneous T cell lymphoma) but also for tumors growing in internal organs (prostate, breast, bladder, lung, esophagus, etc.). The successful clinical application of PDT is a complex interplay of light, oxygen and photosensitizer which generate reactive oxygen species, in time and space-dependent manners, that may destroy the tumor tissue under optimal conditions [57]. When these particular conditions are not achieved, PDT can lead to tumor recurrence [58]. This undesired outcome represents a challenge for the clinical therapeutic applications of PDT in the treatment of cancer.

To enhance the efficacy of PDT in therapy, it is important to nullify the processes that cause cell recurrence and, eventually, invasion and metastasis. A number of studies have examined both the direct and indirect PDT effects upon various non-malignant components of the tumor microenvironment which cause inflammation and

Table 1
Cell-cycle analyses of PC3 cells after combined L-NAME + Pb*a*/PDT repeated treatments. NT, non-treated cells; Pb*a* VIII, cells treated with eight repeated low-dose Pb*a*/PDT treatments; L-NAME, cells treated eight times with 1 mM L-NAME and L-NAME + Pb*a*, cells treated eight times with combined low-dose Pb*a*/PDT + L-NAME treatment.

Treatment	Freq G1	Freq S	Freq G2/M	Freq SubG1
NT	68.5	7.5	8.2	0.4
Pb*a* VIII	66.29	9.61	7.5	0.5
L-NAME	66.27	8.73	7.9	0.6
L-NAME + Pb*a*	68.98	1.52	23.35	2.32

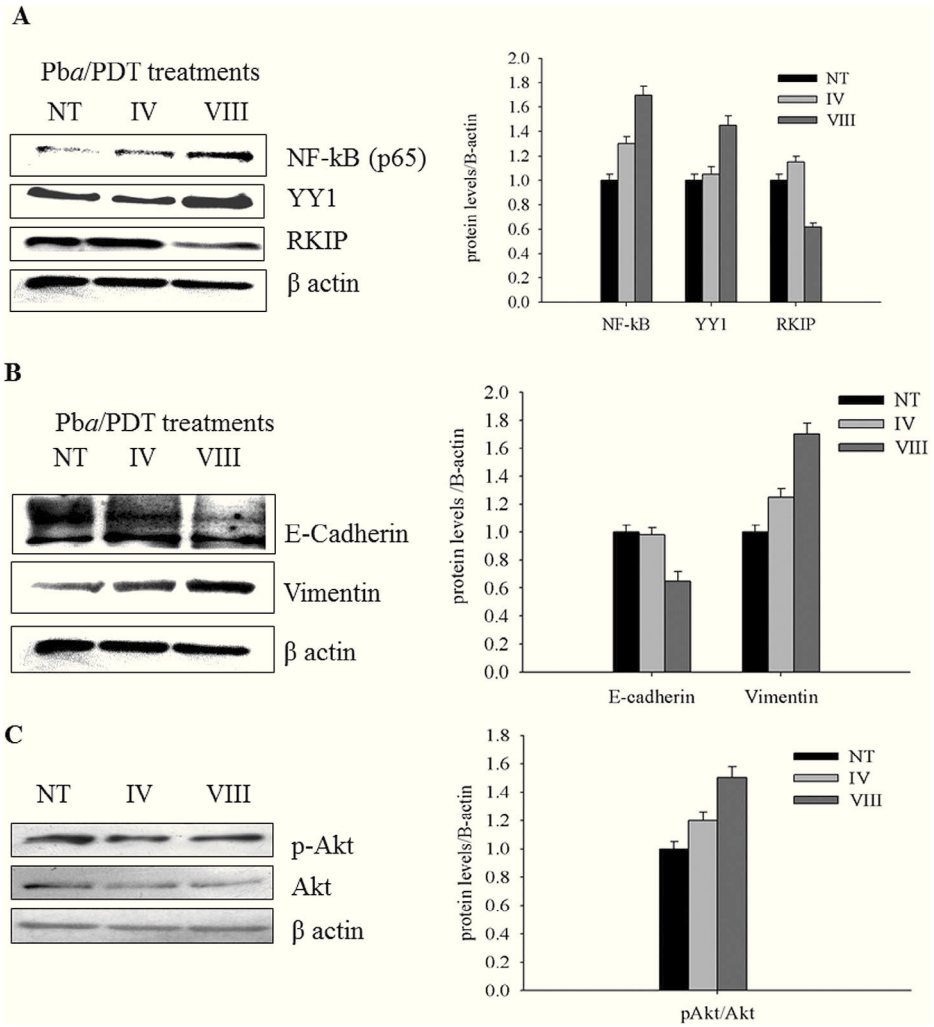

Fig. 5. Western blot analysis of (A) gene products of the NF-kB/YY1/RKIP circuitry; (B) gene products of EMT and C) gene product pAKT/AKT. PC3 cells were treated for four (IV) or eight (VIII) times with a repeated low-dose (40 nM) Pb*a*/PDT. NT represents the non-treated cells. The protein lysates were analyzed 48 h after the last treatment. The histograms report the values of the different protein band intensity determined densitometrically, normalized to β-actin and further normalized to the ratio of non-treated cells /β-actin, fixed to 1.

angiogenesis. The investigation of these particular processes has led to the use of several inhibitors that target the angiogenic and pro-survival molecules in order to enhance PDT effectiveness [59–64].

In the present study, we focused on the role of NO in tumor cells treated with PDT. NO can influence the antitumoral response to PDT both in terms of the endogenous NO [4,11] and the exogenous NO generated by photoactivated PS [7,8].

The controversial role of NO in cancer is found also in PDT: a high-level of NO induced by PDT determines tumor growth arrest [9]; in contrast, low-level NO is cytoprotective [65]. This last effect has

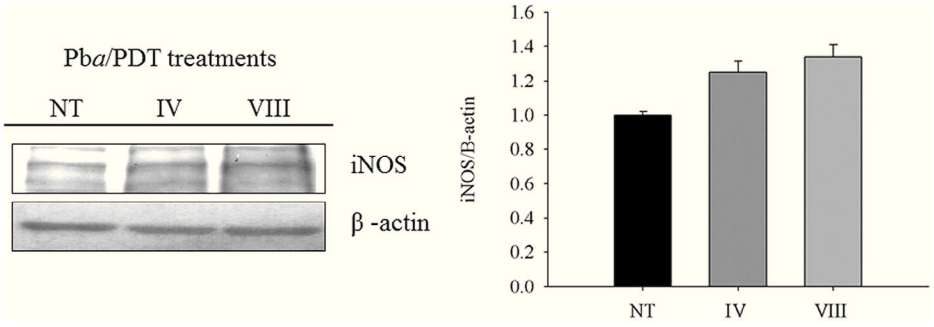

Fig. 6. Expression of iNOS protein during a repeated low-dose Pb*a*/PDT treatment. The protein lysates were analyzed 16 h after the IV and VIII treatments. The histograms report the values of the iNOS band intensity determined densitometrically, normalized to β-actin and further normalized to the ratio of non-treated cells /β-actin, fixed to 1.

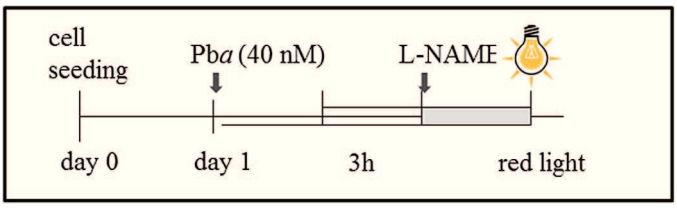

Scheme 3. Schematic panel to describe the combined treatment Pb*a* + L-NAME/PDT during the repeated treatment. L-NAME (1 mM) was administered to the PC3 cells 1 h before light irradiation.

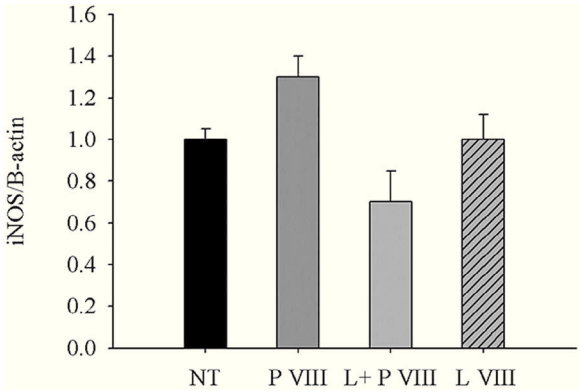

Fig. 7. Reduction of iNOS protein level, induced after a repeated low-dose Pb*a*/PDT, by an iNOS inhibitor. PC3 cells were divided into 4 groups: NT, non-treated cells; P VIII, cells treated with Pb*a* (40 nM) eight times, L + P VIII, cells treated eight times with a combined repeated treatment L-NAME + Pb*a*/PDT; L VIII, cells treated with L-NAME (1 mM) eight times. The protein lysates were analyzed 16 h after the last treatment. The histograms report the values of the iNOS band intensity determined densitometrically, normalized to β-actin and further normalized to the ratio of non-treated cells /β-actin, fixed to 1.

been highlighted through different signaling pathways such as: caspase inactivation by S-nitrosylation [22,23], protein kinase G activation [24] and suppression of pro-apoptotic JNK and p38 MAPK pathways [8,18]. In the present study, we have confirmed a cytoprotective role of NO in prostate cancer cells with a repeated low-dose Pb*a*/PDT treatment, and for the first time, we have highlighted how this effect, through modulation of the NF-kB/YY1/ /RKIP circuitry, can cause cell recurrence and EMT. EMT has been found to promote carcinoma invasion and metastasis [66–68]. It is a highly conserved cellular process that allows polarized, immotile epithelial cells to convert into motile mesenchymal-like cells.

Some studies have described, in different types of tumor cells treated with a photosensitizer, the changes in the morphology, the alteration in the cytoskeleton leading to a different adhesivity [69–74]. But the molecular mechanisms leading to PDT-mediated EMT have not yet been reported. In this study, we have observed that in a prostate carcinoma cell model, under conditions mimicking a suboptimal PDT condition, EMT can be stimulated through the downregulation of the epithelial marker E-cadherin and upregulation of the mesenchymal marker vimentin.

To explain the molecular mechanism leading to EMT, we focused on the NF-kB/Snail/YY1/RKIP circuitry. This particular circuitry is often dysregulated in cancer cells [75–77] and modulated by NO [9,78]. Recently, we have observed in murine amelanotic melanoma B78-H1 cells, both *in vitro* and *in vivo*, that Pb*a*/PDT treatment modulates this circuitry, through the induction of NO, causing either a cell proliferation arrest or a tumor growth stimulation, according to the Pb*a*/PDT concentration used [9,18].

In this study, we examined the relationship among NO, NF-kB/Snail/YY1/RKIP and EMT in PC3 carcinoma cells, considering also the cross-talk of the P13/AKT pathway and the NF-kB pathway and the regulation of EMT [50,51,53]. Since Snail is not well expressed in our prostatic cancer cells (data not shown), we decided to focus on YY1, as it is overexpressed in prostate cancer tissues, as demonstrated by tissue microarray experiments [79]. YY1 is a

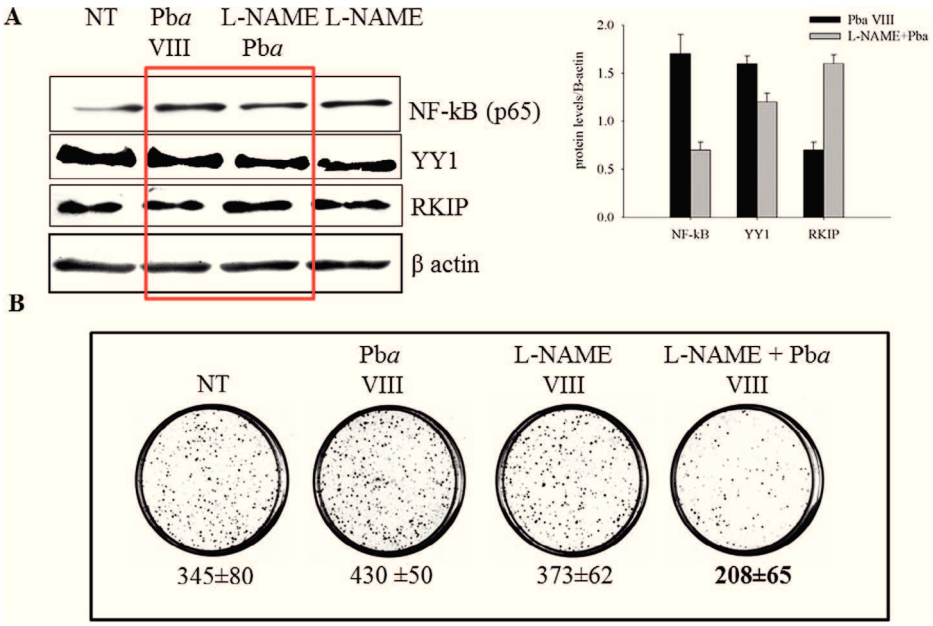

Fig. 8. Role of NO induced by a repeated low-dose Pb*a*/PDT treatment on (A) the NF-kB/YY1/RKIP circuitry. PC3 cells were treated with a combined repeated low-dose Pb*a*/PDT +L-NAME (1 mM) treatment. The protein lysates were analyzed 48 h after the last treatment. The histograms report the values of the different protein band intensity determined densitometrically, normalized to β-actin and further normalized to the ratio of non-treated cells/β-actin, fixed to 1 (B) on clonogenic proliferation. PC3 cells were divided in 4 groups: NT, non-treated cells; Pb*a* VIII, cells treated eight times with repeated low-dose Pb*a*/PDT treatment; L-NAME VIII, cells treated eight times with 1 mM L-NAME and L-NAME + Pb*a* VIII, cells treated eight times with a combined low-dose Pb*a*/PDT + L-NAME treatment. After the last treatment, 500 cells from each group were seeded in a 60 mm Petri plate. After 18 days the colonies were formed, fixed and stained with 2.5% methylene blue in 50% ethanol. The images were obtained with Gel Doc 2000 Bio-Rad. The number of colonies (>50 cells) is reported below each plate. The experiment has been performed in triplicate.

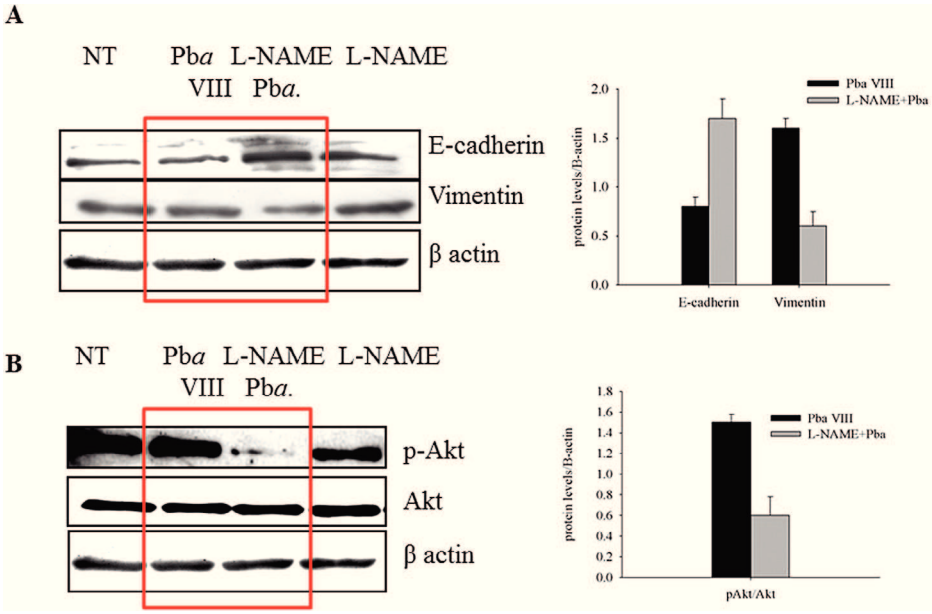

Fig. 9. Role of NO induced by a repeated low-dose Pb*a*/PDT treatment on (A) EMT and (B) pAKT/AKT. PC3 cells were treated with a combined repeated low-dose Pb*a*/PDT +L-NAME (1 mM) treatment. The protein lysates were analyzed 48 h after the last treatment. The histograms report the values of the different protein band intensity determined densitometrically, normalized to β-actin and further normalized to the ratio of non-treated cells /β-actin, fixed to 1.

ubiquitously expressed zinc-finger transcription factor that, when overexpressed or overactivated, leads to cell proliferation and cell resistance [80]. YY1 has been reported to activate the transcription of the EMT-inducer Snail and results in the inhibition of both RKIP and PTEN [35].

By creating a condition characterized by a continuous low induction of NO (this was achieved by a repeated low-dose Pb*a*/PDT) we have demonstrated an increase of the pro-survival NF-kB and YY1 gene products and a concomitant decrease of the pro-apoptotic RKIP: an expression pattern suggesting a cytoprotective role of NO. This was confirmed with the administration of an iNOS inhibitor, L-NAME, which abrogated the effects of gene expression obtained with Pb*a*/PDT as expected, in agreement with the data of Bhowmick and Girotti [8]. Moreover, beside the NF-kB/YY1/RKIP activation, we have also observed a strong activation of the PI3/AKT pathway.

In conclusion, the data reported herein suggest that a suboptimal Pb*a*/PDT, through the induction of low NO levels, induces EMT and cell tumor recurrence in prostate cancer cells through the activation of the NF-kB/YY1/RKIP circuitry. This is a relevant finding as *in vitro* both photosensitizer and light doses can be precisely measured in order to obtain optimal results, while in clinical PDT several variables affecting the outcome cannot be controlled A promising complementary approach to improve PDT could be the inhibition of EMT, by keeping the cells in an epithelial status and inhibiting the invasion in the basement membrane and consequently the formation of metastasis through high levels of NO using combinations of PDT with NO donors or NO–Pb*a* complexes.

Acknowledgments

This work has been carried out with the financial support of the Department of Medical and Biological Sciences, University of Udine.

Appendix: Supplementary materia

Supplementary data to this article can be found online at doi:10.1016/j.niox.2015.02.005.

References

[1] T.J. Dougherty, C.J. Gomer, B.W. Henderson, G. Jori, D. Kessel, M. Korbelik, et al., Photodynamic therapy, J. Natl. Cancer Inst. 90 (1998) 889–905.
[2] P. Agostinis, K. Berg, K.A. Cengel, T.H. Foster, A.W. Girotti, S.O. Gollnick, et al., Photodynamic therapy of cancer: an update, CA Cancer J. Clin. 61 (2011) 250–281.
[3] C.J. Gomer, A. Ferrario, M. Luna, N. Rucker, S. Wong, Photodynamic therapy: combined modality approaches targeting the tumor microenvironment, Lasers Surg. Med. 38 (2006) 516–521.
[4] M. Korbelik, H. Shibuya, I. Cecic, Relevance of nitric oxide to the response of tumours to photodynamic therapy, SPIE 3247 (1998) 98–105.
[5] K.J. Reeves, M.W.R. Reed, N.J. Brown, The role of nitric oxide in the treatment of tumours with aminolevulinic acid-induced photodynamic therapy, J. Photochem. Photobiol. B. 101 (2010) 224–232.
[6] G. Di Venosa, C. Perotti, H. Fukuda, A. Battle, A. Casas, Sensitivity to ALA-PDT of cell lines with different nitric oxide production and resistance to NO cytotoxicity, J. Photochem. Photobiol. B. 80 (2005) 195–202.
[7] S. Gupta, N. Ahmad, H. Mukhtar, Involvement of nitric oxide during phthalocyanine (Pc4) photodynamic therapy-mediated apoptosis, Cancer Res. 58 (1998) 1785–1788.
[8] R. Bhowmick, A.W. Girotti, Pro-survival and pro-growth effects of stress-induced nitric oxide in a prostate cancer photodynamic therapy model, Cancer Lett. 3 (2014) 115–122.
[9] V. Rapozzi, E. Della Pietra, S. Zorzet, M. Zacchigna, B. Bonavida, L.E. Xodo, Nitric oxide-mediated activity in anti-cancer photodynamic therapy, Nitric Oxide 30 (2013) 26–35.
[10] M. Korbelik, C.S. Parkins, H. Shibuya, I. Cecic, M.R. Stratford, D.J. Chaplin, Nitric oxide production by tumor tissue: impact on the response to photodynamic therapy, Br. J. Cancer 82 (2000) 1835–1843.
[11] K.J. Reeves, M.W.R. Reed, N.J. Brown, Is nitric oxide important in photodynamic therapy?, J. Photochem. Photobiol. B 95 (2009) 141–147.
[12] D.A. Wink, Y. Vodovotz, J.A. Cook, M.C. Krishna, S. Kim, D. Coffin, et al., The role of nitric oxide chemistry in cancer treatment, Biochemistry (Mosc) 63 (1998) 802–809.
[13] K. Xie, S. Huang, Contribution of nitric oxide-mediated apoptosis to cancer metastasis inefficiency, Free Radic. Biol. Med. 34 (2003) 969–986.
[14] E.L. Williams, M.B. Djamgoz, Nitric oxide and metastatic cell behaviour, Bioessays 27 (2005) 1228–1238.
[15] D. Fukumura, S. Kashiwagi, R.K. Jain, The role of nitric oxide in tumor progression, Nat. Rev. Cancer 6 (2006) 521–534.
[16] D.D. Thomas, M.G. Espey, L.A. Ridnour, L.J. Hofseth, D. Mancardi, C.C. Harris, et al., Hypoxic inducible factor 1alpha, extracellular signal-regulated kinase, and p53 are regulated by distinct threshold concentrations of nitric oxide, Proc. Natl. Acad. Sci. U.S.A. 101 (2004) 8894–8899.
[17] R. Bhowmick, A.W. Girotti, Cytoprotective signaling associated with nitric oxide upregulation in tumor cells subjected to photodynamic therapy-like oxidative stress, Free Radic. Biol. Med. 57 (2013) 39–48.

[18] V. Rapozzi, K. Umezawa, L.E. Xodo, Role of NF-κB/Snail/RKIP loop in the response of tumor cells to photodynamic therapy, Lasers Surg. Med. 43 (2011) 575–585.
[19] S. Singh, A.K. Gupta, Nitric oxide: role in tumour biology and iNOS/NO-based anticancer therapies, Cancer Chemother. Phatmacol. 67 (2011) 1211–1224.
[20] L. Liu, J.S. Stamler, NO: an inhibitor of cell death, Cell Death Diff. 6 (1999) 937–942.
[21] G. Melino, M.V. Catani, M. Corazzari, P. Guerrieri, F. Bernassola, Nitric oxide can inhibit apoptosis or switch it into necrosis, Cell. Mol. Life Sci. 57 (2000) 612–622.
[22] L. Rossig, B. Fichrlscherer, K. Breitschopf, J. Haendeler, A.M. Zeiher, A. Mülsch, et al., Nitric oxide inhibits caspase-3 by S-nitrosation in vivo, J. Biol. Chem. 274 (1999) 6823–6826.
[23] S. Dimmeler, J. Haendeler, M. Nehls, A.M. Zeiher, Suppression of apoptosis by nitric oxide via inhibition of interleukin-1beta-converting enzyme (ICE)-like and cysteine protease protein (CPP)-32-like proteases, J. Exp. Med. 185 (1997) 601–607.
[24] E.R. Gomes, R.D. Almeida, A.P. Carvalho, C.B. Duarte, Nitric oxide modulates tumor cell death induced by photodynamic therapy through a cGMP-dependent mechanism, Photochem. Photobiol. 76 (2002) 423–430.
[25] C. Min, S.F. Eddy, D.H. Sherr, G.E.J. Sonenshein, NF-kappaB and epithelial to mesenchymal transition of cancer, J. Cell. Biochem. 104 (2008) 733–744.
[26] B.H. Jiang, L.Z. Liu, PI3K/PTEN signaling in angiogenesis and tumorigenesis, Adv. Cancer Res. 102 (2009) 19–65.
[27] W.S. Wu, J.R. Wu, C.T. Hu, Signal cross talks for sustained MAPK activation and cell migration: the potential role of reactive oxygen species, Cancer Metastasis Rev. 27 (2008) 303–314.
[28] J. Suh, A.B. Rabson, NF-kappaB activation in human prostate cancer: important mediator or epiphenomenon?, J. Cell. Biochem. 91 (2004) 100–117.
[29] M.A. Huber, N. Azoitei, B. Baumann, S. Grünert, A. Sommer, H. Pehamberger, et al., NF-kappaB is essential for epithelial-mesenchymal transition and metastasis in a model of breast cancer progression, J. Clin. Invest. 114 (2004) 569–581.
[30] L. Zhang, W. Chen, X. Li, A novel anticancer effect of butein: inhibition of invasion through the ERK1/2 and NF-kappa B signaling pathways in bladder cancer cells, FEBS Lett. 582 (2008) 1821–1828.
[31] K. Tozawa, S. Sakurada, K. Kohri, T. Okamoto, Effects of anti-nuclear factor kappa B reagents in blocking adhesion of human cancer cells to vascular endothelial cells, Cancer Res. 55 (1995) 4162–4167.
[32] S.R. Shin, N. Sánchez-Velar, D.H. Sherr, G.E. Sonenshein, 7,12-dimethylbenz(a)anthracene treatment of a c-rel mouse mammary tumor cell line induces epithelial to mesenchymal transition via activation of nuclear factor-kappaB, Cancer Res. 66 (2006) 2570–2575.
[33] I. Coupienne, G. Fettweis, N. Rubio, P. Agostinis, J. Piette, NF-kappaB inhibition improves the sensitivity of human glioblastoma cells to 5-aminolevulinic acid-based photodynamic therapy, Biochem. Pharmacol. 81 (2011) 606–616.
[34] S. Huerta-Yepez, M. Vega, H. Garban, B. Bonavida, Involvement of the TNF-alpha autocrine-paracrine loop, via NF-kappaB and YY1, in the regulation of tumor cell resistance to Fas-induced apoptosis, Clin. Immunol. 120 (2006) 297–309.
[35] B. Bonavida, S. Baritaki, The novel role of Yin Yang 1 in the regulation of epithelial to mesenchymal transition in cancer via the dysregulated NF-kB/Snail/RKIP/PTEN circuitry, Crit. Rev. Oncog. 16 (2011) 211–226.
[36] V. Rapozzi, M. Miculan, L.E. Xodo, Evidence that photoactivated pheophorbide a causes in human cancer cells a photodynamic effect involving lipid peroxidation, Cancer Biol. Ther. 8 (2009) 1318–1327.
[37] G. Singh, O. Alqawi, M. Espiritu, Metronomic PDT and cell death pathways, Methods Mol. Biol. 635 (2010) 65–78.
[38] S.K. Bisland, L. Lilge, A. Lin, R. Rusnov, B.C. Wilson, Metronomic photodynamic therapy as a new paradigm for photodynamic therapy: rationale and preclinical evaluation of technical feasibility for treating malignant brain tumors, Photochem. Photobiol. 80 (2004) 22–30.
[39] R. Bhowmick, A.W. Girotti, Rapid upregulation of cytoprotective nitric oxide in breast tumor cells subjected to a photodynamic therapy-like oxidative challenge, Photochem. Photobiol. 87 (2011) 378–386.
[40] M.J. Barbera, I. Puig, D. Dominiguez, S. Julien-Grille, S. Guaita-Esteruelas, S. Peiró, et al., Regulation of Snail transcription during epithelial to mesenchymal transition of tumor cells, Oncogene 23 (2004) 7345–7354.
[41] M.A. Nieto, The snail superfamily of zinc-finger transcription factors, Nat. Rev. Mol. Cell Biol. 3 (2002) 155–166.
[42] S. Beach, H. Tang, S. Park, A.S. Dhillon, E.T. Keller, W. Kolch, et al., Snail is a repressor of RKIP transcription in metastatic prostate cancer cells, Oncogene 27 (2008) 2243–2248.
[43] K. Yeung, T. Seitz, S. Li, P. Janosch, B. McFerran, C. Kaiser, et al., Suppression of Raf-1 kinase activity and MAP kinase signalling by RKIP, Nature 401 (1999) 173–177.
[44] K.C. Yeung, D.W. Rose, A.S. Dhillon, D. Yaros, M. Gustafsson, D. Chatterjee, et al., Raf kinase inhibitor protein interacts with NF-kappa B inducing kinase and TAK1 and inhibits NF-kappa B activation, Mol. Cell. Biol. 21 (2001) 7207–7217.
[45] H. Tang, S. Park, S.C. Sun, R. Trumbly, G. Ren, E. Tsung, et al., RKIP inhibits NF-kB in cancer cells by regulating upstream signaling components of the IkB kinase complex, FEBS Lett. 584 (2010) 662–668.
[46] D. Chatterjee, Y. Bai, Z. Wang, S. Beach, S. Mott, R. Roy, et al., RKIP sensitizes prostate and breast cancer cells to drug-induced apoptosis, J. Biol. Chem. 279 (2004) 17515–17523.
[47] H.Z. Li, Y. Gao, X.L. Zhao, Y.X. Liu, B.C. Sun, J. Yang, et al., Effects of raf kinase inhibitor protein expression on metastasis and progression of human epithelial ovarian cancer, Mol. Cancer Res. 6 (2008) 917–928.
[48] B. Boyer, A.M. Vallés, N. Edme, Induction and regulation of epithelial-mesenchymal transitions, Biochem. Pharmacol. 60 (2000) 1091–1099.
[49] M. Guarino, Epithelial mesenchymal transition tumour invasion, Int. J. Biochem. Cell Biol. 39 (2007) 2153–2160.
[50] K. Vleminckx, L. Vakaet Jr., M. Mareel, W. Fiers, F. van Roy, Genetic manipulation of E-cadherin expression by epithelial tumor cells reveals an invasion suppressor role, Cell 66 (1991) 107–119.
[51] E. Batlle, E. Sancho, C. Francí, D. Domínguez, M. Monfar, J. Baulida, et al., The transcription factor snail is a repressor of E-cadherin gene expression in epithelial tumour cells, Nat. Cell Biol. 2 (2000) 84–89.
[52] L. Larue, A. Bellacosa, Epithelial-mesenchymal transition in development and cancer: role of phosphatidylinositol 3′ kinase/AKT pathways, Oncogene 24 (2005) 7443–7454.
[53] S.J. Grille, A. Bellacosa, J. Upson, A.J. Klein-Szanto, F. van Roy, W. Lee-Kwon, et al., The protein kinase Akt induces epithelial mesenchymal transition and promotes enhanced motility and invasiveness of squamous cell carcinoma lines, Cancer Res. 63 (2003) 2172–2178.
[54] S. Baritaki, S. Huerta-Yepez, A. Sahakyan, I. Karagiannides, K. Bakirtzi, A. Jazirehi, et al., Mechanisms of nitric oxide-mediated inhibition of EMT in cancer: inhibition of the metastasis-inducer Snail and induction of the metastasis-suppressor RKIP, Cell Cycle 9 (2010) 4931–4940.
[55] S. Julien, I. Puig, E. Caretti, J. Bonaventure, L. Nelles, F. van Roy, et al., Activation of NF-kappaB by Akt upregulates Snail expression and induces epithelium mesenchyme transition, Oncogene 26 (2007) 7445–7456.
[56] R.S. Di Paola, To arrest or not to G2-M cell-cycle arrest, Clin. Cancer Res. 8 (2002) 3311–3314.
[57] R.R. Allison, K. Moghissi, Oncologic photodynamic therapy: clinical strategies that modulate mechanisms of action, Photodiagnosis Photodyn. Ther. 10 (2013) 331–341.
[58] T. Hasan, Using cellular mechanisms to develop effective combinations of photodynamic therapy and targeted therapies, J. Natl. Compr. Canc. Netw. 10 (Suppl. 2) (2012) S23–S26.
[59] A. Ferrario, K. von Tiehl, S. Wong, M. Luna, C.J. Gomer, Cyclooxygenase-2 inhibitor treatment enhances photodynamic therapy mediated tumor response, Cancer Res. 62 (2002) 3956–3961.
[60] A. Ferrario, K.F. von Tiehl, S. Wong, N. Rucker, M.A. Schwartz, P.S. Gill, et al., Anti-angiogenic treatment enhances photodynamic therapy responsiveness in a mouse mammary carcinoma, Cancer Res. 60 (2000) 4066–4069.
[61] A. Ferrario, C.F. Chantrain, K.F. von Thiel, S. Buckley, N. Rucker, D.R. Shalinsky, et al., The matrix metalloproteinase inhibitor Prinomastat enhances photodynamic therapy responsiveness in a mouse tumor model, Cancer Res. 64 (2004) 2328–2332.
[62] A. Ferrario, N. Rucker, S. Wong, M. Luna, C.J. Gomer, Survivin, a member of the inhibitor of apoptosis family, is induced by photodynamic therapy and is a target for improving treatment response, Cancer Res. 67 (2007) 4989–4995.
[63] A. Ferrario, A. Fisher, N. Rucker, C.J. Gomer, Celecoxib and NS-398 enhance photodynamic therapy by increasing in vitro apoptosis and decreasing in vivo inflammatory and angiogenic factors, Cancer Res. 65 (2005) 9473–9478.
[64] I. Coupienne, S. Bontems, M. Dewaele, N. Rubio, Y. Habraken, S. Fulda, et al., NF-kappaB inhibition improves the sensitivity of human glioblastoma cells to 5-aminolevulinic acid-based photodynamic therapy, Biochem. Pharmacol. 81 (2011) 606–616.
[65] R. Bhowmick, A.W. Girotti, Cytoprotective induction of nitric oxide synthase in a cellular model of 5-aminolevulinic acid-based photodynamic therapy, Free Radic. Biol. Med. 48 (2010) 1296–1301.
[66] T.R. Geiger, D.S. Peeper, Metastasis mechanisms, Biochim. Biophys. Acta 1796 (2009) 293–308.
[67] J.P. Thiery, Epithelial-mesenchymal transitions in tumour progression, Nat. Rev. Cancer 2 (2002) 442–454.
[68] M. Ksiazkiewicz, A. Markiewicz, A.J. Zaczek, Epithelial-mesenchymal transition: a hallmark in metastasis formation linking circulating tumor cells and cancer stem cells, Pathobiology 79 (2012) 195–208.
[69] A. Uzdensky, E. Kolpakova, A. Juzeniene, P. Juzenas, J. Moan, The effect of sub-lethal ALA-PDT on the cytoskeleton and adhesion of cultured human cancer cells, Biochim. Biophys. Acta 1722 (2005) 43–50.
[70] A. Casas, F. Sanz-Rodriguez, G. Di Venosa, L. Rodriguez, L. Mamone, A. Blázquez, et al., Disorganisation of cytoskeleton in cells resistant to photodynamic treatment with decreased metastatic phenotype, Cancer Lett. 270 (2008) 56–65.
[71] T. Tsai, H.T. Ji, P.C. Chiang, R.H. Chou, W.S. Chang, C.T. Chen, ALA-PDT results in phenotypic changes and decreased cellular invasion in surviving cancer cells, Lasers Surg. Med. 41 (2009) 305–315.
[72] V. Vonarx, M.T. Foultier, D.B. Xavier, L. Anasagasti, L. Morlet, T. Patrice, Photodynamic therapy decreases cancer colonic cell adhesiveness and metastatic potential, Res. Exp. Med. (Berl) 195 (1995) 101–116.
[73] N. Rousset, V. Vonarx, S. Eleouet, J. Carre, E. Kerninon, Y. Lajat, et al., Effects of photodynamic therapy on adhesion molecules and metastasis, J. Photochem. Photobiol. B 52 (1999) 65–73.
[74] J.M. Runnels, N. Chen, B. Ortel, D. Kato, T. Hasan, BPD-MA mediated photosensitization in vitro and in vivo: cellular adhesion and beta1 integrin expression in ovarian cancer cells, Br. J. Cancer 80 (1999) 946–953.
[75] S. Baritaki, K. Yeung, M. Palladino, J. Berenson, B. Bonavida, Pivotal roles of Snail inhibition and RKIP induction by the proteosoma inhibitor NPI-0052 in tumor cell chemosensitization, Cancer Res. 69 (2009) 8376–8385.
[76] S. Baritaki, A. Chapman, K. Yeung, D.A. Spandodos, M. Palladino, B. Bonavida, Inhibition of epithelial to mesenchymal transition in metatatic prostate cancer

cells by the novel proteosoma inhibitor NPI-0052; pivotal roles of Snail repression and RKIP induction, Oncogene 28 (2009) 3573–3585.
[77] K. Wu, B. Bonavida, The activated NF-kappaB-Snail-RKIP circuitry in cancer regulates both the metastatic cascade and resistance to apoptosis by cytotoxic drugs, Crit. Rev. Immunol. 29 (2009) 241–254.
[78] H.E. Marshall, J.S. Stamler, Inhibition of NF-kappa B by S-nitrosylation, Biochemistry 40 (2001) 1688–1693.
[79] D. Seligson, S. Horvath, S. Huerta-Yepez, S. Hanna, H. Garban, A. Roberts, et al., Expression of transcription factor Yin Yang 1 in prostate cancer, Int. J. Oncol. 27 (2005) 131–141.
[80] S. Gordon, G. Akopyan, H. Garban, B. Bonavida, transcription factor YY1: structure, function, and therapeutic implication in cancer biology, Oncogene 25 (2006) 1125–1142.